**University of Alberta**


DESIGN AND ANALYSIS OF NEW WIRELESS TRANSMISSION STRATEGIES FOR
COOPERATIVE RELAY NETWORKS


by


**Gayan Lasintha Amarasuriya Aruma Baduge**


A thesis submitted to the Faculty of Graduate Studies and Research
in partial fulfillment of the requirements for the degree of

**Doctor of Philosophy**
in
Communications


Department of Electrical and Computer Engineering


©Gayan Lasintha Amarasuriya Aruma Baduge
Fall 2013
Edmonton, Alberta

*Dedicated to my beloved parents and wife...*

# Abstract

Cooperative relay technologies are currently being researched to address the ever-increasing demand for higher data rates, extended coverage, greater mobility, and enhanced reliability. This thesis thus focuses on (1) developing new physical-layer wireless technologies for cooperative relay networks and (2) ascertaining their viability through performance analysis. Specifically, (i) new system and channel models, (ii) signaling and relay-processing algorithms, (iii) joint relay-antenna selection strategies, (iv) joint transmit-receive beamforming techniques, and (v) comprehensive performance analysis frameworks are developed for one-way, two-way, and multi-way cooperative relay networks.

Our first research focuses on developing a comprehensive analytical framework for deriving closed-form performance bounds of multi-hop amplify-and-forward (AF) relay networks. Specifically, mathematically-tractable, asymptotically-exact end-to-end signal-to-noise ratio bounds are first formulated, and thereby, the outage probability and average bit error rate bounds are derived. In our second work, adaptive multiple-relay selection strategies are designed and analyzed for multi-relay AF networks to optimize the trade-offs among the system performance, complexity, and wireless resource usage. Our third research investigates joint antenna and relay selection strategies, which are optimal in the sense of the achievable diversity gains, for multiple-input multiple-output (MIMO) one-way relay networks and MIMO two-way relay networks. Finally, joint transmit/receive zero forcing transmission strategies are developed for MIMO multi-way relay networks for optimizing the achievable diversity-multiplexing trade-off.

The key design criterion of the aforementioned transmission designs is to leverage spatial diversity and/or spatial multiplexing gains available among distributed single-antenna and/or multiple-antenna wireless terminals through distributed transmission and efficient signal processing. Moreover, the fundamental relationships among the data rate, coverage, and reliability metrics are characterized, and thereby, the detrimental impact of practical wireless transmission impairments on the performance of the aforementioned transmission strategies are quantified. The insights obtained through these analyses are then used to refine

our physical-layer designs to achieve desirable trade-offs between the system performance, resource usage and implementation complexity.

∼

# Acknowledgement

First of all, I express my sincere gratitude and respect to my advisors, Dr. Chintha Tellambura and Dr. Masoud Ardakani. They indeed gave me the total freedom to define and conduct my research, while providing encouragement, guidance, and invaluable expertise throughout my PhD degree program. It was my great pleasure to work and collaborate with them, and their open approach toward research and professionalism have immensely facilitated my PhD studies.

I would also like to thank my PhD examining committee; Dr. Raviraj Adve, Dr. Rambabu Karumudi, and Dr. Yindi Jing for their valuable time spent reading my thesis and providing useful feedback. Furthermore, I am grateful to the faculty and the administrative staff of the ECE for their support and for creating an environment conducive for research excellence.

I also wish to thank the Alberta Innovates Technology Futures (AITF) and the Killam Trusts for the generous financial support I received in the form of the AITF Graduate Scholarship and the Izaak Walton Killam Memorial Scholarship.

My most heartfelt gratitude goes to my beloved parents, my sister, and my loving wife for their immeasurable support and encouragement throughout my graduate studies.

I would also like to thank my labmates, including Damith, Prasanna, Madush, Gongpu, Shuangshuang, Vesh, Yamuna, Amir, Moslem, Mahdi, Raman, Sahar, Zohreh, and Kaveh for the useful discussions we had, immense encouragement they gave, and enjoyable times we spent together. Moreover, the rich and diverse learning environment of my research lab provided me a golden opportunity to gain invaluable experience to excel my research.

$\sim$

# Table of Contents

# List of Figures

# List of Abbreviations

| Abbreviation | Definition |
| --- | --- |
| 4G | fourth generation |
| | |
| AF | amplify-and-forward |
| ANC | analog network coding |
| APR | all-participate relaying |
| AWGN | additive white Gaussian noise |
| | |
| BC | broadcast |
| BER | bit error rate |
| BFSK | binary frequency shift keying |
| BPSK | binary phase shift keying |
| | |
| CA-AF | channel-assisted amplify-and-forward |
| CCDF | complimentary cumulative distribution function |
| CDF | cumulative distribution function |
| CEP | conditional error probability |
| CSI | channel-state information |
| | |
| DF | decode-and-forward |
| DMT | diversity-multiplexing trade-off |
| DoF | degree of freedom |
| | |
| FDF | functional decode-and-forward |
| FG-AF | fixed-gain amplify-and-forward |
| FIR | finite impulse response |
| | |
| GLQ | Gauss-Laguerre quadrature |
| GSC | generalized selection combining |
| | |
| i.i.d. | independent and identically distributed |
| i.n.i.d | independent and non-identically distributed |
| IMT-A | International Mobile Telecommunications-Advanced |
| | |
| LTE | Long Term Evolution |
| LTE-A | Long Term Evolution-Advanced |

| Abbreviation | Definition |
| --- | --- |
| MA-MWR-IC | multiple-access multi-way relay interference channels |
| MAC | multiple-access |
| MGF | moment generating function |
| MIMO | multiple-input multiple-output |
| MISO | multiple-input single-output |
| MMSE | minimum mean square error |
| MRC | maximal ratio combining |
| MRS | multiple relay selection |
| MWRN | multi-way relay network |
| | |
| OT-MRS | output-threshold multiple relay selection |
| OWRN | one-way relay network |
| | |
| PAM | pulse amplitude modulation |
| PDF | probability density function |
| PLNC | physical layer network coding |
| | |
| RF | radio frequency |
| Rx/Tx | receive/transmit |
| | |
| SER | symbol error rate |
| SIMO | single-input multiple-output |
| SISO | single-input single-output |
| SNR | signal-to-noise ratio |
| SRS | single relay selection |
| | |
| TAS | transmit antenna selection |
| TWRN | two-way relay network |
| Tx/Rx | transmit/receive |
| | |
| WiFi | Wireless Fidelity |
| WiMAX | Worldwide Interoperability for Microwave Access |
| | |
| ZF | zero forcing |

# List of Symbols

## Elementary & Special Functions

| Notation | Definition |
|---|---|
| $\lceil \cdot \rceil$ | ceiling function |
| $\lfloor \cdot \rfloor$ | floor function |
| $\exp(\cdot)$ | Exponential function |
| $\log(\cdot)$ | natural logarithm |
| $\log_2(\cdot)$ | logarithm to base 2 |
| $\Gamma(z)$ | Gamma function [1, Eqn. (8.310.1)] |
| $\gamma(\alpha, z)$ | lower incomplete Gamma function [1, Eqn. (8.350.1)] |
| $\Gamma(\alpha, z)$ | upper incomplete Gamma function [1, Eqn. (8.350.2)] |
| $\mathcal{J}_0(\cdot)$ | Bessel function of the first kind of order zero [1, Eqn. (8.402)] |
| $\mathcal{I}_\nu(\cdot)$ | modified Bessel function of the first kind of order $\nu$ [2, Sec. 9.6] |
| $\mathcal{K}_\nu(\cdot)$ | modified Bessel function of the second kind of order $\nu$ [2, Sec. 9.6] |
| $_2\mathcal{F}_1(\cdot, \cdot\,;\cdot\,;\cdot)$ | Gauss Hypergeometric function [1, Eqn. (9.14.1)] |
| $\mathcal{Q}(\cdot)$ | Gaussian $Q$-function [2, Eqn. (26.2.3)] |

## Probability & Statistics

Let $X$ and $\mathcal{A}$ be a random variable and an arbitrary event, respectively.

| Notation | Definition |
|---|---|
| $\mathcal{E}_X\{\cdot\}$ | expected value with respect to $X$; $\mathcal{E}\{\cdot\}$, if $X$ is implied |
| $f_X(\cdot)$ | probability density function (PDF) of $X$ |
| $F_X(\cdot)$ | cumulative distribution function (CDF) of $X$ |
| $\bar{F}_X(\cdot)$ | complimentary cumulative distribution function (CCDF) of $X$ |
| $\mathcal{M}_X(\cdot)$ | moment generating function (MGF) of $X$ |
| $\mathcal{P}[\mathcal{A}]$ | probability of $\mathcal{A}$ |
| $X \sim \mathcal{G}(\alpha, \beta)$ | $X$ is Gamma distributed with shape parameter $\alpha$ and scale parameter $\beta$ |
| $X \sim \mathcal{CN}(\mu, \sigma^2)$ | $X$ is complex normal distributed with mean $\mu$ and variance $\sigma^2$ |

# Vectors and Matrices

Let $\mathbf{a} \in \mathbb{C}^{1 \times n}$ and $\mathbf{A} \in \mathbb{C}^{m \times n}$ denote an $1 \times n$ complex vector and an $m \times n$ complex matrix, respectively.

| Notation | Definition/ interpretation |
|---|---|
| $[\mathbf{a}]_i$ or $\mathbf{a}_i$ | $i$th element of $\mathbf{a}$ |
| $[\mathbf{A}]_{i,j}$ or $\mathbf{A}_{i,j}$ | $i$th element on the $j$th column of $\mathbf{A}$ |
| $\|\mathbf{a}\|$ | Euclidean norm of $\mathbf{a}$ |
| $\|\mathbf{A}\|_F$ | Frobenius norm of $\mathbf{A}$ [3, p.291] |
| $\mathbf{A} = \mathrm{diag}\,(a_1, \ldots, a_n)$ | $\mathbf{A}$ is rectangular diagonal; $a_1$ through $a_n$ are the non-zero diagonal elements |
| $\mathbf{A}^{-1}$ | inverse of $\mathbf{A}$ (for $m = n$) |
| $\mathbf{A}^*$ | conjugate of $\mathbf{A}$ |
| $\mathbf{A}^H$ | conjugate transpose of $\mathbf{A}$ |
| $\mathbf{A}^T$ | transpose of $\mathbf{A}$ |
| $\det(\mathbf{A})$ | determinant of $\mathbf{A}$ |
| $\mathrm{diag}\,(\mathbf{A})$ | elements on the main diagonal of $\mathbf{A}$ |
| $\mathrm{eig}\,(\mathbf{A})$ | eigenvalues of $\mathbf{A}$ (for $m = n$) [4, Ch. 5] |
| $\mathbf{I}_n$ | identity matrix of rank $n$ |
| $\mathbf{0}_{n,m}$ | $(n \times m)$ zero matrix |
| $\mathbf{A} \otimes \mathbf{B}$ | Kronecker product of $\mathbf{A}$ and $\mathbf{B}$ |
| $\mathrm{trace}(\mathbf{A})$ | trace of $\mathbf{A}$ (for $m = n$) [4, p.186] |

# Miscellaneous

| Notation | Definition |
|---|---|
| $|a|$ | absolute value of scalar $a$ |
| $a^*$ | complex conjugate of scalar $a$ |
| $k!$ | factorial of $k$ [2, Eqn. (6.1.5)] |
| $\binom{n}{k}$ | binomial coefficient $n$ choose $k$ [2, Sec. 3.1] |
| $\arg \min_i (a_i)$ | index $i$ corresponding to the smallest $a_i$ |
| $\arg \max_i (a_i)$ | index $i$ corresponding to the largest $a_i$ |
| $\lim_{x \to a} f(x)$ | the limit of function $f(x)$ as $x$ tends to $a$ |
| $\min (a_1, \ldots, a_n)$ | minimum of all scalars $a_i$ for relevant $i$; also $\min_i (a_i)$ |
| $\max (a_1, \ldots, a_n)$ | maximum of all scalars $a_i$ for relevant $i$; also $\max_i (a_i)$ |
| $o(x^n)$ | the remainder in a Maclaurin series [1, Eqn. (0.318.2)] of a function of $x$ after the $x^n$ term |
| $\Re(a)$ | real component of complex scalar $a$ |
| $\Im(a)$ | imaginary component of complex scalar $a$ |

# Chapter 1

# Introduction

Wireless transmission technologies have undergone a tremendous growth recently. For instance, data rate of wireless communication services has increased by about 100 times every six to seven years, and this growth translates into about a million-fold capacity increase since 1957 [5]. The main constituents of this data rate increase are (i) a 25-fold gain from the availability of wider spectrum, (ii) a 5-fold gain by dividing spectrum into smaller slices, (iii) another 5-fold gain from efficient signal/modulation designs, and (iii) an impressive 1600-fold gain due to reduced cell sizes and transmit distances [5]. However, mobile data traffic demand is predicted to grow up to about 11.2 Exabyte per month by 2017, an 13-fold increase over 2012, mainly as a result of the recent proliferation of data-centric portable devices [6]. This exponential demand for data rate will also account for a 16-20% increase in energy consumption and hence will increase the global $CO_2$ emissions by another 2% [7]. As the conventional techniques for increasing data rates, extending coverage, and reducing energy consumption are approaching their fundamental limits, new wireless system architectures and transmission strategies are needed to satisfy the future wireless requirements.

To be more specific, to meet the unprecedented requirement of ubiquitous and ultra fast access, and reliability, the traditional way of exploiting wireless channels in terms of time and frequency dimensions with single-antenna devices is no longer sufficient. For this reason, exploiting the space dimension by sending different streams of data over multiple antennas has become a necessity. This technology, called multiple-input multiple-output (MIMO), meets these requirements better than conventional single-antenna systems [8, 9]. Nevertheless, MIMO technology may itself not be adequate for, for example, extending the coverage area. Thus, the use of relays has been developed [10–13]. A terminal acts as a 'relay' whenever it forwards the signal from one terminal to another. In this way,

although a terminal sacrifices some of its resources (e.g., bandwidth and battery power), such cooperation improves overall network throughput, reliability, and coverage [11–13].

MIMO techniques have already been deployed in latest wireless broadband access networks, for instance, in the standard release IEEE 802.11n of Wireless Fidelity (WiFi) [14], and as well in the standard release IEEE 802.16e of Worldwide Interoperability for Microwave Access (WiMAX) [15]. Moreover, MIMO is an essential component in the next generation cellular networks, and hence, several single-user and multi-user MIMO techniques have been included in the specification of the emerging Long Term Evolution (LTE) and Long Term Evolution-Advanced (LTE-A) standards [16, 17].

Similarly, cooperative relaying techniques have already been standardized in IEEE 802.16j - multi-hop relay specification [18]. In particular, MIMO relay networks [19–21] are the natural generalization of cooperative relay networks for multiple-antenna terminals. To this end, MIMO relaying techniques are currently receiving significant research interest and hence are being investigated for emerging next-generation wireless standards such as LTE-A and International Mobile Telecommunications-Advanced (IMT-A) [22, 23]. Thus, designing and analyzing novel transmission strategies for cooperative relay networks is essential for furthering the aforementioned emerging wireless standards, which are primarily being developed to meet the unprecedentedly increasing demand for faster, reliable, and seamless wireless connectivity.

This doctoral thesis thus focuses on developing novel transmission strategies for cooperative relay networks. To be more specific, the main goals of this thesis are (1) to develop new physical-layer wireless technologies by employing cooperative relaying techniques and multi-antenna technology, and (2) to ascertain their viability through performance analysis. To this end, (i) new system and channel models, (ii) signaling and relay-processing algorithms, (iii) joint relay and antenna selection strategies, and (iv) joint transmit-receive beamforming techniques are designed for one-way, two-way, and multi-way cooperative relay networks. The primary design criterion of these physical-layer designs is to leverage spatial diversity and/or spatial multiplexing gains available among distributed single-antenna and/or multiple-antenna wireless terminals through distributed transmission and efficient signal processing. Furthermore, the fundamental performance metrics such as the data rate, coverage, and reliability metrics are first characterized, and thereby, the detrimental impact of practical wireless propagation impairments on the performance of the aforementioned transmission strategies are quantified. The valuable insights obtained via these analyses are used to fine-tune our transmission strategies to achieve better trade-offs among the system

2

(a) A typical wireless system set-up  (b) Large-scale and small-scale fading [24]
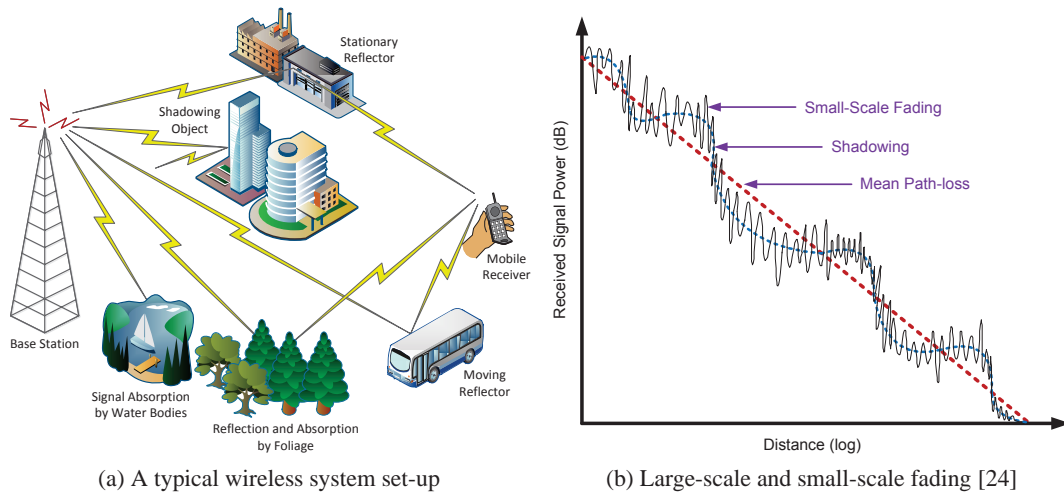
Figure 1.1: Wireless signal propagation and its impairments.

performance, wireless resource usage, and implementation complexity.

The remainder of this chapter consists of technical background, motivation, objectives, significance, outline, and summary of contributions of this thesis.

## 1.1 Technical background

This section presents the technical background necessary for this thesis. To be more specific, the fundamentals of wireless propagation, MIMO, and cooperative relays are discussed by elaborating the underlying technical concepts and terminology. Moreover, the fundamental metrics used for characterizing the wireless system performance are defined, and the corresponding mathematical background is explained.

### 1.1.1 Wireless channels

The wireless channel between a pair of wireless terminals, which are referred to as the transceivers (i.e., transmitters and receivers), generally refers to the multipath fading in the wireless transmission medium. The reliability and the rate of wireless data transfer is mainly governed by the multipath fading effects. The wireless channel thus imposes a fundamental challenge for reliable high-speed communications.

The received signal power over a wireless channel is affected by two different modes of physical phenomena, namely, large-scale propagation effects and small-scale propagation effects [24, 25] (see Fig 1.1). The former includes pathloss and shadowing. Specifically, the mean pathloss typically comes from inverse square power loss, ground reflection and
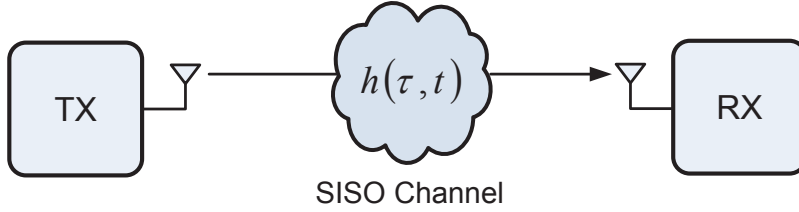
Figure 1.2: A basic wireless communication system.

miscellaneous absorption effects. Shadowing is caused by the large-scale obstacles between the transmitter and receiver, which attenuate signal power due to absorption, reflection, diffraction, and scattering. The small-scale propagation effect is caused mainly due to the constructive and destructive addition of multipath signal components and is also known as short term or fast fading. In particular, multipath propagation results in spreading of the received signal in different dimensions, specifically, in terms of delay, Doppler and angle spreadings.

### 1.1.2   SISO channel

The wireless channel between a single-antenna transmitter-receiver pair is termed as a single-input single-output (SISO) channel (see Fig. 1.2). It is described by the channel impulse response as [24]

$$h(\tau, t) = \sum_{n=0}^{N(t)} \alpha_n(t) e^{-j\phi_n(t)} \delta(\tau - \tau_n(t)), \tag{1.1}$$

where $h(\tau, t)$ is the channel response at time $t$ to an impulse at time $t - \tau$. The time-varying parameters $N(t)$, $\alpha_n(t)$, $\tau_n(t)$, and $\phi_n(t)$ are the number of resolvable multipaths, attenuation, time-delay, and effective phase shift due to delay and Doppler, respectively.

Specifically, for time-invariant channels, i.e., $h(\tau, t) = h(\tau, t + T)$, the time-invariant channel impulse response is given by

$$h(\tau) = \sum_{n=0}^{N} \alpha_n e^{-j\phi_n} \delta(\tau - \tau_n). \tag{1.2}$$

Moreover, whenever the maximum delay spread (i.e., the time difference between the earliest and the latest significant multipath components) of a channel is small relative to the inverse signal bandwidth, the corresponding channel is referred to as a narrowband or flat fading channel and tends to have non-resolvable multiplath components contributing to each term in (1.1). Thus, a narrowband fading channel is a special case of (1.2) and is given

4

by [24]

$$h(\tau, t) = \left( \sum_{n=0}^{N(t)} \alpha_n(t) e^{-j\phi_n(t)} \right) \delta(\tau). \tag{1.3}$$

Under flat and slow fading, the cumulative effect of the wireless channel is thus modeled as a complex channel gain. Moreover, the received signal is generally perturbed by noise introduced by various phenomena pertinent to the wireless channel and the radio transceiver circuitry. The typical received signal may therefore be mathematically modeled as follows [24, 26]:

$$y = hx + n, \tag{1.4}$$

where $h$ and $n$ denote the channel gain and the additive noise, respectively. Besides, $x$ is the data signal mapped onto symbols by using a modulation scheme [24, Ch. 5]. Moreover, the additive noise $n$ arises mainly due to the thermal agitation of electrons in the receiver circuitry and is modeled as white noise uniformly distributed across the entire bandwidth.

**Fading models:**

Various fading channel models are used to model the rapid fluctuations of the received signal in space, time, and frequency dimensions. If the fading is assumed to be caused by the superposition of a large number of independent scattered components, then the in-phase and the quadrature components of the received complex envelope is typically modeled as independent zero mean Gaussian processes. The magnitude of the received complex envelope is then Rayleigh distributed, and its probability density function (PDF) is given by [24, 25]

$$f(x) = \frac{2x}{\Omega} \exp\left( -\frac{x^2}{\Omega} \right) \quad \text{for} \quad x \geq 0, \tag{1.5}$$

where $\Omega$ is the average envelope power.

The Rayleigh fading (1.5) is typically employed to model rich scattering multipath channels. Moreover, the Nakagami-$m$ fading is a more sophisticated/generalized fading model, which is designed to fit empirical data, and is known to provide closer match to experimental data in practical cellular systems. The PDF of the magnitude of the received complex envelope under Nakagami-$m$ fading is given by [27]

$$f(x) = \frac{2m^m x^{2m-1}}{\Gamma(m)\Omega^m} \exp\left( -\frac{mx^2}{\Omega} \right) \quad \text{for} \quad x \geq 0 \quad \text{and} \quad m \geq \frac{1}{2}, \tag{1.6}$$

where $m$ is the parameter used to model either more or less severe fading effects than Rayleigh fading. For example, when $m = 1$, the Nakagami distribution reduces to Rayleigh distribution, and when $m = \frac{1}{2}$, it becomes the one-sided Gaussian distribution. Further, whenever $m \to \infty$, this distribution reduces to an impulse and used to model no-fading.
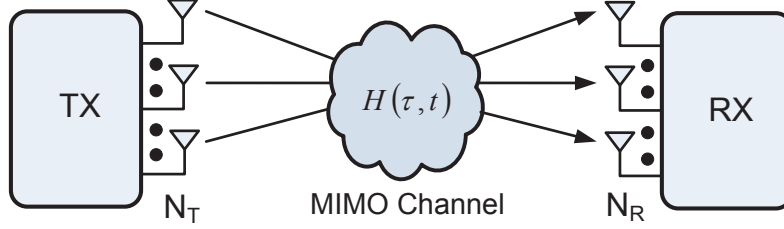
Figure 1.3: MIMO wireless channel.

### 1.1.3 MIMO channel

A MIMO channel is the wireless channel between a multiple-antenna transmitter-receiver pair (Fig. 1.3). For an MIMO system with $N_T$ transmit antennas and $N_R$ receive antennas, the time-varying channel response is represented as a matrix $\mathbf{H}(\tau, t) \in \mathbb{C}^{N_R \times N_T}$ of complex numbers, where its $(i, j)$th element is denoted by $h_{i,j}(\tau, t)$ and is given by (1.1). Here, $h_{i,j}(\tau, t)$ is indeed the time-varying channel impulse response between the $j$th transmit antenna and $i$th receive antenna. The $h_{i,j}$s are not necessarily independent; they may be spatially correlated and the amount of correlation depends on the relative antenna spacing, angles of arrival/departure, and corresponding angular spreads [28]. As wireless channels undergo fading, $h_{i,j}(\tau, t)$ fluctuates randomly, and hence, $\mathbf{H}(\tau, t)$ is typically modeled as a random matrix [25].

Under frequency flat fading and slow fading, the MIMO channel output is modeled as follows:

$$\mathbf{y} = \mathbf{H}\mathbf{x} + \mathbf{n}, \tag{1.7}$$

where $\mathbf{y} \in \mathbb{C}^{N_R \times 1}$, $\mathbf{H} \in \mathbb{C}^{N_R \times N_T}$, and $\mathbf{n} \in \mathbb{C}^{N_R \times 1}$ represent the received signal, channel matrix, and additive noise, respectively.

**Remark 1.1:** Whenever the transmitter and receiver are equipped with multiple-antennas and a single-antenna, respectively, the corresponding wireless channels is called as a multiple-input single-output (MISO) channel. Similarly, the channel associated with a single-antenna transmitter and a multiple-antenna receiver is called as a single-input multiple-output (SIMO) channel.

Next, some of the important system parameters of MIMO systems are briefly summarized.

**Degrees of freedom:**

The degrees of freedom (DoFs) of a communication channel is generally defined to be the dimension of the received signal space [29]. For the MIMO wireless channel with independent and identically distributed (i.i.d.) fading across all antennas, the spatial DoFs govern the maximum number of independent end-to-end data streams in the space dimension [30, 31]. Thus, in general, the DoFs in the space dimension is the rank of the effective MIMO channel. Further, DoFs may exist over the other orthogonal dimensions, namely time and frequency. In such cases, the total number of DoFs is the product of those along individual dimensions [29].

**Diversity combining:**

Both shadowing and fading induce a very large power penalty on the performance of signal transmission over wireless channels. This detrimental effect can successfully be mitigated by coherently combining signals received via independently fading signal paths. This approach is known as diversity combining, and the underlying key idea is the fact that independent signal paths have a low probability of experiencing deep fades simultaneously. Specifically, independently fading signal paths can be achieved in time, frequency and space dimensions.

**Diversity order:**

In general, diversity order quantifies the number of independently faded signal replicas received at the receiver and is defined as [32]

$$G_d = -\lim_{\gamma \to \infty} \frac{\log\left(P_e(\gamma)\right)}{\log\left(\gamma\right)}, \tag{1.8}$$

where $P_e(\gamma)$ is the average probability of error corresponding to the signal-to-noise ratio (SNR) $\gamma$. The diversity order indeed provides insights into how the slope of the average probability of error varies as a function of the average SNR. The maximum diversity order of an $N_R \times N_T$ MIMO system is $N_T N_R$. Whenever the diversity order equals to $N_T N_R$, the underlying MIMO system is said to achieve full diversity order.

The diversity order can also be defined by employing the outage probability as follows [29]:

$$G_d = -\lim_{\gamma \to \infty} \frac{\log\left(P_{\text{out}}(R, \gamma)\right)}{\log\left(\gamma\right)}, \tag{1.9}$$

where $P_{\text{out}}(R, \gamma)$ is the outage probability in the Shanon sense at a given SNR and required rate $R$.

**Array gain:**

Array gain is defined as the average increase in the SNR at the receiver resulted due to coherent signal combining effect of multiple antennas at the receiver or transmitter or both. In general, the coherent combining is realized by spatial post-processing at the receive antennas or/and spatial pre-processing at the transmit antennas. The array gain is manifested by the horizontal shift of the probability of error curve plotted against the average SNR.

For uncoded systems, the diversity order and the array gain can be quantified by using the asymptotic average probability of error analysis in high SNR regime as follows [32]:

$$\lim_{\gamma \to \infty} P_e(\gamma) \approx (G_a \gamma)^{-G_d}, \tag{1.10}$$

where $G_a$ and $G_d$ represent the array gain and the diversity order, respectively.

**Spatial multiplexing gain:**

To contrary to our intuition, fading in MIMO channels can indeed be beneficial for increasing the DoFs available for communication [33]. Specifically, whenever the channel gains between individual transmit-receive antenna pairs fade independently and hence the channel matrix is well conditioned with high probability, then the same MIMO channel can create multiple parallel spatial channels. By transmitting independent data streams in these parallel spatial channels, the data rate can be improved significantly. This effect is known as spatial multiplexing and offers a linear increase in transmission rate for the same bandwidth and same transmit power. Spatial multiplexing gain is therefore defined as [33]

$$r = \lim_{\gamma \to \infty} \frac{R(\gamma)}{\log(\gamma)}, \tag{1.11}$$

where $R(\gamma)$ is the data rate achievable at an average SNR $\gamma$. The spatial multiplexing gain is therefore equivalent to the gradient of the achievable rate curves at the asymptotically high SNRs. For example, an $N_R \times N_T$ MIMO system provides a multiplexing gain of $\min(N_T, N_R)$ [8, 34].

**Diversity-multiplexing trade-off:**

As per the aforementioned discussion, a MIMO system can provide two types of performance gains, namely diversity gain and spatial multiplexing gain. Nevertheless, maximizing one type of gain may not necessarily maximize the other. In fact, in MIMO channels, both type of gains can be simultaneously obtained under the constraint of a fundamental trade-off referred to as the diversity-multiplexing trade-off (DMT), which defines how much of each type of gain any coding scheme can extract [33].
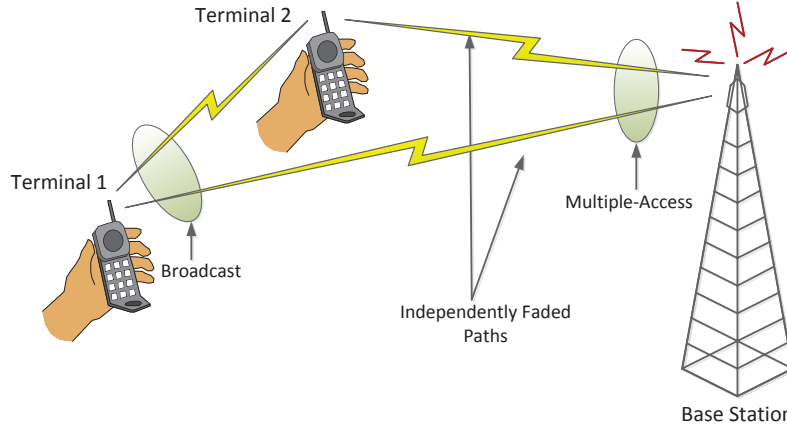
Figure 1.4: A basic cooperative relay network.

A mathematical expression for the DMT can be then formulated by employing the definitions of diversity gain (1.9) and multiplexing gain (1.11) as follows [29, 33]:

$$G_d = - \lim_{\gamma \to \infty} \frac{\log \left( P_{\text{out}}(r \log (\gamma)) \right)}{\log (\gamma)}. \tag{1.12}$$

### 1.1.4 Cooperative relay networks

Although multiple-antenna technology enhances diversity and/or multiplexing gains, it may not be capable of extending the coverage. The traditional way to extend the coverage and data rates simultaneously is to deploy more base-stations to serve in smaller cells, which in effect drives up deployment cost significantly. As a remedy to this problem, cooperative relaying, in which multiple distributed terminals operate cooperatively, has recently emerged [11–13] (see Fig. 1.4). The terminals cooperate with one another by relaying signals intended for others. A terminal is designated as a relay whenever it acts as an intermediate repeater between the transmitter and receiver. This way, each terminal sacrifices some of its resources (e.g., bandwidth and battery power) on behalf of the others, but such cooperation results in an enhanced overall quality-of-service for the whole network. Specifically, such cooperation enables communication between two terminals that are far apart, which is not possible with the traditional single-hop networks.

One key benefit of cooperative relay networks is the cooperative diversity. It is a relatively new form of spatial diversity technique that builds upon the classical relay channel model [10] and cooperative communications [11, 12]. Distributed terminals engage in cooperative communication share their antennas and other wireless resources in order to assist a transmission of a particular terminal. Cooperative diversity arises when these sharing is used primarily to leverage the spatial diversity available among distributed terminals

through distributed transmission and signal processing.

Relay terminals in cooperative networks are generally divided into two general categories (i) amplify-and-forward (AF) and (ii) decode-and-forward (DF), according to their mode of operation [12, 13]. The AF relays simply amplify and retransmit the received signal, while the DF relays decode and estimate the received symbols and re-encode them before retransmission to destination. Noise amplification is a potential drawback of AF relaying, whereas DF relaying suffers from error propagation if errors occur in the symbol estimation at the relay.

In general, cooperation can also be categorized as (i) fixed relaying, (ii) selection relaying and (iii) incremental relaying based on whether adaptive strategies and feedback is employed by the relaying protocol [12, 13]. In the fixed relaying, terminals are allowed to participate in the cooperation either in AF or DF mode throughout the cooperation phase. Whereas the selection relaying builds upon the fixed relaying by allowing transmitting terminals to select a suitable cooperative (or non-cooperative) action based a threshold determined by using the channel-state information (CSI). Finally, the incremental relaying improves the spectral efficiency of both the fixed and the selection relaying by exploiting the limited feedback provided by the destination and relying only when necessary.

Moreover, cooperative relay networks can be divided into three subclasses depending on how many channel-uses are required for mutual data signal exchange. These three subclasses are briefly summarized in following three subsections.

**One-way relay networks (OWRNs):**

In wireless communication systems, the terminals operate on half-duplex mode due to the practical complexity of simultaneous transmissions and receptions. Half-duplex relay networks operating with unidirectional data-flows are referred to as one-way relay networks (OWRNs) in the sequel. For instance, the OWRN in Fig. 1.5 requires four orthogonal channel-uses for two-way data transmission between $T_1$ and $T_2$ via $R$ ($T_1 \rightarrow R$, $R \rightarrow T_2$, $T_2 \rightarrow R$, and $R \rightarrow T_1$). However, only two time-slots are needed without the relay ($T_1 \rightarrow T_2$ and $T_2 \rightarrow T_1$). Thus, in this example, the price for relaying is a 100 % of channel usage. Is there a way to use a relay without incurring this penalty? Two-way relay networks (TWRNs) with physical-layer network coding is a solution to this challenge [35–37].
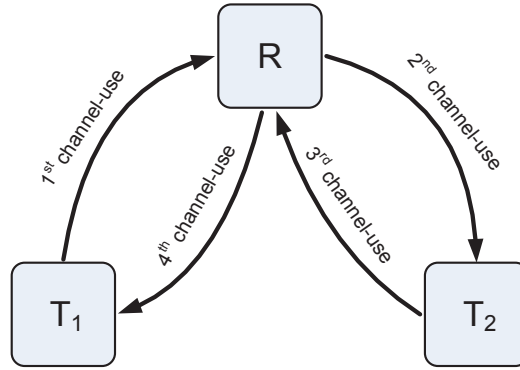
Figure 1.5: A basic one-way relay network.
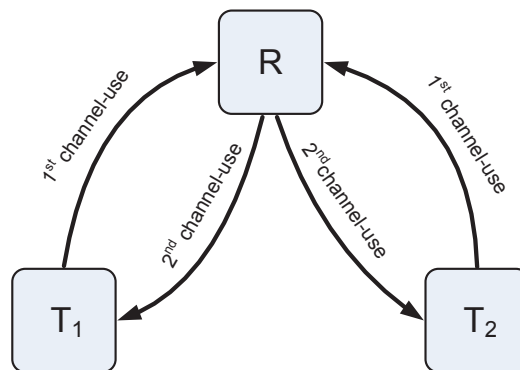


Figure 1.6: A basic two-way relay network.

**Two-way relay networks (TWRNs):**

In TWRNs, both $T_1$ and $T_2$ transmit simultaneously to $R$ during the first channel-use (see Fig. 1.6). Then $R$ generates a network-coded data symbol, a function of data symbols sent from $T_1$ and $T_2$ [35, 38]. In the second channel-use, $R$ broadcasts it back to $T_1$ and $T_2$. Since each terminal knows its own data, by using the network-coded data symbol, $T_1$ can decode the data of $T_2$ and vice versa. Thus, TWRNs require only two channel-uses for two-way data transmission [35–37]. This emerging technology allows the data rate, reliability, and coverage benefits of relaying to be reaped while retaining the efficient use of resources in conventional single-hop networks.

**Multi-way relay networks (MWRNs):**

The TWRNs allow mutual data signal exchange among only two terminals. However, certain practical applications such as multimedia teleconferencing via a satellite or mutual data exchange between sensor nodes and the data fusion center in wireless sensor networks require mutual data exchange among more than just two terminals. To this end, the multi-way

11
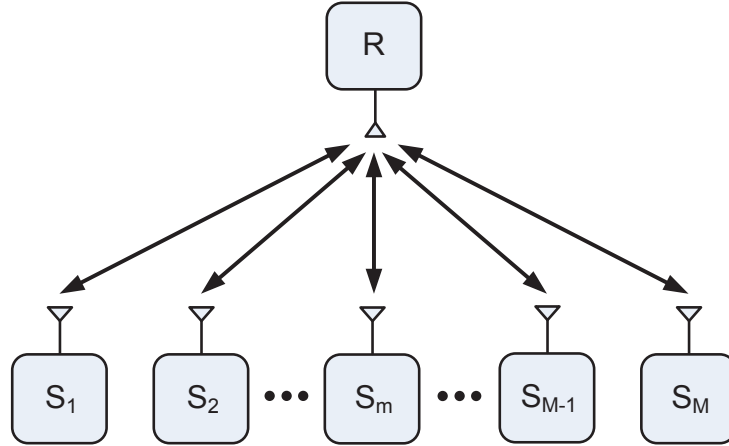
Figure 1.7: A basic multi-way relay network.

relay networks (MWRNs) facilitate mutual data exchange among more than two spatially distributed sources via a relay (see Fig. 1.7). In particular, MWRNs are the natural generalization of conventional OWRNs and TWRNs [39–42]. Moreover, OWRNs have already been included in LTE-A standard, and TWRNs are being studied for relay-based IMT-A systems [43]. Thus, MWRNs are also expected to be an integral part of the next-generation wireless standards.

### 1.1.5 Cooperative MIMO relay networks

The MIMO relay networks consist of all multiple-antenna terminals and achieve both the benefits of cooperative relays and MIMO technology simultaneously [19–21] (see Fig. 1.8). In particular, they achieve some unique benefits, which would not necessarily be achieved by using either relay or MIMO technologies separately. To be more specific, MIMO relay networks provide diversity against large-scale fading, for instance against shadowing, which cannot typically be mitigated with collocated antennas. Moreover, they can be used in applications, where MIMO signal processing alone cannot yield both the diversity and multiplexing gains, however, at the expense of increased signal processing complexity. The natural generalization of MIMO relaying into OWRNs, TWRNs, and MWRNs are referred to as MIMO OWRNs, MIMO MWRNs, and MIMO TWRNs, respectively.

## 1.2 Motivation, objectives and significance

**Motivation:** The fourth generation (4G) and subsequent wireless technologies are currently being researched to address the ever-increasing demand for higher data rates, extended cov-
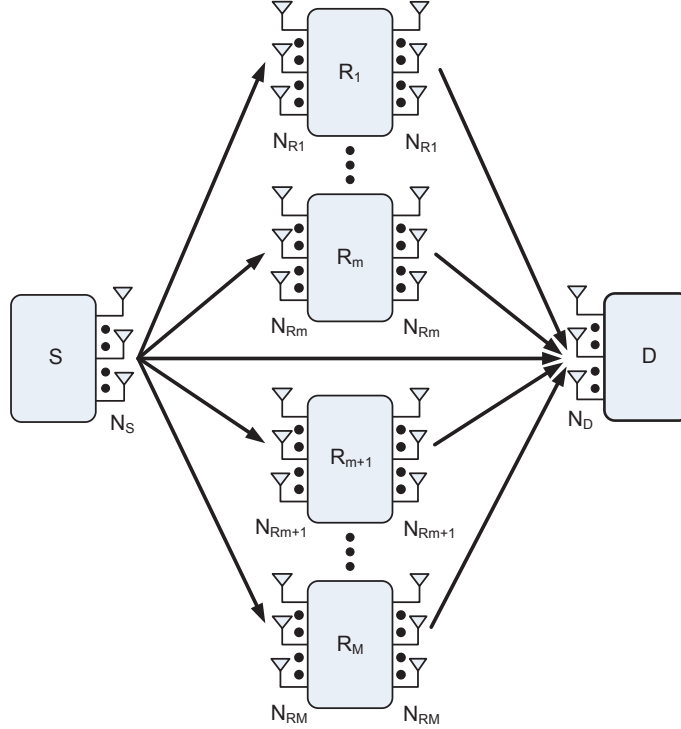
Figure 1.8: A basic MIMO relay network.

erage, greater mobility, and enhanced reliability. To meet these requirements, the traditional techniques of exploiting the wireless channels in terms of time and frequency dimensions with single-antenna devices are not sufficient as they either have already reached their theoretical limits or provide only marginal performance improvements. To circumvent this challenge, cooperative multi-antenna relay networks, which exploit the spatial dimension by sending different streams of bits by using multiple antennas over multiple relayed-hops, are studied for next-generation wireless networks. Thus, this thesis focuses on designing and analyzing new wireless transmission strategies for cooperative relay networks by exploiting cooperative communication and multi-antenna technologies. The specific motivation pertinent to each contribution is explicitly elaborated in Sections 2.1.2, 3.1.2, 4.1.3, and 5.1.3 of Chapters 2, 3, 4, and 5, respectively.

**Objectives:** The main goals of this thesis are (1) to develop new physical-layer wireless technologies by employing cooperative relaying techniques and multi-antenna technology, and (2) to ascertain their viability through performance analysis. To be more specific, (i) new system and channel models, (ii) signaling and relay-processing algorithms, (iii) joint relay-antenna selection strategies, (iv) joint transmit-receive beamforming techniques, and (v) comprehensive performance analysis frameworks are developed for one-way, two-way,

and multi-way cooperative relay networks. These physical layer transmission strategies are designed primarily to leverage spatial diversity and/or spatial multiplexing gains available among distributed single-antenna and/or multiple-antenna wireless terminals through distributed transmission and efficient signal processing. Moreover, important performance metrics, including the outage probability, average probability of error, and achievable diversity/multiplexing trade-off are derived in closed-form. Our analysis indeed characterizes the fundamental relationships among the data rate, coverage, and reliability metrics, and thereby, the detrimental impact of practical wireless propagation impairments on the performance of the aforementioned transmission strategies are quantified. The insights obtained through these analyses are then used to refine our physical layer designs to achieve better trade-offs among the system performance, resource usage, and implementation complexity.

**Significance:** Cooperative single-antenna relay networks have already been included in modern wireless standards such as WiMAX (IEEE 802.16j and IEEE 802.16e) [18, 44]. Going from single-antenna terminals to multiple-antenna terminals can indeed be anticipated not only because of the recent advancements in electronics that make multi-antenna signal processing cost-effective, but also due to the lesser antenna spacing constraints imposed by the higher carrier frequencies of emerging wireless systems such as the 60 GHz frequency band (e.g., IEEE 802.15.3c [45]). Therefore, multiple-antenna cooperative relay networks are currently receiving significant research interest and are being investigated for emerging wireless standards such as LTE-A, and IMT-A [43]. Thus, the proposed transmission designs could significantly contribute to the advancement of these 4G broadband wireless relay standards.

## 1.3 Thesis outline and contributions

This thesis focuses on design and analysis of new transmission strategies for cooperative relay networks. Specifically, Chapters 2–5 of this thesis present (i) comprehensive performance analysis frameworks, (ii) adaptive relay selection strategies, (iii) optimal antenna selection schemes, and (iv) joint transmit/receive beamforming techniques for OWRNs, TWRNs, and MWRNs. Chapter 6 presents the conclusions; the bibliography and the appendices follow.

- Chapter 2 presents a comprehensive performance analysis framework for multi-hop AF relay networks. To be more specific, a new class of SNR upper bounds multi-hop

($N \geq 2$) relay networks is developed by computing the half-harmonic mean of the minimum of the first $P \geq 0$ hop SNRs and the minimum of the remaining $N - P$ hop SNRs. The parameter $P$ varies between $0$ to $N$ and may be chosen to provide the tightest bound. A complete statistical characterization of the SNR bounds is developed by deriving the cumulative distribution function (CDF), the PDF, and the moment generating function (MGF) in closed-form. The resulting outage probability and the average symbol error rate bounds are asymptotically exact. This asymptotic-exactness holds for any $0 \leq P \leq N$ and consequently paves the way to devise a generalized asymptotic performance analysis at high SNRs. Usefulness of the proposed performance bounds is elaborated through two practical examples.

- Chapter 3 develops a new class of multiple relay selection (MRS) scheme for dual-hop multi-branch cooperative wireless networks. The key design criterion is to adaptively select a subset from the available relays to satisfy a preset output threshold SNR. Specifically, in the proposed MRS, the first $L_c$ out of $L$ ($1 \leq L_c \leq L$) relays are sequentially selected such that the output SNR of the maximal ratio combined $L_c$ relayed-paths and the direct path exceeds a preset threshold. The practical viability of the proposed MRS is ascertained by deriving useful performance bounds, including the outage probability, the average symbol error rate (SER), and the average number of selected relays. Our numerical results reveal that the designed adaptive MRS schemes indeed provide more flexibility in utilizing bandwidth and spatial diversity in cooperative relay networks.

- Chapter 4 develops joint antenna and relay selection strategies for MIMO AF OWRNs and TWRNs. More specifically, a comprehensive performance analysis framework is first developed for the optimal transmit antenna selection (TAS) strategy for single-relay MIMO OWRNs, and thereby, the basic performance metrics of the optimal joint antenna and relay selection strategy are derived for multi-relay MIMO OWRNs. Furthermore, the optimal joint transmit/receive antenna and relay selection strategy is designed and analyzed for multi-relay MIMO TWRNs. The design merits are ascertained through deriving basic performance metrics in closed-form. To this end, the probability statistics of the end-to-end SNR are first derived and then used to quantify the outage probability and the average SER. Direct insights into practical system-design are obtained by quantifying the achievable diversity orders and array gains through the asymptotic analysis at high SNRs. Moreover, the amount of performance degradation due to practical transmission impairments such as feedback delays and spatially correlated fading is quantified.

Impact of channel prediction to circumvent outdated CSI for antenna selection due to feedback delay is also studied.

- Chapter 5 designs and analyzes two transmission strategies for MIMO AF MWRNs, namely (i) pairwise zero forcing (ZF) transmission and (ii) non-pairwise ZF transmission. Basic performance metrics such as the outage probability and the fundamental diversity-multiplexing trade-off are derived in closed-form by employing a mathematically tractable statistical characterization of the end-to-end SNR. Our analysis provides insights and guidelines for designing practically viable ZF transmission strategies for MIMO MWRNs. The proposed pairwise ZF transmission strategy possesses a lower practical implementation complexity as each source requires only the instantaneous respective source-to-relay channel knowledge. Contrary, the non-pairwise ZF transmission strategy achieves higher spatial multiplexing gains over the pairwise counterpart at the expense of higher relay processing complexity and more stringent CSI requirements.

$$\sim$$

# Chapter 2

# Performance Bounds for Multi-Hop Relay Networks

This chapter studies a performance analysis framework for multi-hop amplify-and-forward (AF) relay networks over Nakagami-$m$ fading. To this end, a new class of upper bounds on the end-to-end signal-to-noise ratio (SNR) of channel-assisted amplify-and-forward multi-hop ($N \geq 2$) relay networks is presented. It is the half-harmonic mean of the minimum of the first $P \geq 0$ hop SNRs and the minimum of the remaining $N - P$ hop SNRs. The parameter $P$ varies between $0$ to $N$ and may be chosen to provide the tightest bound. The cumulative distribution function, the probability density function, and the moment generating function are derived in closed-form for independent and identically distributed distributed Nakagami-$m$ fading, where $m$ is an integer. The resulting outage probability and the average symbol error rate bounds are asymptotically exact. The asymptotic-exactness holds for any $0 \leq P \leq N$ and consequently paves the way to devise a generalized asymptotic performance analysis at high SNRs. As applications, two applications of multi-hop multi-branch relay networks; (i) the best branch selection and (ii) maximal ratio combining reception are treated. Numerical results are provided to verify the comparative performance against the existing bounds.

The performance analysis framework devised in this chapter serves as a mathematical foundation for analyzing the performance of various wireless relay transmission strategies discussed in the remaining chapters of thesis.

## 2.1   Introduction

Multi-hop relay networks achieve broader coverage and enhanced throughput due to shorter hops and can also provide network connectivity to locations where traditional single-hop

networks may not reach [46]. As well, the battery life of the terminals may be prolonged due to lower power requirements [46]. Moreover, such networks also achieve spatial diversity gains to enhance the system performance. Due to these reasons, their performance has been widely researched [47–57].

Multi-hop relay networks can broadly be divided into two groups: (i) channel-assisted amplify-and-forward (CA-AF) and (ii) fixed-gain amplify-and-forward (FG-AF) [47, 51]. In CA-AF relaying, the amplification factors at the relays are designed to negate the effect of the channel fading. Such an amplification factor indeed depends on different channel realizations and hence is termed as variable-gain amplification as well. On the contrary, in FG-AF relaying, the relay amplification factors are either pre-assigned with constants or designed by employing only the average channel statistics of the fading channels. In general, the CA-AF relays significantly outperform the FG-AF relays in terms of important reliability metrics such as the outage probability and the average symbol error rate (SER). In this chapter, we therefore mainly focus on multi-hop CA-AF relay networks.

### 2.1.1 Prior related research

For a multi-hop CA-AF relay network, exact closed-form analytical performance results for a number of hops $N \geq 3$ appear to be intractable; even for $N = 2$ case, the exact analytical results are rather complicated. Thus, previous performance analyses provide bounds on the end-to-end SNR [47–50] or asymptotic approximations at high SNRs and numerical methods [52–54, 56, 58]. For example, in [47] the multi-hop SNR is upper bounded by the geometric mean of hop SNRs. The moment generating function (MGF), the cumulative distribution function (CDF), and the probability density function (PDF) of this upper bound are then derived. Closed-form lower bounds on the outage probability and the average bit error rate (BER) of the coherent binary modulation are also derived. In [48], the results of [47] is used to study the performance of multi-hop semi-blind relays over generalized fading channels. In [49], the bound of [48] is further employed for performance analysis of fully-connected multi-hop relay networks. Reference [50] proposes an SNR upper bound for a multi-hop CA-AF relay network by using the minimum SNR of all hops [50, Eqn. (11)]. The average BER of several modulation schemes over fading channels is also computed. Reference [59, Ch. 3, pp. 31-38] analyzes the performance of a multi-hop CA-AF relay network over Weibull fading by using the upper bound of [50].

Examples for approximations and/or numerical methods are [52–54, 58] and [56]. In [52], the outage probability of a multi-hop CA-AF relay network over Nakagami-$m$ fading

is evaluated. The MGF of the reciprocal of the SNR is derived in closed-form, and the outage probability is computed via numerical Laplace-transform inversion. A comprehensive performance analysis of a multiple-hop and multiple-branch cooperative network is proposed in [53]. The main idea is to relate the MGF of $X$ to the MGF of $1/X$, which requires numerical integration in some cases. Reference [58] provides an asymptotic analysis of the average error rates of multi-hop multi-branch relay networks. Moreover, the performance of multi-hop AF relays over independent and non-identically distributed (i.n.i.d) Rayleigh fading channels is studied in [54]. In [56], the asymptotic average BER of multi-hop CA-AF relaying over Nakagami-$m$ fading is analyzed.

### 2.1.2 Motivation and contribution

Although the performance bounds of multi-hop CA-AF relay networks presented in [47–49] are tight in low SNRs, they weaken for high SNR and for severe fading environments such as Rayleigh fading. These bounds may thus not provide an accurate assessment of system performance. Specifically, the important system-design parameters such as the diversity order and the coding gains derived by using the bounds of [47, 48] deviate significantly from their exact counterparts. Although the minimum-bound proposed in [50] is also an asymptotically exact bound, it is significantly loose in practical usable SNR regime, particularly, for less severe fading cases ($m > 4$) and for higher number of hops ($N > 4$). Thus, the usefulness of the minimum-bound in practice is limited as the asymptotically exactness is only achieved at significantly low average BER and outage probabilities ($10^{-8}$). Moreover, while the performance analyses of multi-hop CA-AF relay networks [52] and that of multi-hop multi-branch relay network [53] are available, the performance metrics are not in closed-forms. The aforementioned gaps in the performance analysis of multi-hop CA-AF relay networks, arising mainly due to the intractability of the problem, motivated us to develop new asymptotically exact performance bounds and approximations.

In this context, a class of new upper bounds is derived for the end-to-end SNR of a $N$-hop ($N \geq 2$) CA-AF relay network. The key idea is to bound the SNR by the half-harmonic mean of the minimum of the first $P$ hop SNRs and the minimum of the next $N-P$ hop SNR, where $0 \leq P \leq N$. Here, $P$ is a free parameter used to provide flexibility and generality. For example, the special cases $P = 0$ or $P = N$ result in the bounds of Hasna [50]. It may also be viewed as a tunable parameter to get the tightest bound. The CDF, PDF, and MGF of the proposed SNR bound are derived in closed-form. Closed-form lower bounds for the outage probability and the average SER are also derived. Notably, the proposed perfor-

19

mance bounds are asymptotically exact at high SNRs. Consequently, an unified asymptotic performance analysis framework at high SNRs is developed, and thereby, the asymptotic outage probability, asymptotic average SER, diversity order, and array gain are quantified. In particular, our analysis provides valuable insights and guidelines for practical usage, which are useful in system-design and link-budget calculation perspectives.

Numerical results are presented to compare the proposed performance bounds with the existing counterparts [47, 48, 50]. Monte Carlo simulation results are provided to verify the accuracy of our analytical results. Two applications of the proposed bounds, namely (i) best branch selection and (ii) maximal ratio combining reception for the multi-hop/multi-branch relay networks are presented to demonstrate the usefulness of our analysis.

**The chapter is organized as follows:** In Section 2.2, the system model, the channel model, and the proposed SNR bound are presented. Sections 2.3 provides a comprehensive statistical characterization of the proposed SNR bounds. In Section 2.4, the asymptotically exact performance bounds are derived by employing the proposed SNR bound. Section 2.6 presents the numerical results including performance comparisons of the proposed bounds. Section 2.7 concludes the Chapter 2, while proofs are provided in the Appendix A.

## 2.2   System and channel model

We consider a multi-hop relay network consisting of $N$ hops, a source $(S)$, a destination $(D)$ and $N-1$ AF relays $(R_n)$, where $n \in \{1, \cdots, N-1\}$ (see Fig. 2.1). Only single-antenna terminals are used. The relays are CA-AF type [12, 52, 60]. The gain of the CA-AF relay is given by [12, 52]

$$G_n = \sqrt{\frac{\mathcal{P}_n}{\mathcal{P}_n|h_n|^2 + N_{0,n}}} \quad \text{for} \ \ n \in \{1, \cdots, N-1\}, \tag{2.1}$$

where $\mathcal{P}_n$ is the average transmit power at the $n$th relay, $|h_n|$ is the fading amplitude of the $n$-th hop channel, and $N_{0,n}$ is the variance of the zero-mean additive white Gaussian noise at the input of the $n$th receiver. The end-to-end SNR of a multi-hop CA-AF relay network is denoted by $\gamma_{e2e}$ and is given by [52]

$$\gamma_{e2e} = \left[ \prod_{n=1}^{N} \left( 1 + \frac{1}{\gamma_n} \right) - 1 \right]^{-1}, \tag{2.2}$$

where $\gamma_n = \mathcal{P}_n|h_n|^2/N_{0,n}$ is the SNR of the $n$-th hop. Since the exact statistical characterization of $\gamma_{e2e}$ is mathematically intractable, reference [52] shows that $\gamma_{e2e}$ can be tightly
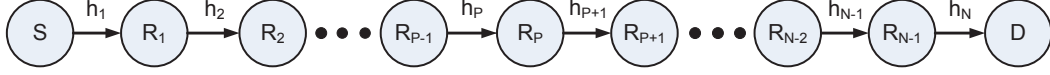
Figure 2.1: A multi-hop relay network.

upper bounded by a more tractable form as follows:

$$\gamma_{\text{e2e}} \leq \left[ \sum_{n=1}^{N} \frac{1}{\gamma_n} \right]^{-1}. \tag{2.3}$$

A quick observation of (2.3) reveals that the SNR upper bound in (2.3) indeed represents the end-to-end SNR pertinent to a multi-hop CA-AF relay network with relay amplification factors given by $G_n = 1/|h_n|$ for $n \in \{1, \cdots, N-1\}$. Intuitively, such relays are capable of inverting the fading channel of the previous hop regardless of its fading state [52] and hence are termed as ideal CA-AF relays. Thus, (2.3) corresponds to the end-to-end SNR of a multi-hop relay network with ideal CA-AF relays, and consequently, the end-to-end SNR of interest is denoted as

$$\gamma_{\text{e2e, ideal}} = \left[ \sum_{n=1}^{N} \frac{1}{\gamma_n} \right]^{-1}. \tag{2.4}$$

The performance measures of multi-hop relay networks with ideal CA-AF relays, in particular, serve as benchmarks for systems with various practical relays.
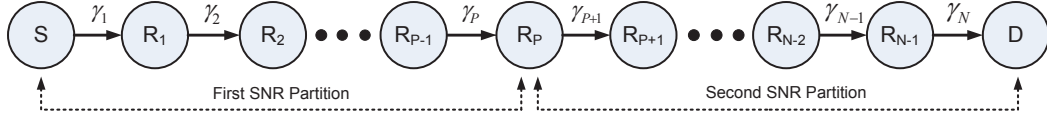


Figure 2.2: The SNR partitioning of the proposed bound.

In order to analyze the system performance, probability statistics of the end-to-end SNR in (2.4) are required. However, the probability distribution of (2.4) is not mathematically tractable, in particular, for $N \geq 3$. Thus, in order to develop a more tractable yet accurate performance analysis framework, we propose a new upper bound for (2.4). The key idea is to partition the set of $\gamma_n$ for $n \in \{1, \cdots, N\}$ into two groups as depicted in Fig. 2.2. The minimum of $\gamma_n$ of each group is then used to bound (2.4) as follows:

$$\gamma_{\text{e2e,ideal}} \leq \gamma_{\text{e2e}}^{\text{ub}} = \left[ \frac{1}{\min\limits_{n \in \{1, \cdots, P\}} (\gamma_n)} + \frac{1}{\min\limits_{n \in \{P+1, \cdots, N\}} (\gamma_n)} \right]^{-1}, \tag{2.5}$$

where $P \in \{1, \cdots, N\}$ is a tunable parameter, which can be used to obtain the tightest bound. The SNR bound $\gamma_{\text{e2e}}^{\text{ub}}$ in (2.5) is indeed the half-harmonic mean of the minimum

21

SNR of the first $P$ hops and the minimum SNR of the next $N - P$ hops. Intuitively, we expect the tightness of the bound to increase as $P$ gets closer to $N - P$. Thus, $P = \lceil \frac{N}{2} \rceil$ is a good choice.

Interestingly, when $P = 0$ or $P = N$, (2.5) reduces to the bound given by Hasna [50, Eqn. (11)]. Note that (2.5) with $N = 2$ and $P = 1$ reduces to the exact end-to-end SNR of the dual-hop relay network with ideal CA-AF relays.

## 2.3 Statistical characterization of the SNR

A comprehensive statistical characterization of the end-to-end SNR bound is indispensable for evaluating the performance metrics in closed-form. To this end, in this section, the CDF, PDF, and MGF of the proposed SNR upper bound are derived in closed-form for independent and identically distributed (i.i.d.) Nakagami-$m$ fading and i.n.i.d Rayleigh fading channels.

Specifically, the CDF, PDF, and MGF of $\gamma_{\text{e2e}}^{\text{ub}}$ in i.i.d. Nakagami-$m$ fading are given by Theorem 2.1.

**Theorem 2.1** *Let $\gamma_n \sim \mathcal{G}(m, \frac{\bar{\gamma}}{m})$ for $n \in \{1, \cdots, N\}$ be independent hop SNRs. The CDF of $\gamma_{\text{e2e}}^{ub}$ is then given by*

$$
\begin{aligned}
F_{\gamma_{\text{e2e}}^{\text{ub}}}(x) &= 1 - \sum_{j=0}^{P(m-1)} \sum_{k=0}^{(N-P-1)(m-1)} \sum_{l=0}^{m+j+k-1} \frac{2}{\Gamma(m)} \binom{m+j+k-1}{l} \\
&\times \frac{\beta_{j,P} \beta_{k,N-P-1} P^{\frac{l-j+1}{2}}}{(N-P)^{\frac{l-j-1}{2}}} \left(\frac{mx}{\bar{\gamma}}\right)^{m+j+k} \exp\left(-\frac{mNx}{\bar{\gamma}}\right) \\
&\times \mathcal{K}_{l-j+1}\left(\frac{2m}{\bar{\gamma}} \sqrt{P(N-P)}\, x\right),
\end{aligned}
\tag{2.6a}
$$

*where*

$$
\beta_{k,N} = \sum_{i=k-m+1}^{k} \frac{\beta_{i,N-1}}{(k-i)!} I_{[0,(N-1)(m-1)]}(i),
\tag{2.6b}
$$

$$
I_{[a,c]}(b) = \begin{cases} 1, & a \le b \le c \\ 0, & \text{otherwise,} \end{cases}
\tag{2.6c}
$$

$$
\tag{2.6d}
$$

$$
\beta_{0,0} = \beta_{0,N} = 1, \beta_{k,1} = 1/\,k!, \text{ and } \beta_{1,N} = N.
\tag{2.6e}
$$

*The PDF of $\gamma_{eq}^{ub}$ is given by*

$$
f_{\gamma_{e2e}^{ub}}(x) = \sum_{i=0}^{3} \sum_{k=0}^{(P-1)(m-1)} \sum_{l=0}^{(N-P-1)(m-1)} \sum_{j=0}^{2m+k+l-2} \frac{2\alpha_i(x)}{(\Gamma(m))^2} \binom{2m+k+l-2}{j}
$$

$$
\times \quad \frac{\beta_{k,P-1}\beta_{l,N-P-1}P^{\frac{j-k-m+4}{2}}}{(N-P)^{\frac{j-m-k}{2}}} \left(\frac{m}{\bar{\gamma}}\right)^{2m+k+l} x^{2m+k+l+j-2}
$$

$$
\times \quad \exp\left(-\frac{mNx}{\bar{\gamma}}\right) \mathcal{K}_{j-k-m+2}\left(\frac{2m}{\bar{\gamma}}\sqrt{P(N-P)}\,x\right), \tag{2.7}
$$

*where $\alpha_1(x) = 1$, $\alpha_2(x) = 2x$, and $\alpha_3(x) = x^2$.*

*The MGF of $\gamma_{eq}^{ub}$ is given by*

$$
\mathcal{M}_{\gamma_{e2e}^{ub}}(s) = 1 - \sum_{j=0}^{P(m-1)} \sum_{k=0}^{(N-P-1)(m-1)} \sum_{l=0}^{m+j+k-1} \frac{2}{\Gamma(m)} \binom{m+j+k-1}{l}
$$

$$
\times \quad \frac{\beta_{j,P}\beta_{k,N-P-1}P^{\frac{l-j+1}{2}}}{(N-P)^{\frac{l-j-1}{2}}} \left(\frac{m}{\bar{\gamma}}\right)^{m+j+k} s\,\mathbb{I}(\mu,\nu,\alpha,\beta), \tag{2.8a}
$$

*where*

$$
\mathbb{I}(\mu,\nu,\alpha,\beta) = \frac{\sqrt{\pi}(2\beta)^\nu\Gamma(\mu+\nu)\Gamma(\mu-\nu)}{\Gamma(\mu+\frac{1}{2})(\alpha+\beta)^{\mu+\nu}} \, {}_2\mathcal{F}_1\left(\mu+\nu,\nu+\frac{1}{2};\mu+\frac{1}{2};\frac{\alpha-\beta}{\alpha+\beta}\right), \tag{2.8b}
$$

$$
\alpha = s + \frac{mN}{\bar{\gamma}}, \beta = \frac{2m}{\bar{\gamma}}\sqrt{P(N-P)}, \tag{2.8c}
$$

$$
\mu = m+j+k+1, \quad and \quad \nu = l-j+1. \tag{2.8d}
$$

**Proof**: See Section A.1 in Appendix A. ∎

**Remark 2.3.1:** The CDF (2.6a), the PDF (2.7), and the MGF (2.8a) do not hold valid for $P = 0$ or $P = N$. Thus, the CDF of $\gamma_{eq}^{ub}$ pertinent to $P = 0$ or $P = N$ is derived explicitly as follows:

$$
F_{\gamma_{e2e}^{ub}}(x) = 1 - \exp\left(-\frac{mNx}{\bar{\gamma}}\right) \sum_{k=0}^{N(m-1)} \beta_{k,N}\left(\frac{mx}{\bar{\gamma}}\right)^k. \tag{2.9}
$$

Similarly, the PDF of $\gamma_{eq}^{ub}$ pertaining to $P = 0$ or $P = N$ is given by

$$
f_{\gamma_{e2e}^{ub}}(x) = \frac{N}{\Gamma(m)}\exp\left(-\frac{mNx}{\bar{\gamma}}\right) \sum_{k=0}^{(N-1)(m-1)} \beta_{k,N-1}\left(\frac{m}{\bar{\gamma}}\right)^{m+k} x^{m+k-1}. \tag{2.10}
$$

The corresponding MGF of $\gamma_{eq}^{ub}$ for $P = 0$ or $P = N$ is then derived as

$$
\mathcal{M}_{\gamma_{e2e}^{ub}}(s) = 1 - \sum_{k=0}^{N(m-1)} \frac{\beta_{k,N}\Gamma(k+1)\bar{\gamma}s}{m}\left(\frac{m}{mN+\bar{\gamma}s}\right)^{k+1}. \tag{2.11}
$$

Furthermore, for the sake of completeness, the CDF, PDF, and MGF of $\gamma_{\text{eq}}^{\text{ub}}$ for i.n.i.d Rayleigh fading case are given as follows: Specifically, the CDF of $\gamma_{\text{e2e}}^{\text{ub}}$ is given by

$$F_{\gamma_{\text{e2e}}^{\text{ub}}}(x) = 1 - 2\sqrt{\lambda_1\lambda_2}\, x \exp\left(-\lambda_0 x\right) \mathcal{K}_1\left(2x\sqrt{\lambda_1\lambda_2}\right), \tag{2.12}$$

where $\lambda_1 = \sum_{n=1}^{N-P} \dfrac{1}{\bar{\gamma}_n}$, $\lambda_2 = \sum_{n=N-P+1}^{N} \dfrac{1}{\bar{\gamma}_n}$ and $\lambda_0 = \lambda_1 + \lambda_2$.

The PDF of $\gamma_{\text{e2e}}^{\text{ub}}$ for i.n.i.d Rayleigh fading is then given by

$$f_{\gamma_{\text{e2e}}^{\text{ub}}}(x) = 2\exp(-\lambda_0 x) \sum_{i=1}^{3} \alpha_i(x)\lambda_1^{\frac{4-i}{2}} \lambda_2^{\frac{i}{2}} x^{2-i} \mathcal{K}_{2-i}\left(2x\sqrt{\lambda_1\lambda_2}\right), \tag{2.13}$$

where $\alpha_1(x) = 1$, $\alpha_2(x) = 2x$, and $\alpha_3(x) = x^2$.

The MGF of $\gamma_{\text{e2e}}^{\text{ub}}$ for i.n.i.d Rayleigh fading is next given by

$$\mathcal{M}_{\gamma_{\text{e2e}}^{\text{ub}}}(x) = 1 - \frac{64}{3}\lambda_1\lambda_2 s \frac{{}_2\mathcal{F}_1\left(3, \frac{3}{2}; \frac{5}{2}; \dfrac{s+\lambda_0-2\sqrt{\lambda_1\lambda_2}}{s+\lambda_0+2\sqrt{\lambda_1\lambda_2}}\right)}{\left(s+\lambda_0+2\sqrt{\lambda_1\lambda_2}\right)^3}. \tag{2.14}$$

The asymptotic analysis of performance metrics in high SNR regime reveals important insights into the system-designing parameters such as the achievable diversity order and the coding gain. The behavior of the CDF or PDF in high SNR regime is equivalent to the behavior of the corresponding statistic around the origin [61]. The first order expansions of the SNR statistics are therefore employed in deriving the asymptotic performance metrics [61]. To this end, generalized first order expansions of the CDF, PDF and MGF of $\gamma_{\text{e2e}}^{\text{ub}}$ (2.5) are given in Theorem 2.2.

**Theorem 2.2** *Let $\gamma_n$, $n \in \{1, \cdots, N\}$ be independent hop SNRs. Suppose that the PDF of $\gamma_n$ can be expanded in a MacLaurin series as $f_{\gamma_n}(x) = \frac{\beta_n}{(C_n\bar{\gamma})^{d_n}} x^{d_n-1} + o\left(x^{d_n-1}\right)$, where $\beta_n$, $C_n$, $d_n$, and $\bar{\gamma}$ are positive constants. The MacLaurin series expansion of the CDF of $\gamma_{\text{e2e}}^{ub}$ is then given by*

$$F_{\gamma_{\text{e2e}}^{\text{ub}}}(x) = \sum_n \left[\frac{\beta_n}{(C_n)^{d_n} d_n}\right] \left(\frac{x}{\bar{\gamma}}\right)^{d_{\min}} + o\left(x^{d_{\min}}\right), \tag{2.15}$$

*where $n \in \{n | d_n = \min(d_1, d_2, \cdots, d_N)\}$ and $d_{\min} = \min\limits_{n\in\{1,\cdots,N\}}(d_n)$.*

The MacLaurin series expansion of the PDF of $\gamma_{\text{e2e}}^{\text{ub}}$ is next given by

$$f_{\gamma_{\text{e2e}}^{\text{ub}}}(x) = \frac{d_{\min}}{(\bar{\gamma})^{d_{\min}}} \sum_n \left[\frac{\beta_n}{(C_n)^{d_n} d_n}\right] x^{d_{\min}-1} + o\left(x^{d_{\min}-1}\right), \tag{2.16}$$

where $n \in \{n | d_n = \min(d_1, d_2, \cdots, d_N)\}$ and $d_{\min} = \min\limits_{n\in\{1,\cdots,N\}}(d_n)$.

The single-term polynomial approximation of the MGF of $\gamma_{\text{e2e}}^{\text{ub}}$ is given by

$$\mathcal{M}_{\gamma_{\text{e2e}}^{\text{ub}}}(s) = \frac{\Gamma(d_{\min})}{(\bar{\gamma})^{d_{\min}}} \sum_n \left[ \frac{\beta_n}{(C_n)^{d_n} d_n} \right] s^{-d_{\min}} + o\left( s^{-d_{\min}} \right), \qquad (2.17)$$

where $n \in \{n | d_n = \min(d_1, d_2, \cdots, d_N)\}$ and $d_{\min} = \min_{n \in \{1, \cdots, N\}} (d_n)$.

**Proof**: See Section A.2 in Appendix A. ∎

**Remark: 2.3.1:** The first order expansions of the CDF, PDF, and MGF of $\gamma_{\text{e2e}}^{\text{ub}}$ presented in the Theorem 2.2 are indeed valid for any type of fading channel models, and hence, they are not just limited to Rayleigh and Nakagami-$m$ fading channels.

## 2.4 Performance analysis

This section presents the performance analysis of multi-hop CA-AF relay networks by employing the proposed SNR bound in (2.5). To this end, the probability distributions of $\gamma_{\text{e2e}}^{\text{ub}}$ provided in Section 2.3 are used to derive the outage probability and the average SER.

### 2.4.1 Outage probability

The outage is the probability that the instantaneous end-to-end SNR falls below a present threshold SNR, $\gamma_{th}$. The lower bounds for the outage probability $P_{out}$ for i.n.i.d Rayleigh and i.i.d. Nakagami-$m$ fading cases can readily be derived by using the CDF results given in (2.12) and (2.6a) as follows:

$$P_{out}^{\text{lb}} = \Pr(\gamma_{\text{e2e}}^{\text{ub}} \leq \gamma_{th}) = F_{\gamma_{\text{e2e}}^{\text{ub}}}(\gamma_{th}). \qquad (2.18)$$

The outage probability lower bound derived by employing our proposed SNR upper bound is asymptotically exact. In order to exploit this asymptotic exactness to obtain direct insights on the achievable diversity order, the asymptotic outage probability at high SNRs is presented in the Corollary 2.1.

**Corollary 2.1** *Let $\gamma_n \sim \mathcal{G}(m, \frac{\bar{\gamma}}{m})$ for $n \in \{1, \cdots, N\}$ be independent hop SNRs. The asymptotic outage probability in high SNR regime derived by using the proposed SNR upper bound is then given by*

$$P_{\text{out}}^{\infty} = \frac{Nm^m}{\Gamma(m+1)} \left( \frac{\gamma_{th}}{\bar{\gamma}} \right)^m + o\left( \bar{\gamma}^{-m} \right), \qquad (2.19)$$

*where $P_{out}^{\infty}$ denotes the asymptotic outage probability as $\bar{\gamma} \to \infty$.*

**Proof**: Proof is a direct application of the Theorem 2.2. ∎

The asymptotic outage probability in high SNR regime for i.n.i.d Rayleigh fading can also be given as a special case of the Corollary 2.1 as

$$P_{\text{out}}^{\infty} = \left( \sum_{n=1}^{N} \frac{1}{C_n} \right) \frac{\gamma_{th}}{\bar{\gamma}} + o\left( \bar{\gamma}^{-1} \right), \tag{2.20}$$

where $C_n = \bar{\gamma}_n / \bar{\gamma}$ for $n \in \{1, \cdots, N\}$.

As our SNR bounds are asymptotically exact in high SNR regime, $P_{\text{out}}^{\infty}$ in (2.19) provides the exact asymptotic outage probability at high SNR for multi-hop CA-AF relay networks. Our Asymptotic outage analysis also reveals that the diversity orders of multi-hop relay networks over i.i.d. Nakagami-$m$ fading and i.n.i.d Rayleigh fading are $m$ and unity, respectively.

### 2.4.2 Average error rate

The average SER is one of the most widely used performance metrics for digital communication systems. The conditional error probability (CEP), $P_e|\gamma$, in this case is averaged over the PDF of $\gamma_{\text{e2e}}$. For example, the CEP of coherent binary phase shift keying (BPSK) and $M$-ary pulse amplitude modulation (PAM) can be expressed as $P_e|\gamma = a\mathcal{Q}\left(\sqrt{b\gamma}\right)$, where $a$ and $b$ are modulation-dependent constants. For example, $(a = 1, b = 2)$ and $(a = 1, b = 1)$ provide the exact CEP of the coherent BPSK and coherent binary frequency shift keying (BFSK), respectively [32].

The average SER can be simplified by integrating by parts as follows [62]:

$$\begin{aligned} \bar{P}_e &= \mathcal{E}_{\gamma_{\text{e2e}}}\left\{ a\mathcal{Q}\left(\sqrt{b\gamma_{\text{e2e}}}\right) \right\} \\ &= \frac{a}{2} - \frac{a}{2}\sqrt{\frac{b}{2\pi}} \int_0^{\infty} x^{-\frac{1}{2}} \exp\left(-\frac{bx}{2}\right) \bar{F}_{\gamma_{\text{e2e}}^{\text{ub}}}(x)\,\mathrm{d}x, \end{aligned} \tag{2.21}$$

where $\bar{F}_{\gamma_{\text{e2e}}^{\text{ub}}}(x)$ denotes the complimentary cumulative distribution function (CCDF) of $\gamma_{\text{e2e}}^{\text{ub}}$ defined as $\bar{F}_{\gamma_{\text{e2e}}^{\text{ub}}}(x) = 1 - F_{\gamma_{\text{e2e}}^{\text{ub}}}(x)$. The average SER bound for i.i.d. Nakagami-$m$ fading is then given by Corollary 2.2.

**Corollary 2.2** *Let $\gamma_n \sim \mathcal{G}(m, \frac{\bar{\gamma}}{m})$ for $n \in \{1, \cdots, N\}$ be independent hop SNRs. The average SER lower bound obtained by using $\gamma_{\text{e2e}}^{\text{ub}}$ is then given by*

$$\begin{aligned} \bar{P}_e^{\text{lb}} &= \frac{a}{2} - a\sqrt{\frac{b}{2\pi}} \sum_{j=0}^{P(m-1)} \sum_{k=0}^{(N-P-1)(m-1)} \sum_{l=0}^{m+j+k-1} \frac{1}{\Gamma(m)} \binom{m+j+k-1}{l} \\ &\quad \times \beta_{j,P}\beta_{k,N-P-1} \frac{P^{\frac{l-j+1}{2}}}{(N-P)^{\frac{l-j-1}{2}}} \left(\frac{m}{\bar{\gamma}}\right)^{m+j+k} \mathbb{I}(\mu, \nu, \alpha, \beta), \end{aligned} \tag{2.22}$$

26

where $\mu = m + j + k + \frac{1}{2}$, $\nu = l - j + 1$, $\alpha = \frac{b}{2} + \frac{mN}{\bar{\gamma}}$, $\beta = \frac{2m}{\bar{\gamma}}\sqrt{P(N-P)}$, and $\mathbb{I}(\mu, \nu, \alpha, \beta)$ is already defined in (2.8a).

**Proof**: The average SER in (2.22) can be derived by substituting (2.6a) into the integral representation of $\bar{P}_e$ in (2.21) and solving the residue integral by using [1, Eqn. (6.621.3)]. ∎

**Remark: 2.4.1:** The average SER lower bound in i.i.d. Nakagami-$m$ fading (2.22) does not hold valid for $P = 0$ or $P = N$ and hence is derived explicitly as follows:

$$\bar{P}_e^{\text{lb}} = \frac{a}{2} - \frac{a}{2}\sqrt{\frac{b}{2\pi}} \sum_{k=0}^{N(m-1)} \beta_{k,N} \Gamma\left(k+\frac{1}{2}\right)\left(\frac{m}{\bar{\gamma}}\right)^k \left(\frac{2\bar{\gamma}}{b\bar{\gamma}+2mN}\right)^{k+\frac{1}{2}}. \tag{2.23}$$

This average SER (2.23) can be derived by first substituting the CCDF of SNR (2.9) into (2.21) and then solving the resulting integral by using [1, Eqn. (8.310.1)].

For the sake of completeness, the average SER lower bound for i.n.i.d Rayleigh fading is also derived as follows:

$$\bar{P}_e^{\text{lb}} = \frac{a}{2} - 3a\pi\lambda_1\lambda_2\sqrt{\frac{b}{2}} \frac{{}_2\mathcal{F}_1\left(\frac{5}{2}, \frac{3}{2}; 2; \frac{\frac{b}{2}+\lambda_0-2\sqrt{\lambda_1\lambda_2}}{\frac{b}{2}+\lambda_0+2\sqrt{\lambda_1\lambda_2}}\right)}{\left(\frac{b}{2}+\lambda_0+2\sqrt{\lambda_1\lambda_2}\right)^{\frac{5}{2}}}. \tag{2.24}$$

The lower bound for the average SER obtained by using our proposed SNR upper bound is asymptotically exact. To prove this claim, we provide the Corollary 2.3.

**Corollary 2.3**  *Let $\gamma_n \sim \mathcal{G}(1, \bar{\gamma}_n)$ for $n \in \{1, \cdots, N\}$ be independent hop SNRs. The asymptotic average SER obtained by using $\gamma_{e2e}^{ub}$ as $\bar{\gamma}_n \to \infty$ is then given by*

$$\bar{P}_e^\infty = \frac{a}{2b} \sum_{n=1}^{N} \frac{1}{C_n \bar{\gamma}} + o\left(\bar{\gamma}^{-1}\right). \tag{2.25}$$

**Proof**: The value at the origin of the PDF of the random variable $\Gamma = \frac{1}{\Gamma_1} + \frac{1}{\Gamma_2}$ can be express by [58, Eqn. (16)]: $f_\Gamma(0) = f_{\Gamma_1}(0) + f_{\Gamma_2}(0)$. The PDF of $\Gamma_1$ and $\Gamma_2$ for i.n.i.d Rayleigh fading case are given by

$$f_{\Gamma_1}(x) = \left(\sum_{n=1}^{P} \frac{1}{\bar{\gamma}_n}\right) \exp\left(-\sum_{n=1}^{N-P} \frac{x}{\bar{\gamma}_n}\right), \quad \text{and} \tag{2.26a}$$

$$f_{\Gamma_2}(x) = \left(\sum_{n=P+1}^{N} \frac{1}{\bar{\gamma}_n}\right) \exp\left(-\sum_{n=N-P+1}^{N} \frac{x}{\bar{\gamma}_n}\right), \tag{2.26b}$$

respectively. Thus, $f_\Gamma(0)$ can readily be obtained as $f_\Gamma(0) = \sum_{n=1}^{N} \frac{1}{\bar{\gamma}_n}$. The asymptotic average SER (2.25) can then be derived by using [58, Eqn. (10)]. ∎

27
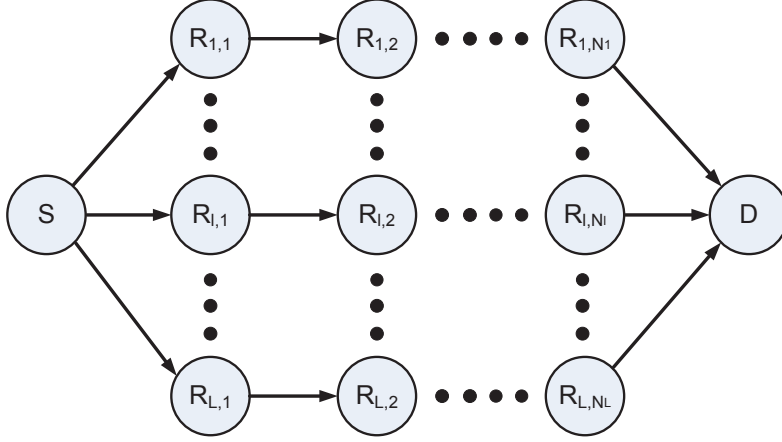
Figure 2.3: A multi-hop multi-branch relay network.

It is worth noticing that (2.25) exactly agrees with the asymptotic exact average SER for multi-hop CA-AF relay networks [58, Eqn. (39)]. Numerical results in Section 2.6 too confirm this asymptotic exactness. The corresponding asymptotic average SER for i.i.d. Nakagami-$m$ fading can be derived by using the Theorem 2.2 as follows:

$$\bar{P}_e^\infty = \frac{aNm^m 2^{m-1}\Gamma(m+\frac{1}{2})}{\sqrt{\pi}(b\bar{\gamma})^m} + o(\bar{\gamma}^{-m}). \tag{2.27}$$

## 2.5 Applications of bounds

The SNR bounds and the corresponding performance bounds proposed for single-branch multi-hop relay networks can readily be employed for accurately accessing the performance of other relaying set-ups. The asymptotic exactness of our bounds, in particular, highlights their practical applicability for wide-range of applications. In this context, this section presents two such applications to further elaborate the usefulness of our proposed bounds.

### 2.5.1 Outage probability of multi-hop multi-branch relay networks with the best branch selection

We consider a multi-hop multi-branch relay network consists of $L$ branches each having $N_l$ hops for $l \in \{1, \cdots, L\}$ (Fig. 2.3). In this set-up, the source-to-destination communication is facilitated by $N_R = \sum_{l=1}^{L} N_l$ ideal CA-AF relays. In this context, we consider the best branch selection, where the destination selects the best branch with multiple hops having the largest instantaneous received SNR. Our proposed upper bound of the end-to-end SNR (2.5) is then employed to obtain an upper bound for the equivalent SNR as $\gamma_{\text{SC}} \leq \gamma_{\text{SC}}^{\text{ub}} = \max\left(\gamma_{\text{e2e},1}^{\text{ub}}, \gamma_{\text{e2e},2}^{\text{ub}}, ..., \gamma_{\text{e2e},L}^{\text{ub}}\right)$, where $\gamma_{\text{e2e},l}^{\text{ub}}$ for $l \in \{1, \cdots, L\}$ is the SNR of $l$-th multi-hop

branch given in (2.5) with $N$ replaced by $N_l$. For independently faded multiple branches, the CDF of $\gamma_{\text{SC}}^{\text{ub}}$ can be derived as

$$F_{\gamma_{\text{SC}}^{\text{ub}}}(x) = \prod_{l=1}^{L} F_{\gamma_{\text{e2e},l}^{\text{ub}}}(x), \qquad (2.28)$$

where $F_{\gamma_{\text{e2e},l}^{\text{ub}}}(x)$ for $l \in \{1, \cdots, L\}$ is the CDF of $\gamma_{\text{e2e},l}^{\text{ub}}$ and can readily be obtained by using (2.6a) and (2.12) for i.i.d. Nakagami-$m$ and i.n.i.d Rayleigh fading, respectively.

In order to obtain direct insights, the asymptotic outage probability at high SNRs for multi-hop multi-branch CA-AF relay networks with best branch selection can be derived by using the Theorem 2.2 as follows:

$$P_{\text{out,SC}}^{\infty} = \prod_{l=1}^{L} \left[ \frac{N_l m_l^{m_l}}{\Gamma(m_l + 1)C_l^{m_l}} \right] \left( \frac{\gamma_{th}}{\bar{\gamma}} \right)^{\sum_{l=1}^{L} m_l} + o\left( \bar{\gamma}^{-\sum_{l=1}^{L} m_l} \right), \qquad (2.29)$$

where $m_l$ for $l = \in \{1, \cdots, L\}$ denotes the severity of fading pertinent to the $l$th branch and $C_l = \bar{\gamma}_l/\bar{\gamma}$. The high SNR outage analysis clearly reveals that the achievable diversity order by the best branch selection over Nakagami-$m$ fading is given by $G_d^{SC} = \sum_{l=1}^{L} m_l$.

### 2.5.2 Average SER of multi-hop multi-branch relay networks with MRC Reception

We consider the same network set-up in Section 2.5.1 (Fig. 2.3), however, in this case, the destination combines the signals received via all branches by using maximal ratio combining (MRC). To this end, an upper bound for the output SNR, $\gamma_{\text{MRC}}$, is derived as follows:

$$\gamma_{\text{MRC}} = \sum_{l=1}^{L} \gamma_{\text{e2e},l} \le \gamma_{\text{MRC}}^{\text{ub}} = \sum_{l=1}^{L} \gamma_{\text{e2e},l}^{\text{ub}}. \qquad (2.30)$$

For independent signals received via multiple branches at the destination, the MGF of $\gamma_{\text{MRC}}^{\text{ub}}$ can be expressed as [63]

$$\mathcal{M}_{\gamma_{\text{MRC}}^{\text{ub}}}(s) = \prod_{l=1}^{L} M_{\gamma_{\text{e2e},l}^{\text{ub}}}(s), \qquad (2.31)$$

where $\mathcal{M}_{\gamma_{\text{eq},l}^{\text{ub}}}(s)$ for $l \in \{1, \cdots, L\}$ is the MGF of the SNR upper bound of $l$-th branch and can readily be derived by employing (2.8a) and (2.14) for Nakagami-$m$ and Rayleigh fading, respectively.

An accurate and computationally efficient average SER bound can then be derived for multi-hop multi-branch CA-AF relay networks with MRC reception at the destination as

follows: The CEP of coherent BFSK and $M$-ary PAM can be expressed in an alternative form as [64]:

$$P_e|\gamma = a\mathcal{Q}(\sqrt{b\gamma}) = \frac{a}{\pi}\sqrt{\frac{b}{2}}\int_0^\infty \frac{\exp(-\gamma(s^2+b/2))}{s^2+b/2}ds.$$ (2.32)

By first using the variable transformation $s^2+b/2 = b/(\gamma+1)$, and then by averaging (2.32) over the PDF of $\gamma$, an alternative average SER expression can be derived as follows [64]:

$$\bar{P}_e = \frac{a}{\pi}\sqrt{\frac{b}{2}}\int_0^\infty \frac{\mathcal{M}_{\gamma_{\mathrm{MRC}}}(s^2+b/2)}{s^2+b/2}ds = \frac{a}{2\pi}\int_{-1}^1 \frac{\mathcal{M}_{\gamma_{\mathrm{MRC}}}(b/(\gamma+1))}{\sqrt{1-\gamma^2}}d\gamma.$$ (2.33)

By first substituting the MGF of $\gamma_{\mathrm{e2e}}^{\mathrm{ub}}$ (2.8a) into (2.31), the MGF of $\gamma_{\mathrm{MRC}}$ can be derived in closed-form. Then, by substituting $\mathcal{M}_{\gamma_{\mathrm{MRC}}}(s)$ into (2.33), a compact and accurate lower bound for the average SER can be then derived by using the Chebyshev-Gauss quadrature rule [2] as

$$\bar{P}_{e,\mathrm{MRC}}^{\mathrm{lb}} = \frac{a}{2N_p}\sum_{j=1}^{N_p} M_{\gamma_{\mathrm{MRC}}^{\mathrm{ub}}}\left(\frac{b}{2}\sec^2(\theta_j)\right) + R_{N_p},$$ (2.34)

where $N_p$ is a small positive integer, $\theta_j = \frac{(2j-1)\pi}{4N_p}$ and $R_{N_p}$ is the remainder term, which becomes negligible as $N_p$ increases, even for small values such as 10 (see Section 2.6).

Again, the asymptotic average SER is derived to obtain direct insights into the achievable diversity order of multi-branch and multi-hop CA-AF relay networks with MRC reception by using the Theorem 2.2 as follows:

$$\bar{P}_{e,\mathrm{MRC}}^\infty = \frac{ab^{-\left(\sum_{l=1}^L m_l\right)}2^{\left(\sum_{l=1}^L m_l-1\right)}\Gamma\left(\sum_{l=1}^L m_l+\frac{1}{2}\right)}{\sqrt{\pi}\Gamma\left(\sum_{l=1}^L m_l+1\right)\bar{\gamma}^{\left(\sum_{l=1}^L m_l\right)}}$$
$$\times \prod_{l=1}^L\left[\frac{N_l m_1^{m_l}}{C_l^{m_l}}\right] + o\left(\bar{\gamma}^{\left(-\sum_{l=1}^L m_l\right)}\right),$$ (2.35)

where $m_l$ for $l \in \{1, \cdots, L\}$ is the severity of fading corresponding to the $l$th branch and $C_l = \bar{\gamma}_l/\bar{\gamma}$. Again, the high SNR average SER analysis clearly reveals that the achievable diversity order of multi-branch and multi-hop relay networks with MRC reception over Nakagami-$m$ fading is given by $G_d^{\mathrm{MRC}} = \sum_{l=1}^L m_l$.

**Remark 1.5.1:** The proposed bounding technique can be used for analyzing the performance of various other multi-hop relay applications. For example, in [65], the proposed SNR bounds are employed to study the multi-antenna multi-hop relay networks with beamforming. Moreover, the proposed outage probability and average SER bounds can be used for accurate optimal power and resource allocation purposes.
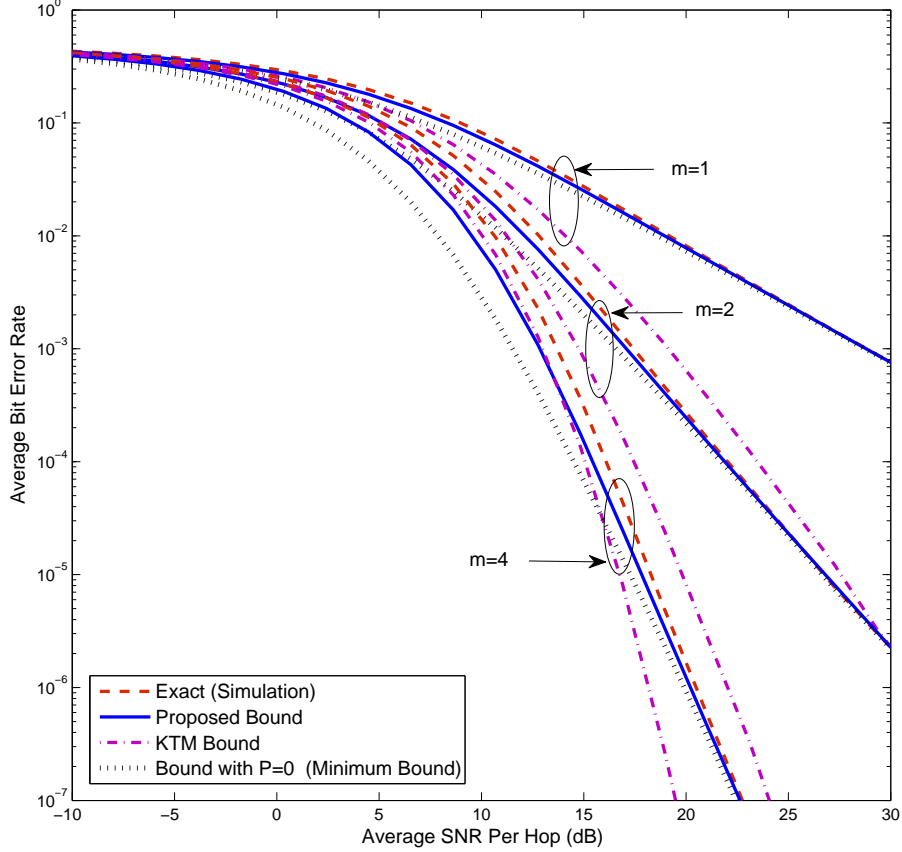
Figure 2.4: The effect of severity of fading on the average BER bounds for a multi-hop relay network in i.i.d. Nakagami-$m$ fading. Here, $N = 3$ and $P = 2$.

## 2.6 Numerical Results

In this section, numerical and simulation results are provided to investigate the tightness of the proposed performance bounds. Accordingly, they are compared with the existing multi-hop performance bounds [47, 50, 59] and exact simulations.

In Fig. 2.4, the proposed lower bounds of BPSK average BER (by letting $a = 1$ and $b = 2$ in (2.22)) are plotted for a three-hop relay network operating over i.i.d. Nakagami-$m$ fading. The BPSK average BER bound of [47, Eqn. (24)] is also plotted for comparison purposes. This bound is named the "KTM". Moreover, the proposed average BER bound with $P = 0$, which simplifies to the bound in [50, Eqn. (11)] and [59, Ch. 3] ("Minimum bound"), is plotted as well for comparison purpose. As expected, the proposed bound is tight, particularly, in medium-to-high SNR regime compared to KTM and Minimum bound. Specifically, our bound converges to the exact average BER curve for high SNRs.
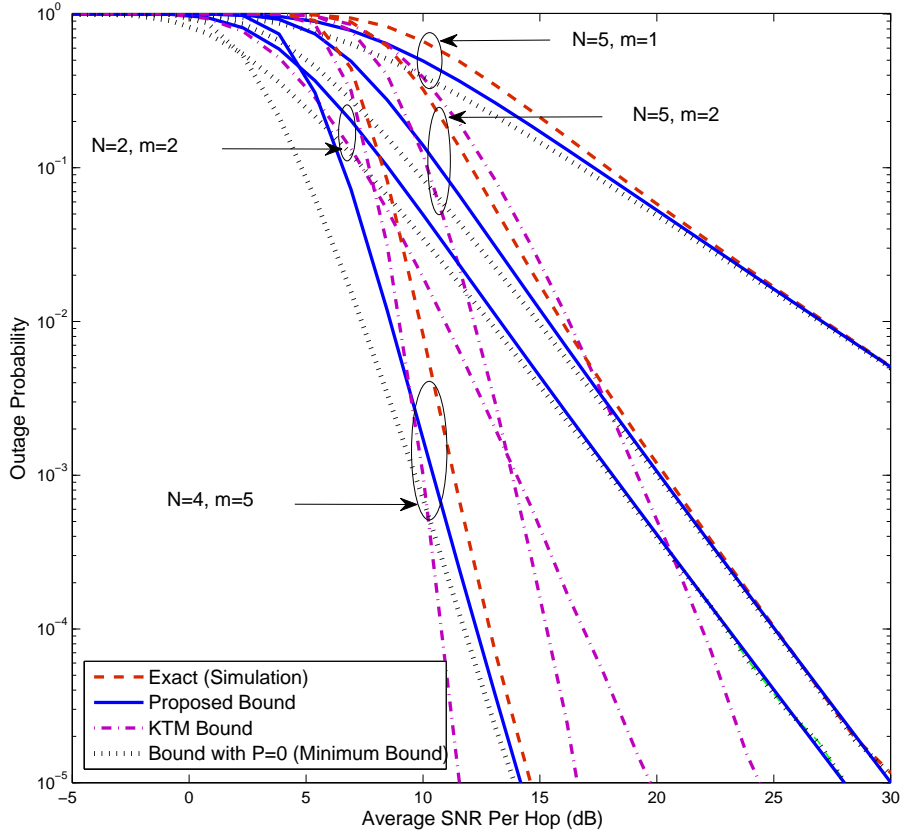
Figure 2.5: A comparison of outage probability bounds of multi-hop relay network over i.i.d. Nakagami-$m$ fading channels. Here, $P = \left\lceil \frac{N}{2} \right\rceil$.

The KTM bound is quite loose for most SNRs ($\bar{\gamma} > 0$ dB) and weakens progressively as the average per hop SNR increases. Although the proposed bound outperforms the KTM bound for moderate-to-high SNRs, the latter is tighter for low-to-moderate SNRs and for less severe fading environments (approximately $m > 5$). However, the KTM bound significantly deviates from the exact average BER for high SNRs. This fact is not surprising because our proposed bounds are asymptotically exact.

In Fig. 2.5, the multi-hop outage probability over Nakagami-$m$ fading is plotted. Although the proposed bound loosens as $N$ and $m$ increase, it is tighter at moderate-to-high SNR than the KTM bound. Similar to the case of the BER bounds, the KTM bound is tighter than our bound for less severe fading conditions (e.g., $m > 5$) and for low-to-moderate SNRs. The outage curve corresponding to $N = 2$ is plotted to verify that our proposed bound reduces to the exact outage probability of dual-hop system with ideal CA-AF relays. The proposed outage bound always outperforms the bound with $P = 0$ ("Minimum
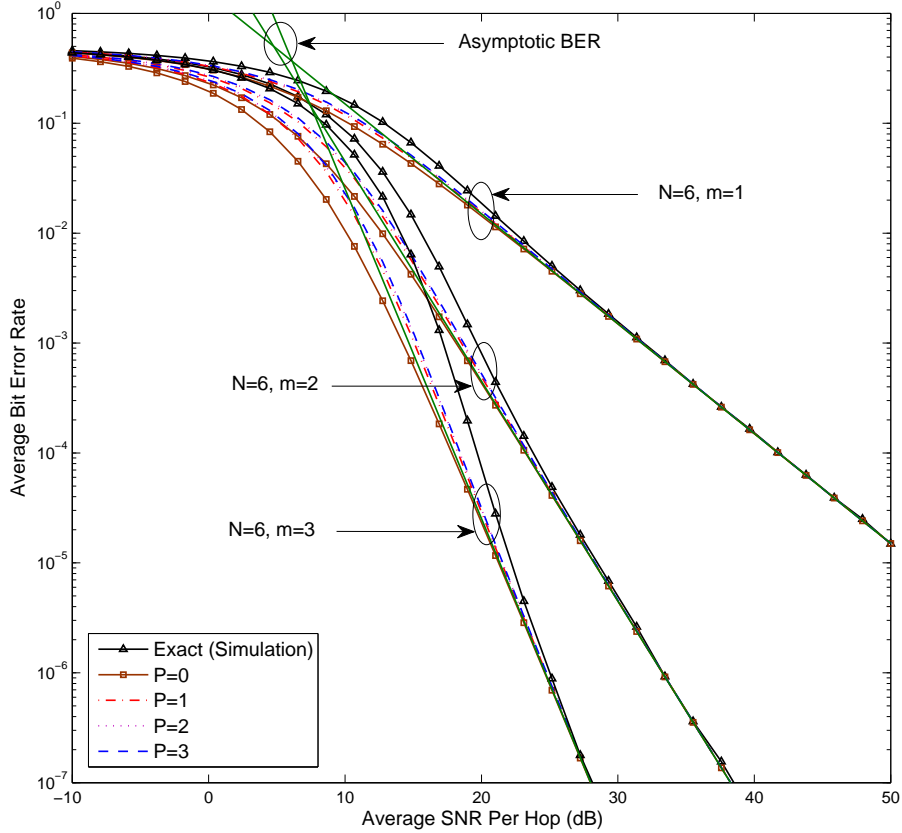
Figure 2.6: The effect number of hops and severity of fading on the proposed BER bounds of a multi-hop relay network over i.i.d. Nakagami-$m$ fading.

bound"). Similar to BER bound, our outage bound is asymptotically exact.

In Fig. 2.6, as a function of $P$, we compare the tightness of different bounds for average BER of BPSK (2.22). For a six-hop relay network over Nakagami-$m$ fading, four different BER bounds are obtained by assigning $P = 0$, $P = 1$, $P = 2$ and $P = 3$. As expected, the bound with $P = 0$, which is equivalent to the bound in [50, Eqn. (11)] and [59, Ch. 3] is significantly weaker than the others. The tightness of the bounds increases as $P$ gets closer to $N - P$. This happens because the criteria $P \approx N - P$ ensures the symmetry of (2.5). Moreover, the gaps between bounds with $P = 1$, $P = 2$ and $P = 3$ are insignificant for severe fading cases. The asymptotic average BER curves are also plotted to verify our high SNR analysis and to demonstrate the asymptotically-exactness of the proposed bounds. These asymptotic BER curves accurately quantify the achievable diversity order and array gains. The proposed performance bounds thus provide valuable insights and guidelines for practical usage for system-design and link-budget calculation perspectives.
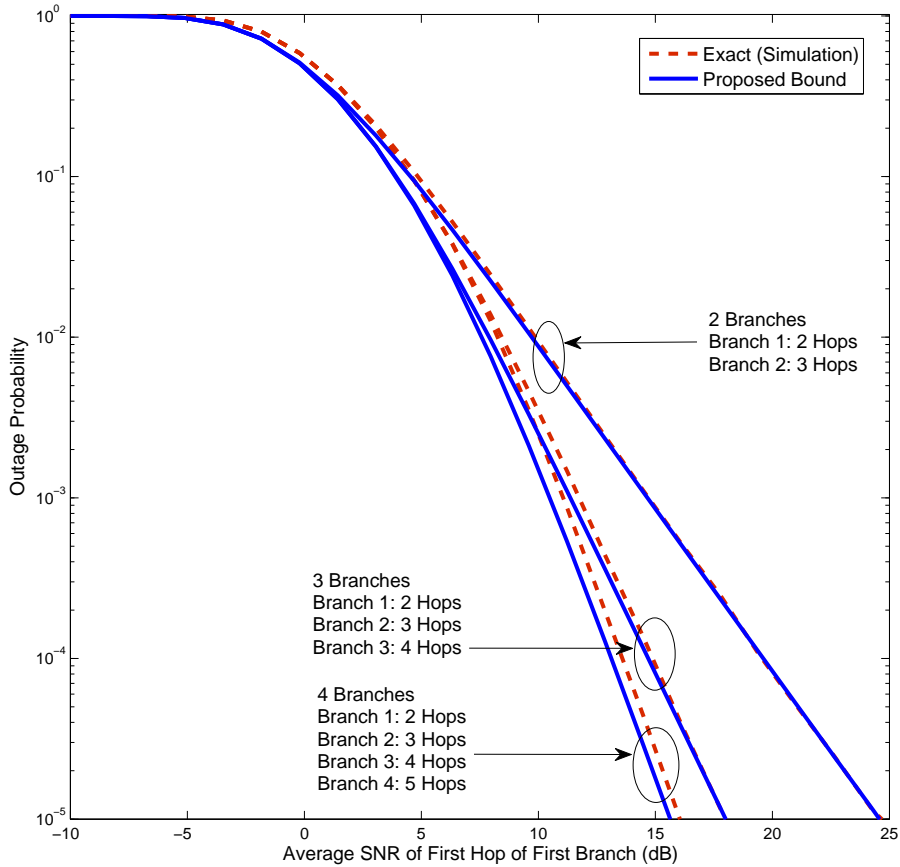
Figure 2.7: The outage probability of multi-hop multi-branch relay networks with selection combining at the destination. System operates over i.n.i.d Rayleigh fading channels. Here, $P_l = \left\lceil \frac{N_l}{2} \right\rceil$.

In Fig. 2.7, the outage probability bounds are plotted for a multi-hop multi-branch CA-AF relay network with best branch selection. The system is assumed to be operating over i.n.i.d Rayleigh fading channels. As expected, the proposed bounds are tighter to the exact curve for a network with fewer hops per branch. In particular, the proposed bounds are tighter in the high SNR regime regardless of the number of hops per branch. Notably, Fig. 2.7 reveals that the proposed outage bound can indeed be employed for an accurate assessment of the achievable diversity order as the proposed outage bound tends to be asymptotically exact at high SNRs.

In Fig. 2.8, we plot the average BER bounds for a multi-hop multi-branch relay network with MRC reception over i.n.i.d Rayleigh fading. The proposed bounds for the average BER lower bounds are tighter to the exact average BER curves at moderate-to-high SNRs. As expected, all BER bounds deteriorate as the number of hops per branch increases. In evalu-
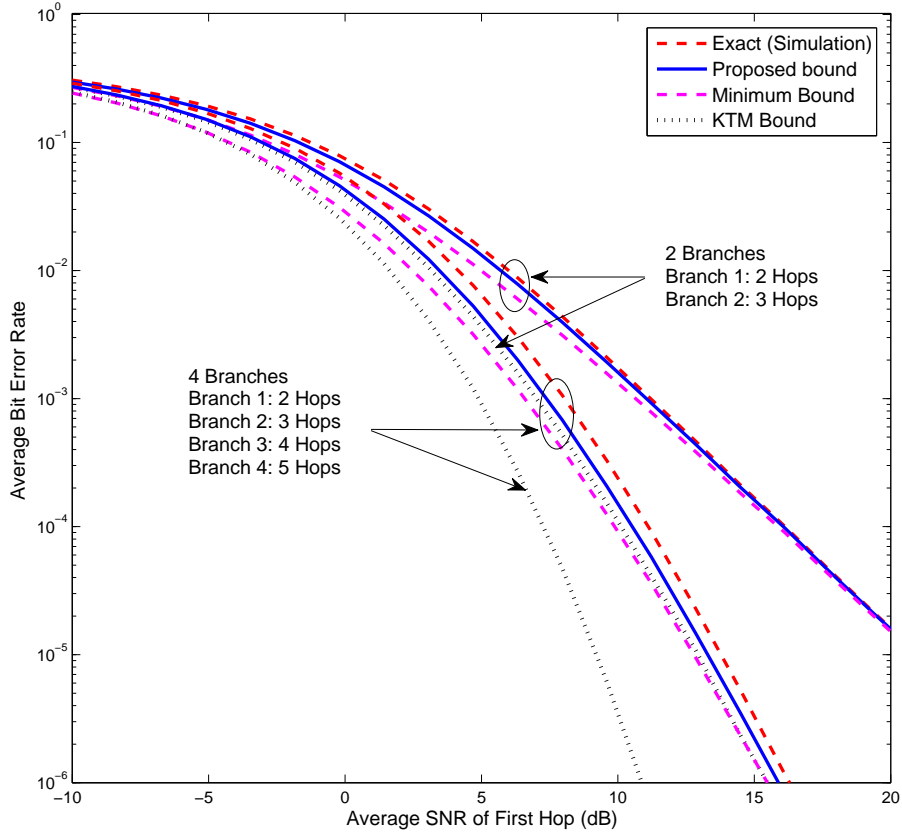
Figure 2.8: The average BER of multi-hop multi-branch relay networks with MRC at the destination. System operates over i.n.i.d Rayleigh fading channels and BPSK modulation scheme is considered. Here, $P_l = \left\lceil \frac{N_l}{2} \right\rceil$.

ating (2.34), we use only ten points ($N_p = 10$). Thus, this result illustrates the accuracy and efficiency of (2.34) for the average BER of multi-hop multi-branch systems. The proposed bound outperforms both KTM and Minimum bounds. Fig. 2.8 clearly shows that the KTM bound would not be employed for accurately quantifying the achievable diversity order of multi-hop multi-branch relay networks because it significantly diverges from the exact average BER curves in high SNR regime. Nevertheless, the asymptotically-exactness of the proposed average BER bounds indeed facilitates accurate quantification of the achievable diversity order.

## 2.7  Conclusion

In this chapter, a new class of SNR upper bounds for multi-hop CA-AF relay networks were proposed and analyzed. The parameter $0 \leq P \leq N$ specifies this class, and $P = \left\lceil \frac{N}{2} \right\rceil$

is a reasonably optimal choice. The closed-form CDF, PDF, and MGF expressions for i.n.i.d Rayleigh fading and for i.i.d. Nakagami-$m$ fading, $m \in \mathbb{Z}^+$ were derived, leading to the average SER and the outage lower bounds. Specifically, the proposed SNR bounds are mathematically more tractable than the previously reported bounds and consequently render them useful for deriving performance metrics of multi-hop relay networks over various fading channels. In particular, these bounds are asymptotically exact and hence pave the way to develop an unified asymptotic analysis framework. Thereby, valuable insights into practical system-design were obtained by quantifying the achievable diversity order and array gains. Moreover, the proposed bounds were used to study the multi-hop multi-branch relay networks. Their asymptotic-exactness may render them useful for other applications; e.g., multiple-antenna beamforming relay networks [65] and optimal power allocation.

$\sim$

# Chapter 3

# Output-Threshold Multiple Relay Selection Schemes

In this chapter, a new class of multiple relay selection (MRS) schemes is developed for dual-hop multi-branch cooperative wireless networks. The key idea is to adaptively select a subset from the available relays to satisfy a preset output threshold signal-to-noise ratio (SNR). Hence, the relay selection of interest is termed as the output-threshold multiple relay selection (OT-MRS). To be more specific, in the OT-MRS, the first $L_c$ out of $L$ relays ($1 \leq L_c \leq L$) are sequentially selected such that the output SNR of the maximal ratio combined $L_c$ relayed-paths and the direct path exceeds the preset threshold SNR. The subset of $L_c$ relays can be selected either from a non-ordered set of $L$ relays or from an ordered set of $L$ relays in the ascending order of the end-to-end SNR. In this context, the latter selection ensures that the minimum number of relays are activated adaptively, because the selected subset now contains the best $L_c$ out of $L$ relays. Consequently, the OT-MRS with SNR ordering is henceforth referred as the minimum-select OT-MRS. For the sake of exposition, the OT-MRS with a non-ordered relay set is termed as the OT-MRS as well.

The performance bounds, including the outage probability, the average symbol error rate, and the average number of selected relays, are derived in closed-form for the OT-MRS scheme. Our numerical results verify the analyses and as well reveal that the OT-MRS outperforms the optimal single relay selection and the generalized selection combining-based multiple relay selection for low-to-moderately high SNRs. Moreover, the minimum-select OT-MRS performs identically to the optimal single relay selection scheme in high SNR regime. The OT-MRS scheme enjoys low channel estimation and no relay ordering requirements as opposed to the minimum-select OT-MRS schemes, however, at the expense of some performance degradation in high SNR regime. The proposed adaptive multiple relay selection schemes indeed provide more flexibility in utilizing bandwidth and spatial

diversity in cooperative wireless networks.

## 3.1 Introduction

Cooperative relay wireless networks achieve distributed spatial diversity, wider coverage, lower transmit power, and reduced interference [12, 66–69]. Selecting a subset of available relays according to some performance metrics can further enhance the performance of cooperative networks [58, 70–78]. In classical adaptive diversity combining techniques, the combiner output is compared against a threshold and the number of diversity branches combined varies adaptively [79–83]. In this work, we utilize such adaptive combining ideas to propose two new output-threshold multiple relay selection (OT-MRS) schemes.

### 3.1.1 Prior related research

The dual-hop multi-branch cooperative network of Laneman and Wornell [67] employs all available relays, which is henceforth called as the all-participate relaying (APR). To circumvent the low spectral efficiency of the APR scheme, which is resulted due to the use of multiple orthogonal channels, miscellaneous relay selection schemes have been developed [58, 70–78]. They can be broadly divided into two categories: (i) single relay selection (SRS) and (ii) multiple relay selection (MRS) [77].

Among single relay selection (SRS) schemes, the selection of the relay whose relayed-path has the maximum end-to-end SNR is the optimal scheme [73, 74, 77, 78]. This scheme achieves the full diversity while maintaining a higher throughput than the others [77]. Various suboptimal SRS schemes having different degrees of trade-offs among the data throughput, reliability, and implementation complexity have been studied in the literature [71, 72, 77]. To be more specific, [71] proposes the nearest neighbor relay selection scheme, which essentially selects the geographically nearest relay to the source or destination. In [77], the best neighbor relay selection, which selects the relay with the strongest channel to the source or the destination in terms of SNR, is proposed and studied. It is shown in [77] that the best neighbor relay selection achieves a mere unity diversity order whenever the direct path does not exist, otherwise, it achieves order two diversity. Moreover, in [72], the performance of the best-worst channel relay selection is investigated for dual-hop multi-branch cooperative networks. The best-worst relay selection scheme selects the relay whose worst channel is the best and hence achieves the full achievable diversity order [77]. Besides, in [72], the best harmonic mean relay selection, which selects the relay having the maximum harmonic mean of the source-relay and relay-destination channel

SNRs, is analytically studied.

The MRS is the natural generalization of SRS into multiple relays. In [75, 77] and [84], several MRS schemes are proposed by generalizing the key ideas of SRS schemes in order to allow multiple relays to cooperate. In [75], an MRS scheme, which minimizes the error probability under total energy constraints, is analytically studied. Further, the MRS schemes of [77] involve maximization of the received SNR subjected to per-relay power constraints. Nevertheless, the complexity of the optimal MRS algorithm of [77] is exponential in the number of relays. Consequently, the optimal MRS is indeed prohibitive in practice for relay networks with large number of relays. To circumvent this issue, in [77], several suboptimal MRS schemes having a linear complexity in the number of relays have also been developed by trading-off the performance to a greater degree to achieve a simpler practical implementation complexity. Recently, in [84], another suboptimal yet effective MRS referred to as generalized selection combining (GSC)-based MRS was proposed and analyzed.

Apart from the aforementioned SRS and MRS schemes, incremental relaying [12] achieves higher spectral efficiencies over APR as the former utilizes the achievable degrees of freedom (DoFs) of the channel effectively with the aid of limited feedback from the destination. In [85], an incremental relaying with the best relay selection scheme is developed for amplify-and-forward (AF) relaying over fading channels.

### 3.1.2 Motivation and contribution

Although SRS schemes achieve higher spectral efficiencies than that of APR, the error rates and outages of SRS are higher. The complexity of the optimal MRS schemes proposed in [75, 77] increases exponentially with the available number of relays. Although the GSC-based MRS [84] achieves considerable performance gains, it requires channel estimation of all the relayed-paths. In addition, the combined SNR may exceed the system requirements, and consequently, more relays than necessary may be selected. The incremental best relay selection scheme of [85] selects only a single-relay and hence does not fully utilize the available degrees of freedom of the wireless relay channel. Thus, MRS schemes yielding better trade-offs among the error performance, implementation complexity, and spectral efficiency are indeed desirable.

In this chapter, we thus develop a new class of OT-MRS schemes by employing orthogonal channeling, spatially-distributed AF relays, and maximal ratio combining (MRC) at the destination. The key concept of OT-MRS is its threshold checking of the output SNR at
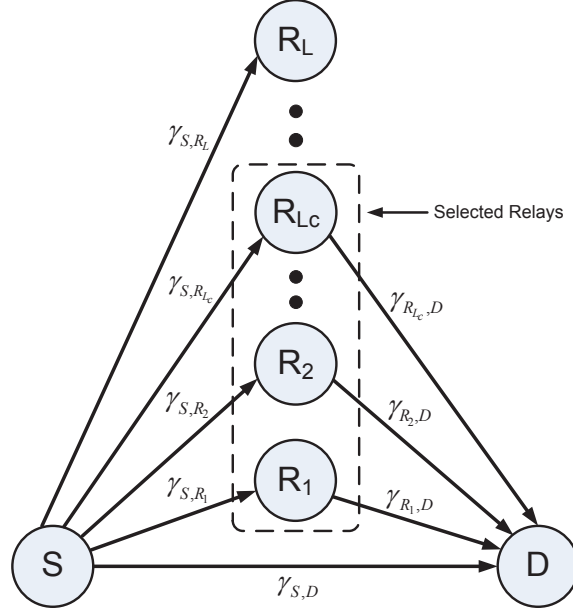
Figure 3.1: The proposed OT-MRS for dual-hop relay networks.

the destination [80, 81]. The cumulative distribution function (CDF), the probability density function (PDF), the moment generating function (MGF), and the first moment of an upper bound of the output SNR are derived. Thereby, closed-form lower bounds for the outage probability, the average symbol error rate (SER), the average number of selected relays, and the ergodic capacity are also derived. The performance of OT-MRS is then compared to that of the existing relay selection schemes. Our numerical results reveal that the proposed OT-MRS indeed facilitate better trade-offs among the bandwidth, performance, and complexity for relay selection schemes.

**This chapter is organized as follows:** Section 3.2 presents the system model and channel model while Section 3.3 describes the mode of operation of the proposed OT-MRS schemes. The statistical characterization of the output SNR is presented in Section 3.4. In Section (3.5), the basic performance metrics of OT-MRS are derived. Section 3.6 presents numerical and simulation results, while Section 3.7 concludes the chapter. All proofs are given in Appendix B.

## 3.2 System and channel model

We consider a cooperative wireless network with $L + 2$ terminals including one source $(S)$, one destination $(D)$, and $L$ AF relays $(R_l)$ for $l \in \{1, \cdots, L\}$ (see Fig. 3.1). Only single antenna terminals are considered. The source-to-destination data transmission takes place

in two phases. In the first phase (broadcast phase), $S$ broadcasts to $L$ relays and $D$. In the second phase (relaying phase), relay selection is applied; i.e., only $L_c$ relays out of $L$ relays ($1 \leq L_c \leq L$) are selected to forward the amplified version of the source signal to $D$. To facilitate the orthogonal transmission in two phases, a time-division channel allocation scheme with $L_c$ time-slots is employed [12]. The channels $S \to R_l$ and $R_l \to D$ for $l \in \{1, \cdots, L\}$ are modeled as independent and identically distributed (i.i.d.) flat-Rayleigh fading. Moreover, the system model contains an independent flat-Rayleigh fading direct channel from $S \to D$. The channel-state information (CSI) of only the selected relays is assumed to be available at $D$ for the OT-MRS. However, for minimum-select OT-MRS, all CSI of all relays needs to be estimated at $D$ for relay ordering. In order to constraint the transmit power at the relays whenever the channel gains of $S \to R_l$ are substantially low, we follow [12] and set the amplification factor of the $l$th relay as

$$G_l = \sqrt{\frac{\mathcal{P}_R}{\mathcal{P}_S |h_{S,R_l}|^2 + \sigma_{R_l}^2}}, \quad \text{for} \ \ l \in \{1, \cdots, L\}, \tag{3.1}$$

where $\mathcal{P}_R$ and $\mathcal{P}_S$ are the average transmit powers at $S$ and $R$, respectively. Furthermore, $h_{S,R_l}$ is the fading amplitude of $S \to R_l$ channel and $\sigma_{R_l}^2$ is the variance of the zero mean additive white Gaussian noise at the input of the $l$th relay's receiver. The combiner at $D$ employs MRC with an output threshold checking [80, 81].

Under the system and channel model of OT-MRS, the instantaneous output SNR, $\Gamma_i$ for $i \in \{1, \cdots, L\}$, at $D$ with $i$ active relays can be written as [86–88]

$$\Gamma_i = \gamma_{S,D} + \sum_{l=1}^{i} \frac{\gamma_{S,R_l} \gamma_{R_l,D}}{\gamma_{S,R_l} + \gamma_{R_l,D} + 1}, \tag{3.2}$$

where $\gamma_{S,D} = \mathcal{P}_S |h_{S,D}|^2 / \sigma_D^2$, $\gamma_{S,R_l} = \mathcal{P}_S |h_{S,R_l}|^2 / \sigma_{R_l}^2$, and $\gamma_{R_l,D} = \mathcal{P}_R |h_{R_l,D}|^2 / \sigma_D^2$ for $l \in \{1, \cdots, i\}$ are instantaneous SNRs pertinent to $S \to D$, $S \to R_l$, and $R_l \to D$ channels, respectively. Specifically, for Rayleigh fading channels, $\gamma_{S,D}$, $\gamma_{S,R_l}$, and $\gamma_{R_l,D}$ are modeled as independent exponential random variables with means $\bar{\gamma}_{S,D}$, $\bar{\gamma}_{S,R}$ and $\bar{\gamma}_{R,D}$, respectively.

In order to accurately analyze the system performance, the probability distribution of $\Gamma_i$ (3.2) is required. However, the derivation of the exact CDF and the PDF of $\Gamma_i$ in close-form is not mathematically tractable. To circumvent this intractability of the problem formulation and hence to facilitate a comprehensive performance analysis, we replace $\Gamma_i$ by a tight upper bound $\Gamma_i^{ub}$ as follows [86–88]:

$$\Gamma_i \leq \Gamma_i^{\text{ub}} = \gamma_{S,D} + \sum_{l=1}^{i} \gamma_{R_l}, \tag{3.3}$$

where $\gamma_{R_l} = \min(\gamma_{S,R_l}, \gamma_{R_l,D})$. The performance metrics derived by using (3.3) serve as tight lower bounds to the exact counterparts. In particular, they are indeed asymptotically exact at high SNRs and consequently serve as benchmarks for practical dual-hop AF relay networks. On the other hand, a tight lower bound on $\Gamma_i$ is given by [86]

$$\Gamma_i \geq \Gamma_i^{\text{lb}} = \gamma_{S,D} + \frac{1}{2} \sum_{l=1}^{i} \gamma_{R_l}. \tag{3.4}$$

The performance metrics derived by using $\Gamma_i^{\text{lb}}$ serves as tight upper bounds on the exact counterparts. However, the theoretical development of the lower and upper bounds follows the same analytical techniques. For the sake of brevity, we thus develop analytical results pertinent to the SNR upper bound (3.4) only.

## 3.3 Proposed relay selection schemes

In this section, the algorithms pertinent to the proposed MRS schemes are presented in detail. To facilitate a concise and clear exposition, the OT-MRS scheme and the minimum-select OT-MRS scheme are described by employing schematic flow-diagrams.

### 3.3.1 OT-MRS scheme

The OT-MRS scheme selects the first $L_c$, $1 \leq L_c \leq L$, (non-ordered) relays such that the combined SNR of the first $L_c$ relayed-paths and the direct path exceeds a preset threshold SNR, $\gamma_{th}$. This SNR threshold can be chosen to be the minimum required SNR for successful symbol decoding for a modulation scheme of interest at an acceptable quality-of-service level. The schematic flow-diagram in Fig. 3.2 illustrates the pertaining relay selection process. First, $D$ receives the signal transmitted by $S$ during the broadcast phase. Next, the first relay (labeled as $R_1$ in Fig. 3.1) forwards the amplified version of the source message to $D$ in the first time-slot of the relaying phase. The combiner at $D$ combines this signal with the signal received via the direct path. If the combiner output SNR exceeds the threshold at this point, no more relays are selected. Otherwise, the remaining relays $R_2, ..., R_L$ are selected in subsequent time-slots until the cumulative output SNR exceeds the threshold. In the worst-case, all $L$ relays are selected. However, in the best-case, just the first relay is sufficient. Note that relays are not ordered based on their SNRs of the corresponding relayed-paths. This is how OT-MRS differs from the minimum-select OT-MRS and GSC-based MRS [84] approaches.
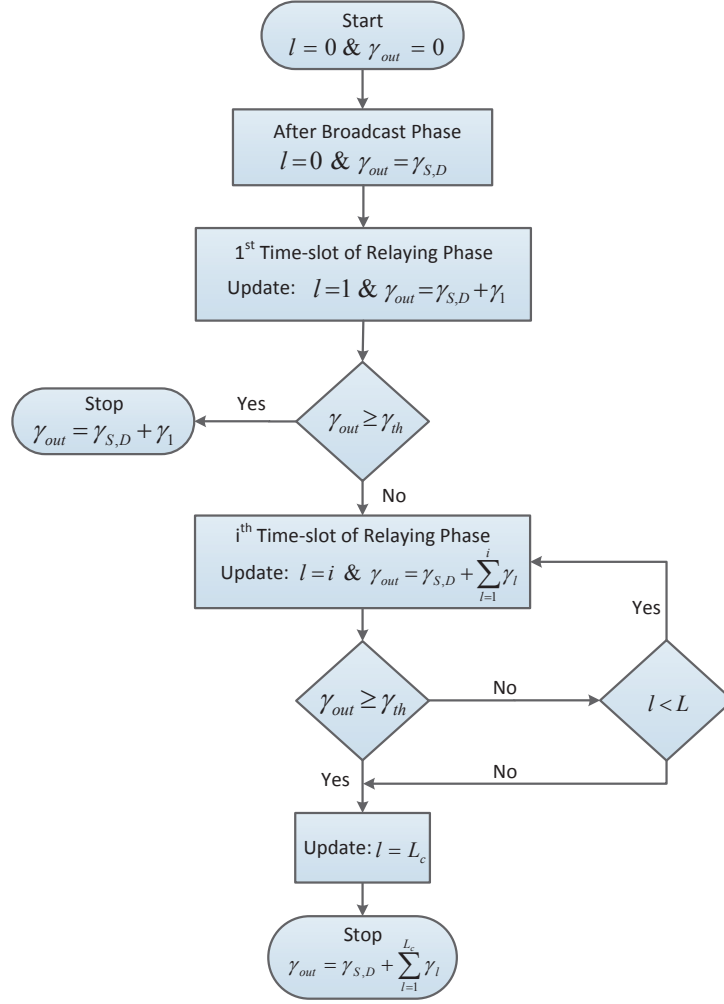
Figure 3.2: Mode of operation of OT-MRS.

### 3.3.2 Minimum-select OT-MRS scheme

In the minimum-select OT-MRS scheme, the $L$ relays are first ordered according to a relay ordering function $\Phi_l(\gamma_{S,R_l}, \gamma_{R_l,D})$ for $i \in \{l = 1, \cdots, L\}$. Suppose that the ordered set of all available relays is denoted as $R_{(1)} < R_{(2)}, < \cdots, < R_{(L)}$. The minimum-select OT-MRS follows the same steps to those of OT-MRS, however, the algorithm now operates on the ordered relay set as depicted in Fig. 3.3. To be more specific, the threshold check is performed on the cumulative combined SNR of the ordered relay set until the output SNR exceeds the preset threshold. In the best case, the minimum-select OT-MRS selects the best available relay, nevertheless, in the worst case, all the relays need to be selected.

The relay ordering process ensures that the minimum number of relays are selected to meet the threshold criterion. To this end, the relays can be ordered in the ascending order
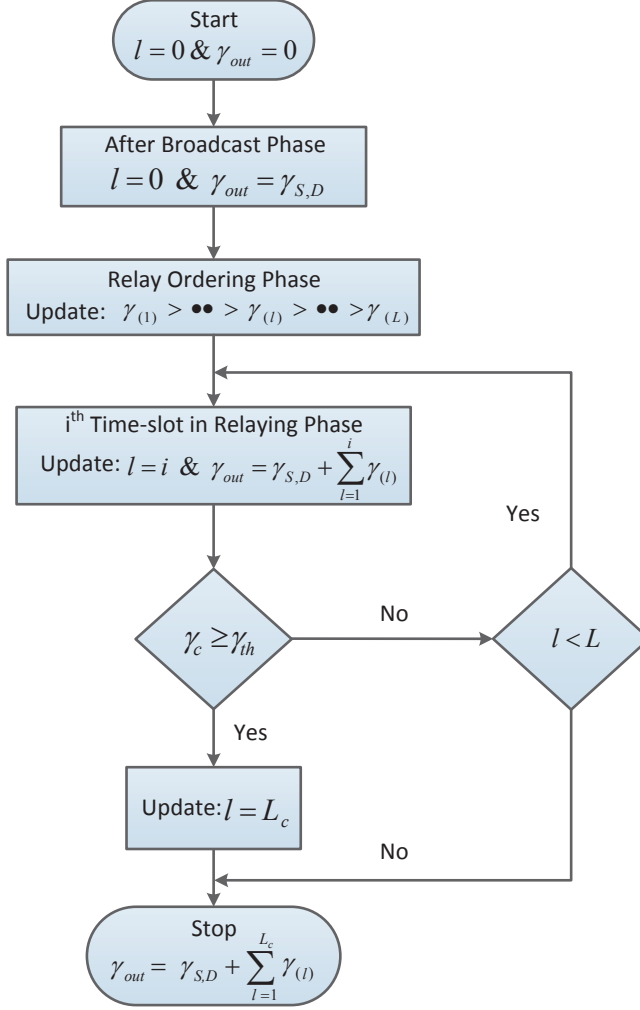
Figure 3.3: Mode of operation of minimum-select OT-MRS.

of their corresponding end-to-end SNR of $S \to R_l \to D$ relayed-path. The SNR relay ordering function is therefore given by

$$\Phi_l(\gamma_{S,R_l}, \gamma_{R_l,D}) = \frac{\gamma_{S,R_l}\gamma_{R_l,D}}{\gamma_{S,R_l} + \gamma_{R_l,D} + 1}. \tag{3.5}$$

Besides the SNR relay ordering, the harmonic mean ordering, $\Phi(\gamma_{S,R_l},\gamma_{R_l,D})=\frac{\gamma_{S,R_l}\gamma_{R_l,D}}{\gamma_{S,R_l}+\gamma_{R_l,D}}$, and the worst channel ordering, $\Phi_l(\gamma_{S,R_l}, \gamma_{R_l,D}) = \min(\gamma_{S,R_l}, \gamma_{R_l,D})$, can be employed as well [77].

**Remark 3.3.1:** The analytical results are provided only for the OT-MRS scheme. The corresponding analysis on minimum-select OT-MRS scheme is omitted due to the mathematical intractability of the problem formulation. However, the comprehensive Monte Carlo simulation results for the minimum-select OT-MRS are provided to obtain useful insights.

### 3.3.3 An important extension to OT-MRS: Modified OT-MRS

In some wireless applications, the direct channel between the source and the destination would be of high fidelity with high probability. For such applications, in certain channel realizations, the SNR of the direct channel at the destination would just be sufficient to exceed the output threshold, and hence, always selecting at least one relay as discussed in Sections 3.3.1 and 3.3.2 results in a lower spectral efficiency unnecessarily. Thus, the afore-mentioned OT-MRS schemes can be readily extended to addressed this issue as follows:

Here, the destination first compares the SNR of the direct channel against the output threshold. If it exceeds the threshold, source-to-destination communication is carried out just using the direct channel. Otherwise, the available relays can be selected in subsequent time-slots until their cumulative SNR exceed the output threshold as discussed in Sections 3.3.1 and 3.3.2. This extended MRS algorithm is illustrated in Fig. 3.4. Thus, this modified OT-MRS saves at least one time-slot in certain channel conditions and thereby further improves the overall spectral efficiency. However, the achievable diversity order at high SNRs is limited to unity, because only the direct channel is selected at very high SNR regime.

The statistical characterization of the end-to-end SNR and derivation of performance bounds of this modified OT-MRS follows the same techniques of that of OT-MRS described in Section 3.3.1. Hence, for the sake of brevity, these results are omitted in this thesis, however, Monte Carlo simulation results are presented in Section 3.6.

## 3.4 Statistical characterization of the SNR

This section provides a comprehensive statistical characterization of the end-to-end SNR of OT-MRS scheme. To be more specific, the CDF, PDF, and MGF of the upper-bounded output SNR of the combiner employed at the destination are derived in closed-form.

In this context, the instantaneous output SNR of the OT-MRS scheme is denoted by $\gamma_{\mathrm{out}}$ and can be written as follows:

$$
\gamma_{\mathrm{out}} = \begin{cases} \gamma_{S,D} + \gamma_{R_1}, & \gamma_{S,D} + \gamma_{R_1} \geq \gamma_{th} \\ \gamma_{S,D} + \displaystyle\sum_{l=1}^{L_c} \gamma_{R_l}, & \gamma_{S,D} + \displaystyle\sum_{l=1}^{L_c} \gamma_{R_l} \geq \gamma_{th} \text{ and } \gamma_{S,D} + \displaystyle\sum_{l=1}^{L_c-1} \gamma_{R_l} \leq \gamma_{th} \\ \gamma_{S,D} + \displaystyle\sum_{l=1}^{L} \gamma_{R_l}, & \text{otherwise,} \end{cases} \tag{3.6}
$$

where $\gamma_{R_l} = \gamma_{S,R_l}\gamma_{R_l,D}/(\gamma_{S,R_l} + \gamma_{R_l,D} + 1)$ for $l \in \{1, \cdots, L\}$ is the non-ordered end-to-end SNR of the relayed-path via the $l$th relay, $R_l$.
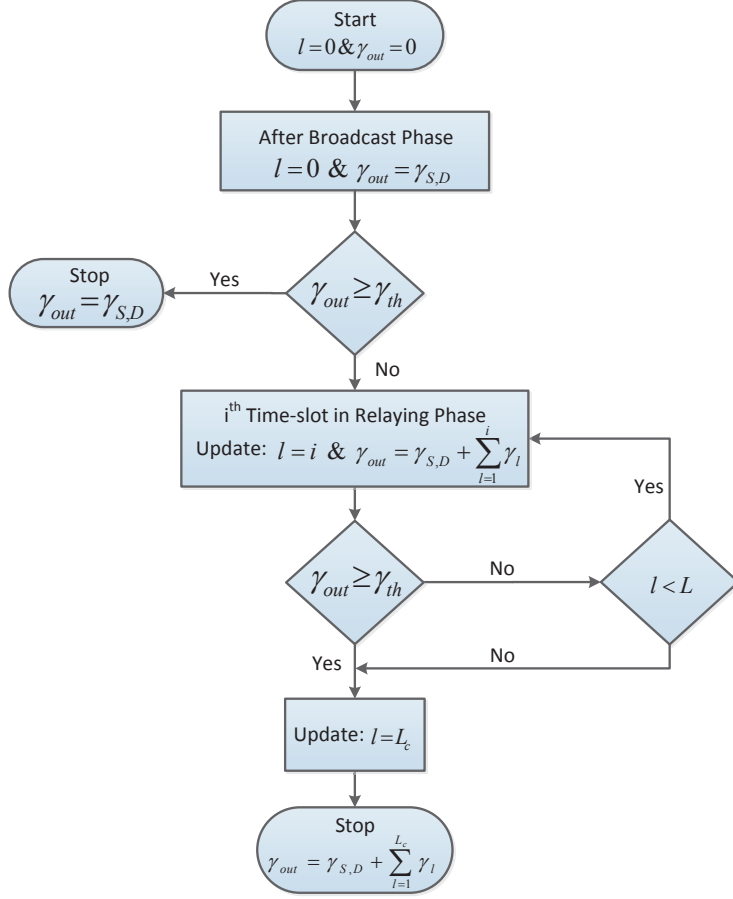
Figure 3.4: Mode of operation of the modified OT-MRS, where the direct channel SNR is first compared against the threshold before selecting at least one relay.

A general expression for the CDF of the output SNR can be then derived by using (3.6) as follows:

$$
\begin{aligned}
F_{\gamma_{\text{out}}}(x) &= \sum_{i=1}^{L} \Pr\left(\left[\gamma_{\text{out}} = \gamma_{S,D} + \sum_{l=1}^{i} \gamma_{R_l}\right] \cap [\gamma_{\text{out}} \leq x]\right) \\
&= \Pr\left(\gamma_{th} \leq \Gamma_1 \leq x\right) + \sum_{i=2}^{L} \Pr\left([\gamma_{th} \leq \Gamma_i \leq x] \cap [0 \leq \Gamma_{i-1} < \gamma_{th}]\right) \\
&+ \Pr\left([0 \leq \Gamma_L \leq x] \cap [0 \leq \Gamma_{L-1} < \gamma_{th}]\right),
\end{aligned}
\tag{3.7}
$$

where $\Gamma_i$ is the combined SNR of the first $i$ relayed-paths and the direct path (3.2). The first term of the second equality of (3.7) accounts for the event in which the combined SNR of the first relayed-path and the direct path exceeds the threshold; i.e., $\Gamma_1 \geq \gamma_{th}$. The second term accounts for the event in which the $i$ relayed-paths are required to be coherently combined with the direct path to form an output whose SNR exceeds the threshold. The third term corresponds to the worst case where the cumulative sum of the first $L-1$ relayed-paths and

the direct path SNRs does not exceed the threshold, and all $L$ relays must be selected. After some manipulations, (3.7) is further simplified to yield a more mathematically tractable form as

$$
F_{\gamma_{\text{out}}}(x) = \begin{cases}
F_{\Gamma_L}(x), & x < \gamma_{th} \\
F_{\Gamma_1}(x) - F_{\Gamma_1}(\gamma_{th}) \\
\quad + \sum_{i=2}^{L} \int_0^{\gamma_{th}} \int_{\gamma_{th}-\Gamma_{i-1}}^{x-\Gamma_{i-1}} f_{\Gamma_{i-1},\gamma_{R_i}}(\Gamma_{i-1},\gamma_{R_i}) \ \mathrm{d}\gamma_{R_i}\mathrm{d}\Gamma_{i-1} & (3.8) \\
\quad + \int_0^{\gamma_{th}} \int_0^{\gamma_{th}-\Gamma_{L-1}} f_{\Gamma_{L-1},\gamma_{R_L}}(\Gamma_{L-1},\gamma_{R_L}) \ \mathrm{d}\gamma_{R_L}\mathrm{d}\Gamma_{L-1}, & x \geq \gamma_{th},
\end{cases}
$$

where $F_{\Gamma_i}(x)$ is the CDF of the combined SNR of the first $i$ relayed-paths and the direct path, and $f_{\Gamma_{i-1},\gamma_{R_i}}(\Gamma_{i-1},\gamma_{R_i})$ is the joint PDF of $\Gamma_{i-1}$ and $\gamma_{R_i}$. To evaluate the CDF of $\gamma_{\text{out}}$, one needs to first derive $F_{\Gamma_{i-1},\gamma_{R_i}}(\Gamma_{i-1},\gamma_{R_i})$ in closed-form. This can be readily derived by first using (3.2) and then identifying the statistically independence of $\Gamma_{i-1}$ and $\gamma_{R_i}$ as follows:

$$
f_{\Gamma_{i-1},\gamma_{R_i}}(\Gamma_{i-1},\gamma_{R_i}) = f_{\Gamma_{i-1}}(\Gamma_{i-1}) \, f_{\gamma_{R_i}}(\gamma_{R_i}) . \tag{3.9}
$$

The PDF of $\Gamma_{i-1}^{ub}$ (3.3) can be next written in closed-form as [88]

$$
f_{\Gamma_{i-1}^{ub}}(x) = \beta_{sd,i-1}\exp\left(-\frac{x}{\bar{\gamma}_{S,D}}\right) + \sum_{l=1}^{i-1} \frac{\beta_{l,i-1}}{(l-1)!} \, x^{l-1} \exp\left(-\frac{x}{\bar{\gamma}}\right), \tag{3.10}
$$

where $\beta_{sd,k} = (\bar{\gamma}_{sd})^{k-1}/(\bar{\gamma}_{sd} - \bar{\gamma})^k$, $\beta_{l,k} = (-\bar{\gamma}_{sd})^{k-l}/\left(\bar{\gamma}^{l-1}(\bar{\gamma} - \bar{\gamma}_{S,D})^{k-l}\right)$, and $\bar{\gamma} = \bar{\gamma}_{S,R}\bar{\gamma}_{R,D}/(\bar{\gamma}_{S,R} + \bar{\gamma}_{R,D})$.

By using (3.10), the CDF of $\Gamma_{i-1}^{ub}$ can be derived as follows:

$$
F_{\Gamma_{i-1}^{ub}}(x) = \beta_{sd,i-1}\bar{\gamma}_{S,D} \left(1 - \exp\left(-\frac{x}{\bar{\gamma}_{S,D}}\right)\right) + \sum_{l=1}^{i-1} \frac{\beta_{l,i-1}\,(\bar{\gamma})^l}{(l-1)!} \, \gamma\left(l,\frac{x}{\bar{\gamma}}\right). \tag{3.11}
$$

Again, by employing (3.8), (3.9), (3.10), and (3.11), the CDF of an upper bound of the output SNR, $\gamma_{\text{out}}^{ub}$, which is obtained by replacing $\gamma_{\text{out}}$ with $\gamma_{\text{out}}^{ub}$ (3.6), can be derived in closed-form as follows:

$$
F_{\gamma_{\text{out}}^{ub}}(x) = \begin{cases}
\beta_{sd,L}\bar{\gamma}_{S,D}\left(1 - \exp\left(-\frac{x}{\bar{\gamma}_{S,D}}\right)\right) \\
\quad + \sum_{l=1}^{L} \frac{\beta_{l,L}\,(\bar{\gamma})^l}{(l-1)!} \, \gamma\left(l,\frac{x}{\bar{\gamma}}\right), & 0 \leq x \leq \gamma_{th} \\
\beta_{sd,1}\bar{\gamma}_{S,D} \exp\left(-\frac{\gamma_{th}}{\bar{\gamma}_{S,D}}\right)\left(1 - \exp\left(-\frac{(x-\gamma_{th})}{\bar{\gamma}_{S,D}}\right)\right) \\
\quad + \lambda \exp\left(-\frac{\gamma_{th}}{\bar{\gamma}}\right)\left(1 - \exp\left(-\frac{(x-\gamma_{th})}{\bar{\gamma}}\right)\right) + \kappa, & x > \gamma_{th},
\end{cases} \tag{3.12a}
$$

47

where $\lambda$ and $\kappa$ are given by

$$\lambda = \beta_{1,1}\bar{\gamma} \ + \ \sum_{i=2}^{L}\left(\beta_{sd,i-1}\left(\frac{\bar{\gamma}\bar{\gamma}_{S,D}}{\bar{\gamma} - \bar{\gamma}_{S,D}}\right)\left(1 - \exp\left(-\frac{\gamma_{th}(\bar{\gamma} - \bar{\gamma}_{S,D})}{\bar{\gamma}\bar{\gamma}_{S,D}}\right)\right)\right.$$

$$+ \ \sum_{l=1}^{i-1}\left.\frac{\beta_{l,i-1}}{l!}\left(\gamma_{th}\right)^l\right). \tag{3.12b}$$

$$\kappa \ = \ \beta_{sd,L-1}\bar{\gamma}_{S,D}\left(1 + \frac{1}{\bar{\gamma} - \bar{\gamma}_{S,D}}\left(\bar{\gamma}_{S,D}\exp\left(-\frac{\gamma_{th}}{\bar{\gamma}_{sd}}\right) - \bar{\gamma}\exp\left(-\frac{\gamma_{th}}{\bar{\gamma}}\right)\right)\right)$$

$$+ \ \sum_{l=1}^{L-1}\beta_{l,L-1}\left(\frac{(\bar{\gamma})^l}{(l-1)!}\gamma\left(l,\frac{\gamma_{th}}{\bar{\gamma}}\right) - \frac{(\gamma_{th})^l}{l!}\exp\left(-\frac{\gamma_{th}}{\bar{\gamma}}\right)\right). \tag{3.12c}$$

The PDF of $\gamma_{\text{out}}^{ub}$ can be then derived by differentiating (3.12a) as follows:

$$f_{\gamma_{\text{out}}^{ub}}(x) = \begin{cases} \beta_{sd,L}\exp\left(-\dfrac{x}{\bar{\gamma}_{S,D}}\right) + \displaystyle\sum_{l=1}^{L}\dfrac{\beta_{l,L}}{(l-1)!}x^{l-1}\exp\left(-\dfrac{x}{\bar{\gamma}}\right), & 0 \leq x \leq \gamma_{th} \\[3mm] \beta_{sd,1}\exp\left(-\dfrac{x}{\bar{\gamma}_{S,D}}\right) + \dfrac{\lambda}{\bar{\gamma}}\exp\left(-\dfrac{x}{\bar{\gamma}}\right), & x > \gamma_{th} \end{cases} \tag{3.13}$$

Moreover, the MGF of $\gamma_{\text{out}}^{ub}$ can be derived by taking the Laplace transform of the PDF of $\gamma_{\text{out}}^{ub}$ (3.13) as

$$\mathcal{M}_{\gamma_{\text{out}}^{ub}}(s) \ = \ \mathcal{E}_{\gamma_{\text{out}}^{ub}}\{\exp(-sx)\}$$

$$= \ \left(s + \frac{1}{\bar{\gamma}_{S,D}}\right)^{-1}\beta_{sd,L} + (\beta_{sd,1} - \beta_{sd,L})\exp\left(-\gamma_{th}\left(s + \frac{1}{\bar{\gamma}_{S,D}}\right)\right)$$

$$+ \ \sum_{l=1}^{L}\frac{\beta_{l,L}}{(i-1)!}\left(s + \frac{1}{\bar{\gamma}}\right)^{-l}\gamma\left(l,\gamma_{th}\left(s + \frac{1}{\bar{\gamma}}\right)\right)$$

$$+ \ \left(s + \frac{1}{\bar{\gamma}}\right)^{-1}\frac{\lambda}{\bar{\gamma}}\exp\left(-\gamma_{th}\left(s + \frac{1}{\bar{\gamma}}\right)\right). \tag{3.14}$$

The moments of the output SNR are useful as signal quality indicators. They can be used as an alternative performance measure to average error rate analysis. The $n$th moment of $\gamma_{\text{out}}^{ub}$ is defined as

$$\overline{(\gamma_{\text{out}}^{ub})^n} = \mathcal{E}\left\{\left(\gamma_{\text{out}}^{ub}\right)^n\right\} = \int_0^{\infty} x^n f_{\gamma_{\text{out}}^{ub}}(x)\mathrm{d}x = (-1)^n \left.\frac{\mathrm{d}^n M_{\gamma_{\text{out}}^{ub}}(s)}{\mathrm{d}s^n}\right|_{s=0}. \tag{3.15}$$

Among them, the average output SNR, $\bar{\gamma}_{\text{out}}$, is an important comparative performance metric. Thus, an upper bound for $\bar{\gamma}_{\text{out}}$ of the OT-MRS is next derived by first substituting (3.13)

into (3.15) and then letting $n = 1$ as follows:

$$
\begin{aligned}
\overline{\gamma_{\text{out}}^{ub}} &= \left. -\frac{\mathrm{d}M_{\gamma_{\text{out}}^{ub}}(s)}{\mathrm{d}s} \right|_{s=0} \\
&= (\bar{\gamma}_{sd})^2 \left( \beta_{sd,L} + (\beta_{sd,1} - \beta_{sd,L}) \left( 1 + \frac{\gamma_{th}}{\bar{\gamma}_{sd}} \right) \exp\left( -\frac{\gamma_{th}}{\bar{\gamma}_{sd}} \right) \right) \\
&+ \bar{\gamma}\lambda \left( 1 + \frac{\gamma_{th}}{\bar{\gamma}} \right) \exp\left( -\frac{\gamma_{th}}{\bar{\gamma}} \right) + \sum_{l=1}^{L} \frac{\beta_{l,L}}{(l-1)!} \bar{\gamma}^{(l+1)} \gamma\left( l+1, \frac{\gamma_{th}}{\bar{\gamma}} \right). \quad (3.16)
\end{aligned}
$$

## 3.5 Performance analysis

In this section, the performance metrics of the proposed OT-MRS are derived in closed-form. To this end, closed-form lower bounds for the outage probability, the average SER, and the average number of selected relays are derived by employing the probability statistics of the output SNR presented in Section 3.4.

### 3.5.1 Outage probability

The outage probability is denoted by $P_{\text{out}}$ and is defined as the probability that the instantaneous output SNR, $\gamma_{\text{out}}$, falls below a certain target SNR, $\gamma_0$. For the proposed OT-MRS, this target SNR is indeed equal to the output threshold SNR, $\gamma_{th}$. A closed-form lower bound on the outage probability, $P_{\text{out}}^{lb}$, can be therefore obtained by evaluating $F_{\gamma_{\text{out}}^{ub}}(x)$ given in (3.12a) at $x = \gamma_{th}$ as follows:

$$
P_{\text{out}}^{lb} = \Pr\left( \gamma_{\text{out}}^{ub} \leq \gamma_{th} \right) = F_{\gamma_{\text{out}}^{ub}}(\gamma_{th}). \quad (3.17)
$$

Next, by employing (3.12a) and (3.17), $P_{\text{out}}^{lb}$ can be explicitly derived as

$$
P_{\text{out}}^{lb} = \beta_{sd,L}\bar{\gamma}_{S,D} \left( 1 - \exp\left( -\frac{\gamma_{th}}{\bar{\gamma}_{S,D}} \right) \right) + \sum_{l=1}^{L} \frac{\beta_{l,L}(\bar{\gamma})^l}{(l-1)!} \gamma\left( l, \frac{\gamma_{th}}{\bar{\gamma}} \right), \quad (3.18a)
$$

where $\lambda$ and $\kappa$ are defined in (3.12b) and (3.12c), respectively.

### 3.5.2 Average error rate

The average SER is derived by averaging the conditional error probability (CEP) over the PDF of the output SNR, $\gamma_{\text{out}}$. A closed-form lower bound on the average SER pertinent to the CEP, $P_e|\gamma = \zeta \mathcal{Q}\left( \sqrt{\eta\gamma} \right)$, can be then derived as follows (see Section B.1 of Appendix

B for the proof):

$$
\begin{aligned}
\bar{P}_e^{lb} &= \frac{\zeta}{2}\beta_{sd,L}\bar{\gamma}_{S,D}(1-\mu_{sd}) + \zeta\left(\beta_{sd,1}-\beta_{sd,L}\right)\bar{\gamma}_{S,D} \\
&\quad\times\ \left(\mathcal{Q}\left(\sqrt{\eta\gamma_{th}}\right)\exp\left(-\frac{\gamma_{th}}{\bar{\gamma}_{S,D}}\right) - \mu_{sd}\mathcal{Q}\left(\sqrt{2\nu_{sd}}\right)\right) \\
&\quad + \zeta\lambda\left(\exp\left(-\frac{\gamma_{th}}{\bar{\gamma}}\right)\mathcal{Q}\left(\sqrt{\eta\gamma_{th}}\right) - \mu\mathcal{Q}\left(\sqrt{2\nu}\right)\right) \\
&\quad + \sum_{l=1}^{L}\zeta\beta_{l,L}\bar{\gamma}^l\left(\frac{1}{2} - \mathcal{Q}\left(\sqrt{\eta\gamma_{th}}\right)\left(1 - \frac{\gamma\left(l,\frac{\gamma_{th}}{\bar{\gamma}}\right)}{(l-1)!}\right)\right. \\
&\quad\left. - \sum_{j=0}^{l-1}\frac{2^{j-1}\mu^{(2j+1)}\gamma\left(j+\frac{1}{2},\nu\right)}{\sqrt{\pi}\, j!(\eta\bar{\gamma})^j}\right),
\end{aligned}
\tag{3.19}
$$

where $\mu_{sd} = \sqrt{\frac{\eta\bar{\gamma}_{sd}}{2+\eta\bar{\gamma}_{sd}}}$, $\mu = \sqrt{\frac{\eta\bar{\gamma}}{2+\eta\bar{\gamma}}}$, $\nu_{sd} = \frac{\gamma_{th}(2+\eta\bar{\gamma}_{sd})}{2\bar{\gamma}_{sd}}$, and $\nu = \frac{\gamma_{th}(2+\eta\bar{\gamma})}{2\bar{\gamma}}$.

### 3.5.3 Average number of selected relays

The number of selected relays $L_c$ by the proposed OT-MRS fluctuates with the channel fading states. Consequently, $L_c$ is a discrete random variable with the range $1 \leq L_c \leq L$. This range indeed yields notable trade-offs among spectral efficiency, power consumption, and performance. For example, whenever $L_c$ equals to $L$, OT-MRS essentially reverts to APR. On the contrary, whenever $L_c$ is less than $L$, OT-MRS requires fewer number of orthogonal channels than that of APR and hence achieves higher spectral efficiency and lower power consumption. However, a low $L_c$ yields a lower diversity gain than that of APR. To obtain more insight into such trade-offs, in this section, the average the number of selected relays by the proposed OT-MRS is derived.

In this context, the average number of selected relays is denoted by $\bar{L}_c$ and can be defined as

$$
\bar{L}_c = \sum_{l=1}^{L} l\ \Pr(L_c = l),
\tag{3.20}
$$

where $\Pr(L_c = l)$ denotes the probability that the selected number of relays equals to $l$. A lower bound for the average number of selected relays by the OT-MRS can then be derived

in closed-form as follows (see Section B.2 of Appendix B for the proof):

$$\bar{L}_c^{lb} = L\beta_{sd,L-1}\bar{\gamma}_{S,D} + (\beta_{sd,1} - L\beta_{sd,L-1})\,\bar{\gamma}_{S,D}\exp\left(-\frac{\gamma_{th}}{\bar{\gamma}_{S,D}}\right) + \beta_{1,1}\bar{\gamma}\exp\left(-\frac{\gamma_{th}}{\bar{\gamma}}\right)$$
$$+ \sum_{i=1}^{L-1}\frac{L\beta_{i,L-1}\,(\bar{\gamma})^i}{(i-1)!}\gamma\left(i,\frac{\gamma_{th}}{\bar{\gamma}}\right) + \sum_{l=2}^{L-1}\left(l\beta_{sd,l-1}\left(\frac{\bar{\gamma}\bar{\gamma}_{S,D}}{\bar{\gamma}-\bar{\gamma}_{S,D}}\right)\right.$$
$$\times\left.\left(1-\exp\left(-\frac{\gamma_{th}(\bar{\gamma}-\bar{\gamma}_{S,D})}{\bar{\gamma}\bar{\gamma}_{S,D}}\right)\right)\exp\left(-\frac{\gamma_{th}}{\bar{\gamma}}\right) + \sum_{i=1}^{l-1}\frac{l\beta_{i,l-1}\,(\gamma_{th})^i}{i!}\exp\left(-\frac{\gamma th}{\bar{\gamma}}\right)\right).$$

$$(3.21)$$

### 3.5.4 Ergodic Capacity

The channel capacity is defined as the maximum rate at which information can be transmitted across a noisy channel with arbitrary reliability. In particular, the ergodic capacity is a basic performance measure of digital communications over fading channels. Thus, the ergodic capacity, $C$, is defined as the expected value of the instantaneous maximum mutual information ($I$) between the source and the destination. The achievable mutual information by the OT-MRS schemes is therefore given by

$$I = \frac{1}{L_c + 1}\log_2(1 + \gamma_{\text{out}}), \tag{3.22}$$

where $L_c$ is the number of selected relays, and $\gamma_c$ is the output SNR at the destination. The ergodic capacity can then be defined as the joint expectation of $I$ with respect to $\gamma_{\text{out}}$ and $L_c$ as

$$C = \mathcal{E}_{\gamma_c, L_c}\left\{\frac{1}{L_c + 1}\left[\log_2(1 + \gamma_{\text{out}})\right]\right\}. \tag{3.23}$$

Since the exact closed-form evaluation of (3.23) appears mathematically intractable, an upper bound of $C$ is derived as follows: First, the dependency of $L_c$ in the expectation in (3.23) is removed by replacing $L_c$ by its expected value, $\bar{L}_c$, derived in (3.21) as

$$C \lesssim \mathcal{E}_{\gamma_{\text{out}}}\left\{\frac{1}{\bar{L}_c + 1}\left[\log_2(1 + \gamma_{\text{out}})\right]\right\}. \tag{3.24}$$

Next, by first knowing that $\log_2(\cdot)$ is a concave function and then by using Jensen's inequality [1], $C$ can be upper bounded as

$$C \lesssim \frac{1}{\bar{L}_c + 1}\log_2\left(1 + \mathcal{E}\{\gamma_{\text{out}}\}\right). \tag{3.25}$$

Finally, an upper bound for the ergodic capacity of the OT-MRS can be derived in closed-form by using the proposed bounds for the average number of selected relays and average SNR as follows:

$$C \lesssim \frac{1}{\bar{L}_c^{lb} + 1}\log_2\left(1 + \overline{\gamma_{\text{out}}^{ub}}\right). \tag{3.26}$$

where $\mathcal{E}\{\gamma_{\text{out}}^{ub}\}$ is the average output SNR upper bound at the destination and is defined in (3.16). Moreover, $\bar{L}_c^{lb}$ the lower bound for the average number of selected relays defined in (3.21).

In particular, the ergodic capacity bound (3.26) serves as an important measure of the achievable spectral efficiency by the proposed OT-MRS schemes. Specifically, (3.26) reveals that the ergodic capacity is dominated by the pre-log factor, $1/(\bar{L}_c+1)$, which directly relates to the average number of selected relays, and hence, to the orthogonal time-slots required for a complete transmission cycle. Thus, by maximizing this pre-log factor, the achievable spectral efficiency can further be maximized. To this end, the modified OT-MRS schemes discussed in Section 3.3.3 serves as an important extension of the proposed OT-MRS as they ensure that no relays will be selected, whenever the direct channel SNR exceeds the output threshold, for scenarios in which the source-to-destination channel is of high fidelity with high probability.

## 3.6   Numerical results

In this section, our numerical results are presented to illustrate and compare the important performance metrics of the proposed OT-MRS and the minimum-select OT-MRS schemes. To be more specific, numerical results for the average bit error rate (BER) of binary phase shift keying (BPSK), the outage probability, the average number of selected relays, and the ergodic capacity are provided. Moreover, the performance of the proposed MRS schemes is compared with the competing SRS and MRS schemes.

In Fig. 3.5, the average BER of BPSK of the OT-MRS and the minimum-select OT-MRS schemes is plotted for dual-hop networks having six relays and ten relays. The average BER lower bound of the OT-MRS is plotted by letting $\zeta = 1$ and $\eta = 2$ in (3.19). Furthermore, the average BER curves corresponding to the minimum-select OT-MRS is plotted by using Monte Carlo simulations. In particular, the average BER of the direct transmission (without relaying) is plotted for comparison purposes. Fig. 3.5 clearly reveals that both OT-MRS and minimum-select OT-MRS schemes perform almost identically in low SNR regime. This observation is not surprising as both schemes need to select all the relays at very low SNRs in order to exceed the output threshold SNR. On the contrary, in high SNR regime, minimum-select OT-MRS outperforms the OT-MRS, because the former selects best relays out of an ordered relay set, while the latter selects a arbitrary set of relays from a non-ordered relay set. As the average SNR increases, the BER curves experience a
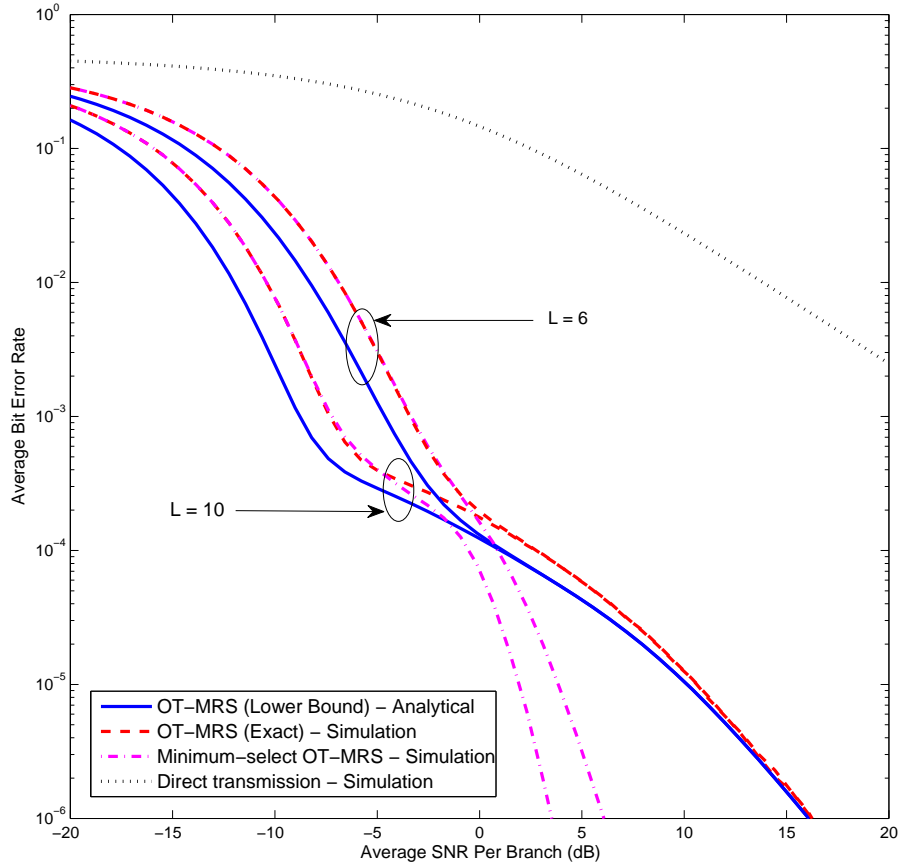
Figure 3.5: The average BER of BPSK against the average transmit SNR per branch. The output threshold $\gamma_{th}$ is set to 5 dB.

sudden kink. This kink is resulted due to the fact that the OT-MRS and the minimum-select OT-MRS select only an arbitrary relay and the best relay, respectively at very high SNRs. Fig. 3.5 reveals that the OT-MRS achieves a substantial performance gain compared to the direct transmission. For example, at an average BER of $10^{-3}$, MRS schemes achieve more than 20 dB SNR gain compared to the direct transmission. Moreover, our analytical average BER curves are tighter to the exact counterpart in moderate-to-high SNR regime, and they are indeed asymptotically exact at very high SNRs.

In Fig. 3.6 the average number of selected relays by the proposed OT-MRS scheme is plotted against the average transmit SNR. The analytical lower bounds are plotted by using (3.21) whereas the exact curves are plotted by using Monte Carlo simulation results. Fig. 3.6 clearly shows that the OT-MRS selects all the available relays in very low SNR regime, nevertheless, the number of selected relays indeed decreases as the SNR increases. As
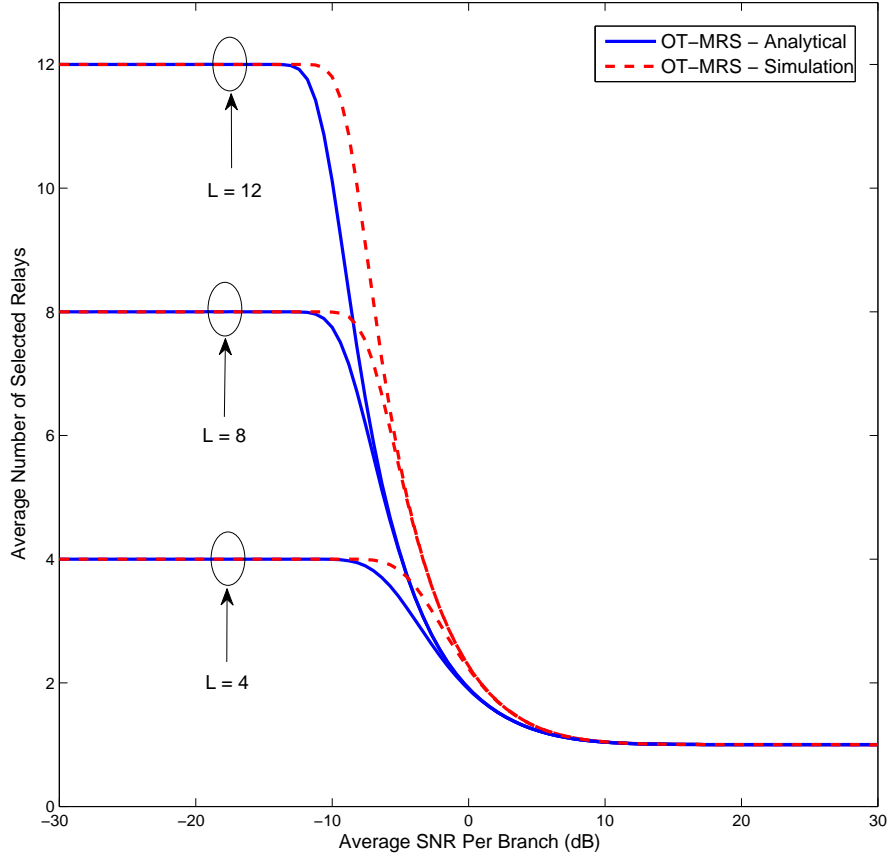
Figure 3.6: The average number of selected relays against the average SNR. The output threshold $\gamma_{th} = 10\,\text{dB}$.

expected, in the best case, the OT-MRS selects just one relay. Again, our analytical bounds are tighter to the exact curves, and hence, they serve as benchmarks for the practical system-designing. Fig. 3.6 confirms that our proposed MRS schemes adapt the number of selected relays, and hence, the number of orthogonal time-slots required for a complete transmission cycle according to the channel fading conditions. Interestingly, the number of the selected relays by the OT-MRS is directly related to the achievable spectral efficiency as per (3.26). Thus, the achievable spectral efficiency of the OT-MRS increases as the channel condition improves, while satisfying the required output threshold SNR. Therefore, this observation clearly reveals that the proposed OT-MRS indeed utilizes the channel resource adaptively offering better trade-offs between the spectral efficiency and reliability metrics.

In Fig. 3.7, the average number of selected relays by both the OT-MRS and the minimum-select OT-MRS is again plotted, however, now as a function of the normalized output thresh-
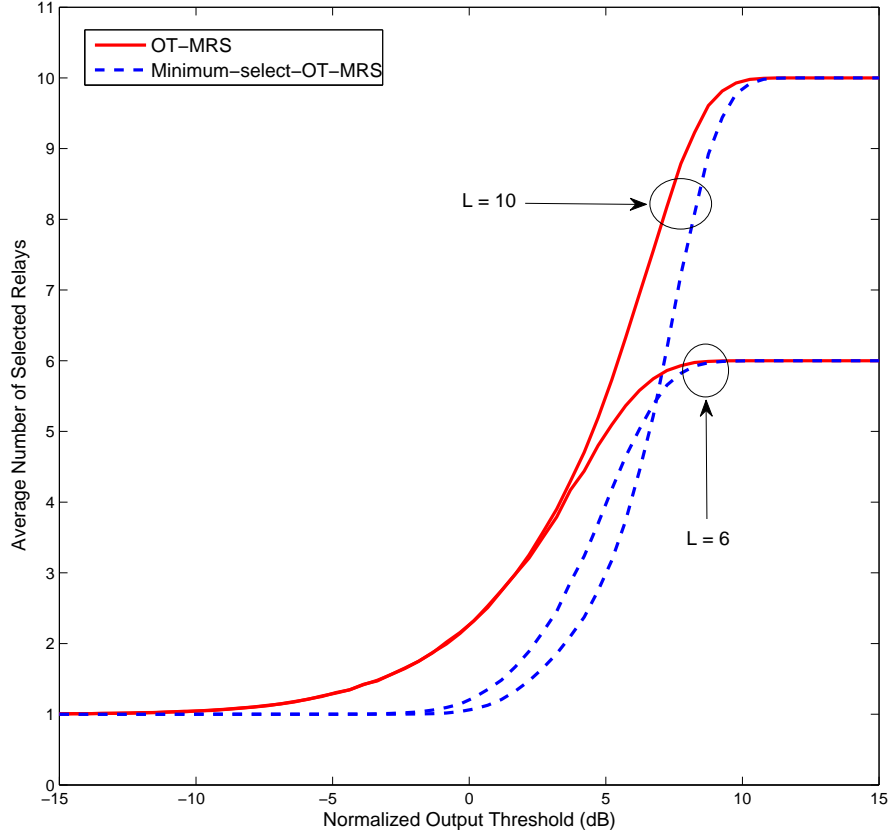
Figure 3.7: The average number of selected relays against the threshold SNR. The normalized threshold SNR is defined as $\gamma_{th}/\bar{\gamma}$.

old SNR. A dual-hop relay network with six and ten relays are considered. Fig. 3.7 confirms that the minimum-select OT-MRS indeed selects a lower number of relays than that of the OT-MRS for a given normalized output threshold. For example, at an output threshold of $0\,\mathrm{dB}$, the OT-MRS selects two relays as opposed to the single relay selected by the minimum-select OT-MRS. Furthermore, at very low threshold SNRs, all the available relays need to be selected, however, at very high SNRs, only one relay would be able to provide the required received SNR.

In Fig. 3.8, a comparison of average number of relays selected by OT-MRS, minimum-select OT-MRS, modified OT-MRS, and modified minimum-select OT-MRS is presented. Here, a relay network with six relays has been considered. Figure 3.8 clearly reveals that the average number of relays selected by modified OT-MRS schemes approached zero at very high SNRs, whereas, the corresponding number of relays is one for the conventional OT-MRS schemes. Thus, the modified OT-MRS schemes further improves the spectral effi-
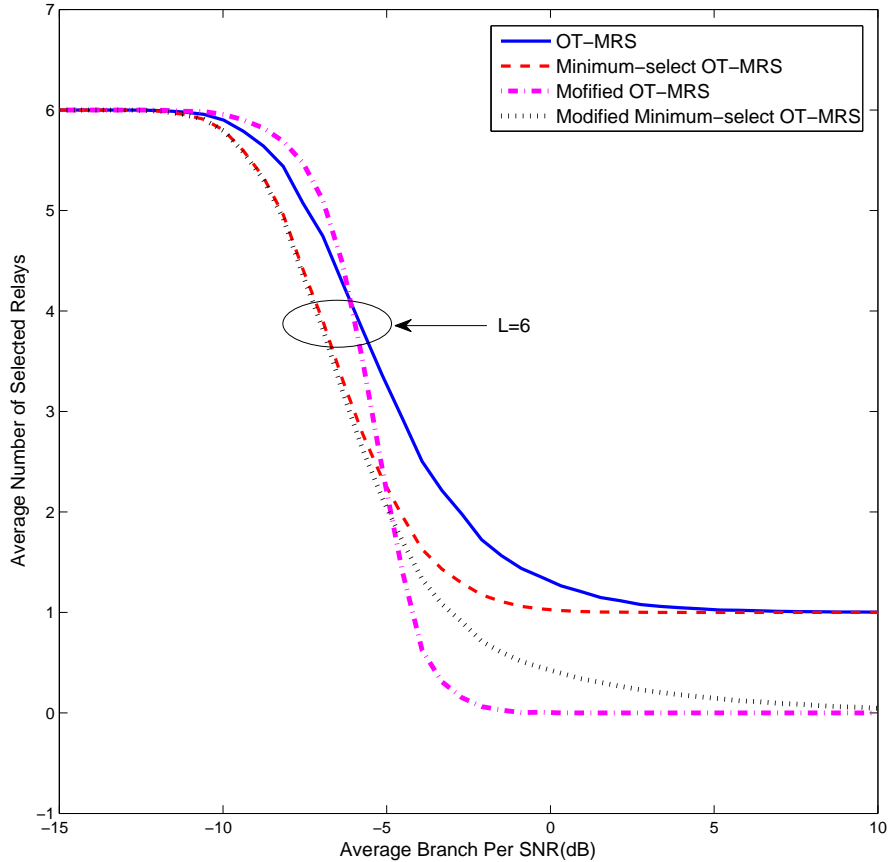
Figure 3.8: A comparison of the average number of relays selected by the four OT-MRS schemes. The relay network consists of six relays, and the output threshold SNR is set to 10 dB.

ciency by selecting fewer relays in moderate-to-high SNR regime as they effectively minimizes the required number of orthogonal time-slots in the relay-to-destination transmission phase at least by one.

In Fig. 3.9, the average BER of BPSK for OT-MRS and the minimum-select OT-MRS is compared with that of the best relay selection [73], GSC-based MRS which selects best 4 out of 6 relays [84], and the APR [12]. In particular, the APR scheme is included as a benchmark for comparison purposes. The average BER of fixed $L_n$ out of $L$ relay selection is also plotted as a comparison between a fixed versus adaptive relay selection. In low-to-moderate SNRs, both OT-MRS and minimum-select OT-MRS perform identical to the APR and hence outperform the competing counterparts. As expected, the OT-MRS looses diversity gain for the SNRs significantly higher than the threshold as it only uses the signals from the direct path and one relayed-path at very high SNRs. However, the minimum-select
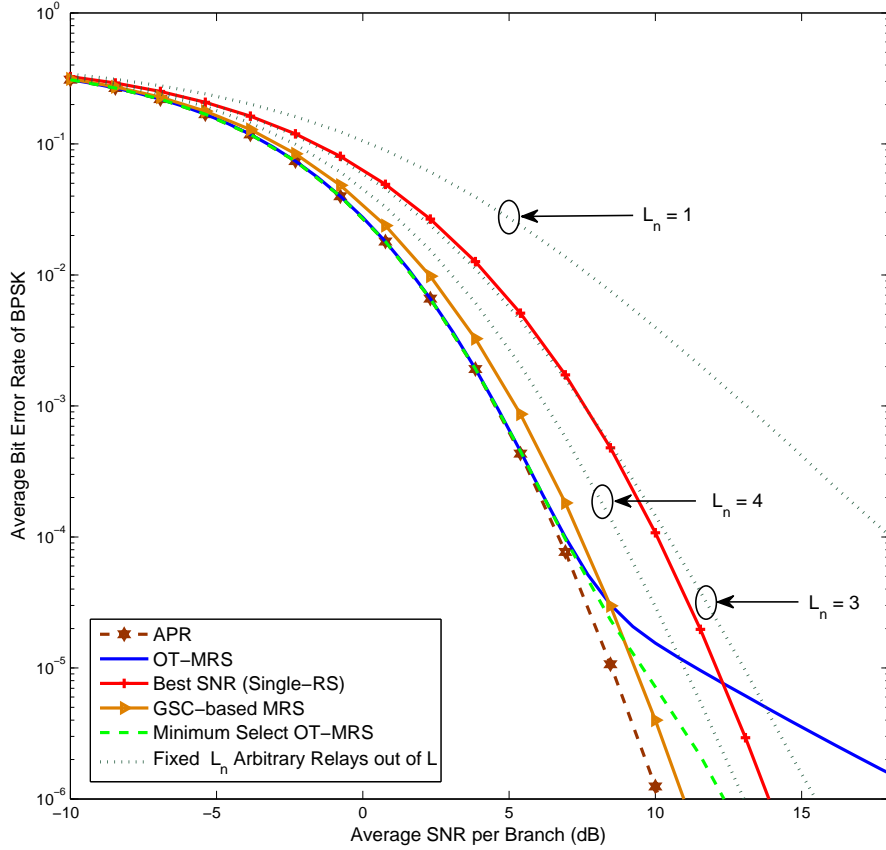
Figure 3.9: The average BER comparison of OT-MRS and minimum-select OT-MRS with the competing SRS and MRS schemes. The number of available relays, $L$, is set to 6.

OT-MRS circumvents this drawback by selecting and combining signals from both the best relay and direct path. It is worth noticing that the minimum-select OT-MRS achieves this performance gain at the cost of additional feedback overhead, channel estimation, relay ordering, and power requirements compared to the OT-MRS scheme. The aforementioned observations/insights obtained through Fig. 3.9 therefore clearly reveal the SNR adaptivity of our proposed MRS as they provide flexibility to adapt in fading, and enables better trade-offs among the bandwidth, performance, and complexity in cooperative relay networks.

Fig. 3.10 presents a comparison of the outage probability of the proposed OT-MRS against the competing SRS and MRS. The proposed OT-MRS outperforms all the other relay selection schemes in entire SNR regime apart from the APR. Indeed, the OT-MRS and the APR perform identically. This happens because OT-MRS selects relays sequentially until the cumulative output SNR exceeds the preset threshold $\gamma_{th}$, and an outage event occurs only when the cumulative output SNR of all $L$ relays is less than $\gamma_{th}$. Consequently,
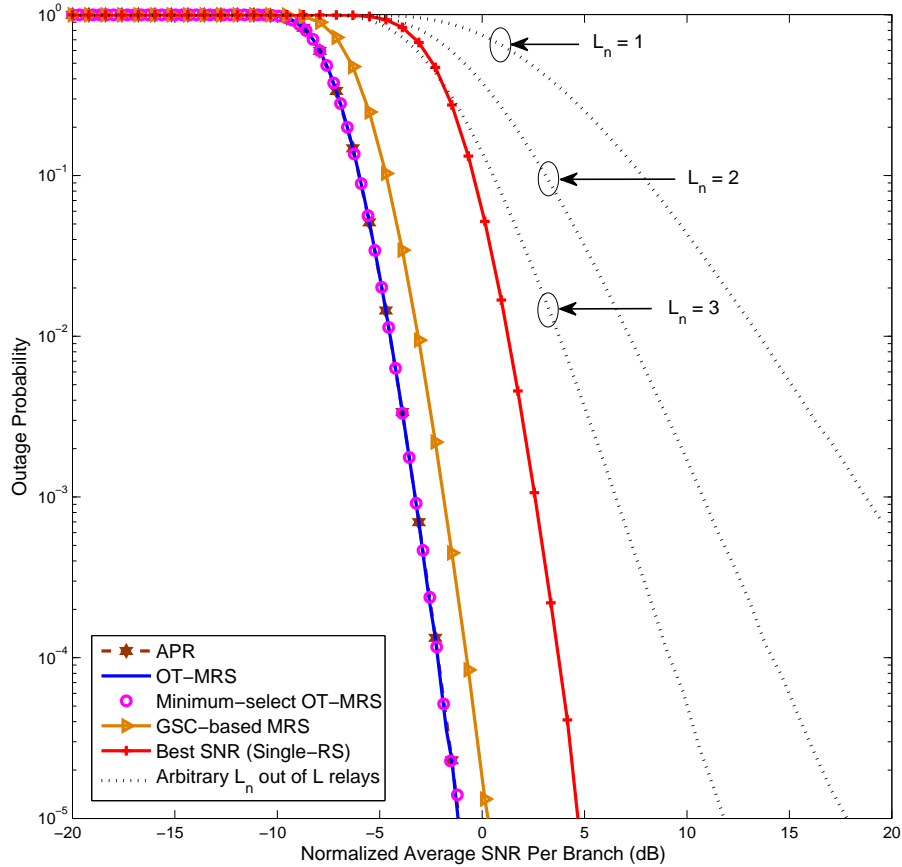
Figure 3.10: The comparison of the outage probability. The number of available relays, $L$, is set to 10, and the output threshold is assumed to be the same as the target SNR, i.e., $\gamma_{th} = \gamma_0 = 6.98\,\text{dB}$. The GSC-based MRS selects the best 5 out of 10 relays. The normalized average SNR is defined as $\bar{\gamma}^* = \bar{\gamma}/\gamma_{th}$.

the minimum-select OT-MRS performs just as the same as the OT-MRS because they now have the same outage event definition. Fig. 3.10 shows that the proposed OT-MRS schemes clearly outperform the optimal SRS and GSC-based MRS in terms of outage probability as well.

In Fig. 3.11, the average BER of the competing relay selection schemes is plotted as a function of the normalized output threshold SNR. The average BER curves of the minimum-select OT-MRS corresponding to three relay ordering functions; namely, (i) SNR ordering, (ii) harmonic-mean ordering, and (iii) worst channel ordering are plotted for comparison purposes as well. Fig.3.11 reveals the dependence of the average BER of the OT-MRS schemes on the output threshold. Whenever, the output threshold is significantly higher than the average SNR per branch, the OT-MRS selects all $L$ relays and performs identical to
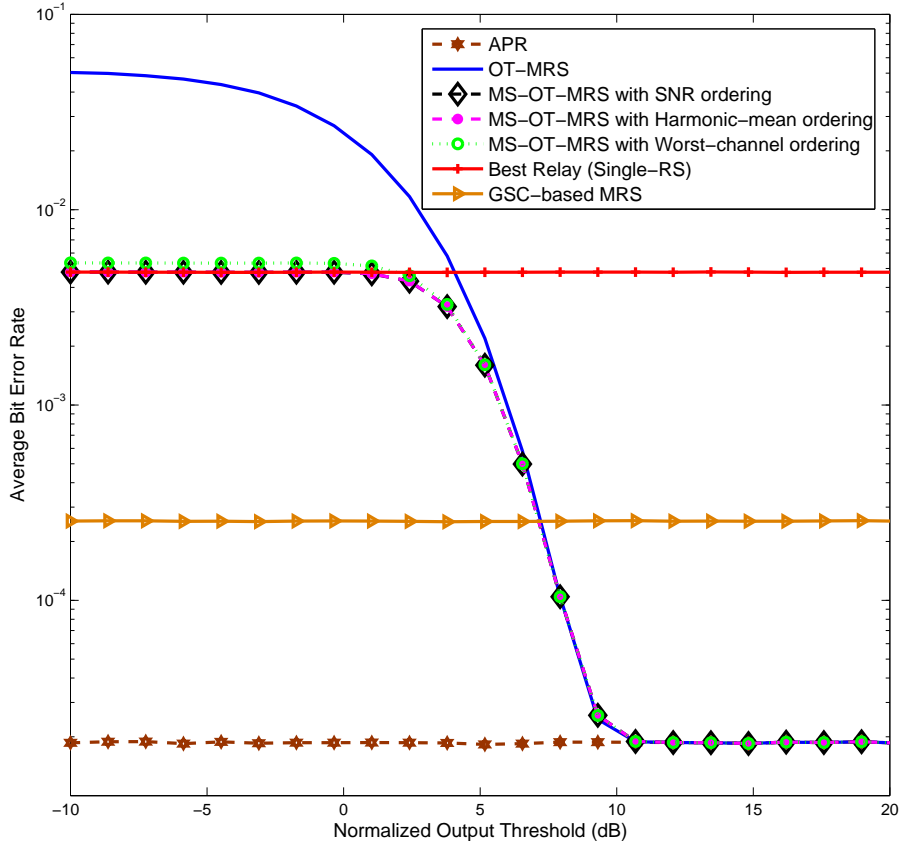
Figure 3.11: The average BER against normalized output threshold. The available number of relays $L$ is set to 10. The GSC-based MRS scheme selects the best five relays out of ten available relays. The normalized output threshold is defined as $\gamma_{th}^* = \gamma_{th}/\bar{\gamma}$.

the APR. On the contrary, for very low normalized threshold SNRs, the average BER of the minimum-select OT-MRS and the optimal SRS is identical, because the former selects only the best available relay just as the latter. Fig. 3.11 therefore confirms that the proposed OT-MRS schemes utilize the wireless resources adaptively to improve the system performance.

In Fig.3.12, the ergodic capacity is plotted for both OT-MRS and minimum-select OT-MRS schemes. The capacity upper bound of OT-MRS is plotted by using (3.26), while the exact capacity curves are plotted by using Monte Carlo simulations. The ergodic capacity of both schemes are identical in very low SNRs, while at high SNRs, the minimum-select OT-MRS outperforms the OT-MRS. This observation is not surprising as at low SNRs, both schemes select all the available relays, whereas, at moderate-to-high SNR, the former selects fewer number of relays than that of the latter. Moreover, at very high SNRs, for both schemes, just one relay would be able to exceed the output threshold, and hence, the gap
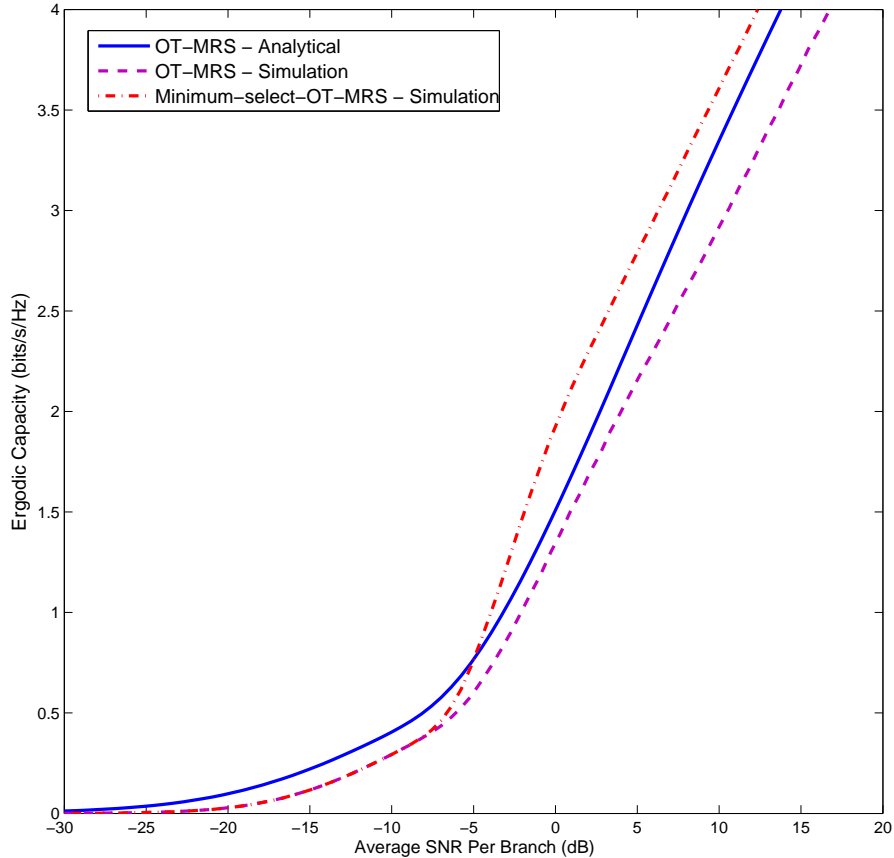
Figure 3.12: The Ergodic capacity against the average SNR per branch. The available number of relays $L$ is set to 10, and the output threshold is fixed to $\gamma_{th} = 10\,\mathrm{dB}$.

between the ergodic capacity curves remains fixed.

## 3.7  Conclusion

In this chapter, two OT-MRS schemes were developed for cooperative wireless relay networks. The proposed OT-MRS schemes can adapt to fading channel conditions and consequently select a subset of all available relays to satisfy the preset network quality-of-service level. The basic performance metrics were quantified, and thereby, important insights into practical system-implementation were obtained. Specifically, the CDF, PDF, and MGF of the upper-bounded output SNR were first derived and then used to quantify closed-form lower bounds for the outage probability, average SER, and the average number of selected relays. The numerical and simulation results were presented and compared with the competing SRS and MRS including the optimal SRS and the GSC-based MRS. Numerical results

reveal that the OT-MRS schemes outperform these competing schemes for low-to-moderate SNRs. The proposed MRS schemes provide flexibility to adapt in fading and hence enable resolving trade-offs among the bandwidth, performance, and complexity for practically implementing cooperative relay networks.

$\sim$

# Chapter 4

# Antenna and Relay Selection Strategies for One-way and Two-way MIMO Relay Networks

In this chapter, joint antenna and relay selection strategies are developed for multiple-input multiple-output (MIMO) amplify-and-forward (AF) relay networks. Two subclasses of relay networks, namely, (i) one-way relay networks (OWRNs) and (ii) two-way relay networks (TWRNs) are treated. Specifically, a comprehensive performance analysis framework is developed for the optimal transmit antenna selection (TAS) strategy for single-relay MIMO OWRNs. Thereby, the basic performance metrics of the optimal joint antenna and relay selection strategy are derived for multi-relay MIMO OWRNs. Moreover, the optimal joint transmit/receive antenna and relay selection strategy is proposed and analyzed for multi-relay MIMO TWRNs.

The basic performance metrics of the aforementioned transmission strategies are derived in closed-form. To this end, the probability statistics of the end-to-end signal-to-noise ratio (SNR) are first derived and then used to quantify the outage probability and the average symbol error rate (SER). Direct insights into practical system-design is obtained by quantifying the achievable diversity orders and array gains through the asymptotic analysis at high SNRs. Interestingly, our outage probability results reveal that the joint relay and antenna selection strategies achieve significant diversity and array gains over those of their single relay counterparts. In fact, the diversity orders of individual relayed-branches accumulate to yield the overall diversity of the multi-relay networks. Moreover, the amount of performance degradation due to practical transmission impairments such as feedback delays and spatially correlated fading is studied by deriving the asymptotic outage probability and the average SER, and thereby, the reduction of diversity order and array gain is quanti-

fied. Impact of channel prediction to circumvent outdated channel-state information (CSI) for antenna selection due to feedback delay is also studied. All the derivations are validated through Monte Carlo simulations.

## 4.1 Introduction

Cooperative relay networks are currently being investigated for emerging wireless system standards such as Worldwide Interoperability for Microwave Access (WiMAX), particular in IEEE 802.16j and IEEE 802.16m releases, and 3GPP Long Term Evolution-Advanced (LTE-A) [22, 23]. There are two specific subclasses of cooperative relay networks. They are generally referred to as (i) one-way relay networks (OWRNs) [12] and (ii) two-way relay networks (TWRNs) [35]. To be more specific, the half-duplex relay networks operating with unidirectional data flows are referred to as OWRNs and require four orthogonal channel-uses for two-way data transmission. On the other hand, the half-duplex relay networks operating with bidirectional data flows are generally known as TWRNs and consume only two orthogonal channel-uses for two-way data transmission. Thus, two-way relaying is a promising spectral efficient transmission protocol for wireless networks with half-duplex terminals [35, 37, 38, 89, 90]. Specifically, TWRNs avoid the pre-log factor of one-half in capacity expressions and thus are as twice spectrally efficient as the conventional OWRNs [35, 38]. However, TWRNs achieve this spectral efficiency gain over OWRNs at the expense of more stringent synchronization and signal processing complexity at the relay terminals.

The performance of both OWRNs and TWRNs can be further improved by integrating MIMO transmission technology [20, 21, 39, 40, 91, 92]. However, the main drawback of any MIMO system is the increased system complexity due to the additional cost for enabling multiple transmit and receive radio frequency (RF) chains[1] [93]. Antenna selection for single-hop MIMO systems has been widely studied to circumvent these drawbacks [93]. In particular, antenna selection reduces the complexity and the power requirements of the MIMO transmitter much more than most other transmit diversity schemes such as beamforming [94].

Moreover, relay selection strategies can be employed to improve the diversity and spectral efficiency improvements of both OWRNs and TWRNs [73, 78, 95]. Interestingly, for multi-relay MIMO relay networks, both antennas and relays can be selected jointly for fur-

---

[1]Passive antenna elements and additional digital signal processing are becoming increasingly cheaper; however, RF elements are still expensive and do not follow Moore's law [93].

ther maximizing the achievable diversity and spectral efficiency gains. Thus, in this chapter, joint antenna and relay selection strategies for cooperative multi-relay MIMO OWRNs and TWRNs are proposed and analyzed.

### 4.1.1 Prior related research on antenna selection for OWRNs

The optimal TAS strategy for dual-hop MIMO AF cooperative relay networks involves maximizing the end-to-end SNR by selecting the best transmit antenna at the source and relay by an exhaustive search [96]. Although the optimal TAS strategy achieves the full diversity order, its implementation complexity is relatively high due to the requirement of CSI of all three channels (i.e., $S \rightarrow D$, $S \rightarrow R$, and $R \rightarrow D$) at the source. As a remedy, reference [97] proposes two suboptimal yet low-complexity TAS strategies. The complexity reduction is achieved by maximizing the individual channel SNRs rather than the end-to-end SNR. The performance of these three TAS strategies has been evaluated by using Monte Carlo simulations only, without analysis [96, 97].

Other studies of TAS for MIMO AF relaying [17, 98–105] all differ from [96, 97]. These studies either employ TAS for only one of $S$ or $R$, or they all ignore the $S \rightarrow D$ direct path. Thus, their TAS algorithms are completely different from those of optimal and suboptimal TAS strategies of [96, 97]. In [17], the outage probability of multi-hop MIMO relaying with TAS is derived semi-analytically. In [98], the relay is limited to a single antenna, and the source and the destination employ TAS and maximal ratio combining (MRC), respectively. The outage and average SER are derived. In [100], transmit/receive (Tx/Rx) antenna pair selection is proposed for dual-hop MIMO AF relay networks. Here, the end-to-end transmission takes place by selecting the best Tx/Rx antenna pair at both the $S \rightarrow R$ and $R \rightarrow D$ MIMO channels. Reference [101] extends [100] by deriving the asymptotic outage probability and average SER. In addition, [106] extends the analysis of [100] for Nakagami-$m$ fading. In [99], the diversity order of a suboptimal TAS for MIMO relay networks is derived. In [103–105], the performance of TAS for dual-hop AF relay networks is studied by ignoring the direct path between $S$ and $D$. Further, in [102], three TAS strategies, which are optimal in terms of the outage probability, are developed for MIMO decode-and-forward (DF) relaying.

### 4.1.2 Prior related research on antenna selection for TWRNs

In the wide body of relay literature, there appear only few studies, [107–109], dealing with the issue of antenna selection for TWRNs. In [107], the upper bounds for the average

symbol error probability of network-coded DF TWRNs having two single-antenna sources and a dual-antenna relay are studied. In [107], during the first time-slot, two independent symbols are transmitted simultaneously by both sources to the relay. At the relay, these two symbols are decoded separately, and in the second time-slot, the relay transmits a physical layer network-coded symbol (the XOR of the two symbols) to the two sources by using Alamouti coding or antenna selection. Reference [108] extends the results of [107] by using either max-min antenna selection or maximal ratio transmission in the second time-slot. In particular, the transmission strategy in [108] achieves a diversity gain in the order of the number of antennas at the relay. Moreover, in [109], the computationally efficient relay antenna subset selection algorithms are investigated for maximizing the sum rate of MIMO TWRNs. Specifically, in [109], two antenna selection strategies namely, the joint-antenna selection and separate-antenna selection, are studied for reducing the computational complexity of relay antenna subset selection.

In addition to the above studies, [39, 40, 91] investigate the designing of optimal transmit precoders and receiver filters for MIMO TWRNs with the availability of perfect CSI. Moreover, [92] studies the effects of channel estimation errors on the receivers of MIMO AF TWRNs.

### 4.1.3 Motivation and contribution

The best relay selection for dual-hop cooperative OWRNs and TWRNs has been widely studied [73, 78, 85, 90, 95, 110]. In best relay selection, a single relay with maximum end-to-end SNR is selected for relaying. This scheme achieves the full diversity while maintaining a higher throughput than the repetition-based relaying [95]. However, in [73, 78, 85, 90, 95, 110] and many others, the selection of a relay is considered, but no antenna selection is considered.

Nevertheless, for multi-relay MIMO relay networks, both relays and antennas can be jointly selected. In the wide body of relay literature, there appear only three references, [90], [111], and [112], dealing with the issue of joint selection for MIMO OWRNs. In [90], joint antenna and relay selection is studied for MIMO DF relay networks. References [111] and [112] investigate the joint antenna and relay selection to maximize the channel capacity. Specifically, [111] uses the transmit antenna selection algorithm from [113] with instantaneous CSI, while [112] extends [111] for statistical CSI. Therefore, to the best of our knowledge, joint relay and antenna selection strategies for minimizing the outage probability and hence for maximizing the achievable diversity gains have not yet been studied

for dual-hop MIMO AF OWRNs. Note that the basic performance metrics of the optimal TAS for even the single-relay MIMO OWRNs have not yet been reported.

Moreover, references [107, 108] investigate antenna selection only for DF TWRNs, where individual symbols from the two sources are first decoded separately and then a network-coded symbol is broadcast back to these sources. In particular, the system models in both [107][2] and [108] employ multiple antennas at the relay only, and each source is equipped with a single antenna. Furthermore, in [107, 108], the transmit antenna selection is considered in the second time-slot (broadcast phase) only. The precoder/decoder designs proposed in [39, 40, 91, 92] require employing multiple Tx/Rx RF chains at each terminal and hence increase both complexity and cost, which clearly loosens one of the main trade-offs of deploying relay networks; i.e., the cost versus performance. Therefore, to the best of our knowledge, both Tx/Rx antenna selection for single-relay MIMO AF TWRNs, and joint relay and antenna selection for multi-relay MIMO AF TWRNs have not yet been studied.

This chapter fills the aforementioned gaps in MIMO relay literature by proposing and analyzing new joint antenna and relay selection strategies and the corresponding performance analysis frameworks for both MIMO AF OWRNs and MIMO AF TWRNs. To be more specific, the contribution of this chapter can be enumerated as follows:

1. A comprehensive performance analysis framework is developed for the optimal TAS strategy for dual-hop single-relay MIMO AF OWRNs.

2. The optimal joint antenna and relay selection strategy for minimizing the outage probability and hence maximizing the achievable diversity order is proposed for multi-relay MIMO AF OWRNs.

3. A novel antenna selection strategy, which selects the best Tx/Rx antennas at the two sources and relay, based on maximizing the end-to-end SNR of the worst source and hence minimizing the overall outage probability is developed for MIMO AF TWRNs.

4. Two useful generalizations, namely (i) the multi-relay OWRNs and (i) the multi-relay TWRNs, are also treated by proposing and analyzing the corresponding joint relay and Tx/Rx antenna selection strategies.

5. The basic performance metrics such as the outage probability and the average SER are derived by employing the statistical characterization of the end-to-end SNR. The

---

[2]The system model in [107] is restricted to a dual-antenna relay terminal.

achievable diversity orders and array gains are derived through an insightful high SNR analysis.

6. The performance degradations incurred due to the practical transmission impairments such as (i) feedback delays and (ii) spatially correlated fading are quantified in closed-form. Specifically, the asymptotic performance degradation is quantified to obtain valuable insights into practical system-design.

7. The impact of channel prediction to circumvent the adverse effects of outdated CSI is studied by presenting and analyzing a linear finite impulse response (FIR) channel prediction strategy for MIMO TWRNs.

8. Insightful numerical results are provided to show the performance gains of the proposed strategies, and our analysis is validated through Monte Carlo simulations.

**The chapter is organized as follows:** Section 4.2 outlines the system model and channel model pertinent to both OWRNs and TWRNs. Section 4.4 presents the antenna and relay selection strategies. Section 4.6 provides the statistical characterization of the end-to-end SNR. In Section 4.7, the basic performance metrics of antenna selection strategies are investigated. Section 4.10 provides numerical results, while Section 4.11 draws concluding remarks. All the proofs are provided in Appendix C.

## 4.2 System and channel model

In this section, the system and the channel models pertinent to the OWRNs and TWRNs are presented.

### 4.2.1 System and channel model for OWRNs

We consider a dual-hop cooperative AF OWRN with MIMO-enabled source ($S$), relay ($R$), and destination ($D$) having $N_S$, $N_R$ and $N_D$ antennas, respectively (Fig. 4.1). All terminals operate in the half-duplex mode, and hence, the end-to-end data transmission takes place in two orthogonal time-slots [12]. The CSI and the feedback channels are assumed to be perfect unless otherwise stated[3]. The channel matrix from terminal $X$ to terminal $Y$, where $X \in \{S, R\}, Y \in \{R, D\}$, and $X \neq Y$, is denoted by $\mathbf{H}_{X,Y}$. The $(i, j)$th element of $\mathbf{H}_{X,Y}$ is denoted by $h_{X,Y}^{i,j}$. The channel gains are assumed to be independent and identically distributed (i.i.d.) Nakagami-$m$ fading (with integer $m$). The channel vector from the $j$th

---

[3]In Section 4.9.1, the detrimental impact of feedback delays due to outdated CSI is studied.
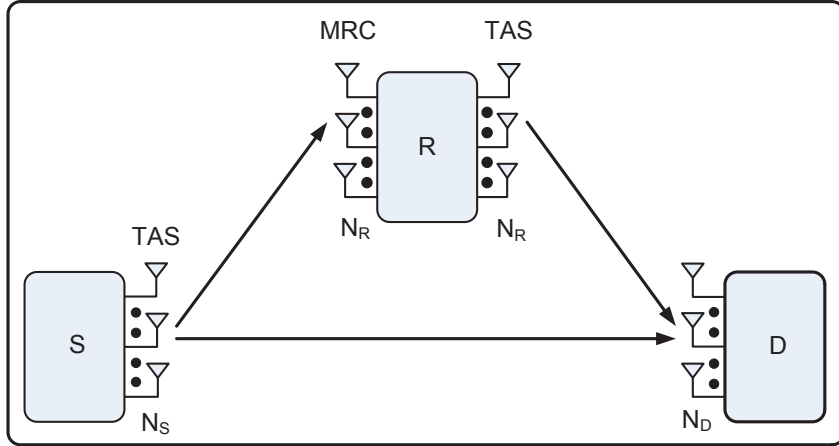
Figure 4.1: The optimal TAS for MIMO OWRNs.
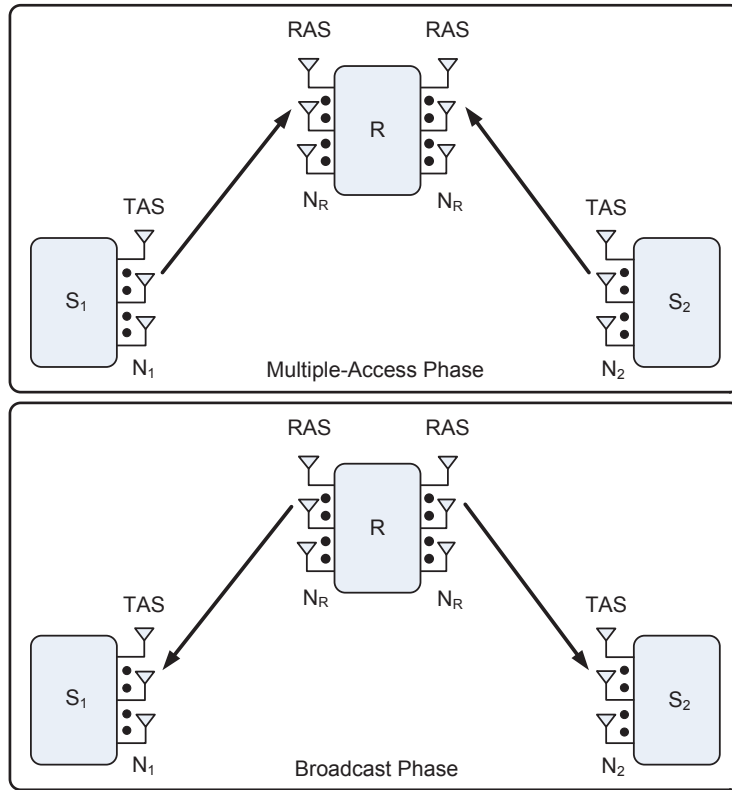


Figure 4.2: The optimal Tx/Rx antenna selection for MIMO TWRNs.

transmit antenna at $X$ to $Y$ is denoted by $\mathbf{h}_{X,Y}^{(j)}$. Moreover, the additive noise at the nodes is modeled as complex zero mean white Gaussian noise.

### 4.2.2 System and channel model for TWRNs

We consider a cooperative MIMO AF TWRN consisting of two source nodes ($S_1$ and $S_2$), and one relay node ($R$) as depicted in Fig. 4.2. Specifically, $S_1$, $S_2$ and $R$ are equipped with $N_1$, $N_2$ and $N_R$ antennas, respectively. All nodes are assumed to be half-duplex, and all channel amplitudes are assumed to be i.i.d. frequency-flat Rayleigh fading. The feedbacks for antenna selection are assumed to be perfect unless otherwise stated[4]. The channel matrix from $S_i$ to $R$ is denoted by $H_{S_i,R}$ for $i \in \{1, 2\}$. In particular, all the channel coefficients are assumed to be fixed over two consecutive time-slots unless otherwise stated [35]. Thus, the channels matrix from $R$ to $S_i$ for $i \in \{1, 2\}$ can be denoted as $(H_{S_i,R})^T$. Moreover, the $(k, l)$th element[5] of $H_{S_i,R}$ is denoted by $h_{S_i,R}^{k,l}$ and is modeled as $h_{S_i,R}^{k,l} \sim \mathcal{CN}(0, \zeta_i)$. Here, $\zeta_i$ for $i \in \{1, 2\}$ accounts for the pathloss effect and is modeled as $\zeta_i \propto (d_{S_i,R})^{-\varpi_i}$, where $d_{S_i,R}$ is the distance between $S_i$ and $R$, and $\varpi$ is the pathloss exponent of $S_i \to R$ channel. The additive noise at all the receivers is modeled as complex zero mean white Gaussian noise. The direct channel between $S_1$ and $S_2$ is assumed to be unavailable due to heavy pathloss and shadowing [35, 37].

## 4.3 Signal model and end-to-end SNR

In this section the signal models for both OWRNs and TWRNs are first presented, and thereby, the respective end-to-end SNRs are derived.

### 4.3.1 Signal model and end-to-end SNR for OWRNs

In the first time-slot, $S$ broadcasts to $R$ and $D$ by employing TAS, and $R$ employs MRC reception. Here, we consider an ideal channel-assisted amplify-and-forward (CA-AF) relay with a gain $G = \sqrt{\frac{\mathcal{P}_R}{\mathcal{P}_S||\mathbf{h}_{SR}^{(i)}||^2}}$ [17, 52, 114] for the sake of mathematical tractability of the moment generating function (MGF) of the end-to-end SNR. In particular, the ideal CA-AF relays invert the source-to-relay channel gain regardless of its fading state. The performance metrics obtained by using ideal CA-AF relays serves as tight (in low-to-high SNR regime) and asymptotically exact lower bounds (in high SNR regime) to that of practical CA-AF relays [17, 52, 114], in which the relay gain is given by $G = \sqrt{\frac{\mathcal{P}_R}{\mathcal{P}_S||\mathbf{h}_{SR}^{(i)}||^2+\sigma_R^2}}$, where $\sigma_R^2$ is the noise variance at the relay. Specifically, the performance metrics derived by using ideal CA-AF relays serve as useful benchmarks for practical CA-AF relay network designing

---

[4]The performance degradation incurred due to feedback delays is analytically studied in Section 4.9.2
[5]Here, $h_{S_i,R}^{k,l}$ is the channel coefficient from the $l$th transmit antenna of $S_i$ to the $k$th receive antenna of $R$.

[52].

In the second time-slot, $R$ first amplifies the received signal and then broadcasts it to $D$ again by employing TAS. Then $D$ combines the two signals received in the two time-slots by applying the optimal receiver filter in the minimum mean square error (MMSE) sense [96, 98]. Under this system model, the post-processing end-to-end SNR at $D$ when $S$ and $R$ transmit from the $i$th antenna and the $k$th antenna, respectively, is given by [96]

$$\gamma_{\text{e2e}}^{(i,k)} = \gamma_{S,D}^{(i)} + \frac{\gamma_{S,R}^{(i)}\gamma_{R,D}^{(k)}}{\gamma_{S,R}^{(i)} + \gamma_{R,D}^{(k)}}, \tag{4.1}$$

where $\gamma_{S,D}^{(i)} = \bar{\gamma}_{S,D}\left|\left|\mathbf{h}_{S,D}^{(i)}\right|\right|_F^2$, $\gamma_{S,R}^{(i)} = \bar{\gamma}_{S,R}\left|\left|\mathbf{h}_{S,R}^{(i)}\right|\right|_F^2$ and $\gamma_{R,D}^{(k)} = \bar{\gamma}_{R,D}\left|\left|\mathbf{h}_{R,D}^{(k)}\right|\right|_F^2$ are the equivalent instantaneous SNRs, and $\bar{\gamma}_{SD}$, $\bar{\gamma}_{SR}$, and $\bar{\gamma}_{RD}$ are the average transmit SNRs of the $S \to D$, $S \to R$, and $R \to D$ channels, respectively. Here, $\gamma_{S,D}^{(i)}$, $\gamma_{S,R}^{(i)}$ and $\gamma_{R,D}^{(k)}$ are independent Gamma distributed random variables; $\gamma_{S,D}^{(i)} \sim \mathcal{G}\left(M_0, \beta_0\right)$, $\gamma_{S,R}^{(i)} \sim \mathcal{G}\left(M_1, \beta_1\right)$ and $\gamma_{R,D}^{(k)} \sim \mathcal{G}\left(M_2, \beta_2\right)$, where $M_0 = m_0 N_D$, $M_1 = m_1 N_R$, $M_2 = m_2 N_D$, $\beta_0 = \frac{\bar{\gamma}_{S,D}}{m_0}$, $\beta_1 = \frac{\bar{\gamma}_{S,R}}{m_1}$ and $\beta_2 = \frac{\bar{\gamma}_{R,D}}{m_2}$. Moreover, $m_0$, $m_1$ and $m_2$ are the integer severity of the fading parameters of the Nakagami fading in the $S \to D$, $S \to R$ and $R \to D$ channels, respectively.

### 4.3.2 Signal model and end-to-end SNR for TWRNs

In two-way relaying, $S_1$ and $S_2$ exchange their information-bearing symbols[6], $\mathbf{x}_1$ and $\mathbf{x}_2$, respectively, in two time-slots. In the first time-slot, both $S_1$ and $S_2$ transmit $\mathbf{x}_1$ and $\mathbf{x}_2$ simultaneously by selecting the $j$th and $l$th transmit antennas, respectively, to $R$ over a multiple access channel. Then $R$ receives the superimposed-signal[7] by selecting the $m$th receive antenna as follows:

$$y_R = \sqrt{\mathcal{P}_{S_1}}h_{S_1,R}^{m,j}\mathbf{x}_1 + \sqrt{\mathcal{P}_{S_2}}h_{S_2,R}^{m,l}\mathbf{x}_2 + n_R, \tag{4.2}$$

where $\mathcal{P}_{S_i}$ for $i \in \{1, 2\}$ is the transmit power of $S_i$, and $n_R$ is the additive white Gaussian noise (AWGN) at $R$ having mean zero and variance $\sigma_R^2$.

In the second time slot, $R$ first amplifies $y_R$ with the following relay amplification factor

$$G = \sqrt{\frac{\mathcal{P}_R}{\left(\mathcal{P}_{S_1}\left|h_{S_1,R}^{m,j}\right|^2 + \mathcal{P}_{S_2}\left|h_{S_2,R}^{m,l}\right|^2 + \sigma_R^2\right)}}. \tag{4.3}$$

---

[6]The information-bearing symbols have unit symbol energies; i.e., $\mathcal{E}\{|\mathbf{x}_1|^2\} = 1$ and $\mathcal{E}\{|\mathbf{x}_2|^2\} = 1$.
[7]This superimposed-signal is also known as the analog network code in the two-way relay networks [38, 91].

and then broadcasts the amplified signal again by using the $m$th transmit antenna to $S_i$ for $i \in \{1, 2\}$ over the broadcast channel. Here, $\mathcal{P}_R$ is the transmit power at $R$. Then, $S_1$ and $S_2$ receive the signals by again using the $j$th and $l$th receive antennas[8], respectively, as follows:

$$y_{S_1} = G h_{S_1,R}^{m,j} Y_R + n_1 \quad \text{and} \quad y_{S_2} = G h_{S_2,R}^{m,l} Y_R + n_2, \tag{4.4}$$

where $n_i \sim \mathcal{CN}\left(0, \sigma_i^2\right)$ for $i \in \{1, 2\}$ is the AWGN at $S_i$. By first substituting (4.2) into (4.4) and then by removing the self-interference[9] [35], the end-to-end SNR at $S_i$ can be derived as

$$\gamma_{S_1}^{(j,l,m)} = \frac{\left(\dfrac{\mathcal{P}_R |h_{S_1,R}^{m,j}|^2}{\sigma_1^2}\right)\left(\dfrac{\mathcal{P}_{S_2} |h_{S_2,R}^{m,l}|^2}{\sigma_R^2}\right)}{\left(\dfrac{\mathcal{P}_R}{\sigma_1^2} + \dfrac{\mathcal{P}_{S_1}}{\sigma_R^2}\right)|h_{S_1,R}^{m,j}|^2 + \dfrac{\mathcal{P}_{S_2} |h_{S_2,R}^{m,l}|^2}{\sigma_R^2} + 1} \quad \text{and}$$

$$\gamma_{S_2}^{(j,l,m)} = \frac{\left(\dfrac{\mathcal{P}_{S_1} |h_{S_1,R}^{m,j}|^2}{\sigma_2^2}\right)\left(\dfrac{\mathcal{P}_R |h_{S_2,R}^{m,l}|^2}{\sigma_R^2}\right)}{\dfrac{\mathcal{P}_{S_1} |h_{S_1,R}^{m,j}|^2}{\sigma_R^2} + \left(\dfrac{\mathcal{P}_R}{\sigma_2^2} + \dfrac{\mathcal{P}_{S_2}}{\sigma_R^2}\right)|h_{S_2,R}^{m,l}|^2 + 1}. \tag{4.5}$$

In Section 4.4.2, the optimal selection of antenna indices ($j$, $l$, and $m$) is described in detail.

## 4.4 Antenna selection strategies

In this section, the antenna selection strategies are presented for both single-relay OWRNs and TWRNs.

### 4.4.1 Optimal transmit antenna selection for OWRNs

The end-to-end SNR $\gamma_{\text{e2e}}^{(i,k)}$ for MIMO OWRNs can be maximized by selecting the best transmit antennas at $S$ and $R$ as follows [96]:

$$(I, K) = \underset{i \in \{1, \cdots, N_S\}, \, k \in \{1, \cdots, N_R\}}{\arg\max} \left(\gamma_{\text{e2e}}^{(i,k)}\right), \tag{4.6}$$

where $\gamma_{\text{e2e}}^{(i,k)}$ is given by (4.1). Besides, $I$ and $K$ are the optimal antenna indexes at $S$ and $R$, respectively. By substituting (4.1) into (4.6), the optimal TAS strategy can be decomposed

---

[8]In the second phase, one would alternatively select the antenna tuple $(j', l', m')$ at $S_1$, $S_2$, and $R$, respectively, which are not necessarily same as $(j, l, m)$. However, the overall achievable diversity order would be the same for both the cases.

[9]It is assumed that $S_i$ knows its own information-bearing symbol $\mathcal{X}_i$ and all the channel coefficients.

as follows:

$$K = \operatorname*{argmax}_{k\in\{1,\cdots,N_R\}} \left(\gamma_{R,D}^{(k)}\right) \quad \text{and} \quad I = \operatorname*{argmax}_{i\in\{1,\cdots,N_S\}} \left(\gamma_{S,D}^{(i)} + \frac{\gamma_{S,R}^{(i)}\gamma_{R,D}^{(K)}}{\gamma_{S,R}^{(i)} + \gamma_{R,D}^{(K)}}\right). \quad (4.7)$$

The decomposition in (4.7) follows from the fact that the end-to-end SNR for a given source transmit antenna can indeed be maximized by maximizing the relay-to-destination channel SNR, and consequently, the antenna selection at the relay is independent of that of the source.

In practice, the direct channel between $S$ and $D$ may be unavailable entirely due to the transmission impairments such as heavy shadowing and pathloss. In this scenario, the optimal TAS strategy selects the transmit antennas at $S$ and $R$ separately to maximize the SNR of the $S \to R$ and $R \to D$ channels, respectively, without considering the $S \to D$ channel. In this context, the optimal TAS strategy which maximizes the end-to-end SNR can be given by

$$I = \operatorname*{argmax}_{i\in\{1,\cdots,N_S\}} \left(\gamma_{SR}^{(i)}\right) \quad \text{and} \quad K = \operatorname*{argmax}_{k\in\{1,\cdots,N_R\}} \left(\gamma_{RD}^{(k)}\right). \quad (4.8)$$

### 4.4.2  Optimal transmit/receive antenna selection for TWRNs

The overall performance of multi-source systems is governed by the performance of the weakest source [26]. Thus, the TWRN is in outage whenever either $S_1$ or $S_2$ is in outage. This observation motivates our antenna selection criterion for TWRNs; the joint maximization of the end-to-end SNR of the weakest source. To this end, the antenna indices at $S_1$, $S_2$ and $R$ are selected to maximize the end-to-end SNR of the worst source and thereby to minimize the overall system outage probability[10] as follows:

$$\{J, L, M\} = \operatorname*{argmax}_{\substack{j\in\{1,\cdots,N_1\},l\in\{1,\cdots,N_2\}\\ m\in\{1,\cdots,N_R\}}} \left(\min\left(\gamma_{S_1}^{(j,l,m)}, \gamma_{S_2}^{(j,l,m)}\right)\right), \quad (4.9)$$

where $J$, $L$, and $M$ are the optimal antenna indices at $S_1$, $S_2$ and $R$, respectively[11], selected to minimize the overall outage probability of TWRNs.

---

[10]Alternatively, the Tx/Rx selection strategy for TWRNs can be seen as the maximization of the mutual information achievable at the worst source. Equivalently, the antenna selection becomes $\{J, L, M\} = \operatorname*{argmax}_{\substack{j\in\{1,\cdots,N_1\},\, l\in\{1,\cdots,N_2\}\\ m\in\{1,\cdots,N_R\}}} \left(\min\left(\mathcal{I}_{S_1}^{(j,l,m)}, \mathcal{I}_{S_2}^{(j,l,m)}\right)\right)$, where $\mathcal{I}_{S_1}^{(j,l,m)} = \frac{1}{2}\log\left(1 + \gamma_{S_1}^{(j,l,m)}\right)$ and $\mathcal{I}_{S_2}^{(j,l,m)} = \frac{1}{2}\log\left(1 + \gamma_{S_2}^{(j,l,m)}\right)$ are the the mutual information at $S_1$ and $S_2$, respectively.

[11]Since the channel matrices, $H_{S_1,R}$ and $H_{S_2,R}$, remain static over the two time-slots, $S_1$, $S_2$ and $R$ can use the $J$th, $L$th and $M$th antennas, respectively, for both transmission and reception.
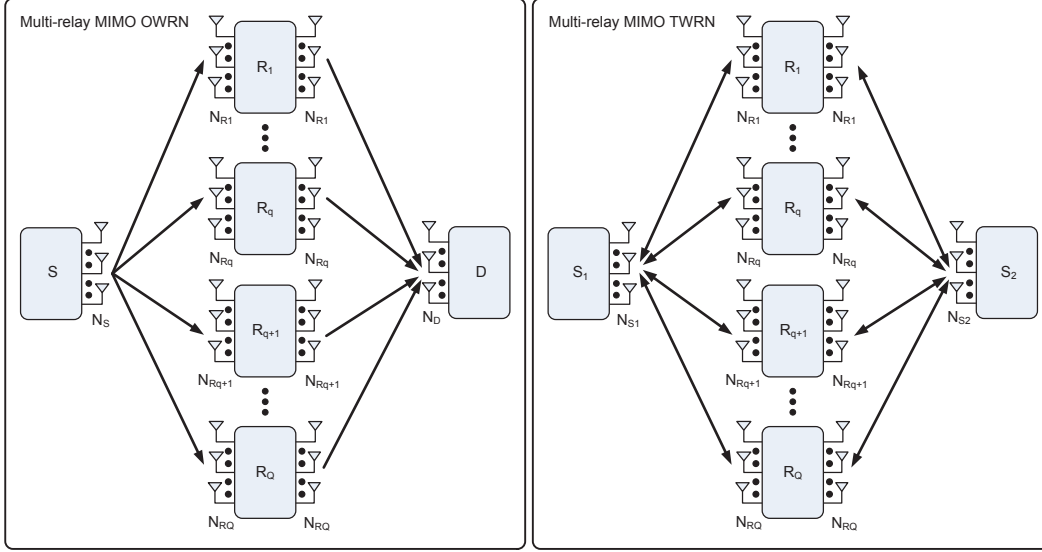
Figure 4.3: Joint antenna and relay selection for MIMO OWRNs/TWRNs.

## 4.5 Joint antenna and relay selection strategies

In this section, the joint antenna and relay selection strategies are proposed for multi-relay OWRNs and TWRNs. To this end, we consider the same system model in Section 4.2. Nevertheless, we now assume that multiple relays are available for cooperation (see Fig. 4.3). Thus, $Q$ relays each having $N_{R_q}$ antennas are assumed to be available, and the $q$th relay is denoted by $R_q$ for $q \in \{1, \cdots, Q\}$. In this context, antennas and relays can indeed be selected jointly to maximize the achievable diversity and spectral efficiency gains.

### 4.5.1 Joint antenna and relay selection for OWRNs

The optimal joint transmit antenna and relay selection strategy for the multi-relay MIMO OWRNs is given by

$$\{I, K, Q^*\} = \operatorname*{argmax}_{\substack{i \in \{1, \cdots, N_S\}, \, k \in \{1, \cdots, N_{R_q}\} \\ q \in \{1, \cdots, Q\}}} \left( \gamma_{\text{e2e}}^{(i,k,q)} \right), \tag{4.10}$$

where $I$, $K$, and $Q^*$ are the best transmit antenna indexes at $S$ and $R$, and the best relay, Moreover, the end-to-end SNR pertinent to the $q$th relay is denoted by $\gamma_{\text{e2e}}^{(i,k,q)}$ and given by[12]

$$\gamma_{\text{e2e}}^{(i,k,q)} = \frac{\gamma_{S,R_q}^{(i)} \gamma_{R_q,D}^{(k)}}{\gamma_{S,R_q}^{(i)} + \gamma_{R_q,D}^{(k)}}, \tag{4.11}$$

---

[12]The direct channel between the source and the destination is assumed to be unavailable due to heavy shadowing and pathloss.

where $\gamma_{S,R_q}^{(i)} = \bar{\gamma}_{S,R_q}||\mathbf{h}_{S,R_q}^{(i)}||^2$ and $\gamma_{R_q,D}^{(k)} = \bar{\gamma}_{R_q,D}||\mathbf{h}_{R_q,D}^{(k)}||^2$ are the equivalent instantaneous SNRs having $\bar{\gamma}_{SR_q}$ and $\bar{\gamma}_{R_qD}$ as the average transmit SNRs of the $S \to R_q$ and $R_q \to D$ channels, respectively. Moreover, $\gamma_{S,R_q}^{(i)}$ and $\gamma_{R_q,D}^{(k)}$ are independent Gamma distributed random variables; $\gamma_{S,R_q}^{(i)} \sim \mathcal{G}\left(m_{SR_q}N_{R_q}, \beta_{SR_q}\right)$ and $\gamma_{R_qD}^{(k)} \sim \mathcal{G}\left(m_{R_qD}N_D, \beta_{R_qD}\right)$, where $\beta_{SR_q} = \bar{\gamma}_{S,R_q}/m_{SR_q}$ and $\beta_{R_qD} = \bar{\gamma}_{R_q,D}/m_{R_qD}$. Besides, $m_{SR_q}$ and $m_{R_qD}$ are the integer severity of the fading parameters of the Nakagami fading in the $S \to R$ and $R \to D$ channels, respectively.

### 4.5.2 Joint antenna and relay selection for TWRNs

The key design criterion of the joint Tx/Rx and relay selection for TWRNs is the joint selection of the best relay ($R_{Q^*}$), and the best antenna indices, $J$, $K$, and $M_{Q^*}$ of $S_1$, $S_2$ and $R_{Q^*}$, respectively, to minimize the overall outage probability. In this context, the joint relay and antenna selection criterion for maximizing the end-to-end SNR of the worst source and thereby for minimizing the overall outage probability is given by

$$\{J, L, Q^*, M_{Q^*}\} = \underset{\substack{i\in\{1,\cdots,N_1\},\, l\in\{1,\cdots,N_2\} \\ q\in\{1,\cdots,Q\},\, m_q\in\{1,\cdots,N_{R_q}\}}}{\mathrm{argmax}} \left(\min\left(\gamma_{S_1}^{(j,l,m_q)}, \gamma_{S_2}^{(j,l,m_q)}\right)\right), \qquad (4.12)$$

where $\gamma_{S_1}^{(j,l,m_q)}$ and $\gamma_{S_2}^{(j,l,m_q)}$ are instantaneous SNRs at $S_1$ and $S_2$ through the $q$th relay $R_q$. Moreover, $\gamma_{S_1}^{(j,l,m_q)}$ and $\gamma_{S_2}^{(j,l,m_q)}$ are defined in (4.5).

## 4.6 Statistical characterization of the SNR

In this section, the statistical characterizations of the end-to-end SNR corresponding to both OWRNs and TWRNs are presented. To be more specific, the cumulative distribution function (CDF) and the MGF of the end-to-end SNR are derived in closed-form.

### 4.6.1 Statistical characterization of the SNR of OWRNs

The statistical characterization of the exact end-to-end SNR of the optimal TAS for OWRNs is mathematically intractable, and hence, a lower bound of the end-to-end SNR is employed. Consequently, the CDF and the MGF of this SNR lower bound are derived as follows:

The CDF of a lower bound of the end-to-end SNR can be derived as (see Appendix C.1

for the proof)

$$F_{\gamma_{e2e}^{lb}}(x) = \left[1 - \sum_{a,b,p,q,l} \mathcal{A}_1\, x^{M_2+b+q} \exp\left(-x\kappa\right) \mathcal{K}_{l-b+1}\left(x\lambda\right)\right]$$

$$\times \left[\sum_{u=0}^{N_S} \sum_{v=0}^{u(M_2-1)} \mathcal{B}_1 x^v \exp\left(-\frac{ux}{\beta_0}\right)\right], \qquad (4.13a)$$

where $\mathcal{A}_1$, $\mathcal{B}_1$, $\kappa$ and $\lambda$ are defined as

$$\mathcal{A}_1 = \frac{2N_R\binom{N_s}{a}\binom{N_R-1}{p}\binom{M_1+b+q-1}{l}(-1)^{a+p+1}\phi_{b,a,M_1}\phi_{q,p,M_2}}{\Gamma(M_2)a^{\frac{b-l-1}{2}}(p+1)^{\frac{l-b+1}{2}}\beta_1^{\frac{l+b+1}{2}}\beta_2^{\frac{2M_2+2q-l+b-1}{2}}} \qquad (4.13b)$$

$$\mathcal{B}_1 = (-1)^u \binom{N_S}{u} \frac{\phi_{v,u,M_0}}{\beta_0}, \quad \kappa = \frac{a}{\beta_1} + \frac{p+1}{\beta_2} \quad \text{and} \qquad (4.13c)$$

$$\lambda = 2\sqrt{\frac{a(p+1)}{\beta_1\beta_2}}, \quad \text{respectively.} \qquad (4.13d)$$

Further, $\displaystyle\sum_{a,b,p,q,l} = \sum_{a=1}^{N_S}\sum_{b=0}^{a(M_1-1)}\sum_{p=0}^{N_R-1}\sum_{q=0}^{p(M_2-1)}\sum_{l=0}^{M_2+b+q-1}$ and $\phi_{k,N,L}$ is the coefficient of the

expansion of $\displaystyle\left[\sum_{u=0}^{L-1}\frac{1}{u!}\left(\frac{x}{\bar\gamma}\right)^u\right]^N = \sum_{k=0}^{N(L-1)}\phi_{k,N,L}\left(\frac{x}{\bar\gamma}\right)^k$ and given by [115, Eqn. (44)]

$$\phi_{k,N,L} = \sum_{i=k-L+1}^{k}\frac{\phi_{i,N-1,L}}{(k-i)!}I_{[0,(N-1)(L-1)]}(i), \qquad (4.14)$$

$\phi_{0,0,L} = \phi_{0,N,L} = 1$, $\phi_{k,1,L} = 1/\ k!$, $\phi_{1,N,L} = N$ and $I_{[a,c]}(b) = \begin{cases} 1, & a \le b \le c \\ 0, & \text{otherwise} \end{cases}$.

The CDF of the end-to-end SNR for the optimal TAS strategy of MIMO OWRNs without having the direct channel is next derived as (see Appendix C.2 for the proof)

$$F_{\gamma_{e2e}}(x) = 1 - \sum_{p=1}^{N_R}\sum_{q=0}^{p(M_2-1)}\sum_{a=0}^{N_S-1}\sum_{b=0}^{a(M_1-1)}\sum_{c=0}^{M_1+q+b-1}\mathcal{A}_2 x^{M_1+b+q}\,e^{-\delta x}\mathcal{K}_{c-q+1}(\epsilon x), \quad (4.15a)$$

where $\mathcal{A}_3$ is given by

$$\mathcal{A}_2 = \frac{2(-1)^{p+q+1}N_S p^{\frac{\zeta}{2}}\binom{N_R}{p}\binom{N_S-1}{a}\binom{M_1+q+b-1}{c}\phi_{q,p,M_2}\phi_{b,a,M_1}}{\Gamma(M_1)(a+1)^{\frac{\zeta}{2}}\beta_1^{\frac{2M_1+q+2b-c-1}{2}}\beta_2^{\frac{c+q+1}{2}}}. \qquad (4.15b)$$

Besides, in (4.15a) and (4.15b), $\delta = \frac{a+1}{\beta_1} + \frac{p}{\beta_2}$ and $\epsilon = 2\sqrt{\frac{p(a+1)}{\beta_1\beta_2}}$.

The MGF of $\gamma_{\text{e2e}}^{lb}$ is defined as

$$\mathcal{M}_{\gamma_{\text{e2e}}^{lb}}(s) = \mathcal{E}_{\gamma_{\text{e2e}}^{lb}}\{\exp(-s\gamma)\} = \int_0^\infty sF_{\gamma_{\text{e2e}}^{lb}}(\gamma)\exp(-s\gamma)\,\mathrm{d}\gamma. \tag{4.16}$$

The MGF of $\gamma_{\text{e2e}}^{lb}$ can be derived by first substituting (4.13a) into (4.16) and by using [1, Eqn. (6.621.3)] as follows:

$$
\begin{aligned}
\mathcal{M}_{\gamma_{\text{e2e}}^{lb}}(s) &= \sum_{u=0}^{N_S}\sum_{v=0}^{u(M_0-1)}\mathcal{B}_1\beta_0^2\Gamma(v+1)\frac{s}{(u+s\beta_0)^{v+1}} \\
&\quad - \sum_{a,b,p,q,l}\sum_{u=0}^{N_S}\sum_{v=0}^{m(M_0-1)}\frac{\mathcal{A}_1\sqrt{\pi}(-1)^u(2\lambda)^\zeta\Gamma(\eta+\zeta)\Gamma(\eta-\zeta)}{\beta_0^v\Gamma(\eta+\frac{1}{2})} \\
&\quad \times \frac{s\ _2\mathcal{F}_1\left(\eta+\zeta,\zeta+\frac{1}{2};\eta+\frac{1}{2};\frac{s+\kappa-\lambda}{s+\kappa+\lambda}\right)}{(s+\kappa+\lambda)^{\eta+\zeta}},
\end{aligned} \tag{4.17}
$$

where $\sum\limits_{a,b,p,q,l}$ is defined in (4.13a). Besides, $\eta$, $\zeta$, $\kappa$, and $\lambda$ depend on the summation variables and are defined as $\eta = M_2 + b + q + v + 1$, $\zeta = l - b + 1$, $\kappa = \frac{a}{\beta_1} + \frac{p+1}{\beta_2}$, and $\lambda = 2\sqrt{\frac{a(p+1)}{\beta_1\beta_2}}$, respectively.

The MGF of the end-to-end SNR for the optimal TAS strategy of MIMO OWRNs without having the direct channel is next derived as

$$
\begin{aligned}
\mathcal{M}_{\gamma_{\text{e2e}}}(s) &= 1 - \sum_{p,q,a,b,c} = \sum_{p=1}^{N_R}\sum_{q=0}^{p(M_2-1)}\sum_{a=0}^{N_S-1}\sum_{b=0}^{a(M_1-1)}\sum_{c=0}^{M_1+q+b-1}\mathcal{A}_2\sqrt{\pi}(2\epsilon)^{c-q+1} \\
&\quad \times \frac{\Gamma(\eta+\zeta)\Gamma(\eta-\zeta)s\ _2\mathcal{F}_1\left(\eta+\zeta,\zeta+\frac{1}{2};\eta+\frac{1}{2};\frac{s+\delta-\epsilon}{s+\delta+\epsilon}\right)}{\Gamma(\eta+\frac{1}{2})(s+\delta+\epsilon)^{\eta+\zeta}},
\end{aligned} \tag{4.18}
$$

where $\mathcal{A}_2$ is given by (4.15b). Moreover, the parameters $\delta$, $\eta$, $\zeta$, and $\epsilon$ depend on the summation variables and are defined as $\delta = \frac{a+1}{\beta_1} + \frac{p}{\beta_2}$, $\eta = M_1 + b + q + 1$, $\zeta = c - q + 1$ and $\epsilon = 2\sqrt{\frac{p(a+1)}{\beta_1\beta_2}}$, respectively.

The PDF of $\gamma_{\text{e2e}}^{lb}$ can be readily derived by differentiating the CDF of $\gamma_{\text{e2e}}^{lb}$ with respect to $x$ by using [1, Eqn. (8.486.12)]. However, the probability density function (PDF) result is omitted for the sake of brevity.

## 4.6.2 Statistical characterization of the SNR of TWRNs

In analyzing the performance of the proposed Tx/Rx selection strategy for TWRNs, the statistical characterization of the instantaneous end-to-end SNR of the weakest source is essential. Thus, the end-to-end SNR of the weakest source is defined as

$$Z = \max_{\substack{j\in\{1,\cdots,N_1\},\,l\in\{1,\cdots,N_2\} \\ m\in\{1,\cdots,N_R\}}}\left(\min\left(\gamma_{S_1}^{(j,l,m)},\gamma_{S_2}^{(j,l,m)}\right)\right). \tag{4.19}$$

The CDF of the random variable $Z$ is then derived as (see Appendix C.4 for the proof)

$$
\begin{aligned}
F_Z(z) &= \left[ \mathbb{F}\left( z, \frac{p+1}{\zeta_1}, \frac{q+1}{\zeta_2}, \frac{q}{\zeta_2}, \frac{N_1}{\zeta_1}, N_1 - 1, N_2 \right) \right. \\
&\quad + \left. \mathbb{F}\left( z, \frac{q+1}{\zeta_2}, \frac{p+1}{\zeta_1}, \frac{p}{\zeta_1}, \frac{N_2}{\zeta_2}, N_1, N_2 - 1 \right) \right]^{N_R},
\end{aligned}
\tag{4.20}
$$

where the function $\mathbb{F}\left( z, a, b, c, d, u, v \right)$ is given by

$$
\begin{aligned}
\mathbb{F}\left( z, a, b, c, d, u, v \right) &= \sum_{p=0}^{N_1-1} \sum_{q=0}^{N_2-1} \frac{N_1 N_2 \binom{N_1-1}{p}\binom{N_2-1}{q}(-1)^{p+q}}{b\zeta_1\zeta_2} \\
&\times \left[ \frac{1 - \exp\left(-a\beta z\right)}{a} - \frac{1 - \exp\left(-(a+b)\beta z\right)}{a+c} \right] \\
&+ \sum_{p=0}^{u} \sum_{q=0}^{v} d\binom{u}{p}\binom{v}{q}(-1)^{p+q} \left[ \frac{\exp\left(-(a+c)\beta z\right)\left(1 - \exp\left(-(a+c)\phi(z)\right)\right)}{a+c} \right. \\
&\times \left. - \frac{\exp\left(-(a\phi(z) + (a\beta + c\alpha)z)\right)}{a} \mathcal{J}(z) \right].
\end{aligned}
\tag{4.21}
$$

In (4.21), $\alpha = \frac{\bar{\gamma}_S\bar{\gamma}_R}{\bar{\gamma}_R+\bar{\gamma}_T}$, $\beta = \frac{1}{\bar{\gamma}_R}$, $\phi(z) = \frac{1}{\bar{\gamma}_S\bar{\gamma}_R}\sqrt{(\bar{\gamma}_S^2 + \bar{\gamma}_S\bar{\gamma}_R + \bar{\gamma}_R^2/4)z^2 + \bar{\gamma}_S\bar{\gamma}_R z} + \frac{z}{2\bar{\gamma}_S}$. Moreover, the function $\mathcal{J}(z)$ in (4.21) can be given in two forms as follows:

1. By using Gauss-Laguerre quadrature (GLQ) [116, Eqn. (25.4.45)], $\mathcal{J}(z)$ can be evaluated as

$$
\mathcal{J}(z) = \sum_{t=1}^{T_g} w_t \exp\left( -\frac{acz(\alpha\beta z + \eta)}{x_t + a\phi(z)} \right) + \mathcal{R}_{T_g}.
\tag{4.22}
$$

where $\eta = \frac{1}{\bar{\gamma}_S\bar{\gamma}_S}$. Here, $x_t$ and $w_t$ for $t \in \{1, \cdots, T_g\}$ are the abscissas and weights of the GLQ, respectively, and they can be efficiently computed by using the classical algorithm in [117] (see Appendix C.4 for more details). Moreover, $T_g$ is the number of terms used for the GLQ, and $\mathcal{R}_{T_g}$ is the remainder term, which diminishes as $T_g$ approaches as small as 10 [117].

2. Alternatively, by using Taylor series expansion, the function $\mathcal{J}(z)$ can be derived as

$$
\mathcal{J}(z) = \sum_{i=0}^{\infty} \frac{(-1)^i}{i!}(acz(\alpha\beta z + \eta))^i \exp\left(a\phi(z)\right) \Gamma\left(1 - i, a\phi(z)\right).
\tag{4.23}
$$

The convergence of the infinite series in $\mathcal{J}(x)$ is discussed in Appendix C.4.

## 4.7  Performance analysis of antenna selection

In this section, the basic performance metrics of the antenna and relay selection strategies for both OWRNs and TWRNs are presented. To be more specific, the outage probability,

77

the average SER, and the corresponding high SNR approximations are derived, and thereby, valuable insights and guidelines into practical system-designing are obtained by deriving the achievable diversity order and the array gains.

### 4.7.1   Outage probability of optimal TAS for OWRNs

The outage probability[13] of the optimal TAS strategy for MIMO OWRNs is denoted by $P_{out}$ and defined as the probability that the end-to-end SNR falls below a preset threshold $\gamma_{th}$. Thus, $P_{out}$ is given by

$$P_{out} = \Pr\left(\gamma_{\text{e2e}}^{(I,K)} \leq \gamma_{th}\right) = \Pr\left(\max_{i \in \{1,\cdots,N_S\},\, k \in \{1,\cdots,N_R\}}\left(\gamma_{\text{e2e}}^{(i,k)}\right) \leq \gamma_{th}\right), \quad (4.24)$$

where $\gamma_{\text{e2e}}^{(i,k)}$ is defined in (4.1). An upper bound for the outage probability of MIMO OWRNs having the direct channel can be now derived in closed-form by evaluating the CDF of the SNR lower bound in (4.13a) at the threshold SNR, $\gamma_{th}$. Moreover, the exact outage probability of the MIMO OWRNs without having the direct channel can be then derived by evaluating the CDF of the exact SNR in (4.15a) at $\gamma_{th}$.

In order to obtain direct insights into the achievable diversity order and array gain, the asymptotic outage probability at high SNRs pertinent to the optimal TAS strategy for MIMO OWRNs with the direct channel is derived as follows (see Appendix C.3 for the proof):

$$P_{out}^\infty = \begin{cases} \Omega_1\left(\frac{\gamma_{th}}{\bar{\gamma}}\right)^{m_0 N_S N_d + m_1 N_S N_R} + o\left(\bar{\gamma}^{-(m_0 N_S N_d + m_1 N_S N_R)}\right), & m_1 N_S < m_2 N_D \\ \Omega_2\left(\frac{\gamma_{th}}{\bar{\gamma}}\right)^{m_0 N_S N_D + m_2 N_R N_D} + o\left(\bar{\gamma}^{-(m_0 N_S N_D + m_2 N_R N_D)}\right), & m_1 N_S > m_2 N_D \\ (\Omega_1 + \Omega_2)\left(\frac{\gamma_{th}}{\bar{\gamma}}\right)^{m_0 N_S N_D + mN N_R} + o\left(x^{m_0 N_S N_D + mN N_R}\right), & m_1 N_s = m_2 N_d = mN, \end{cases} \quad (4.25a)$$

where $\Omega_1$ and $\Omega_2$ are given by

$$\Omega_1 = \frac{(m_0/k_0)^{m_0 N_S N_D}(m_1/k_1)^{m_1 N_S N_R}\,(m_1 N_S N_R)!\,(m_0 N_S N_D)!}{\left((m_0 N_D)!\,(m_1 N_R)!\right)^{N_S}\,(m_0 N_S N_D + m_1 N_S N_R)!}, \quad (4.25b)$$

$$\Omega_2 = \frac{(m_0/k_0)^{m_0 N_S N_D}(m_2/k_2)^{m_2 N_R N_D}\,(m_2 N_R N_D)!\,(m_0 N_S N_D)!}{\left((m_0 N_D)!\,(m_2 N_D)!\right)^{N_S}\,(m_0 N_S N_D + m_2 N_R N_D)!}. \quad (4.25c)$$

In (4.25b) and (4.25c), $k_0$, $k_1$, and $k_2$ are defined as $k_0 = \bar{\gamma}_{S,D}/\bar{\gamma}$, $k_1 = \bar{\gamma}_{S,R}/\bar{\gamma}$, and $k_2 = \bar{\gamma}_{R,D}/\bar{\gamma}$, respectively. By using (4.25a), the achievable diversity order of the optimal TAS strategy for MIMO OWRNs can be quantified as $G_d = m_0 N_S N_D + N_R \min\left(m_1 N_S, m_2 N_D\right)$.

---

[13]The information capacity outage probability can be defined as the probability that the instantaneous mutual information $\mathcal{I}$ falls below the target rate $\mathcal{R}_{th}$; $\Pr\left(\frac{1}{2}\log\left(1 + \gamma_{\text{e2e}}^{(I,K)}\right) \leq \mathcal{R}_{th}\right) = F_{\gamma_{\text{e2e}}}(\gamma_{th})$, where $\gamma_{th} = 2^{2\mathcal{R}_{th}} - 1$.

Similarly, the asymptotic outage probability at high SNRs of the optimal TAS strategy for MIMO OWRNs without having the direct channel is derived as follows (see Appendix C.3 for the proof):

$$P_{out}^\infty = \begin{cases} \Pi_1 \left(\frac{\gamma_{th}}{\bar{\gamma}}\right)^{m_1 N_S N_R} + o\left(\bar{\gamma}^{-(m_1 N_S N_R+1)}\right), & m_1 N_S < m_2 N_D \\ \Pi_2 \left(\frac{\gamma_{th}}{\bar{\gamma}}\right)^{m_2 N_R N_D} + o\left(\bar{\gamma}^{-(m_2 N_R N_D)}\right), & m_1 N_S > m_2 N_D \\ (\Pi_1 + \Pi_2) \left(\frac{\gamma_{th}}{\bar{\gamma}}\right)^{m_1 N_S N_R} + o\left(\bar{\gamma}^{-(mNN_R)}\right), & m_1 N_S = m_2 N_D = mN, \end{cases} \quad (4.26)$$

where $\Pi_1$ and $\Pi_2$ are given by

$$\Pi_1 = \frac{(m_1/k_1)^{m_1 N_S N_R}}{\left((m_1 N_R)!\right)^{N_S}} \quad \text{and} \quad \Pi_2 = \frac{(m_2/k_2)^{m_2 N_R N_D}}{\left((m_2 N_D)!\right)^{N_R}}. \quad (4.27)$$

Again, the achievable diversity order of the optimal TAS for MIMO OWRNs without having the direct channel is quantified to be $G_d = N_R \min(m_1 N_S, m_2 N_D)$.

### 4.7.2   Outage probability of optimal Tx/Rx antenna selection for TWRNs

The outage probability performance of multi-source systems is governed by the performance of the weakest source [26]. Thus, the TWRN of interest is indeed considered as a multi-source system, and hence, it is in outage if either $S_1$ or $S_2$ is in outage. This observation motivates the our outage probability definition of TWRNs. The outage probability of the optimal Tx/Rx antenna selection for MIMO TWRNs is therefore defined as the probability that the end-to-end SNR of the weakest source falls below a preset threshold $(\gamma_{th})$ and is given by

$$P_{out} = \Pr\left[ Z = \max_{\substack{j \in \{1,\cdots,N_1\}, \, j \in \{1,\cdots,N_2\} \\ m \in \{1,\cdots,N_R\}}} \left(\min\left(\gamma_{S_1}^{(j,l,m)}, \gamma_{S_2}^{(j,l,m)}\right)\right) \leq \gamma_{th} \right]. \quad (4.28)$$

The outage probability of interest can be then derived by evaluating the CDF of $Z$ given in (4.20) at the preset threshold, $\gamma_{th}$, as

$$\begin{aligned} P_{out} &= \Bigg[ \mathbb{F}\left(\gamma_{th}, \frac{p+1}{\zeta_1}, \frac{q+1}{\zeta_2}, \frac{q}{\zeta_2}, \frac{N_1}{\zeta_1}, N_1 - 1, N_2\right) \\ &\quad + \mathbb{F}\left(\gamma_{th}, \frac{q+1}{\zeta_2}, \frac{p+1}{\zeta_1}, \frac{p}{\zeta_1}, \frac{N_2}{\zeta_2}, N_1, N_2 - 1\right) \Bigg]^{N_R}, \end{aligned} \quad (4.29)$$

where the function $\mathbb{F}(z, a, b, c, d, u, v)$ has already been defined in (4.21).

To obtain direct insights, the asymptotic outage probability at high SNRs of the optimal Tx/Rx antenna selection for the MIMO TWRNs is derived as (see Appendix C.5 for the proof)

$$P_{out}^\infty = \Delta \left(\frac{\gamma_{th}}{\bar{\gamma}}\right)^{G_d} + o\left(\bar{\gamma}^{-G_d}\right), \quad (4.30a)$$

where $G_d$ is the achievable diversity order and given by

$$G_d = N_R \min (N_1, N_2).$$ (4.30b)

Furthermore, the system-dependent parameter $\Delta$ is given by

$$\Delta = \begin{cases} \left(\frac{C_S+C_R}{\zeta_1 C_S C_R}\right)^{N_1 N_R}, & N_1 < N_2 \\ \left(\frac{C_S+C_R}{\zeta_2 C_S C_R}\right)^{N_2 N_R}, & N_1 > N_2 \\ \left(\frac{1}{\zeta_1^N} + \frac{1}{\zeta_2^N}\right)^{N_R} \left(\frac{C_S+C_R}{C_S C_R}\right)^{N N_R}, & N_1 = N_2 = N, \end{cases}$$ (4.30c)

where $C_S$ and $C_R$ are the ratios of the source and relay average transmit SNR to the reference average transmit SNR ($\bar{\gamma}$), respectively; i.e., $C_S = \bar{\gamma}_S/\bar{\gamma}$ and $C_R = \bar{\gamma}_R/\bar{\gamma}$.

### 4.7.3 Average symbol error rate of optimal TAS for OWRNs

The average SER of the optimal TAS strategy is derived by averaging the conditional error probability (CEP) over the PDF of the end-to-end SNR. The CEP of the coherent binary phase shift keying (BPSK) and $M$-ary pulse amplitude modulation (PAM) can be expressed as $P_e|\gamma = \alpha Q(\sqrt{\varphi \gamma})$, where $\alpha$ and $\varphi$ are modulation-dependent constants [32, 62]. Thus, an upper bound for the average SER for MIMO OWRNs with the direct channel can be derived by first substituting (4.13a) into the SER integral [62], $\bar{P}_e^{ub} = \frac{\alpha}{2}\sqrt{\frac{\varphi}{2\pi}} \int_0^\infty x^{-\frac{1}{2}} e^{-\frac{\varphi x}{2}} F_{\gamma_{e2e}^{lb}}(x) \, \mathrm{d}x$, and then solving the resulting integral by using [1, Eqn. (6.621.3)] as follows:

$$\bar{P}_e^{ub} = \sum_{u=0}^{N_S} \sum_{v=0}^{u(M_2-1)} \frac{2^{v-1}\alpha\sqrt{\varphi}\beta_0^{\frac{3}{2}}\Gamma(v+\frac{1}{2})}{\sqrt{\pi}(2u+\varphi\beta_0)^{v+\frac{1}{2}}} - \sum_{a,b,p,q,l} \sum_{u=0}^{N_S} \sum_{v=0}^{u(M_2-1)} \frac{\mathcal{A}_1\alpha\sqrt{\varphi}(-1)^u}{2^{\frac{3}{2}}\beta_0^v\Gamma(\eta+\frac{1}{2})}$$

$$\times \frac{(2\lambda)^\zeta\Gamma(\eta+\zeta)\Gamma(\eta-\zeta) \, {}_2F_1\left(\eta+\zeta, \zeta+\frac{1}{2}; \eta+\frac{1}{2}; \frac{\psi-\lambda}{\psi+\lambda}\right)}{(\psi+\lambda)^{\eta+\zeta}},$$ (4.31)

where $\mathcal{A}_1$ and $\sum_{a,b,p,q,l}$ are defined in (4.13a). Besides, $\psi$, $\eta$, $\zeta$, and $\lambda$ depend on the summation variables and are defined as $\psi = \frac{\varphi}{2} + \frac{u}{\beta_0} + \frac{a}{\beta_1} + \frac{p+1}{\beta_2}$, $\eta = M_2 + b + q + v + \frac{1}{2}$, $\zeta = l - b + 1$ and $\lambda = 2\sqrt{\frac{a(p+1)}{\beta_1\beta_2}}$, respectively.

The average SER of the optimal TAS strategy for MIMO OWRNs without having the direct channel is then derived as

$$\bar{P}_e = \frac{\alpha}{2} - \frac{\alpha}{2}\sqrt{\frac{\varphi}{2}} \sum_{p=1}^{N_R} \sum_{q=0}^{p(M_2-1)} \sum_{a=0}^{N_S-1} \sum_{b=0}^{a(M_1-1)} \sum_{c=0}^{M_1+q+b-1} \frac{\mathcal{A}_3(2\epsilon)^\nu\Gamma(\mu+\nu)\Gamma(\mu-\nu)}{\Gamma(\mu+\frac{1}{2})}$$

$$\times \frac{{}_2F_1\left(\mu+\nu, \nu+\frac{1}{2}; \mu+\frac{1}{2}; \frac{\frac{\varphi}{2}+\delta-\epsilon}{\frac{\varphi}{2}+\delta+\epsilon}\right)}{(\frac{\varphi}{2}+\delta+\epsilon)^{\mu+\nu}},$$ (4.32a)

where $\mathcal{A}_3$ is given by

$$\mathcal{A}_3 = \frac{2N_S\binom{N_R}{p}\binom{N_S-1}{a}\binom{M_1+q+b-1}{c}(-1)^{p+q+1}p^{\frac{c-q+1}{2}}\phi_{q,p,M_2}\phi_{b,a,M_1}}{\Gamma(M_1)(a+1)^{\frac{c-q+1}{2}}\beta_1^{\frac{2M_1+2b+q-c-1}{2}}\beta_2^{\frac{c+q+1}{2}}}. \tag{4.32b}$$

In (4.32a), $\mu$, $\nu$, $\delta$, and $\epsilon$ depend on the summation variables and are defined as $\mu = M_1 + b + q + 1/2$, $\nu = l - q + 1$, $\delta = \frac{a+1}{\beta_1} + \frac{p}{\beta_2}$ and $\epsilon = 2\sqrt{\frac{p(a+1)}{\beta_1\beta_2}}$, respectively.

To obtain valuable insights into the achievable diversity order and the array gain, the asymptotic average SER at high SNRs for MIMO OWRNs with the direct channel is derived as follows (see Appendix C.3 for the proof):

$$P_e^\infty = \frac{\Omega\alpha 2^{G_d-1}\Gamma(G_d+1/2)}{\sqrt{\pi}(\varphi\bar{\gamma})^{G_d}} + o\left(\bar{\gamma}^{-G_d}\right). \tag{4.33a}$$

In (4.33a), the system dependent parameter $\Omega$ is defined as

$$\Omega = \begin{cases} \Omega_1, & m_1N_S < m_2N_D \\ \Omega_2, & m_1N_S > m_2N_D \\ \Omega_1 + \Omega_2, & m_1N_s = m_2N_d = mN, \end{cases} \tag{4.33b}$$

where $\Omega_1$ and $\Omega_2$ are defined in (4.25b) and (4.25c), respectively. Moreover, the achievable diversity order and the array gain are given by

$$G_d = m_0N_SN_D + N_R\min\left(m_1N_S, m_2N_D\right), \tag{4.33c}$$

$$G_a = \left(\frac{\Omega\alpha 2^{G_d-1}\Gamma(G_d+\frac{1}{2})}{\sqrt{\pi}(\varphi)^{G_d}}\right)^{-\frac{1}{G_d}}. \tag{4.33d}$$

The high SNR asymptotic average SER of the optimal TAS for the MIMO OWRNs without having the direct channel can also be obtained by replacing $\Omega$ and $G_d$ of (4.33b) with

$$\Pi = \begin{cases} \Pi_1, & m_1N_S < m_2N_D \\ \Pi_2, & m_1N_S > m_2N_D \\ \Pi_1 + \Pi_2, & m_1N_s = m_2N_d = mN \end{cases} \text{and} \quad G_d = N_R\min\left(m_1N_S, m_2N_D\right), \tag{4.34}$$

where $\Pi_1$ and $\Pi_2$ are defined in (4.27).

### 4.7.4 Average symbol error rate of optimal antenna selection for TWRNs

The derivation of the exact average SER of the optimal Tx/Rx antenna selection for MIMO TWRNs appears mathematically intractable. However, in order to obtain useful insights into system-designing parameters such as the diversity order and the array gain, the asymptotic average SER at high SNRs can indeed be derived as follows:

$$P_e^\infty = \frac{\Delta\alpha 2^{G_d-1}\Gamma(G_d+1/2)}{\sqrt{\pi}(\varphi\bar{\gamma})^{G_d}} + o\left(\bar{\gamma}^{-G_d}\right), \tag{4.35a}$$

81

where the system dependent parameter $\Delta$ is defined in (4.30c). Besides, the achievable diversity order and the array gain are given by

$$G_d = N_R \min(N_1, N_2),$$ (4.35b)

$$G_a = \left( \frac{\Delta \alpha 2^{G_d-1} \Gamma(G_d+\frac{1}{2})}{\sqrt{\pi}(\varphi)^{G_d}} \right)^{-\frac{1}{G_d}}.$$ (4.35c)

## 4.8 Performance analysis of joint antenna and relay selection

In this section, the performance of the proposed joint antenna and relay selection strategies is investigated for both MIMO OWRNs and MIMO TWRNs. To this end, the overall outage probability, high SNR outage approximation, and the achievable diversity order are derived in closed-form.

### 4.8.1 Outage probability of joint antenna and relay selection for OWRNs

The overall outage probability of the optimal joint transmit antenna and relay selection for MIMO OWRNs can be derived as

$$
\begin{aligned}
P_{out} &= \Pr\left( \max_{\substack{i\in\{1,\cdots,N_S\},\, k\in\{1,\cdots,N_{R_q}\} \\ q\in\{1,\cdots,Q\}}} \left( \frac{\gamma_{S,R_q}^{(i)}\gamma_{R_q,D}^{(k)}}{\gamma_{S,R_q}^{(i)}+\gamma_{R_q,D}^{(k)}} \right) \le \gamma_{th} \right) \\
&= \Pr\left( \max_{q\in\{1,\cdots,Q\}} \left( \max_{\substack{i\in\{1,\cdots,N_S\} \\ k\in\{1,\cdots,N_{R_q}\}}} \left( \frac{\gamma_{S,R_q}^{(i)}\gamma_{R_q,D}^{(k)}}{\gamma_{S,R_q}^{(i)}+\gamma_{R_q,D}^{(k)}} \right) \right) \le \gamma_{th} \right).
\end{aligned}
$$ (4.36)

The second equality of (4.36) yields from the mutual independence of $\gamma_{S,R_q}^{(i)}$ and $\gamma_{R_q,D}^{(k)}$ for $q \in \{1, \cdots, Q\}$. Next, (4.36) can be further simplified by solving the inner maximization problem as

$$P_{out} = \Pr\left( \max_{q\in\{1,\cdots,Q\}} \left( \frac{\gamma_{S,R_q}^{(I)}\gamma_{R_q,D}^{(K)}}{\gamma_{S,R_q}^{(I)}+\gamma_{R_q,D}^{(K)}} \right) \le \gamma_{th} \right),$$ (4.37)

where $\gamma_{S,R_q}^{(I)} = \max\limits_{i\in\{1,\cdots,N_S\}} \left( \gamma_{S,R_q}^{(i)} \right)$ and $\gamma_{R_q,D}^{(K)} = \max\limits_{k\in\{1,\cdots,N_{R_q}\}} \left( \gamma_{R_q,D}^{(k)} \right)$. The overall outage probability of the joint transmit antenna and relay selection for MIMO OWRNs can be then derived in closed-form as follows:

$$
\begin{aligned}
P_{out} &= \prod_{q=1}^{Q} \left[ 1 - \sum_{a=0}^{\mu_q-1} \sum_{b=0}^{a(\lambda_q-1)} \sum_{p=1}^{\psi_q} \sum_{l=0}^{p(\xi_q-1)} \sum_{u=0}^{l} \sum_{v=0}^{\lambda_q+b-1} \mathcal{A}_4 \gamma_{th}^{\lambda_q+b+l} \right. \\
&\quad \times \left. \exp\left( -\gamma_{th}\left( \frac{a+1}{\beta_{SR_q}} + \frac{p}{\beta_{R_qD}} \right) \right) \mathcal{K}_{u+v-l+1}\left( 2\gamma_{th}\sqrt{\frac{p(a+1)}{\beta_{SR_q}\beta_{R_qD}}} \right) \right],
\end{aligned}
$$ (4.38)

where $\mathcal{A}_4$ is given by

$$\mathcal{A}_4 = \frac{2(-1)^{a+p+1}\mu_q\binom{\psi_q}{p}\binom{\mu_q-1}{a}\binom{l}{u}\binom{\lambda_q+b-1}{v}p^{\frac{u+v-l+1}{2}}\phi_{b,a,\lambda_q}\phi_{q,p,\xi_q}}{\Gamma(\lambda_q)(a+1)^{\frac{u+v-l+1}{2}}(\beta_{SRq})^{\frac{2\lambda_q+2b+l-u-v-1}{2}}(\beta_{R_qD})^{\frac{u+v+l+1}{2}}}. \tag{4.39}$$

Here, in (4.38) and (4.39), the system dependent $\lambda_q$, $\mu_q$, $\xi_q$, and $\psi_q$ are defined as $\lambda_q = m_{SR_q}N_{R_q}$, $\mu_q = N_S$, $\xi_q = m_{R_qD}N_D$, and $\psi_q = N_{R_q}$, respectively.

To obtain direct insights into the achievable diversity order of the joint antenna and relay selection for MIMO OWRNs, the asymptotic outage probability at high SNRs is derived as follows:

$$P_{\text{out}}^{\infty} = \left[\prod_{q=1}^{Q}\Omega_q\right]\left(\frac{\gamma_{th}}{\bar{\gamma}}\right)^{G_d} + o\left(\bar{\gamma}^{-G_d}\right), \tag{4.40}$$

where $\Omega_q$ is given by

$$\Omega_q = \begin{cases} \frac{(m_{SR_q}/u_q)^{m_{SR_q}N_SN_{R_q}}}{\left((m_{SR_q}N_{R_q})!\right)^{N_S}}, & m_{SR_q}N_S < m_{R_qD}N_D \\[4mm] \left[\frac{(m_{SR_q}/u_q)^{m_{SR_q}N_SN_{R_q}}}{\left((m_{SR_q}N_{R_q})!\right)^{N_S}} \right. \\[2mm] \left. + \frac{(m_{R_qD}/v_q)^{m_{R_qD}N_DN_{R_q}}}{\left((m_{R_qD}N_D)!\right)^{N_{R_q}N_D}}\right], & m_{SR_q}N_S = m_{R_qD}N_D \\[4mm] \frac{(m_{R_qD}/v_q)^{m_{R_qD}N_{R_q}N_D}}{\left((m_{R_qD}N_D)!\right)^{N_{R_q}N_D}}, & m_{SR_q}N_S > m_{R_qD}N_D. \end{cases} \tag{4.41}$$

Moreover, in (4.40) the achievable diversity order is denoted by $G_d$ and is given by

$$G_d = \sum_{q=1}^{Q}N_{R_q}\min\left(m_{SR_q}N_S, m_{R_qD}N_D\right). \tag{4.42}$$

### 4.8.2 Asymptotic SER of joint antenna and relay selection for OWRNs

The derivation of the exact average SER of the optimal joint antenna and relay selection for OWRNs is mathematically intractable. Nevertheless, to obtain valuable insights into the average SER at high SNRs, the asymptotic average SER is derived as follows:

$$P_e^{\infty} = \frac{\alpha\left(\prod_{q=1}^{Q}\Omega_q\right)2^{G_d-1}\Gamma\left(G_d+\frac{1}{2}\right)}{\sqrt{\pi}(\varphi\bar{\gamma})^{G_d}} + o\left(\bar{\gamma}^{-G_d}\right), \tag{4.43}$$

where $\Omega_q$ is given by (4.41). The diversity order is given in (4.42) and the array gain can be derived as

$$G_a = \left(\frac{\alpha 2^{G_d-1}}{\sqrt{\pi}(\varphi)^{G_d}}\left(\prod_{q=1}^{Q}\Omega_q\right)\Gamma\left(G_d+\frac{1}{2}\right)\right)^{-\frac{1}{G_d}}. \tag{4.44}$$

### 4.8.3 Outage probability of joint antenna and relay selection for TWRNs

The overall outage probability of the joint Tx/Rx antenna and relay selection for MIMO TWRNs is defined as

$$
\begin{aligned}
P_{out} &= \Pr\left( \max_{\substack{i\in\{1,\cdots,N_1\},\, l\in\{1,\cdots,N_2\} \\ q\in\{1,\cdots,Q\},\, m_q\in\{1,\cdots,N_{R_q}\}}} \left( \min\left( \gamma_{S_1}^{(j,l,m_q)}, \gamma_{S_2}^{(j,l,m_q)} \right) \le \gamma_{th} \right) \right) \\
&= \Pr\left( \min\left( \gamma_{S_1}^{(J,L,M_{Q^*})}, \gamma_{S_2}^{(J,L,M_{Q^*})} \right) \le \gamma_{th} \right).
\end{aligned}
\tag{4.45}
$$

where $J$, $L$ and $M_{Q^*}$ are the optimal antenna and relay indices. The overall outage probability can be then derived in closed-form as follows:

$$
\begin{aligned}
P_{out} &= \prod_{q=1}^{Q} \left\{ \left[ \mathbb{F}\left( \gamma_{th}, \frac{p+1}{\zeta_{1,q}}, \frac{u+1}{\zeta_{2,q}}, \frac{u}{\zeta_{2,q}}, \frac{N_1}{\zeta_{1,q}}, N_1-1, N_2 \right) \right. \right. \\
&\quad + \left. \left. \mathbb{F}\left( \gamma_{th}, \frac{u+1}{\zeta_{2,q}}, \frac{p+1}{\zeta_{1,q}}, \frac{p}{\zeta_{1,q}}, \frac{N_2}{\zeta_{2,q}}, N_1, N_2-1 \right) \right]^{N_{R_q}} \right\},
\end{aligned}
\tag{4.46}
$$

where $\mathbb{F}(\cdot,\cdot,\cdot,\cdot,\cdot)$ is given by (4.21) upon replacing $\zeta_1$, $\zeta_2$, $N_R$, $\alpha$, $\beta$, and $\phi(z)$ with the corresponding parameters pertinent to multi-relay TWRNs as $\zeta_{1,k}$, $\zeta_{2,q}$, $N_{R_q}$, $\alpha_q = \frac{\bar{\gamma}_S + \bar{\gamma}_{R_q}}{\bar{\gamma}_S \bar{\gamma}_{R_q}}$, $\beta_q = \frac{1}{\bar{\gamma}_{R_q}}$ and $\phi_q(z) = \frac{1}{\bar{\gamma}_S \bar{\gamma}_{R_q}} \sqrt{(\bar{\gamma}_S^2 + \bar{\gamma}_S \bar{\gamma}_{R_q} + \bar{\gamma}_{R_q}^2/4)z^2 + \bar{\gamma}_S \bar{\gamma}_{R_q} z} + \frac{z}{2\bar{\gamma}_S}$, respectively.

Again, the direct insights into the achievable diversity order of the joint Tx/Rx antenna and relay selection for TWRNs are obtained by deriving the asymptotic outage probability at high SNRs as follows:

$$
P_{out}^{\infty} = \left( \prod_{q=1}^{Q} \Delta_q \right) \left( \frac{\gamma_{th}}{\bar{\gamma}} \right)^{\sum_{q=1}^{Q} G_{d_q}} + o\left( \bar{\gamma}^{-\left(\sum_{q=1}^{Q} G_{d_q}\right)} \right),
\tag{4.47a}
$$

where the achievable diversity order $G_d$ is given by

$$
G_d = \sum_{q=1}^{Q} G_{d_q} = \min(N_1, N_2) \sum_{q=1}^{K} N_{R_q}.
\tag{4.47b}
$$

In (4.47a), $\Delta_q$ is obtained again by replacing $\zeta_1$, $\zeta_2$ and $C_R$ of (4.30c) with $\zeta_{1,q}$, $\zeta_{2,q}$ and $C_{R_q} = \bar{\gamma}_{R_q}/\bar{\gamma}$, respectively.

### 4.8.4 Asymptotic SER of joint Tx/Rx antenna and relay selection for TWRNs

The derivation of the exact SER in closed-form for the joint Tx/Rx antenna and relay selection for TWRNs is again mathematically intractable. However, in order to obtain further

insights into the achievable diversity order and the array gain, the asymptotic average SER is derived as follows:

$$P_e^\infty = \frac{\alpha \left(\prod_{q=1}^{Q} \Delta_q\right) 2^{G_d-1} \Gamma\left(G_d + \frac{1}{2}\right)}{\sqrt{\pi}(\varphi\bar{\gamma})^{G_d}} + o\left(\bar{\gamma}^{-G_d}\right), \tag{4.48}$$

where $\Delta_q$ is obtained by replacing $\zeta_1$, $\zeta_2$ and $C_R$ of (4.30c) with $\zeta_{1,q}$, $\zeta_{2,q}$ and $C_{R_q} = \bar{\gamma}_{R_q}/\bar{\gamma}$, respectively. The achievable diversity order is given in (4.47b) and the array gain can be derived as

$$G_a = \left(\frac{\alpha 2^{G_d-1}}{\sqrt{\pi}(\varphi)^{G_d}} \left(\prod_{q=1}^{Q} \Delta_q\right) \Gamma\left(G_d + \frac{1}{2}\right)\right)^{-\frac{1}{G_d}}. \tag{4.49}$$

## 4.9  Impact of practical transmission impairments

In this section, the detrimental impact of practical transmission impairments on the performance of antenna selection for both OWRNs and TWRNs is studied. Specifically, the performance degradation incurred due to feedback delays and spatially-correlated fading is quantified to obtain valuable insights into practical system designing.

### 4.9.1  Impact of feedback delay on optimal TAS for OWRNs

In practical systems, the feedback channel from the receiver to the transmitter experiences delays. We thus assume that the transmit antennas at $S$ and $R$ are selected based on the outdated CSI received via feedback channels of $S \to R$ and $R \to D$ having $\tau_1$ and $\tau_2$ time delays, respectively[14]. The first hop and the second hop channels are denoted by $\mathbf{H}_1(t)$ and $\mathbf{H}_2(t)$, respectively, and are modeled as [118, 119]

$$\mathbf{H}_l(t) = \rho_l \mathbf{H}_l(t - \tau_l) + \mathbf{E}_{d,l} \quad \text{for} \quad l \in \{1, 2\}, \tag{4.50}$$

where $\rho_l$ is the normalized correlation coefficients between $h_l^{i,j}(t)$ and $h_l^{i,j}(t - \tau_l)$. For Clarke's scattering model, $\rho_l = \mathcal{J}_0(2\pi f_l \tau_l)$, where $f_l$ is the Doppler fading bandwidth. Furthermore, $\mathbf{E}_{d,l}$ is the error matrix, incurred due to feedback delay, having mean zero and variance $(1 - \rho_l^2)$ Gaussian entries.

In the first time-slot, $S$ selects the $I$th transmit antenna based on the outdated CSI received by the local $R \to S$ feedback channel, which is assumed to experience a time delay $\tau_1$. Similarly, in the second time-slot, the relay $R$ selects the $K$th transmit antenna based on the $\tau_2$-delayed CSI.

---

[14]The direct channel is assumed unavailable due to heavy shadowing and pathloss.

**Outage probability of optimal TAS for OWRNs under feedback delays:**

Under this channel model, the exact CDF of the end-to-end SNR can be derived as (see Appendix C.6 for the proof)

$$
\begin{aligned}
F_{\tilde{\gamma}_{e2e}}(x) \;=\; & 1 - \sum_{a,b,k,l}\,\sum_{p,q,u,v} \beta_1^b \beta_2^q \rho_1^{2k}(1-\rho_1^2)^{b-k}\rho_2^{2u}(1-\rho_2^2)^{q-u}\Psi\Phi^{\frac{2b+v+l+1}{2}} \\
& \times\; \Theta^{\frac{2(M_2+q+u)+v-l+1}{2}} x^{M_2+u+l} e^{-(\Phi+\Theta)x}\mathcal{K}_{v-l+1}\left(2x\sqrt{\Phi\Theta}\right),
\end{aligned}
\tag{4.51a}
$$

where $\Psi$, $\Phi$, and $\Theta$ depend on the summation variables and are defined as

$$
\begin{aligned}
\Psi \;=\; & \frac{2(-1)^{a+p}N_S N_R\binom{N_S-1}{a}\binom{N_R-1}{p}\binom{b}{k}\binom{q}{u}\binom{M_2+u+l-1}{v}}{\Gamma(M_1)\Gamma(M_2)\Gamma(M_2+u)\,(l)!} \\
& \times\; \frac{\phi_{b,a,M_1}\phi_{q,b,M_2}\Gamma(M_1+b)\Gamma(M_2+q)}{(a+1)^{M_1+b+k}(p+1)^{M_2+q+u}},
\end{aligned}
\tag{4.51b}
$$

$$
\Phi = \frac{a+1}{\beta_1(1+a(1-\rho_1^2))} \quad\text{and}\quad \Theta = \frac{p+1}{\beta_2(1+p(1-\rho_2^2))}.
\tag{4.51c}
$$

In (4.51a), the two summations are defined as $\displaystyle\sum_{a,b,k,l} = \sum_{a=0}^{N_S-1}\sum_{b=0}^{a(M_1-1)}\sum_{k=0}^{b}\sum_{l=1}^{M_1+k-1}$ and

$$
\sum_{p,q,u,v} = \sum_{p=0}^{N_R-1}\sum_{q=0}^{p(M_2-1)}\sum_{u=0}^{q}\sum_{v=0}^{M_2+u+l-1}.
$$

The outage probability of the optimal TAS for MIMO OWRNs under the outdated CSI can be readily obtained by evaluating (4.51a) at $\gamma_{th}$ as $P_{out} = F_{\tilde{\gamma}_{e2e}}(\gamma_{th})$.

In order to obtain useful insights into the amount of performance degradation incurred due to feedback delays, the asymptotic outage probability of the optimal TAS for MIMO OWRNs under the outdated CSI can be next derived as follows (see Appendix C.6 for the proof):

$$
P_{out}^{\infty} = \begin{cases} \Phi_1\left(\frac{\gamma_{th}}{\bar{\gamma}}\right)^{m_1 N_R} + o\left(\bar{\gamma}^{-m_1 N_R}\right), & m_1 N_R < m_2 N_D \\[2mm] \Phi_2\left(\frac{\gamma_{th}}{\bar{\gamma}}\right)^{m_2 N_d} + o\left(\bar{\gamma}^{-m_2 N_d}\right), & m_1 N_R > m_2 N_D \\[2mm] (\Phi_1+\Phi_2)\left(\frac{\gamma_{th}}{\bar{\gamma}}\right)^{mN} + o\left(\bar{\gamma}^{-mN}\right), & m_1 N_R = m_2 N_D = mN, \end{cases}
\tag{4.52a}
$$

where $\Phi_1$ and $\Phi_2$ are given by

$$
\Phi_1 \;=\; \sum_{a=0}^{N_S-1}\sum_{b=0}^{a(M_1-1)} \frac{N_S m_1^{M_1}\binom{N_S-1}{a}(-1)^a \phi_{b,a,M_1}\Gamma(M_1+b)(1-\rho_1)^b}{M_1 k_1^{M_1}\Gamma^2(M_1)(1+a(1-\rho_1^2))^{M_1+b}},
\tag{4.52b}
$$

$$
\Phi_2 \;=\; \sum_{a=0}^{N_R-1}\sum_{b=0}^{a(M_2-1)} \frac{N_R m_2^{M_2}\binom{N_R-1}{a}(-1)^a \phi_{b,a,M_2}\Gamma(M_2+b)(1-\rho_2)^b}{M_2 k_2^{M_2}\Gamma^2(M_2)(1+a(1-\rho_2^2))^{M_2+b}}.
\tag{4.52c}
$$

Moreover, in (4.52b) and (4.52c), $\rho_j = \mathcal{J}_0(2\pi f_j \tau_j)$ for $j \in \{1, 2\}$, where $f_j$ is the Doppler fading frequency and $\tau_j$ is the time delay for $S \to R$ and $R \to D$ channels, respectively.

The achievable diversity order can be then derived by using (4.52a) as

$$
G_d = \begin{cases} m_1 N_R, & m_1 N_R < m_2 N_D \\ m_2 N_D, & m_1 N_R > m_2 N_D \\ mN, & m_1 N_R = m_2 N_D = mN \end{cases} \quad \text{or} \ \ G_d = \min\left(m_1 N_R, m_2 N_D\right). \quad (4.53)
$$

**Average SER of optimal TAS for OWRNs under feedback delays:**

The average SER of the optimal TAS for MIMO OWRNs under outdated CSI can be then derived as follows:

$$
\begin{aligned}
\bar{P}_e \ = \ & \frac{\alpha}{2} - \alpha\sqrt{\varphi} \sum_{a,b,k,l} \sum_{p,q,u,v} 2^{v-l-\frac{1}{2}} \beta_1^b \beta_2^q \rho_1^{2k}(1-\rho_1^2)^{b-k} \rho_2^{2u}(1-\rho_2^2)^{q-u} \Psi \Phi^{b+v+1} \\
& \times \ \frac{\Theta^{M_2+q+u+v-l+1} \Gamma(\mu+\nu)\, \Gamma(\mu-\nu)\ {}_2\mathcal{F}_1\left(\mu+\nu, \nu+\frac{1}{2}; \mu+\frac{1}{2}; \frac{\frac{\varphi}{2}+\delta-\epsilon}{\frac{\varphi}{2}+\delta+\epsilon}\right)}{\Gamma\left(\mu+\frac{1}{2}\right)\left(\frac{\varphi}{2}+\delta+\epsilon\right)^{\mu+\nu}}, \quad (4.54)
\end{aligned}
$$

where $\mu$, $\nu$, $\delta$, and $\epsilon$ depend on the summation variables and are defined as $\mu = M_2 + u + l + \frac{1}{2}$, $\nu = v - l + 1$, $\delta = \Phi + \Theta$, and $\epsilon = 2\sqrt{\Phi\Theta}$, respectively.

The degradation of the achievable diversity order and the array gain of the optimal TAS for OWRNs incurred due to the feedback delays is next quantified by deriving the asymptotic average SER at high SNRs as follows:

$$
P_e^\infty = \frac{\alpha \Phi 2^{G_d-1} \Gamma\left(G_d + \frac{1}{2}\right)}{\sqrt{\pi}(\varphi\bar{\gamma})^{G_d}} + o\left(\bar{\gamma}^{-G_d}\right), \quad (4.55a)
$$

where the system dependent parameter $\Phi$ is given by

$$
\Phi = \begin{cases} \Phi_1, & m_1 N_R < m_2 N_D \\ \Phi_2, & m_1 N_R > m_2 N_D \\ \Phi_1 + \Phi_2, & m_1 N_R = m_2 N_D. \end{cases} \quad (4.55b)
$$

Moreover, $\Phi_1$ and $\Phi_2$ are defined in (4.52b) and (4.52c), respectively. In particular, the achievable diversity order is given by $G_d = \min\left(m_1 N_R, m_2 N_D\right)$ and the array gain is derived as

$$
G_a = \left(\frac{\alpha \Phi 2^{G_d-1}}{\sqrt{\pi}(\varphi)^{G_d}} \Gamma\left(G_d + \frac{1}{2}\right)\right)^{-\frac{1}{G_d}}. \quad (4.55c)
$$

The amount of performance degradation of the optimal TAS for MIMO OWRNs incurred due to feedback delay can be now quantified by employing the our high SNR analysis given in Section 4.7 and Section 4.9.1. The diversity order reduction resulted due to

feedback delay effect over the perfect CSI case is quantified as

$$G_d^{\text{reduction}} = N_R \min\left(m_1 N_S, m_2 N_D\right) - \min\left(m_1 N_R, m_2 N_D\right).\tag{4.56}$$

The array gain is degraded by a factor of $G_a^{\text{perfect}}/G_a^{\text{imperfect}}$, where $G_a^{\text{perfect}}$ and $G_a^{\text{imperfect}}$ are defined in (4.33c) and (4.55c), respectively.

### 4.9.2 Impact of feedback delay on optimal antenna selection for TWRNs

In practical MIMO TWRNs, the performance of antennas selection could be severely affected from the outdated CSI due to feedback delays. In this subsection, the feedback delay effect on the performance of the optimal Tx/Rx antenna selection for TWRNs is studied.

In this context, the feedback channel from the receiver to the transmitter is assumed to experience delays. We thus assume that Tx/Rx antennas at $S_1$, $S_2$ and $R$ are selected based on the outdated CSI received via the feedback channels of $S_1 \rightarrow R$, and $S_2 \rightarrow R$ having $\tau_1$ and $\tau_2$ time delays, respectively. These two channels can be modeled as [118]

$$\mathbf{H}_{S_i,R}(t) = \rho_i \mathbf{H}_{S_i,R}(t - \tau_i) + \mathbf{E}_i, \quad \text{for} \quad i \in \{1, 2\},\tag{4.57}$$

where $\rho_i$ is the normalized correlation coefficients between $h_{S_i,R}^{k,l}(t)$ and $h_{S_i,R}^{k,l}(t - \tau_i)$. For Clarke's scattering model, $\rho_i = \mathcal{J}_0(2\pi f_i \tau_i)$, where $f_i$ is the Doppler fading bandwidth[15]. Besides, $\mathbf{E}_i$ is the error matrix incurred by the feedback delay, and is having mean zero and variance $(1 - \rho_i^2)$ Gaussian entries. For the sake of mathematical tractability, we consider single-antenna relays only. Nevertheless, both $S_1$ and $S_2$ are equipped with multiple-antennas.

**Outage probability of optimal Tx/Rx antenna selection for TWRNs under feedback delays:**

Under the aforementioned channel and system model, the overall outage probability of Tx/Rx antenna selection for MIMO TWRNs based on minimizing the overall outage probability is derived as (see Appendix C.7 for the proof)

$$\begin{aligned} P_{out} = F_Z(\gamma_{th}) &= \mathbb{G}\left(\gamma_{th}, \frac{p+1}{\hat{\zeta}_{1,p}}, \frac{q+1}{\hat{\zeta}_{2,q}}, \frac{1}{(q+1)\hat{\zeta}_{1,p}}, N_1\right) \\ &+ \mathbb{G}\left(\gamma_{th}, \frac{q+1}{\hat{\zeta}_{2,q}}, \frac{p+1}{\hat{\zeta}_{1,p}}, \frac{1}{(p+1)\hat{\zeta}_{2,q}}, N_2\right), \end{aligned}\tag{4.58a}$$

---

[15]Here, $\mathcal{J}_0(z)$ is the Bessel function of the first kind of order zero [1, Eqn. (8.402)].

where the function $\mathbb{G}\left(\cdot, \cdot, \cdot, \cdot, \cdot\right)$ is defined as

$$
\begin{aligned}
\mathbb{G}\left(z, a, b, c, d\right) = & \sum_{p=0}^{N_1-1} \sum_{q=0}^{N_2-1} N_1 N_2 \binom{N_1-1}{p}\binom{N_2-1}{q}(-1)^{p+q} \\
& \times \left[\frac{1}{b\hat{\zeta}_{1,p}\hat{\zeta}_{2,q}}\left(\frac{1-\exp\left(-a\beta z\right)}{a} - \frac{1-\exp\left(-(a+b)\beta z\right)}{a+b}\right)\right. \\
& \left. - c\left(\frac{\exp\left(-(a+b)\beta z\right)\left(1-\exp\left(-(a+b)\phi(z)\right)\right)}{a+b} - \frac{\mathrm{e}^{-(a\phi(z)+(a\beta+b\alpha)z)}}{a}\mathcal{J}(z)\right)\right] \\
& + \sum_{p=0}^{d-1}(-1)^p\binom{d}{p+1}\exp\left(-a\beta z\right).
\end{aligned} \tag{4.58b}
$$

In (4.58b), $\alpha$, $\zeta$, $\phi(z)$, and $\mathcal{J}(z)$ are defined as in (4.21). Moreover, $\hat{\zeta}_{1,p}$ and $\hat{\zeta}_{2,q}$ are given by $\hat{\zeta}_{1,p} = \zeta_1\left(1+p(1-\rho_1^2)\right)$ and $\hat{\zeta}_{2,q} = \zeta_2\left(1+q(1-\rho_2^2)\right)$, respectively.

Further insights into the detrimental effect of feedback delays on the performance of Tx/Rx antenna selection can be obtained by deriving the asymptotic outage probability at high SNRs as follows (see Appendix C.7 for the proof):

$$
P_{out}^{\infty} = \begin{cases}
\Theta_1\left(\frac{\gamma_{th}}{\bar{\gamma}}\right) + o\left(\bar{\gamma}^{-1}\right), & \rho_1 = 1 \quad \text{and} \quad 0 \leq \rho_2 < 1 \\
\Theta_2\left(\frac{\gamma_{th}}{\bar{\gamma}}\right) + o\left(\bar{\gamma}^{-1}\right), & \rho_2 = 1 \quad \text{and} \quad 0 \leq \rho_1 < 1 \\
(\Theta_1 + \Theta_2)\left(\frac{\gamma_{th}}{\bar{\gamma}}\right) + o\left(\bar{\gamma}^{-1}\right), & 0 \leq \rho_1 < 1 \quad \text{and} \quad 0 \leq \rho_2 < 1,
\end{cases} \tag{4.59a}
$$

where $\Theta_1$ and $\Theta_2$ are given by

$$
\Theta_1 = \left(\frac{C_S + C_R}{C_S C_R}\right)\sum_{q=0}^{N_2-1}\frac{(-1)^q N_2\binom{N_2-1}{q}}{\hat{\zeta}_{2,q}}, \tag{4.59b}
$$

$$
\Theta_2 = \left(\frac{C_S + C_R}{C_S C_R}\right)\sum_{p=0}^{N_1-1}\frac{(-1)^p N_1\binom{N_1-1}{p}}{\hat{\zeta}_{1,p}}. \tag{4.59c}
$$

Eqn. (4.59a) clearly reveals that the achievable diversity order of the optimal Tx/Rx antenna selection for TWRNs is unity. Thus, the outdated CSI incurred due to feedback delay effect has a severely detrimental effect on the outage probability, in effect, the achievable diversity order diminishes from $\min\left(N_1, N_2\right)$ to one.

**Average SER of optimal Tx/Rx antenna selection for TWRNs under feedback delays:**

The derivation of the exact average SER of the optimal Tx/Rx for TWRNs is mathematically intractable, and hence, only the asymptotic average SER is derived. Specifically, useful insights into the amount of degradation of the achievable diversity order and the array gain

incurred due to the feedback delays can be obtained by deriving the asymptotic average SER at high SNRs as follows:

$$P_e^\infty = \frac{\alpha \Theta 2^{G_d - 1} \Gamma\left(G_d + \frac{1}{2}\right)}{\sqrt{\pi}(\varphi\bar{\gamma})^{G_d}} + o\left(\bar{\gamma}^{-G_d}\right), \tag{4.60a}$$

where the system dependent parameter $\Phi$ is given by

$$\Theta = \begin{cases} \Theta_1, & \rho_1 = 1 \quad \text{and} \quad 0 \le \rho_2 < 1 \\ \Theta_2, & \rho_2 = 1 \quad \text{and} \quad 0 \le \rho_1 < 1 \\ \Theta_1 + \Theta_2, & 0 \le \rho_1 < 1 \quad \text{and} \quad 0 \le \rho_2 < 1 \end{cases} \tag{4.60b}$$

In (4.60b), $\Theta_1$ and $\Theta_2$ are defined in (4.59b) and (4.59c), respectively. Besides, the achievable diversity order and the array gain are derived as

$$G_d = 1 \quad \text{and} \quad G_a = \left(\frac{\alpha \Theta 2^{G_d - 1}}{\sqrt{\pi}(\varphi)^{G_d}} \Gamma\left(G_d + \frac{1}{2}\right)\right)^{-\frac{1}{G_d}}. \tag{4.60c}$$

The amount of diversity degradation for optimal Tx/Rx antenna selection for TWRNs can be quantified by using (4.30b) and (4.60c) as follows: $G_d^{\text{reduction}} = N_R \min\left(N_S, N_D\right) - 1$. Similarly, the array gain degradation factor is quantified to be $G_a^{\text{perfect}}/G_a^{\text{imperfect}}$, where $G_a^{\text{perfect}}$ and $G_a^{\text{imperfect}}$ are given in (4.35b) and (4.60c), respectively.

### 4.9.3 Channel prediction for circumventing feedback delay effect of Tx/Rx antenna selection for TWRNs

Linear channel prediction can be employed to circumvent outdated CSI due to feedback delays in time varying channels [120, 121]. Thus, in this subsection, such a linear channel prediction strategy is used to minify the adverse effects of feedback delay for Tx/Rx antenna selection in MIMO TWRNs.

For each block-length ($L_b$ symbols of each with symbol duration $T_s$), the $(k, l)$th entry of the estimated channel matrix $\hat{H}_{S_i, R}(t)$ for $i \in \{1, 2\}$ is given by

$$\hat{h}_{S_i, R}^{k,l}(t) = h_{S_i, R}^{k,l}(t) + e_{S_i, R}^{k,l}(t), \quad \text{for} \quad i \in \{1, 2\}, \tag{4.61}$$

where $h_{S_i, R}^{k,l}(t)$ is the $(k, l)$th entry of the actual channel matrix $H_{S_i, R}(t)$ and $e_{S_i, R}^{k,l}(t) \sim \mathcal{CN}(0, \sigma_{e,i}^2)$ is the Gaussian channel estimation error. Here, the channel estimation error variance can be explicitly defined as $\sigma_{e,i}^2 = \sigma_i^2/E_p$, where $\sigma_i^2$ and $E_p$ are the noise power at each receive antenna and the power of the pilot symbol. Moreover, $h_{S_i, R}^{k,l}(t)$ and $e_{S_i, R}^{k,l}(t)$ are statistically independent.

By employing classical theory of linear FIR channel prediction [120, 121], the $L$-block ahead predicted channel entry is derived as[16]

$$\tilde{h}_{S_i,R}^{k,l}(t + LL_bT_s) = \mathbf{w}_{\text{opt},i}^H \hat{\mathbf{h}}_{S_i,R}^{k,l}, \quad \text{for} \quad i \in \{1,2\}, \tag{4.62}$$

where $\hat{\mathbf{h}}_{S_i,R}^{k,l} = [\hat{h}_{S_i,R}^{k,l}(t), \hat{h}_{S_iR}^{k,l}(t - L_bT_s), \cdots \hat{h}_{S_i,R}^{k,l}(t - (L-1)L_bT_s)]^T$ is the vector of estimated fading amplitudes corresponding to the prediction length $L$. Further, $\mathbf{w}_{\text{opt},i}^H$ is the optimal weighting vector corresponding to Wiener-Hopf equation [120, 121] and is derived as $\mathbf{w}_{\text{opt}} = \mathbf{R}_i^{-1}\mathbf{r}_i$, where the $(m,n)$th entry of $L \times L$ matrix $\mathbf{R}_i$ is given by $[\mathbf{R}_i]_{m,n} = \mathcal{J}_0(2\pi f_i|m-n|L_bT_s) + \sigma_{e,i}^2\delta(m-n)$, and $l$th entry of $L \times 1$ vector $\mathbf{r}_i$ is given by $[\mathbf{r}_i]_l = \mathcal{J}_0(2\pi f_i|L+l-1|L_bT_s)$. This optimal weighting vector is derived to minimize the mean square error (MSE) as $\min\limits_{\mathbf{w}_{\text{opt},i}} \left(\sigma_e^2\right) = \sigma_h^2 - \mathbf{r}_w^H\mathbf{R}_w^{-1}\mathbf{r}_w$, where $\sigma_e^2$ is the predictor error variance [120, 121].

Next, it can readily be seen that the normalized correlation coefficient between the true and the predicted fading amplitude is given by $\hat{\rho}_i = \sqrt{\mathbf{r}_i^H\mathbf{R}_i^{-1}\mathbf{r}_i}$. Consequently, the $(k,l)$th entry of the $L$-block ahead true channel matrix $H_{S_i,R}$ can be written as

$$h_{S_i,R}^{k,l} = \hat{\rho}_i \, \tilde{h}_{S_i,R}^{k,l} + \sqrt{1 - \hat{\rho}_i^2} \, n_{S_i,R}^{k,l}, \quad \text{for} \quad \in \{1,2\}, \tag{4.63}$$

where $n_{S_i,R}^{k,l}$ is the Gaussian residue error with zero mean and unit variance. It is worth noticing that (4.57) is indeed the special case of the unit tap form of (4.63). Thus, the exact overall outage probability and its high SNR approximation of Tx/Rx antenna selection with channel prediction for MIMO TWRNs can be derived by simply replacing $\rho_i$ in (4.58a) and (4.59a), respectively, by $\hat{\rho}_i = \sqrt{\mathbf{r}_i^H\mathbf{R}_i^{-1}\mathbf{r}_i}$.

### 4.9.4 Impact of spatially-correlated fading on Tx/Rx antenna selection for TWRNs

In this subsection, the impact of spatially-correlated fading among multiple antenna elements on the performance of the optimal Tx/Rx antenna selection for MIMO TWRNs is studied. To this end, the exact amount of asymptotic performance degradation due to correlated fading is quantified in closed-form. The system model of interest is same as that of Section 4.9.2, and the corresponding channel model is presented as follows:

---

[16]On the contrary to our assumption in Section 4.2, here, a more practical signaling scheme, where each transmission phase is assumed to last $L$-blocks, is employed. Interestingly, the feedback time delay $\tau_i$ defined in (4.57) can now be defined as $\tau_i = LL_bT_s$.

**Correlated fading channel model**

The channel vector from $S_i$ to $R$ is assumed to be spatially-correlated flat Rayleigh fading and is given by $\boldsymbol{\Psi}_i^{\frac{1}{2}} \mathbf{h}_{S_i,R}$ for $i \in \{1,2\}$, where $\boldsymbol{\Psi}_i$ is the $N_i \times N_i$ covariance matrix at $S_i$ and $\mathbf{h}_{S_i,R}$ is a $N_i \times 1$ vector with independent Rayleigh fading entries. The $(p,q)$th element of $\boldsymbol{\Psi}_i$ for $i \in \{1,2\}$ is given by [122, Eqn. (8.1.5)]

$$\boldsymbol{\Psi}_i^{p,q} = \begin{cases} \rho_{i,p}\rho_{i,q}, & p \neq q \\ 1, & p = q, \end{cases} \quad \text{where} \quad 0 \leq (\rho_{i,p}, \rho_{i,q}) < 1. \tag{4.64}$$

Hence, $\boldsymbol{\Psi}_i$ can be parameterized by an $1 \times N_i$ vector $\rho_i$ with the $p$th element $\rho_{i,p}$.

**Asymptotic outage probability at high SNRs under spatially correlated fading:**

The asymptotic overall outage probability at high SNRs for Tx/Rx antenna selection for MIMO TWRNs over correlated Rayleigh fading is derived by employing similar techniques to those in Appendix C.5 as follows:

$$P_{out}^{\infty} = \Omega_{Corr} \left( \frac{\gamma_{th}}{\bar{\gamma}} \right)^{G_{d,Corr}} + o\left( \bar{\gamma}^{-(G_{d,Corr})} \right), \tag{4.65a}$$

where the achievable diversity order is given by

$$G_{d,Corr} = \min\left(N_1, N_2\right). \tag{4.65b}$$

Moreover, the system dependent coefficient, $\Omega_{Corr}$, is given by

$$\Omega_{Corr} = \begin{cases} \omega_1 \left( \frac{C_S + C_R}{\zeta_1 C_S C_R} \right)^{N_1}, & N_1 < N_2 \\ \omega_2 \left( \frac{C_S + C_R}{\zeta_2 C_S C_R} \right)^{N_2}, & N_1 > N_2 \\ \left( \omega_1/\zeta_1^N + \omega_2/\zeta_2^N \right) \left( \frac{C_S + C_R}{C_S C_R} \right)^N, & N_1 = N_2 = N, \end{cases} \tag{4.65c}$$

where $\omega_1$ and $\omega_2$ are given by

$$\omega_1 = \left( \left[ 1 + \sum_{n=1}^{N_1} \frac{\rho_{1,n}}{1 - \rho_{1,n}} \right] \prod_{n=1}^{N_1} [1 - \rho_{1,n}] \right)^{-1} \quad \text{and} \tag{4.65d}$$

$$\omega_2 = \left( \left[ 1 + \sum_{n=1}^{N_2} \frac{\rho_{2,n}}{1 - \rho_{2,n}} \right] \prod_{n=1}^{N_2} [1 - \rho_{2,n}] \right)^{-1}. \tag{4.65e}$$

**Asymptotic average SER at high SNRs under spatially correlated fading:**

The asymptotic average SER at high SNRs of the optimal Tx/Rx antenna selection for the TWRNs operating over spatially correlated fading is derived as follows:

$$P_e^{\infty} = \frac{\alpha 2^{G_{d,Corr}-1} \Omega_{Corr} \Gamma\left(G_{d,Corr} + \frac{1}{2}\right)}{\sqrt{\pi}(\varphi\bar{\gamma})^{G_{d,Corr}}} + o\left( \bar{\gamma}^{-G_{d,Corr}} \right), \tag{4.66a}$$

In (4.66a), $\Omega_{Corr}$ is defined in (4.65c). Moreover, the achievable diversity order is given in (4.65b) and the array gain is derived as

$$G_{a,Corr} = \left( \frac{\alpha\Omega_{Corr}2^{G_{d,Corr}-1}}{\sqrt{\pi}(\varphi)^{G_{d,Corr}}}\Gamma\left(G_{d,Corr} + \frac{1}{2}\right) \right)^{-\frac{1}{G_{d,Corr}}}. \tag{4.66b}$$

**Amount of performance degradation due to correlated fading**

The amount of performance degradation due to correlated fading is next quantified analytically. It is worth noticing that the achievable diversity order (4.65b) of Tx/Rx antenna selection for MIMO TWRNs remains the same even over the correlated Rayleigh fading. However, the array gain is severely affected. In this context, the asymptotic average transmit SNR gap at high SNRs ($\bar{\gamma}_{\mathrm{gap}}^{\infty}$), which is defined as the ratio of the average transmit SNRs of uncorrelated and correlated cases at a fixed outage probability for a given threshold SNR, is derived as

$$\bar{\gamma}_{\mathrm{gap}}^{\infty} = \begin{cases} (\omega_1)^{-1/G_d}, & N_1 < N_2 \\ (\omega_2)^{-1/G_d}, & N_1 > N_2 \\ \left[\left(\zeta_1^N + \zeta_2^N\right) / \left(\zeta_1^N\omega_2 + \zeta_2^N\omega_1\right)\right]^{-1/G_d}, & N_1 = N_2 = N. \end{cases} \tag{4.67}$$

It is worth noticing that $\bar{\gamma}_{\mathrm{gap}}^{\infty}$ can now be used to design the required fade-margins to countermeasure the SNR loss due to spatially-correlated fading in practical MIMO TWRNs set-ups.

## 4.10 Numerical results

In this section, our numerical results are presented for both OWRNs and TWRNs. Specifically, the outage probability and the average bit error rate (BER) of BPSK pertinent to optimal TAS and optimal joint antenna and relay selection strategies are plotted by employing both Monte Carlo simulation results and our analytical results. To capture the effect of the network geometry, the average SNR of the $i$th hop is modeled by $\bar{\gamma}_i = \bar{\gamma}_0 \left(\frac{l_0}{l_i}\right)^{\varpi}$ for $i \in \{1, 2\}$, where $\bar{\gamma}_0$ is the average transmit SNR of direct channel and $\varpi$ is the pathloss exponent. The distances between the terminals $S \to D$, $S \to R$, and $R \to D$ are denoted by $d_0$, $d_1$ and $d_2$, respectively.

**Outage probability of the optimal TAS for OWRNs:**

In Fig. 4.4, the exact outage probability of the optimal TAS for the MIMO OWRNs obtained via Monte Carlo simulations is compared with the analytical outage upper bound (4.13a) for several antenna configurations. The outage probability of the single-antenna OWRN
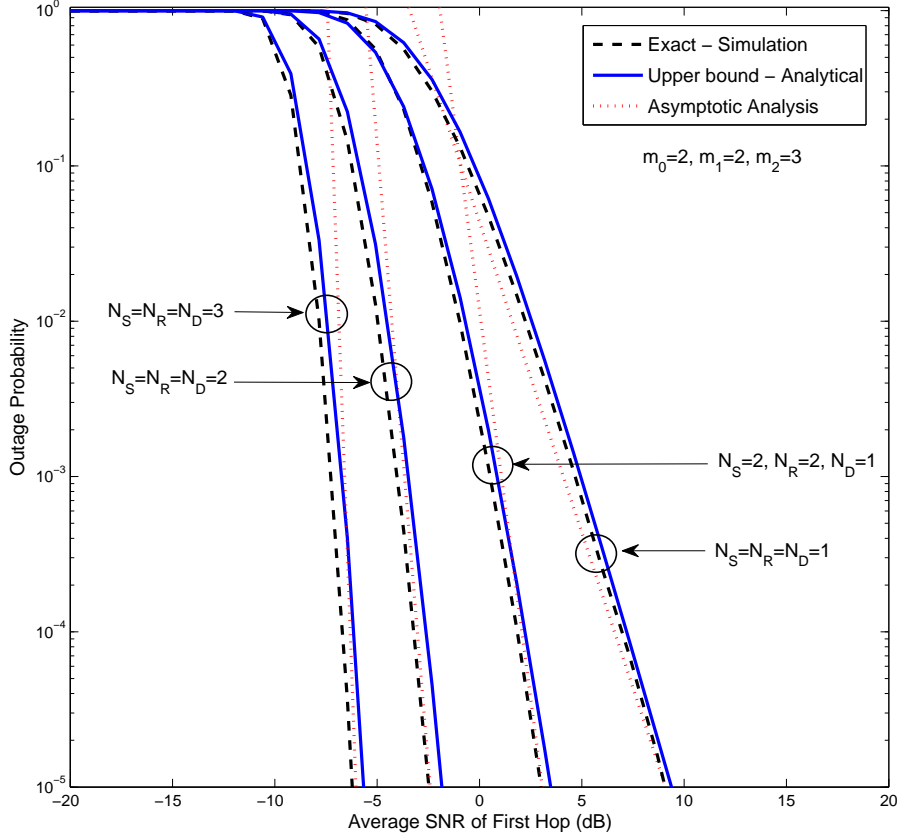
Figure 4.4: The outage probability of optimal TAS for OWRNs. The direct channel is assumed available. The hop distances are $d_1 = \frac{d_0}{3}, d_2 = \frac{2d_0}{3}$ and the pathloss exponent is assumed to be $\varpi = 2.5$.

is also plotted for comparison purposes. For example, at an outage of $10^{-4}$, the triple-antenna OWRN with optimal TAS achieves almost 12 dB SNR gain over the single-antenna counterpart. Our outage upper bound is considerably tight to the exact outage and just a fraction of a dB off of the exact. The asymptotic outage curves are plotted to obtain direct insights about the diversity order and array gain. Thus, the outage bound provides accurate insights into the important system parameters such as the diversity order and can be used as a benchmark for designing practical MIMO TAS for OWRNs.

**Average BER of the optimal TAS for OWRNs:**

In Fig. 4.5, the closed-form upper bound for the average BER of BPSK of the optimal TAS for MIMO OWRNs is compared for several antenna set-ups at the source, relay and destination. Fig. 4.5 also shows the tightness of our BER bound for different fading parameters

94
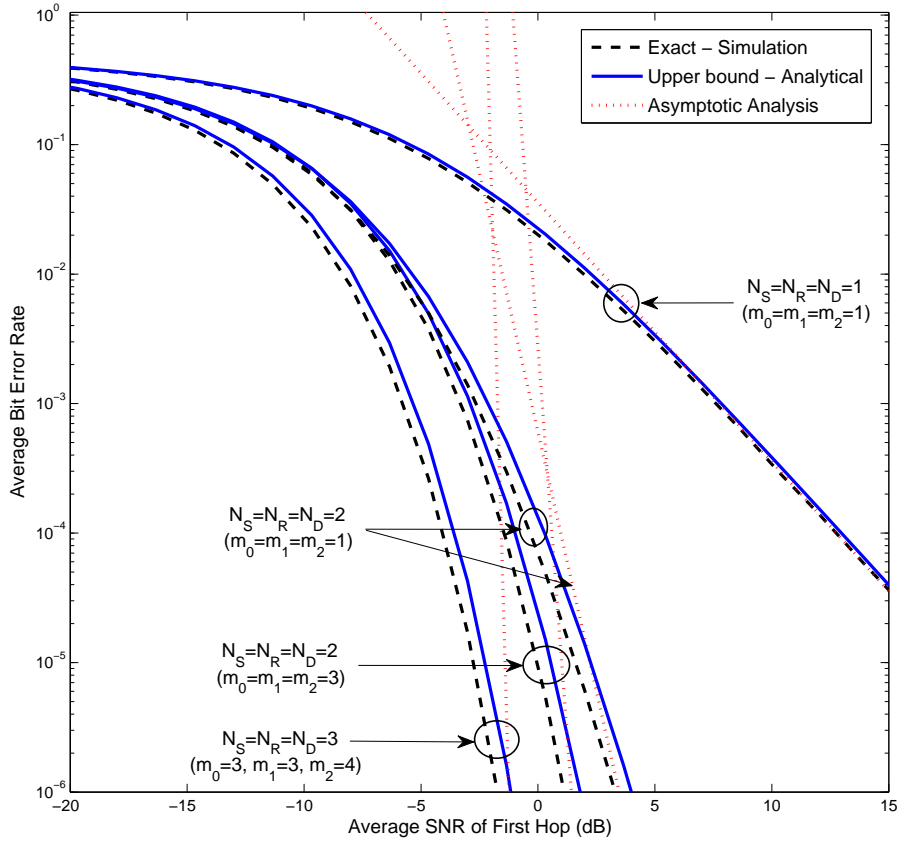
Figure 4.5: The average BER of BPSK of optimal TAS for OWRN. The direct channel is assumed available. The hop distances are $d_1 = \frac{d_0}{3}, d_2 = \frac{2d_0}{3}$ and the path-loss exponent is $\varpi = 2.5$.

(i.e., $m_0$, $m_1$ and $m_2$). Similar to the outage bound, the BER bound is always exact within 1 dB and predicts the diversity order accurately. The asymptotic BER curves are plotted to obtain valuable system-design insights such as diversity order and array gain. Fig. 4.5 clearly reveals that the optimal TAS for MIMO OWRNs achieves significant gains in terms of the average BER. For instance, at an average BER of $10^{-3}$, the dual-antenna OWRN achieves more than 10 dB SNR gain over the single-antenna counterpart.

**Impact of feedback delays on outage probability of optimal TAS for OWRNs:**

In Fig. 4.6, the detrimental impact of outdated CSI incurred due to feedback delays on the outage probability of the optimal TAS for MIMO OWRNs is shown. The exact outage curves are plotted by using (4.51a), whereas the asymptotic outage curves is plotted by using (4.52a). The TAS at $S$ and $R$ is performed based on the outdated CSI received via
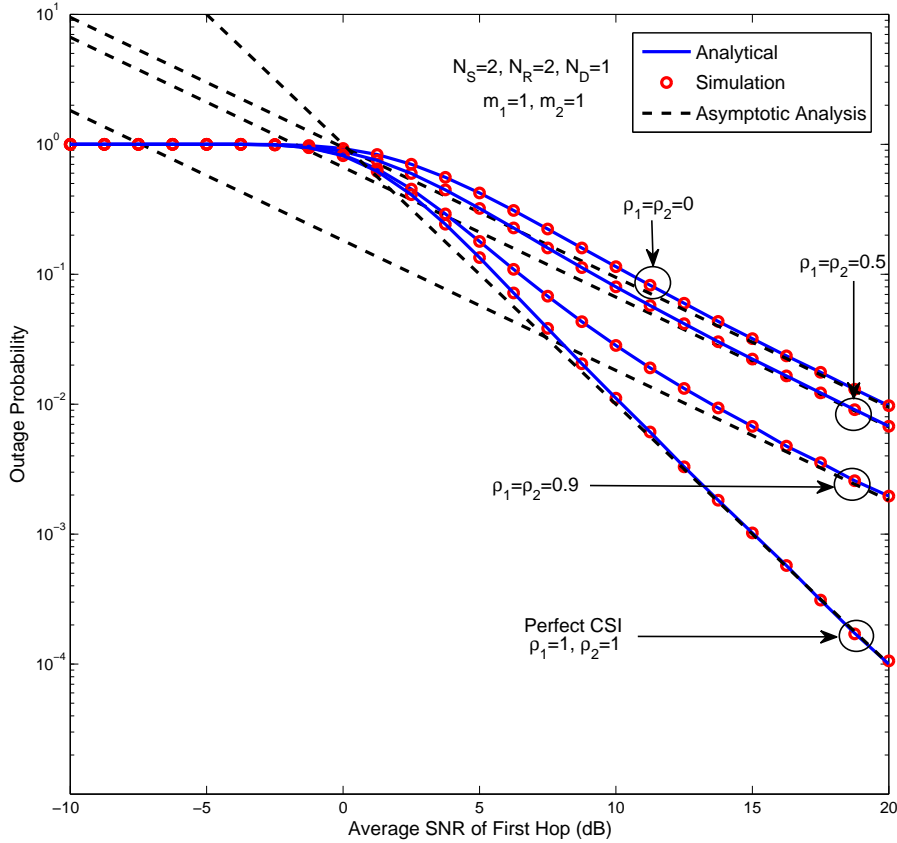
Figure 4.6: The impact of feedback delay on the outage performance of optimal TAS for OWRNs. The direct path is assumed unavailable. The hop distances are $d_1 = d_2 = l_0/2$ and the pathloss exponent is assumed to be $\varpi = 2.5$.

the local feedbacks $R \to S$ and $D \to R$ having time delays $\tau_1$ and $\tau_2$, respectively. Several outage curves are obtained by changing $\rho_1$ and $\rho_2$, where $\rho_l$ is related to $\tau_l$ by following Clarke's scattering model; $\rho_l = \mathcal{J}_0(2\pi f_l \tau_l)$ for $l \in \{1,2\}$, where $f_l$ is the Doppler fading frequency. The two extreme cases, $\rho_l = 1$ and $\rho_l = 0$, correspond to the perfect and fully outdated CSI cases. The outage probability is severely degraded due to the presence of feedback delays. For example, at an outage probability of $10^{-3}$ the fully outdated CSI case results in 10 dB SNR loss over the perfect CSI case. The asymptotic outage curves in Fig. 4.6 reveal that the feedback delays has a significant detrimental effect on the achievable diversity order as well.
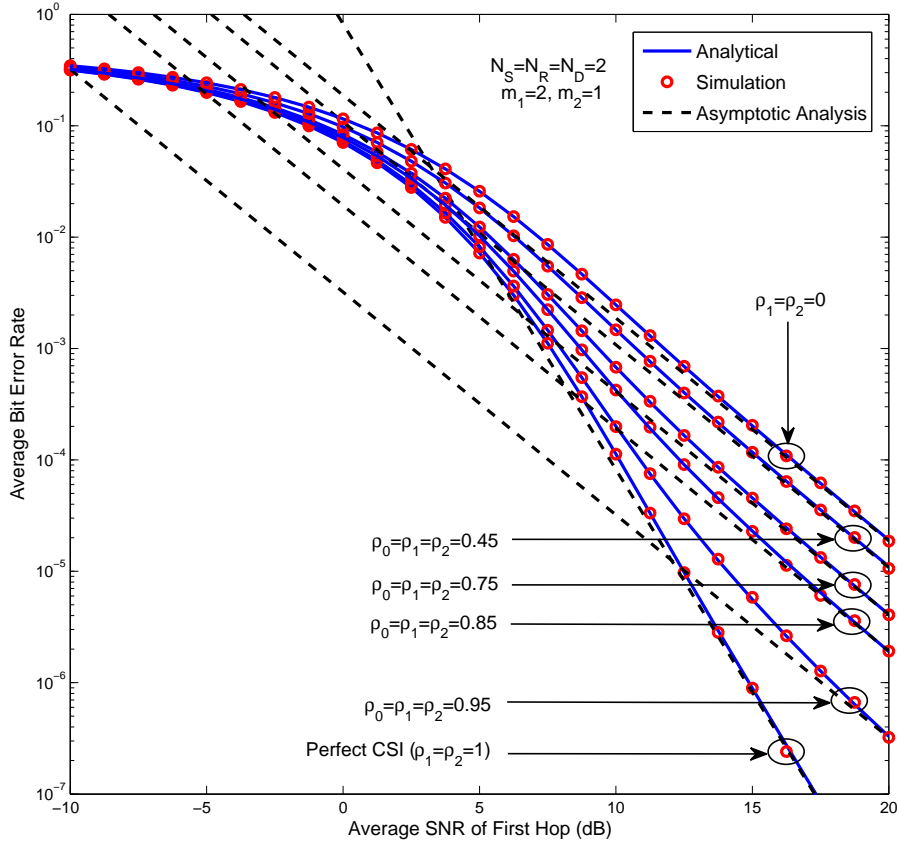
Figure 4.7: The impact of outdated CSI on the average BER of the optimal TAS for OWRNs. Direct channel is assumed unavailable. The hop distances are $d_1 = d_2 = d_0/2$ and the pathloss exponent is assumed to be $\varpi = 2.5$.

**Impact of feedback delays on average SER of optimal TAS for OWRNs:**

Similarly, in Fig. 4.7, the feedback delay effect on the BPSK average BER of the optimal TAS for OWRNs is depicted. To this end, the exact BER curves and the asymptotic BER curves are plotted by using (4.54) and (4.55a), respectively. In particular, Fig. 4.7 shows that just as in outage probability case, feedback delay in TAS has a severe detrimental effect on the average BER. The asymptotic BER curves are plotted to depict the reduction of the diversity order and array gain due to feedback delay. For example, the achievable diversity order of the system reduces to $G_d = \min(m_1 N_R, m_2 N_D)$ from the full diversity order; $G_d = N_R \min(m_1 N_S, m_2 N_D)$. Further, the array gain is severely affected whenever a slight time delay in the feedback channel is incurred as well. Thus, the presence of feedback delays in OWRNs with TAS results in significant detrimental effects on the average BER.
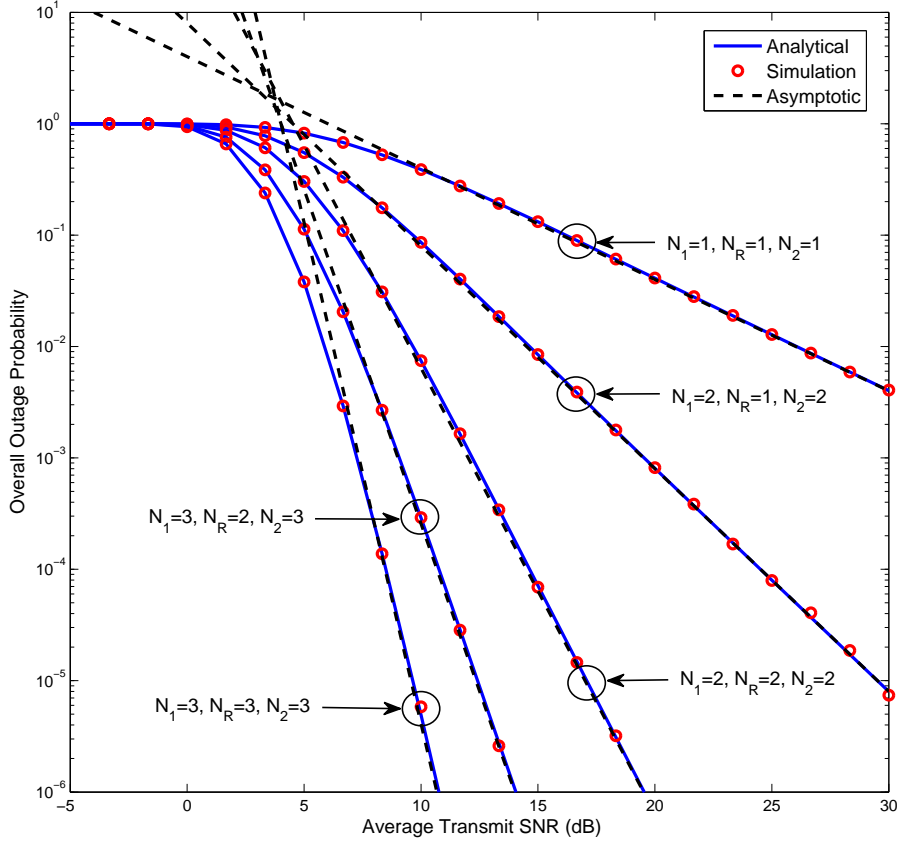
Figure 4.8: The outage probability of optimal Tx/Rx antenna selection for TWRNs. The target rate of the whole system is $R_{th} = 2$ bits/Hz/s. Since the two source nodes are identical, their individual target rates are considered as $\frac{R_{th}}{2}$. The hop distances are $d_{S_1,R} = d_{S_2,R}$ and the pathloss exponent is assumed to be $\varpi = 3.5$.

**Outage probability of the optimal Tx/Rx for TWRNs:**

Fig. 4.8 shows the overall outage probability of the optimal Tx/Rx antenna selection strategy for the single-relay MIMO TWRNs. The analytical outage curves are plotted for several antenna set-ups by using (4.29) and (4.30a). In particular, the outage curve corresponding to the single-antenna TWRN is plotted as a benchmark. Fig. 4.8 clearly reveals that the optimal Tx/Rx antenna selection for multi-antenna TWRNs provide significant gains over the single-antenna TWRNs. For example, at $10^{-2}$ outage probability, the triple-antenna TWRNs provides a 20.34 dB SNR gain over the single-antenna TWRN. The asymptotic outage curves, which are exact at high SNRs, clearly reveal the diversity order of the system and provide insights into practical two-way relay system designing. The exact match between Monte Carlo simulations and analytical curves verifies the accuracy of our derivations.
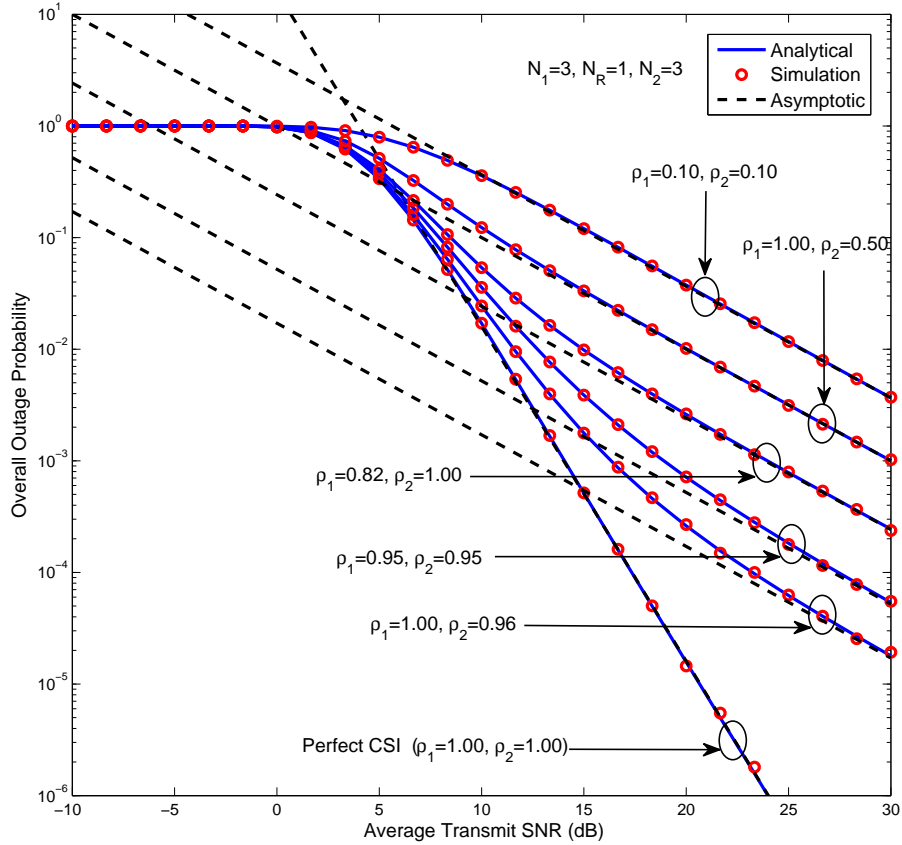
Figure 4.9: The feedback delay effect on the outage probability of Tx/Rx antenna selection for TWRNs. The hop distances are $d_{S_1,R} = d_{S_2,R}$ and the pathloss exponent is assumed to be $\varpi = 3.5$.

**Impact of feedback delay on outage probability of optimal Tx/Rx for TWRNs:**

Fig. 4.9 shows the impact of feedback delays on the outage probability of the optimal Tx/Rx antenna selection by considering the MIMO TWRN with $N_1 = 3$, $N_R = 1$ and $N_2 = 3$. The outage probability is plotted for several feedback delay scenarios by changing $\rho_1$ and $\rho_2$. The outage curve with $\rho_1 = \rho_2 = 1$ corresponds to the perfect CSI case (i.e., antenna selection with perfect CSI), whereas the curve with $0 \leq \rho_1, \rho_2 < 1$ corresponds to the imperfect CSI case. As $\rho_1$ and $\rho_2$ decrease from 1 to 0 (i.e., as the feedback delay increases), the performance of Tx/Rx antenna selection degrades significantly. In particular, Fig. 4.9 shows that even a slight feedback delay in either hop results in severe degradation of the diversity order. This result is clearly revealed by the curves corresponding to ($\rho_1 = 1$, $\rho_2 = 0.95$) and ($\rho_1 = 0.82$, $\rho_2 = 1$), respectively, where one hop has no feedback delays, and the other hop has a slight feedback delay. Specifically, our asymptotic analysis clearly
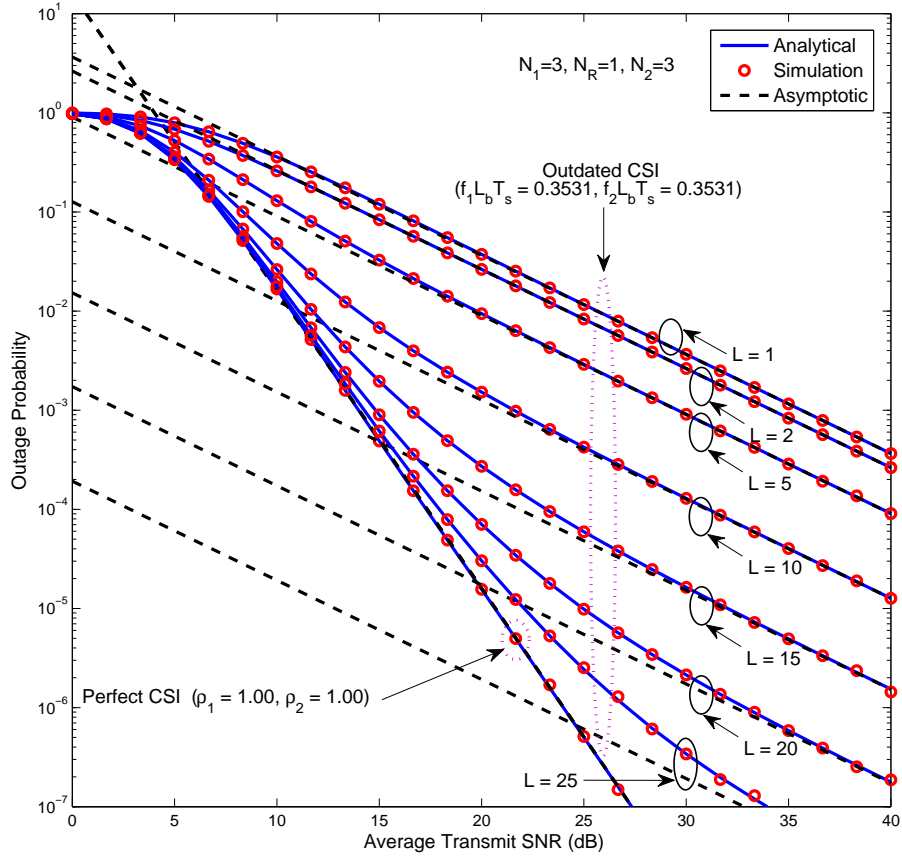
Figure 4.10: The impact of channel prediction to circumvent the outdated CSI for Tx/Rx antenna selection. The FIR channel predictor length for each individual hop is denoted by $L$. The hop distances are $d_{S_1 R} = d_{S_2 R}$ and the path-loss exponent is $\varpi = 3.5$.

reveals that the Tx/Rx antenna selection based on the perfect CSI achieves the full diversity available in the MIMO two-way relay channel; $G_d = \min(N_1, N_2)$. However, when the antennas are selected based on the outdated CSI, this diversity gain decreases to unity. Specifically, at $10^{-3}$ outage probability, a 15.76 dB performance loss is incurred when the antenna selection is based on CSI related to $\rho_1 = 1$ and $\rho_2 = 0.5$ over the perfect CSI case. The exact match between the Monte Carlo simulation points and the analytical results verifies the accuracy of our analysis.

**Effect of channel prediction to circumvent outdated CSI:**

In Fig. 4.10, the effect of linear channel prediction to circumvent the detrimental impact of outdated CSI due to feedback delay is studied for the MIMO TWRN with ($N_1 = 3$, $N_R = 1$, $N_2 = 3$) antenna configuration. A set of outage curves are plotted by varying
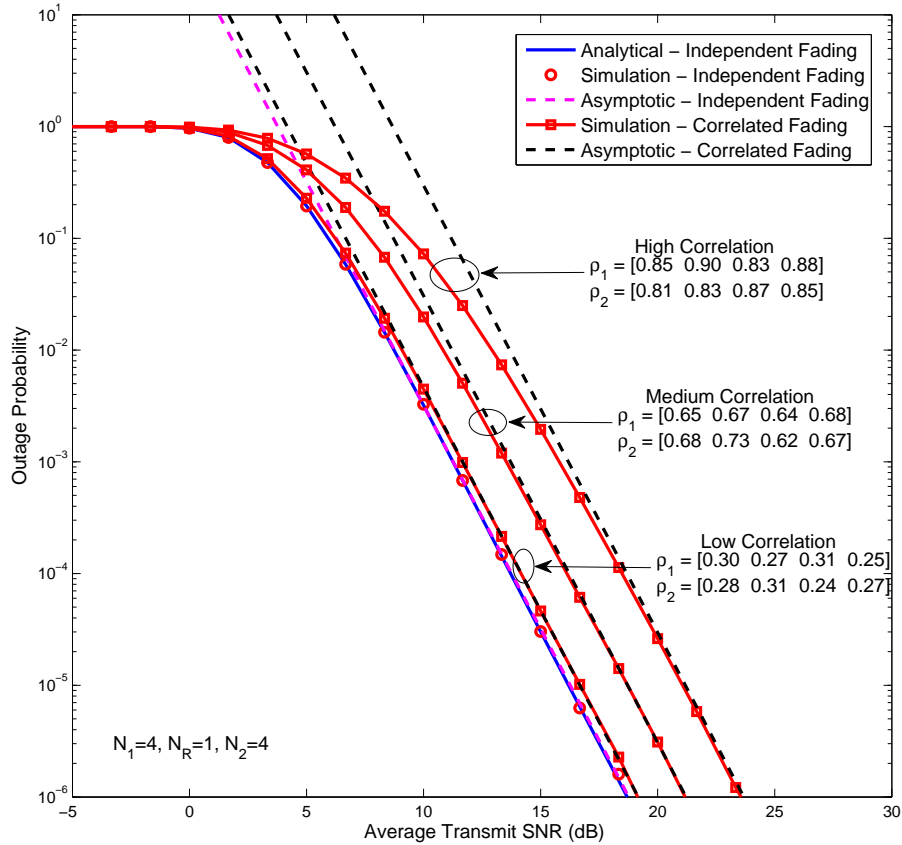
Figure 4.11: The impact of correlated fading on the outage probability of Tx/Rx antenna selection for TWRNs. The hop distances are $d_{S_1,R} = d_{S_2,R}$ and the pathloss exponent is $\varpi = 3.5$.

the FIR channel predictor length $L$. Fig. 4.10 clearly reveal that a significant performance improvement can be obtained by increasing the predictor length. For example, at $10^{-3}$ outage probability, a FIR predictor with 20 taps provides almost 21 dB SNR gain over a single-tap predictor. It is also worth noticing that the diversity order loss can not be fully recovered by the FIR linear prediction. However, a significant fraction of outage probability loss resulted from the outdated CSI can be recovered by using causal FIR prediction. For instance, at $10^{-5}$ outage probability, a 25 tap FIR predictor only looses 1.3 dB compared to the perfect CSI case. Intuitively, it can be concluded that an infinite impulse response (IIR) predictor would fully recover the diversity order loss resulted from feedback delay effect.

**Impact of correlated fading on outage probability of antenna selection for TWRNs:**

Fig. 4.11 shows the impact of correlated fading on the overall outage probability of Tx/Rx antenna selection for the MIMO TWRN with ($N_1 = 4$, $N_R = 1$, $N_2 = 4$) antenna set-up. Four specific spatial correlation effects are considered; (i) independent fading (ii) low correlation, (iii) medium correlation, and (iv) high correlation by varying relative antenna spacing, angle of arrival/departure, and angular spread. Our asymptotic outage curves clearly reveal that the spatial correlation degrades the outage probability significantly. It is also worth noticing that while spatial correlation does not degrade the achievable diversity order, it does degrade the array gain. For instance, at $10^{-5}$ outage probability, high correlation results in almost 5 dB SNR loss with respective to independent fading case. This asymptotic outage loss agrees well with our analytical results presented in Section 4.9.4 and hence render it useful for obtaining valuable insights into practical MIMO TWRN system-designing.

**Outage probability of joint antenna and relay selection for OWRNs:**

In Fig. 4.12, the exact outage probability of the optimal joint transmit antenna and relay selection for dual-relay MIMO OWRNs is plotted over Nakagami-$m$ fading channels. To this end, the outage probability of a dual-relay ($Q = 2$) OWRN having dual-antenna terminals is plotted. In order to depict the achievable diversity order clearly, the asymptotic outage curves are plotted by using (4.40). In particular, the outage probability of a dual-relay network having single-antenna terminals is also plotted by using (4.38) with $N_S = 1$, $N_D = 1$ and $N_{R_q}\big|_{q=1}^{2} = 1$ for comparison purposes. Fig. 4.12 clearly reveals that the dual-relay OWRN with joint relay and antenna selection outperforms the dual-relay OWRN having singe-antenna terminals. For example, at an outage of $10^{-4}$, the former system set-up achieves 10 dB SNR gain over the latter. Furthermore, a dual-hop single-relay OWRN is also treated as a reference set-up to show the performance gains obtained by using relay and/or antenna selection strategies. Specifically, the joint antenna and relay selection for dual-antenna OWRN achieves almost 20 dB SNR gain over the single-antenna/single relay OWRN.

**Outage probability of joint antenna and relay selection for TWRNs:**

In Fig. 4.13, the overall outage probability of multi-relay MIMO TWRNs with dual-antenna terminals is plotted. Specifically, the joint Tx/Rx antenna and relay selection is performed based on minimizing the overall outage probability. The analytical curves are plotted by using (4.46) and (4.47a). The outage curves corresponding to the single-relay TWRN is
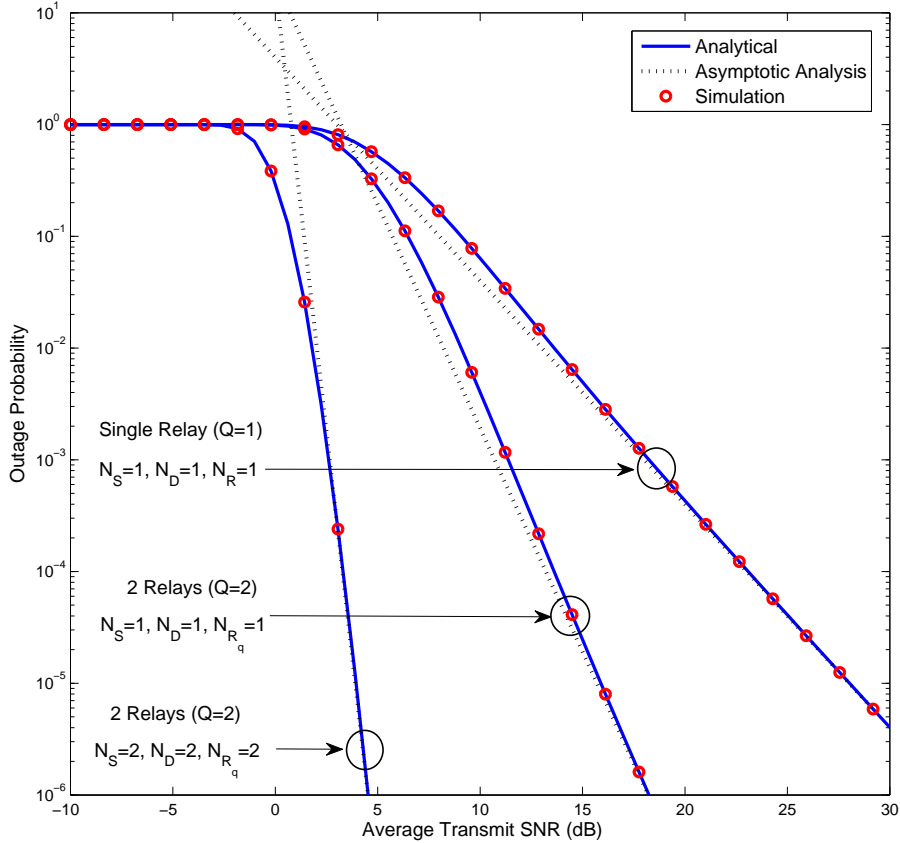
Figure 4.12: The outage probability of joint antenna and relay selection for OWRNs. The direct channel is assumed unavailable and the pathloss exponent is assumed to be $\varpi = 3.5$. The severity of the Nakagami fading channel is set to $m_{SR_q} = 2$ and $m_{R_qD} = 2$ for $q \in \{1, 2\}$, where $q$ is the relay index.

plotted as a benchmark for comparison purposes. Fig. 4.13 clearly illustrates the performance gains of joint antenna and relay selection for the multi-relay TWRNs over that of their single-relay counterpart. For example, at $10^{-5}$ outage probability, the quadruple-relay TWRN provides a SNR gain of 9.5 dB over that of its single-relay counterpart. Furthermore, the asymptotic outage curves verify our diversity order analysis. Monte Carlo simulations agree exactly with analytical outage curves, validating our analysis.

## 4.11 Conclusion

In this chapter, the optimal antenna and relay selection strategies were developed for both multi-antenna OWRNs and TWRNs. To this end, the optimal antenna selection strategies were first studied for single-relay OWRNs/TWRNs, and thereby, the optimal joint and relay
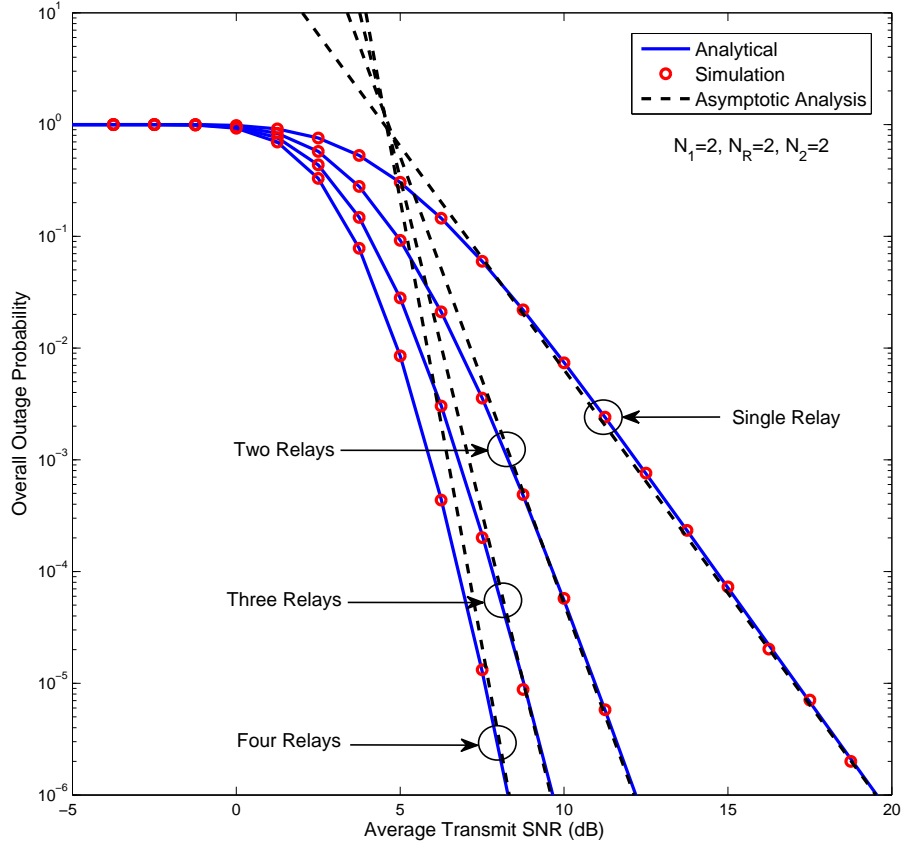
Figure 4.13: The overall outage probability of the optimal joint antenna and relay selection for TWRNs. The target rate of the overall system and individual sources are 2 bits/Hz/s and 1 bits/Hz/s, respectively. The hop distances are $d_{S_1,R} = d_{S_2,R}$, and the pathloss exponent is assumed to be $\varpi = 3.5$.

selection strategies were developed for multiple-relay OWRNs/TWRNs. The performance of the proposed strategies were investigated by deriving the overall outage probability, average SER, and the respective asymptotic approximations at high SNRs. In particular, our asymptotic performance analysis was employed to quantify the achievable diversity order and the array gain, and hence, valuable insights and guidelines for practical system-design perspective were obtained.

The detrimental impact of practical transmission impairments, including the feedback delays and the spatially correlated fading, on the performance of antenna selection was analytically investigated. Specifically, the exact outage probability was derived, and thereby, the amount of performance degradation was quantified in closed-form. In particular, the reduction of the achievable diversity order and the array gain due to feedback delays and

correlated fading were derived, and consequently, valuable insights into practical antenna selection implementation were obtained. Our results reveal that these transmission impairments yield in severe performance degradations. To this end, an efficient linear FIR channel prediction strategy was studied to circumvent the adverse effects of outdated CSI.

Numerical results were provided to show the system performance and thereby elaborating the detrimental impact of practical transmission impairments to obtain useful design insights. Notably, our proposed selection strategies were optimal in the sense of outage probability and hence in the sense of diversity order as well. In particular, the joint relay and antenna selection strategies improve the diversity gains over the single-relay counterparts by a factor equal to the total number of all available antennas at the relays. Our antenna and relay selection strategies indeed achieve full diversity gains while minimizing the cost of implementing multiple Tx/Rx RF chains.

$$\sim$$

# Chapter 5

# Multi-Way MIMO Relay Networks With Zero-Forcing Transmissions

In this chapter, two transmission strategies, namely (i) pairwise zero-forcing transmission and (ii) non-pairwise zero-forcing transmission, are analytically studied for multiple-input multiple-output (MIMO) amplify-and-forward (AF) multi-way relay networks. To this end, lower and upper bounds of the outage probability, the corresponding high signal-to-noise ratio outage probability approximations, and the fundamental diversity-multiplexing trade-off are derived in closed-form. The proposed pairwise zero-forcing transmission strategy possesses a lower practical implementation complexity as each source requires only the instantaneous respective source-to-relay channel knowledge. Counter intuitively, the non-pairwise zero-forcing transmission strategy achieves higher spatial multiplexing gains over the pairwise counterpart at the expense of higher relay processing complexity and more stringent channel state information requirements. Moreover, numerical results are presented to further validate our analysis and thereby to obtain valuable insights into practical MIMO AF multi-way relay network implementation.

## 5.1 Introduction

In multi-way relay networks (MWRNs), $M \geq 2$ spatially-distributed sources mutually exchange their data signals via an intermediate relay. This communication system configuration may arise in many practical scenarios, for example, in multimedia teleconferencing applications via a satellite or in data exchange between sensor nodes and the data fusion center in wireless sensor networks. In particular, MWRNs are the natural generalization of conventional one-way relay networks (OWRNs) and two-way relay networks (TWRNs) [39–42], and consequently, they allow mutual data exchange among more than

two sources. Moreover, OWRNs have already been included in Long Term Evolution-Advanced (LTE-A) standard, and TWRNs are being studied for relay-based International Mobile Telecommunications-Advanced (IMT-A) systems [43]. Thus, MWRNs are also expected to be an integral part of the next-generation wireless standards. However, a comprehensive performance analysis of multiple-antenna MWRNs has been lacking. To this end, in this chapter, two MIMO transmission strategies are developed and analyzed for AF MWRNs.

### 5.1.1   Prior related research on single-antenna MWRNs

Although, multi-way communication channels were first studied more than three decades ago [123], their practical significance has not been fully exploited until the emergence of modern cooperative relay communication research. To this end, in [124–132], the multi-way channel has been exploited with the aid of relays leading to MWRNs. To be more specific, in [124], the achievable symmetric rate of full-duplex MWRNs, where all the sources and the relay operate in full-duplex mode, are studied for several relay processing strategies. However, half-duplex MWRNs may be preferred in practice over full-duplex MWRNs as the practical implementation of the latter is significantly complicated. Thus, in [125], a pairwise half-duplex transmission strategy is studied for MWRNs by employing so-called functional decode-and-forward (FDF) relay processing. Furthermore, the FDF strategy of [125] has been shown to achieve the common-rate capacity of the binary MWRNs whenever the multiple sources exchange signals via a relay at a common-rate. Reference [126] extends the FDF transmission strategy for common-rate binary MWRNs of [125] to the general-rate MWRNs over a finite field by deriving capacity regions. Besides, [127] derives the common-rate capacity of Gaussian MWRNs, where all sources transmit at the same power. In [128], pairwise decode-and-forward (DF) MWRNs based on deterministic broadcasting with side information have been shown to be optimal in the sense of sum-capacity. Recently, in [129], we derived the conditional outage probability and average bit error rate of pairwise AF MWRNs in closed-form. All the aforementioned studies except [129] consider single-antenna MWRNs, where all the sources and the relay are equipped with a single-antenna, and employ the DF protocol exploiting inherent benefits of physical layer network coding.

### 5.1.2   Prior related research on multiple-antenna MWRNs

In [130], a new transceiver strategy is proposed for half-duplex DF MWRNs, where multiple single-antenna sources exchange their signals through a multiple-antenna relay by em-

ploying beamforming techniques. Moreover, [130] derives the transmit beamformer at the relay by employing semidefinite optimization techniques based on relay power minimization criterion. Reference [131] extends [130] to cater AF TWRNs and thereby studying the achievable sum rate for both symmetric and asymmetric traffic scenarios by using simulations. In addition, [133] studies the multi-group AF MWRNs by employing unicast, multicast, and hybrid unicast-multicast transmission strategies. Besides, [132] studies a special case of MWRNs[1] in which signals are exchanged only between predefined pairs of sources. To be more specific, [132] employs a proactive relay precoder design to align messages from the same pair of sources by first eliminating inter-pair interference and then utilizing intra-pair interference for symbol decoding via network coding. All the aforementioned references treat MWRNs with multiple-antenna relays; however, all the sources are single-antenna terminals.

### 5.1.3 Motivation

Although single-antenna MWRNs have been heavily investigated, their achievable spectral efficiency improvement is limited [129]. Thus, more spectrally-efficient MWRNs can be designed by exploiting the additional degrees of freedom (DoFs) provided by multiple-antennas at the sources as well as at the relay. For example, these DoFs can be used for spatial beamforming to eliminate inter-pair/intra-pair interferences and thereby improving the achievable spatial multiplexing gains. To the best of our knowledge, multiple-antenna AF MWRNs, where all sources and relay are equipped with multiple-antennas, have not yet been studied. For instance, the MWRNs considered in [124–129] consist of all single-antenna terminals, while those in [130–132] allow multiple-antenna relays, however, all sources are restricted to single-antenna terminals. Moreover, important system performance metrics of MIMO MWRNs such as the outage probability and the fundamental diversity-multiplexing trade-off (DMT) have not been derived in closed-form.

### 5.1.4 Our contribution

This chapter thus fills the aforementioned gaps in transmission designing and performance analysis of MIMO MWRNs by developing and analyzing two transmission strategies, which are primarily based on transmit/receive (Tx/Rx) zero forcing (ZF), for MIMO AF MWRNs consisting of $M \geq 2$ MIMO-enabled sources and a single MIMO-enabled relay. We term

---

[1]Specifically, the transmission strategy of [132] is only applicable whenever the transmit beamforming at the relay cannot be employed due to the relay antenna array constraints, where there are not enough degrees of freedom to eliminate inter-pair interference.

the MWRNs transmission schemes treated in this chapter as (i) Pairwise ZF transmissions and (ii) Non-pairwise ZF transmissions.

To be more specific, in the pairwise ZF transmission strategy, $M$ sources exchange $M$ independent symbol vectors in two consecutive multiple-access (MAC) and broadcast (BC) phases each having $M-1$ time-slots. In the MAC phase, the $i$th and the $(i+1)$th pair of sources, where $i \in \{1, \cdots, M-1\}$, transmit to the relay by employing transmit-ZF precoding, while the relay receives a superimposed-signal without using a specific receiver reconstruction filtering. This pairwise MAC transmission takes place until the completion of the last pair's transmission. In the BC phase, relay performs a simple AF operation for each superimposed-signal received during the MAC phase by employing a specific gain, which is designed to constraint the long-term total transmission power at the relay. The relay then broadcasts these $M-1$ signals in $M-1$ consecutive time-slots in the BC phase, where all the $M$ sources receive these amplified superimposed-signals by employing their corresponding receive-ZF reconstruction filters. Consequently, each source now has $M-1$ independent signals from which the data signal vectors belonging to the remaining $M-1$ sources can readily be decoded by using self-interference cancellation and back-propagated successive known interference cancellation.

On the other hand, the non-pairwise ZF transmission strategy is capable of exchanging all $M$ data signals among all the participating sources in $M$ time-slots, which contain one MAC phase transmission and $M-1$ BC phase transmissions[2]. In the MAC phase, all the MIMO-enabled sources simultaneously transmit to the relay, where a concatenated-signal vector is recovered by employing the receive-ZF reconstruction filtering. In the next subsequent BC phase transmissions, the relay forwards an amplified-and-permuted[3] version of its received signal back to all the sources by employing a joint transmit-ZF precoding technique.

In this chapter, the basic performance metrics of the two aforementioned MIMO MWRN transmission strategies are derived to obtain valuable insights into their practical implementation. To this end, two novel end-to-end signal-to-noise ratio (SNR) expressions are first developed and then used to derive closed-form lower and upper bounds of the overall outage probability. Mathematically tractable high SNR outage probability approximations are derived, and thereby, the fundamental DMT and maximum achievable diversity/multiplexing

---

[2]This transmission strategy can be considered as an extension of [131] to enable multiple-antenna sources in order to reap both diversity and multiplexing benefits subjected to a fundamental DMT.

[3]To be more specific, this permutation is performed such that the signals belonging to all the sources are fully exchanged among themselves at the end of the final BC phase transmission.

gains are quantified as well in order to obtain valuable insights into practical MIMO MWRN system-design and implementation. Moreover, useful numerical results are presented to further validate the insights provided by our analysis.

### 5.1.5 Significance

It is worth noticing that the two aforementioned transmission strategies are applicable to two specific antenna configurations. Specifically, to employ joint Tx/Rx ZF in the pairwise transmission strategy, the number of antennas at the relay must not exceed the minimum antenna count at any of the sources. On the contrary, the non-pairwise transmission strategy requires the relay to be equipped with a larger antenna array than the summation of all the source antennas in order to retain adequate DoFs to eliminate all inter-pair/intra-pair interferences in the BC phases.

Our pairwise ZF transmission strategy enjoys two-fold benefits over the non-pairwise counterpart; (i) it allows simple practical implementation as each source requires only the corresponding source-to-relay channel knowledge as opposed to the global channel-state information (CSI) requirement, and (ii) it yields lower relay processing complexity as the relay does not either employ any receive-filtering/precoding or require CSI. However, these benefits come at the expense of lower achievable spatial multiplexing gains as shown in Section 5.3.4. Counter intuitively, the non-pairwise ZF transmission strategy enjoys a much higher spatial multiplexing gain, however, by compromising most of the benefits inherent to the pairwise counterpart. To be more specific, non-pairwise strategy requires relay to be equipped with a much larger antenna array in order to enable its joint receive/transmit (Rx/Tx) ZF and thereby substantially increasing the relay processing complexity. Besides, both pairwise and non-pairwise transmission strategies reap substantial diversity and multiplexing gains inherent to MIMO systems, however, subjected to the fundamental DMT. It is worth noticing that our two transmission strategies for MIMO MWRNs can be employed in various practical implementation scenarios by carefully analyzing the performance versus complexity trade-off, which is the most important trade-off in deploying practical cooperative communication systems.

**This chapter is organized as follows:** Section 5.2 outlines the system, channel, and signal models of both pairwise and non-pairwise transmission schemes. In Sections 5.3 and 5.4, the performance metrics of pairwise and non-pairwise transmission strategies are derived. Section 5.5 presents the numerical results, while Section 5.6 outlines the concluding remarks. All proofs are provided in Appendix D.
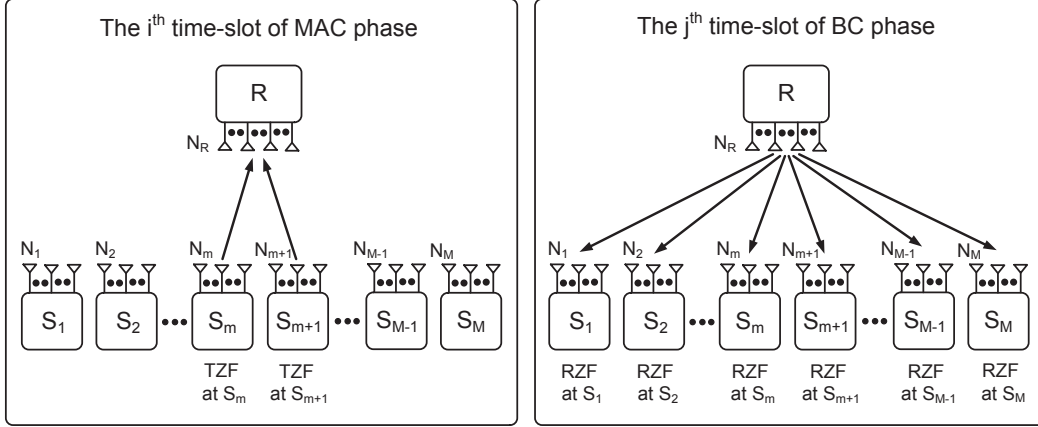
Figure 5.1: The schematic system diagram of pairwise transmission strategy depicting the $i$th time of the MAC phase and the $j$th time-slot of the BC phase, where $i \in \{1, \cdots, M-1\}$ and $j \in \{1, \cdots, M-1\}$. The terms TZF and RZF are referred to the transmit zero-forcing and receive zero-forcing, respectively.

## 5.2 System, channel and signal models

In this section, the system, channel, and signal models pertaining to the two transmission strategies of MIMO AF MWRNs are presented. Specifically, we consider an AF MIMO MWRN consisting of $M$ sources ($S_m$) for $m \in \{1, \cdots, M\}$ and one relay node ($R$), where each of them operates in half-duplex mode. The $m$th source and the relay are equipped with $N_m$ and $N_R$ antennas respectively. All the channels are assumed to be independently distributed frequency-flat Rayleigh fading. Moreover, the noise at all the receivers is modeled as complex zero mean additive white Gaussian noise (AWGN). The direct channel between $S_m$ and $S_{m'}$ for $m \neq m'$ is assumed to be unavailable due to transmission impairments such as heavy pathloss and shadowing [35]. The channel matrix from $S_m$ to $R$ in the $i$th time-slot of the MAC phase is denoted as $\mathbf{H}_{m,R}^{(i)} \sim \mathcal{CN}_{N_R \times N_m}\left(\mathbf{0}_{N_R \times N_m}, \mathbf{I}_{N_R} \otimes \mathbf{I}_{N_m}\right)$. The channel matrix from $R$ to $S_m$ in the $j$th time-slot of the BC phase is denoted as $\mathbf{H}_{R,m}^{(j)} \sim \mathcal{CN}_{N_m \times N_R}\left(\mathbf{0}_{N_m \times N_R}, \mathbf{I}_{N_m} \otimes \mathbf{I}_{N_R}\right)$. Moreover, all the channel matrices are assumed to be remain fixed over one time-slot. Besides, $\mathbf{H}_{m,R}^{(i)}$ and $\mathbf{H}_{m',R}^{(i')}$ are independent for $(m, m') \in \{1, \cdots, M\}$, $(i, i') \in \{1, \cdots, M-1\}$ and $m \neq m'$. Similarly, $\mathbf{H}_{R,m}^{(j)}$ and $\mathbf{H}_{R,m'}^{(j')}$ are independent for $(j, j') \in \{1, \cdots, M-1\}$, $(m, m') \in \{1, \cdots, M\}$, $j \neq j'$ and $m \neq m'$.

In the next two subsections, signal models for pairwise ZF transmissions and non-pairwise ZF transmissions are presented in detail. Specifically, the MAC and BC phase signaling models, signal decoding process, and end-to-end SNR formulation of both trans-
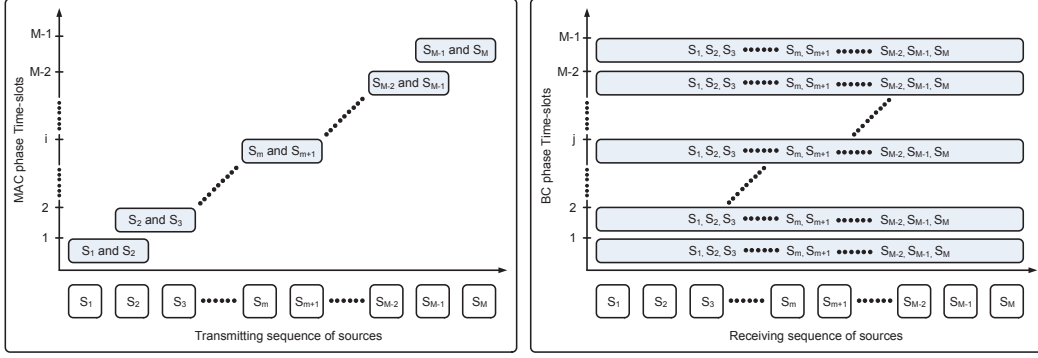
Figure 5.2: The schematic timing diagram of pairwise transmission strategy depicting the MAC phase and BC phase time-slots and transmission/reception sequence.

mission strategies are explicitly described by employing schematic timing diagrams and concrete examples.

### 5.2.1 Signal model of MIMO AF MWRNs with pairwise transmissions

In the MIMO AF MWRNs with pairwise ZF transmissions[4], all $M$ sources exchange their data signal vectors, $\mathbf{x}_m$, satisfying $\mathcal{E}\left[\mathbf{x}_m\mathbf{x}_m^H\right] = \mathbf{I}_{N_R}$, each other in two consecutive MAC and BC transmission phases each of them having $M - 1$ time-slots.

**MAC phase of pairwise transmission strategy:**

Let us consider an intermediate stage of the MAC phase, i.e., its $i$th time-slot (see Fig. 5.1 and Fig. 5.2). In the $i$th time-slot of the MAC phase, the pair of sources, $S_m$ and $S_{m+1}$ transmit $\mathbf{x}_m$ and $\mathbf{x}_{m+1}$ simultaneously to $R$ by employing transmit-ZF precoding. The received superimposed-signal vector at $R$ in the $i$th time-slot of MAC phase is given by

$$\mathbf{y}_R^{(i)} = \mathbf{H}_{m,R}^{(i)}\left(g_m\mathbf{U}_m^{(i)}\mathbf{x}_m\right) + \mathbf{H}_{m+1,R}^{(i)}\left(g_{m+1}\mathbf{U}_{m+1}^{(i)}\mathbf{x}_{m+1}\right) + \mathbf{n}_R^{(i)}, \qquad (5.1)$$

where $i \in \{1, \cdots, M - 1\}$, $\mathbf{H}_{m,R}^{(i)}$ is the channel matrix from $S_m$ to $R$, and $\mathbf{n}_R^{(i)}$ is the $N_R \times 1$ zero mean AWGN vector at $R$ in the $i$th time-slot of the MAC phase satisfying $\mathcal{E}\left[\mathbf{n}_R^{(i)}\left(\mathbf{n}_R^{(i)}\right)^H\right] = \mathbf{I}_{N_R}\sigma_R^2$. In (5.1), $g_m\mathbf{U}_m^{(i)}\mathbf{x}_m$ is the precoded transmit signal at $S_m$ with the dimension[5] $N_m \times 1$. Moreover, $\mathbf{U}_m^{(i)}$ is the transmit-ZF precoding matrix at $S_m$ in the

---

[4]In MIMO AF MWRN with pairwise transmissions, the constraint $N_R < \min\left(N_1, \cdots, N_M\right)$ is imposed to employ joint transmit/receiver ZF for the same antenna configuration [134]. Consequently, the maximum number of end-to-end data subchannels from $S_i$ to $R$ is constrained to $N_R$.

[5]Note that the precoded transmit signal at $S_m$ is of dimension $N_m \times 1$, and hence, no transmit antenna is discarded arbitrarily.

$i$th time-slot of the MAC phase, and is given by [134]

$$\mathbf{U}_m^{(i)} = \left(\mathbf{H}_{m,R}^{(i)}\right)^H \left(\mathbf{H}_{m,R}^{(i)} \left(\mathbf{H}_{m,R}^{(i)}\right)^H\right)^{-1},\tag{5.2}$$

Besides, in (5.1), $g_m$ is the power normalizing factor, which constraints the long-term total power at $S_m$, and is given by

$$g_m = \sqrt{\mathcal{P}_m/\mathrm{Tr}\left(\mathcal{E}\left[\mathbf{U}_m^{(i)}\left(\mathbf{U}_m^{(i)}\right)^H\right]\right)} = \sqrt{\mathcal{P}_m/\mathcal{T}_m},\tag{5.3}$$

where $\mathcal{T}_m \triangleq \mathrm{Tr}\left(\mathcal{E}\left[\mathbf{U}_m^{(i)}(\mathbf{U}_m^{(i)})^H\right]\right) = \frac{N_R}{N_m - N_R}$ [135] and $\mathcal{P}_m$ is the transmit power at $S_m$.

**Remark:** Only $N_R$ independent data symbols can be sent from each node to the relay as it has only $N_R$ receive antennas. To ensure this constraint at each node, the symbol vectors of arbitrary lengths are multiplied by a permutation matrix as follows:

$$\mathbf{x}_m = \mathbf{\Pi}_m \mathbf{d}_m,\tag{5.4}$$

where $\mathbf{d}_m$ is a symbol vector at $S_m$ with dimension $l_m \times 1$. Further in (5.4), $\mathbf{\Pi}_m$ is the $N_R \times l_m$ permutation matrix[6], which ensures only $N_R$ independent data streams are transmitted to the relay by each node to avoid any data symbol loss.

The aforementioned MAC phase continues until the last pair of sources, $S_{M-1}$ and $S_M$, complete their transmission (see Fig. 5.2), and consequently, $R$ has now received $M-1$ pairwise transmissions containing $M-1$ superimposed-signals in the form of (5.1).

**BC phase of pairwise transmission strategy:**

During the BC phase, $R$ broadcasts the amplified versions of the $M-1$ received signals back to all $M$ sources in $M-1$ consecutive time-slots (see Fig. 5.1 and Fig. 5.2). Again, we consider the $j$th time-slot, an intermediate stage of the BC phase for the sake of the brevity of the exposition. Furthermore, let us assume that $\mathbf{y}_R^{(i)}$ in (5.1), which is the signal received by $R$ in the $i$th time-slot of the MAC phase, is scheduled to be transmitted in the $j$th time-slot of the BC phase. In the $j$th time-slot of the BC phase, the transmitted signal by $R$ is given by

$$\mathbf{x}_R^{(j)} = G_j \mathbf{y}_R^{(i)} \quad \text{for } j \in \{1, \cdots, M-1\},\tag{5.5}$$

where $G_j = \sqrt{\mathcal{P}_R/(g_m^2 + g_{m+1}^2 + \sigma_R^2)}$ is the relay power normalizing constant corresponding to $\mathbf{y}_R^{(i)}$ in (5.1) and is designed to constraint the long-term total relay transmit

---

[6]The permutation matrix, $\mathbf{\Pi}_m$, is constructed by horizontally concatenating a $N_R \times N_R$ permutation matrix and a $N_R \times (l_m - N_R)$ zero matrix, where $m \in \{1, \cdots, M\}$.

power. Note that in (5.5), $\mathbf{y}_R^{(i)}$ can be either of $M-1$ superimposed-signals received by $R$ during the MAC phase. The broadcast signal in (5.5) is then received by all the $M$ sources. During the $j$th time-slot of the BC phase, the received signal at the $m$th source is given by

$$\mathbf{y}_{S_m}^{(j)} = \mathbf{V}_m^{(j)}\Big(G_j\mathbf{H}_{R,m}^{(j)}\mathbf{y}_R^{(i)} + \mathbf{n}_m^{(j)}\Big),\tag{5.6}$$

where $j \in \{1,\cdots,M-1\}$ and $m \in \{1,\cdots,M\}$. Besides, $\mathbf{H}_{R,m}^{(j)}$ is the channel matrix from $R$ to $S_m$ in the $j$th time-slot of the BC phase, and is assumed to be statistically independent for different $m \in \{1,\cdots,M\}$ and $j \in \{1,\cdots,M-1\}$. Moreover, in (5.6), $\mathbf{n}_m^{(j)}$ is the $N_m \times 1$ zero mean AWGN vector at $S_m$ satisfying $\mathcal{E}\left[\mathbf{n}_m^{(j)}\left(\mathbf{n}_m^{(j)}\right)^H\right] = \mathbf{I}_{N_m}\sigma_m^2$ for $m \in \{1,\cdots,M\}$ and $\mathbf{V}_m^{(j)}$ is the receive-ZF matrix at $S_m$ employed in the $j$th time-slot, and is given by [134]

$$\mathbf{V}_m^{(j)} = \left(\left(\mathbf{H}_{R,m}^{(j)}\right)^H\mathbf{H}_{R,m}^{(j)}\right)^{-1}\left(\mathbf{H}_{R,m}^{(j)}\right)^H,\tag{5.7}$$

where $j \in \{1,\cdots,M-1\}$ and $m \in \{1,\cdots,M\}$. The aforementioned BC phase transmissions continue until all $M-1$ superimposed-signals are broadcast by $R$ during $M-1$ successive BC phase time-slots in order to ensure that each source receives adequate number of independent signals from which the signals belonging to other $M-1$ sources can readily be decoded.

**Signal decoding process of pairwise transmission strategy:**

Upon the completion of the MAC phase and the BC phase, mutual exchange of all $M$ source signal vectors via the relay is accomplished. Each source therefore has received $M-1$ independent signals, which indeed carry the data of the remaining $M-1$ sources. Now by employing self-interference cancellation and back-propagated known-interference cancellation successively [25,125,131], each source can readily decode the data of the other $M-1$ sources.

For the sake of the exposition of signal decoding, let us consider a three-way relay network consisting of three sources and a single relay. By first substituting (5.1) and (5.7) into (5.6), and then letting $M = 3$, $i \in \{1,2\}$, $j \in \{1,2\}$ and $m \in \{1,2,3\}$, the signals received at $S_i$ for $i \in \{1,2,3\}$ during the first time-slot of BC phase are given by

$$\mathbf{y}_{S_1}^{(1)} = G_1\left(g_1\mathbf{x}_1 + g_2\mathbf{x}_2 + \mathbf{n}_R^{(1)}\right) + \mathbf{V}_1^{(1)}\mathbf{n}_1^{(1)}\tag{5.8a}$$

$$\mathbf{y}_{S_2}^{(1)} = G_1\left(g_1\mathbf{x}_1 + g_2\mathbf{x}_2 + \mathbf{n}_R^{(1)}\right) + \mathbf{V}_2^{(1)}\mathbf{n}_2^{(1)}\tag{5.8b}$$

$$\mathbf{y}_{S_3}^{(1)} = G_1\left(g_1\mathbf{x}_1 + g_2\mathbf{x}_2 + \mathbf{n}_R^{(1)}\right) + \mathbf{V}_3^{(1)}\mathbf{n}_3^{(1)},\tag{5.8c}$$

where $G_1 = \sqrt{\mathcal{P}_R/(g_1^2 + g_2^2 + \sigma_R^2)}$. Similarly, the signals received at the three sources in the second time-slot of the BC phase are next given by

$$\mathbf{y}_{S_1}^{(2)} = G_2 \left( g_2\mathbf{x}_2 + g_3\mathbf{x}_3 + \mathbf{n}_R^{(2)} \right) + \mathbf{V}_1^{(2)}\mathbf{n}_1^{(2)} \tag{5.9a}$$

$$\mathbf{y}_{S_2}^{(2)} = G_2 \left( g_2\mathbf{x}_2 + g_3\mathbf{x}_3 + \mathbf{n}_R^{(2)} \right) + \mathbf{V}_2^{(2)}\mathbf{n}_2^{(2)} \tag{5.9b}$$

$$\mathbf{y}_{S_3}^{(2)} = G_2 \left( g_2\mathbf{x}_2 + g_3\mathbf{x}_3 + \mathbf{n}_R^{(2)} \right) + \mathbf{V}_3^{(2)}\mathbf{n}_3^{(2)}, \tag{5.9c}$$

where $G_2 = \sqrt{\mathcal{P}_R/(g_2^2 + g_3^2 + \sigma_R^2)}$.

The signals received by $S_1$ are given by (5.8a) and (5.9a). From (5.8a), the self-interference, i.e., the term involving $\mathbf{x}_1$, can be readily canceled, and consequently, the signal vector belonging to $S_2$, i.e., $\mathbf{x}_2$, can now be decoded at $S_1$ by employing standard ZF MIMO decoding [25]. Next, by knowing $\mathbf{x}_2$ from the previous decoding step, the interference owing $\mathbf{x}_2$ in (5.9a) can be eliminated and thus paving the way to decoding of $\mathbf{x}_3$ at $S_1$. This step of interference cancellation is referred to as back-propagated known-interference cancellation [125, 131]. Similarly, by employing self-interference and back-propagated known-interference cancellations successively, the the signals received at $S_2$ and $S_3$ can be decoded as well.

**End-to-end SNR of pairwise ZF transmission strategy:**

In this subsection, we develop a general end-to-end SNR expression for an arbitrary data subchannel. To this end, by again substituting (5.1) and (5.7) into (5.6), and then by employing back-propagated successive self-interference and known-interference cancellation[7], the signal vector pertinent to the $n$th source, received at the $m$th source in the $j$th time-slot of the BC phase is derived as

$$\mathbf{y}_{S_m}^{(j,n)} = G_j \left( g_n\mathbf{x}_n + \mathbf{n}_R^{(j)} \right) + \mathbf{V}_m^{(j)}\mathbf{n}_m^{(j)}, \tag{5.10}$$

where $j \in \{1, \cdots, M-1\}$, $m \in \{1, \cdots, M\}$, $n \in \{1, \cdots, M\}$, and $m \neq n$. Then the post-processing end-to-end SNR of the $k$th data subchannel of $\mathbf{y}_{S_m}^{(j,n)}$ in (5.10) can be derived as follows: (see Appendix D.1 for the proof)

$$\left[ \gamma_{S_m^{(j,n)}} \right]_k = \frac{\bar{\gamma}_{R,m}\bar{\gamma}_{n,R}\mathcal{T}_j\mathcal{T}_{j+1}\mathcal{T}_n^{-1}}{\bar{\gamma}_{R,m}\mathcal{T}_j\mathcal{T}_{j+1} + (\bar{\gamma}_{j,R}\mathcal{T}_{j+1} + \bar{\gamma}_{j+1,R}\mathcal{T}_j + \mathcal{T}_j\mathcal{T}_{j+1}) \left[ \left( \left( \mathbf{H}_{R,m}^{(j)} \right)^H \mathbf{H}_{R,m}^{(j)} \right)^{-1} \right]_{k,k}} \tag{5.11}$$

---

[7]It is assumed that $S_m$ knows its own data symbol vector, $\mathbf{x}_m$, CSI of $\mathbf{H}_{m,R}^{(i)}$, and $G_j$, which requires $g_m$.
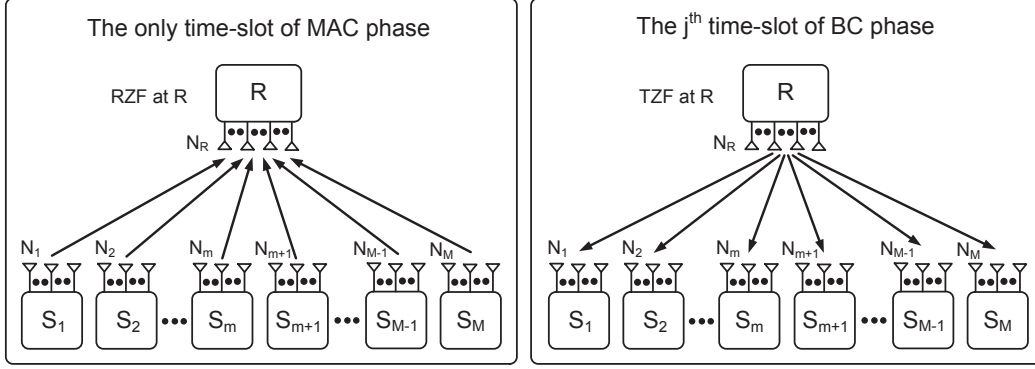
Figure 5.3: The schematic system diagram of non-pairwise transmission strategy depicting the only time of the MAC phase and the $j$th time-slot of the BC phase, where $j \in \{1, \cdots, M-1\}$. The terms TZF and RZF are referred to the transmit zero-forcing and receive zero-forcing, respectively.

where $k \in \{1, \cdots, N_R\}$, $\bar{\gamma}_{R,m} = P_R/\sigma_m^2$, $\bar{\gamma}_{j,R} = P_j/\sigma_R^2$, and $\bar{\gamma}_{n,R} = P_n/\sigma_R^2$[8]. Furthermore, $\mathcal{T}_j$s are defined in (5.3) and given by $\mathcal{T}_j = N_R/(N_j - N_R)$, $\mathcal{T}_{j+1} = N_R/(N_{j+1} - N_R)$, and $\mathcal{T}_n = N_R/(N_n - N_R)$.

**Remark II.1:** The end-to-end SNR random variables, $\left[\gamma_{S_m^{(j,n)}}\right]_k$, for $k \in \{1, \cdots, N_R\}$ in (5.11) are statistically correlated for a given set of $j$, $m$, and $n$ values as noise term in (5.10) is colored due to $\mathbf{V}_m^{(j)}$. However, the set of $\left[\gamma_{S_m^{(j,n)}}\right]_k$ belonging to different $j$, $m$ and $n$ values are statistically independent.

### 5.2.2 Signal model of MIMO AF MWRNs with non-pairwise ZF transmissions

In the MIMO AF MWRNs with non-pairwise ZF transmissions[9], all $M$ sources exchange their data signal vectors in $M$ time-slots. The MAC phase consists of only one time-slot, whereas the BC phase contains $M - 1$ time-slots.

**MAC phase of non-pairwise transmission strategy:**

During the MAC phase, all the sources transmit simultaneously their signals to $R$ without employing any transmit precoding strategy (see Fig. 5.3 and Fig. 5.4). The pre-processed

---

[8]It is worth noticing that the index pair $(j, n)$ in (5.10) and (5.11) is used only to differentiate the sequence of symbol vectors received by a particular source in each time-slot of the BC phase from the remaining set of sources. Thus, each pair of $(j, n)$ has a one-to-one correspondence, and hence, without loss of generality, the index $n$ is removed herein for the sake of notational simplicity.

[9]In the MIMO AF MWRNs with non-pairwise transmissions, the constraint $N_R > \sum_{i=1}^{M} N_i$ is imposed to employ joint receiver and transmit ZF at the relay. Consequently, the maximum number of end-to-end data subchannels from all the sources to the relay is constrained to $\sum_{i=1}^{M} N_{\min}$, where $N_{\min} = \min_{i \in \{1, \cdots, M\}} (N_i)$.
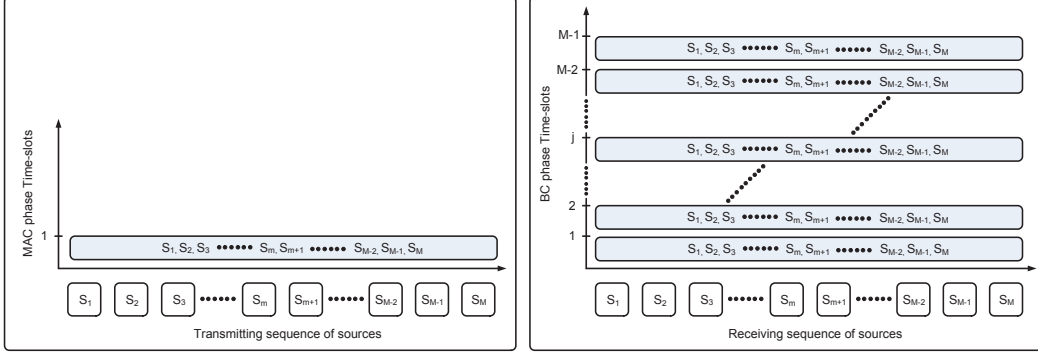
Figure 5.4: The schematic timing diagram of non-pairwise transmission strategy depicting the MAC phase and BC phase time-slots and transmission/reception sequence.

superimposed-signal vector received at $R$ is given by

$$\mathbf{y}_R = \sum_{m=1}^{M} \sqrt{\frac{\mathcal{P}_m}{N_m}} \mathbf{H}_{m,R} \mathbf{\Pi}_m \mathbf{x}_m + \mathbf{n}_R, \qquad (5.12)$$

where $\mathbf{n}_R$ is a noise vector at $R$ satisfying $\mathcal{E}\left[\mathbf{n}_R \mathbf{n}_R^H\right] = \mathbf{I}_{N_R} \sigma_R^2$. Moreover, $\mathbf{\Pi}_m$ for $m \in \{1, \cdots, M\}$ is the permutation matrix at $S_m$ and used to ensure that only $N_{\min} = \min_{m \in \{1, \cdots, M\}} (N_m)$ data subchannels are transmitted by any $S_m$ in order to eliminate any lost of data subchannels in the BC phase at the sources[10]. Next, the pre-processed signal at $R$ given in (5.12) can alternatively be rewritten as

$$\mathbf{y}_R = \mathbf{H}_{S,R} \mathbf{x}_S + \mathbf{n}_R, \qquad (5.13)$$

where $\mathbf{H}_{S,R} \in \mathbb{C}^{N_R \times \sum_{m=1}^{M} N_m}$ is the effective channel matrix formed by horizontally concatenating individual channel matrices as follows:

$$\mathbf{H}_{S,R} = [\mathbf{H}_{1,R}, \mathbf{H}_{2,R}, \cdots, \mathbf{H}_{M,R}]. \qquad (5.14)$$

Furthermore, $\mathbf{x}_S$ is the effective transmit signal vector obtained by vertically concatenating the weighted individual source transmit vectors $\mathbf{x}_i$ and can be written as $\mathbf{x}_S = \left[\sqrt{\mathcal{P}_1/N_1}\mathbf{\Pi}_1\mathbf{x}_1; \sqrt{\mathcal{P}_2/N_2}\mathbf{\Pi}_2\mathbf{x}_2; \cdots; \sqrt{\mathcal{P}_M/N_M}\mathbf{\Pi}_M\mathbf{x}_M\right]$. The relay then employs the receive-ZF reconstruction matrix, $\mathbf{W}_r$, to receive this superimposed-signal vector as follows:

$$\tilde{\mathbf{y}}_R = \mathbf{W}_r \mathbf{y}_R = \mathbf{x}_S + \mathbf{W}_r \mathbf{n}_R, \qquad (5.15)$$

where $\mathbf{W}_r = \left(\mathbf{H}_{S,R}^H \mathbf{H}_{S,R}\right)^{-1} \mathbf{H}_{S,R}^H$.

---

[10]Moreover, the permutation matrix, $\mathbf{\Pi}_m$, for $m \in \{1, \cdots, M\}$ is constructed by first horizontally concatenating an $\mathbf{I}_{N_{\min}}$ and $\mathbf{O}_{N_{\min} \times (N_m - N_{\min})}$ matrices, and then vertically concatenating this resulting matrix with another $\mathbf{O}_{(N_m - N_{\min}) \times N_m}$ matrix.

**BC phase of non-pairwise transmission strategy:**

During the BC phase, $R$ employs the transmit-ZF precoding to broadcast an amplified-and-permuted version of $\tilde{\mathbf{y}}_R$ back to all the sources in $M-1$ subsequent time-slots (see Fig. 5.3 and Fig. 5.4). For the sake of exposition of the BC phase transmissions, an intermediate $j$th time-slot of the BC phase is considered. To this end, the transmitted signal by $R$ in the $j$th time-slot of the BC phase can be written as

$$\tilde{\mathbf{y}}_R^{(j)} = \mathbf{W}_t^{(j)} G^{(j)} \mathbf{\Pi}^{(j)} \mathbf{W}_r \mathbf{y}_R, \tag{5.16}$$

where $\mathbf{W}_t^{(j)} = \left(\mathbf{H}_{R,S}^{(j)}\right)^H \left(\mathbf{H}_{R,S}^{(j)} \left(\mathbf{H}_{R,S}^{(j)}\right)^H\right)^{-1}$ is the transmit precoding matrix at $R$. Here, $\mathbf{H}_{R,S}^{(j)} \in \mathbb{C}^{\sum_{i=1}^M N_i \times N_R}$ is the effective channel matrix from $R$ to all the sources and constructed by vertically concatenating individual channel matrices as follows:

$$\mathbf{H}_{R,S} = [\mathbf{H}_{R,1}; \mathbf{H}_{R,1}; \cdots ; \mathbf{H}_{R,M}]. \tag{5.17}$$

In (5.16), the amplification gain, $G^{(j)}$, is designed to constraint long-term relay transmit power as

$$G^{(j)} = \sqrt{\mathcal{P}_R \left[\left(\sum_{i=1}^M \frac{\mathcal{P}_i}{N_i}\right)\alpha + \beta\right]^{-1}}, \tag{5.18}$$

where $\alpha = \mathrm{Tr}\left(\mathcal{E}\left[\mathbf{W}_t^{(j)}\left(\mathbf{W}_t^{(j)}\right)^H\right]\right)$ and $\beta = \mathrm{Tr}\left(\mathcal{E}\left[(\mathbf{W}_t^{(j)}\mathbf{W}_r\mathbf{n}_R)(\mathbf{W}_t^{(j)}\mathbf{W}_r\mathbf{n}_R)^H\right]\right)$. Moreover, in (5.16), $\mathbf{\Pi}^{(j)}$ is the permutation matrix at the $j$th time-slot of the BC phase, and designed to ensure that the signal belonging to $S_{m+1}$ is transmitted to $S_m$ for all $m \in \{1, \cdots, M\}$ with $S_{M+1} \triangleq S_1$. To this end, $\mathbf{\Pi}^{(j)}$ for $j \in \{1, \cdots M-1\}$ is constructed as $\mathbf{\Pi}^{(j)} = (\mathbf{\Pi}_P)^j$, where $\mathbf{\Pi}_P$ is the primary permutation matrix with $\sum_{m=1}^M N_m \times \sum_{m=1}^M N_m$ dimension and given by

$$\mathbf{\Pi}_P = \begin{bmatrix} \mathbf{O}_{N_2 \times N_1} & \mathbf{I}_{N_2} & \mathbf{O}_{N_2 \times N_3} \cdots & \mathbf{O}_{N_2 \times N_{M-1}} & \mathbf{O}_{N_2 \times N_M} \\ \mathbf{O}_{N_3 \times N_1} & \mathbf{O}_{N_3 \times N_2} & \mathbf{I}_{N_3} \cdots & \mathbf{O}_{N_2 \times N_{M-1}} & \mathbf{O}_{N_3 \times N_M} \\ \vdots & \vdots & \ddots & \vdots & \vdots \\ \mathbf{O}_{N_{M-1} \times N_1} & \mathbf{O}_{N_{M-1} \times N_2} \cdots & \cdots & \mathbf{I}_{N_{M-1}} & \mathbf{O}_{N_{M-1} \times N_M} \\ \mathbf{O}_{N_M \times N_1} & \mathbf{O}_{N_M \times N_2} \cdots & \cdots & \mathbf{O}_{N_M \times N_{M-1}} & \mathbf{I}_{N_M} \\ \mathbf{I}_{N_1} & \mathbf{O}_{N_1 \times N_2} \cdots & \cdots & \mathbf{O}_{N_1 \times N_{M-1}} & \mathbf{O}_{N_1 \times N_M} \end{bmatrix} \tag{5.19}$$

The concatenated received signal vector at the sources in the $j$th time-slot of the BC phase can then be written as

$$\mathbf{y}_S^{(j)} = \mathbf{H}_{R,S}^{(j)} \mathbf{W}_t^{(j)} G^{(j)} \mathbf{\Pi}^{(j)} \mathbf{W}_r \mathbf{y}_R + \mathbf{n}_S, \quad \text{for} \quad j \in \{1, \cdots, M-1\}, \tag{5.20}$$

where $\mathbf{n}_S$ is the concatenated-AWGN vector at all the sources satisfying $\mathcal{E}\left[\mathbf{n}_S\mathbf{n}_S^H\right] = \sigma_R^2\mathbf{I}_{\sum_{i=1}^M N_i}$. The BC phase continues until the completion of all $M-1$ relay transmissions in $M-1$ consecutive time-slots.

**Signal decoding process of non-pairwise transmission strategy:**

Upon the completion of the MAC and BC phases, each source has now received the $M-1$ noise perturbed signal vectors belonging to other $M-1$ sources. This full data signal exchange is achieved due to the fact that the relay has enough degrees of freedom which can readily be exploited for spatial beamforming to eliminate inter-source/intra-stream interferences by virtue of successive $M-1$ transmit ZF transmissions of the carefully permuted signal vector in the BC phase. This permutation ensures every source receives $M-1$ signal vectors corresponding to the remaining $M-1$ sources within the $M-1$ BC phase transmit ZF transmissions. The each of $M-1$ signals received by any particular source can readily be decoded by employing standard MIMO signal detection techniques developed for MIMO ZF systems [25].

In the next subsection, the end-to-end SNR of an arbitrary data subchannel at the sources for the non-pairwise ZF transmission strategy is derived in closed-form.

**End-to-end SNR of non-pairwise ZF transmission strategy:**

By employing similar techniques to those in Appendix D.1, the end-to-end SNR of the $k$th subchannel of $\mathbf{y}_S^{(j)}$ in (5.20) is derived as

$$\left[\gamma_{\mathbf{y}_S^{(j)}}\right]_k = \frac{\bar{\gamma}_{R,k'}\bar{\gamma}_{k',R}}{N_{k'}\mathcal{Q}_j' + N_{k'}\mathcal{Q}_j\displaystyle\sum_{i=1}^M \frac{\bar{\gamma}_{i,R}}{N_i} + N_{k'}\bar{\gamma}_{R,k'}\left[\left((\mathbf{H}_{S,R})^H\mathbf{H}_{S,R}\right)^{-1}\right]_{k',k'}}, \tag{5.21}$$

where $k \in \{1, \cdots, N_S\}$, $\bar{\gamma}_{k',R} \triangleq \frac{\mathcal{P}_{k'}}{\sigma_R^2}$, $\bar{\gamma}_{R,k'} \triangleq \frac{\mathcal{P}_R}{\sigma_{k'}^2}$, $N_S = \sum_{m=1}^M N_m$, and $k' = \pi(j,k)$, which is determined by the permutation matrix $\mathbf{\Pi}^{(j)}$. Moreover, the system dependent parameters $\mathcal{Q}$ and $\mathcal{Q}'$ are given by

$$\mathcal{Q}_j = \mathrm{Tr}\Big(\mathcal{E}\left[\mathbf{W}_t^{(j)}(\mathbf{W}_t^{(j)})^H\right]\Big) = \mathrm{Tr}\Big(\mathcal{E}\left[\left(\mathbf{H}_{R,S}^{(j)}(\mathbf{H}_{R,S}^{(j)})^H\right)^{-1}\right]\Big), \tag{5.22}$$

$$\mathcal{Q}_j' = \mathrm{Tr}\Big(\mathcal{E}\big[(\mathbf{W}_t^{(j)}\mathbf{W}_r)(\mathbf{W}_t^{(j)}\mathbf{W}_r)^H\big]\Big) = \mathrm{Tr}\Big(\mathcal{E}\big[\left((\mathbf{H}_{R,S}^{(j)})^H\mathbf{H}_{S,R}^H\mathbf{H}_{S,R}\mathbf{H}_{R,S}^{(j)}\right)^{-1}\big]\Big)$$

The end-to-end SNR of the $k$th data subchannel of $S_m$ belonging to $S_j$ for $(m,j) \in$

$\{1, \cdots, M\}$ and $m \neq j$ can then be written by using (5.21) as follows:

$$\left[\gamma_{S_m^{(j)}}\right]_k = \frac{\bar{\gamma}_{R,m}\bar{\gamma}_{j,R}}{N_j\mathcal{Q}_j' + N_j\mathcal{Q}_j \sum_{m=1}^{M} \frac{\bar{\gamma}_{i,R}}{N_m} + N_j\bar{\gamma}_{R,m}\left[\left((\mathbf{H}_{S,R})^H\mathbf{H}_{S,R}\right)^{-1}\right]_{k_{m,j},k_{m,j}}}, \quad (5.23)$$

where $k \in \{1, \cdots, N_{\min}\}$. Moreover, in (5.23), $k_{m,j} \in \{1, \cdots, MN_{\min}\}$ and the relationship between $k$ and $k_{m,j}$ strictly depends[11] on the permutation matrix, $\mathbf{\Pi}^{(j)}$.

**Remark II.2:** It is worth noting that the end-to-end SNR random variables of data sub-channels of $S_m$, $\left[\gamma_{S_m^{(j)}}\right]_k$, for $j \in \{1, \cdots, M\}$, $m \neq j$ and $k \in \{1, \cdots, N_{\min}\}$ in (5.23) are statistically correlated due to the colored noise at $R$ resulted from $\mathbf{W}_r$. Moreover, $\left[\gamma_{S_m^{(j)}}\right]_k$ for $m \in \{1, \cdots, M\}$ and $\left[\gamma_{S_{m'}^{(j)}}\right]_k$ for $m' \in \{1, \cdots, M\}$ can share the same random variable, $\left[\left((\mathbf{H}_{S,R})^H\mathbf{H}_{S,R}\right)^{-1}\right]_{k',k'}$, for $k' \in \{1, \cdots, MN_{\min}\}$ as the relay broadcasts a permuted version of the same noise perturbed signal, which is received in the MAC phase, $M - 1$ times in the BC phase.

**Remark II.3:** The end-to-end SNR expressions corresponding to MIMO MWRNs with both pairwise and non-pairwise transmissions in (5.11) and (5.23), respectively, possess the same form of $\gamma = \eta/(\zeta + \mu X)$, where $\eta$, $\zeta$ and $\mu$ are system dependent parameters and $X$ is the random variable. Thus, the statistical characterization of both (5.11) and (5.23) follow the same techniques.

**Remark II.4:** In both pairwise and non-pairwise transmissions schemes, antenna selection algorithms can be employed at the sources to further optimize the overall performance. In this context, optimal antenna subset selection algorithms based on maximizing the achievable sum-rate or minimizing the overall outage probability can be developed. Development of such optimal antenna selection algorithms and other performance optimizing techniques remain as important, interesting open research problems, and will be considered in our future research directions.

### 5.2.3 Alternative source-grouping strategies

The pairwise and non-pairwise ZF transmission strategies discussed in Section 5.2.1 and Section 5.2.2, respectively, follow the pairwise source-grouping and the all-simultaneous source-grouping, which are indeed the two extreme cases of source-grouping schemes. Besides, there exists arbitrary source-grouping schemes in which each group may consist of

---

[11]Random variable $\left[\left((\mathbf{H}_{S,R})^H\mathbf{H}_{S,R}\right)^{-1}\right]_{k_{m,j},k_{m,j}}$ for $k_{m,j} \in \{1, \cdots, MN_{\min}\}$ are in fact identically distributed, and hence, the exact relationship between $k$ and $k_{m,j}$ does not affect the performance analysis.

an arbitrary number of sources, and hence, they lie in between the two extreme source-grouping schemes. To be more specific, $L$ source groups can be first formed from the available $M$ sources. The $l$th group consists of $M_l$ sources and the $m$th source belonging to the $l$th group, $S_{l,m}$, is equipped with $N_{l,m}$ antennas, where $l \in \{1, \cdots, L\}$ and $m \in \{1, \cdots, M_l\}$. The total number of antennas of the $l$th group's sources can be therefore quantified as $N_l = \sum_{i=1}^{M_l} N_{l,i}$. Further, the total number of all source antennas is $N_S = \sum_{l=1}^{L} N_l = \sum_{l=1}^{L} \sum_{i=1}^{M_l} N_{l,i}$. In particular, these groups are formed to satisfy specific antenna constraints to ensure that each group possesses adequate amount of degrees of freedom to eliminate inter-group, inter-user, and inter-stream interferences.

The performance of these alternative source-grouping schemes would indeed lie in between those of the two extreme cases treated in this chapter. For example, as shown in Sections 5.3 and 5.4, the all-simultaneous source-grouping scheme achieves the maximum spatial multiplexing gain of $r_{\max} = \min_{m \in \{1, \cdots, M\}} (N_m)$ whereas the pairwise source-grouping scheme achieves the minimum multiplexing gain of $r_{\min} = M N_R / (2(M-1))$. The spatial multiplexing gain of any alternative grouping strategy will therefore lies in between these two extremes values, $r_{\max}$ and $r_{\min}$. Providing a comprehensive performance analysis of other grouping strategies is out of the scope of this chapter and hence will be considered in future research. Moreover, development of alternative source-grouping schemes is an important open research problem and will be further investigated in our future research.

## 5.3 Performance analysis of MWRNs with pairwise Tx/Rx ZF transmissions

In this section, the basic performance metrics of the MIMO AF MWRN with pairwise Tx/Rx ZF transmissions are derived. Specifically, the lower and upper bounds of the outage probability of an arbitrary source are first derived in closed-form and then used to derive the corresponding bounds of the overall outage probability. Moreover, the high SNR outage probability approximations and the DMT are derived to obtain valuable insights into practical MIMO MWRN designs.

### 5.3.1 The outage probability of an arbitrary source of MWRNs with pairwise ZF transmissions

In this subsection, the outage probability of the $m$th source for $m \in \{1, \cdots, M\}$ is derived. In the MWRN with pairwise Tx/Rx ZF transmissions, the $m$th source receives $M-1$ symbol vectors pertaining to the remaining $M - 1$ sources in the BC phase. In this context, the

outage probability of a multi-subchannel system is governed by the performance of the weakest subchannel [26]. Thus, the outage probability of the $m$th source is defined as

$$P_{\text{out,m}} = \Pr\left(\min_{\substack{k\in\{1,\cdots,N_R\} \\ j\in\{1,\cdots,M-1\}}} \left(\left[\gamma_{S_m^{(j)}}\right]_k\right) \leq \gamma_{th}\right), \tag{5.24}$$

where $\gamma_{th}$ is the threshold SNR[12]. The direct computation of (5.24) is mathematically intractable due to the correlation of $[\gamma_{S_m^{(j)}}]_k$ for $k \in \{1\cdots N_R\}$ for a given $j$. Thus, simple lower and upper bounds of the outage probability are derived in closed-form.

**Lower bound of $P_{\text{out,m}}$:**

The lower bound of the outage probability of the $m$th source can be derived as (see Appendix D.2 for the proof)

$$P_{\text{out,m}}^{\text{lb}} = 1 - \prod_{j=1}^{M-1}\left(1 - F_{\gamma_{S_{m,\min}}^{(j),\text{ub}}}(\gamma_{th})\right), \tag{5.25}$$

where $F_{\gamma_{S_{m,\min}}^{(j),\text{ub}}}(x)$ is the cumulative distribution function (CDF) of $\gamma_{S_{m,\min}}^{(j),\text{ub}}$, and is given by

$$F_{\gamma_{S_{m,\min}}^{(j),\text{ub}}}(x) = \begin{cases} \dfrac{\gamma\left(N_m-N_R+1,\frac{\mu_m^{(j)}x}{\eta_m^{(j)}-\zeta_m^{(j)}x}\right)}{\Gamma(N_m-N_R+1)}, & 0 < x < \dfrac{\eta_m^{(j)}}{\zeta_m^{(j)}} \\ 1, & x \geq \dfrac{\eta_m^{(j)}}{\zeta_m^{(j)}}, \end{cases} \tag{5.26}$$

where $\mu_m^{(j)} = \bar{\gamma}_{j,R}\mathcal{T}_{j+1} + \bar{\gamma}_{j+1,R}\mathcal{T}_j + \mathcal{T}_j\mathcal{T}_{j+1}$, $\eta_m^{(j)} = \bar{\gamma}_{R,m}\bar{\gamma}_{n,R}\mathcal{T}_j\mathcal{T}_{j+1}\mathcal{T}_n^{-1}$, and $\zeta_m^{(j)} = \bar{\gamma}_{R,m}\mathcal{T}_j\mathcal{T}_{j+1}$, where $m \in \{1,\cdots,M\}$, and $j \in \{1,\cdots,M-1\}$.

**Upper bound of $P_{\text{out,m}}$:**

The upper bound of the outage probability of the $m$th source can be derived as (see Appendix D.3 for the proof)

$$P_{\text{out,m}}^{\text{ub}} = 1 - \prod_{j=1}^{M-1}\left(1 - F_{\gamma_{S_{m,\min}}^{(j),\text{lb}}}(\gamma_{th})\right), \tag{5.27}$$

where $F_{\gamma_{S_{m,\min}}^{(j),\text{lb}}}(x)$ is the CDF of $\gamma_{S_{m,\min}}^{(j),\text{lb}}$ and is given by

$$F_{\gamma_{S_{i,\min}}^{(j),\text{lb}}}(x) = \begin{cases} 1 - \dfrac{\det\left[\mathbf{Q}_m\left(\frac{\mu_m^{(j)}x}{\eta_m^{(j)}-\zeta_m^{(j)}x}\right)\right]}{\prod_{l=1}^{N_R}[\Gamma(N_i-l+1)\Gamma(N_R-l+1)]}, & 0 < x < \dfrac{\eta_m^{(j)}}{\zeta_m^{(j)}} \\ 1, & x \geq \dfrac{\eta_m^{(j)}}{\zeta_m^{(j)}}. \end{cases} \tag{5.28}$$

---

[12]This threshold SNR, $\gamma_{th}$, is set to satisfy the minimum service-rate constraint; $\gamma_{th} = 2^{\mathcal{R}_{th}} - 1$, where $\mathcal{R}_{th}$ is the target rate [26].

The $(u, v)$th element of $N_R \times N_R$ matrix, $\mathbf{Q}_m(x)$ in (5.28) is given by [136, Eqn. (2.73)]

$$[\mathbf{Q}_m(x)]_{u,v} = \Gamma(N_m - N_R + u + v - 1, x). \tag{5.29}$$

### 5.3.2 Overall outage probability of MWRNs with pairwise ZF transmissions

The outage probability of a multi-source/multi-subchannel system is governed by the performance of the smallest subchannel of the weakest source. Thus, the overall outage probability of the MIMO AF MWRN with pairwise ZF transmissions is defined as the probability that the smallest subchannel of the weakest source falls bellow a preset threshold as follows:

$$P_{\text{out}} = \Pr\left(\min_{\substack{k \in \{1,\cdots,N_R\}, j \in \{1,\cdots,M-1\} \\ m \in \{1,\cdots,M\}}} \left(\left[\gamma_{S_m^{(j)}}\right]_k\right) \le \gamma_{th}\right). \tag{5.30}$$

Again, the closed-form evaluation of (5.30) appears mathematically intractable, and hence, tight lower and upper bounds of the overall outage probability are derived.

**Lower bound of the overall outage probability:**

The lower bound of the overall outage probability can be defined by using (D.6) as follows:

$$P_{\text{out}} \ge P_{\text{out}}^{\text{lb}} = \Pr\left(\min_{m \in \{1,\cdots,M\}} \left(\gamma_{S_{m,\min}}^{\text{ub}}\right) \le \gamma_{th}\right), \tag{5.31}$$

where $\gamma_{S_{m,\min}}^{\text{lb}} = \min_{j \in \{1,\cdots,M-1\}} \left(\gamma_{S_{m,\min}}^{(j),\text{ub}}\right)$ is defined in (D.6). Next, $P_{\text{out}}^{\text{lb}}$ can be derived in closed-form by using (5.25) as

$$P_{\text{out}}^{\text{lb}} = 1 - \prod_{m=1}^{M} \prod_{j=1}^{M-1} \left(1 - F_{\gamma_{S_{m,\min}}^{(j),\text{ub}}}(\gamma_{th})\right), \tag{5.32}$$

where $F_{\gamma_{S_{m,\min}}^{(j),\text{ub}}}(x)$ is defined in (5.26).

**Upper bound of the overall outage probability:**

The upper bound of the overall outage probability is defined by using (D.13) as follows:

$$P_{\text{out}} \le P_{\text{out}}^{\text{ub}} = \Pr\left(\min_{m \in \{1,\cdots,M\}} \left(\gamma_{S_{m,\min}}^{\text{lb}}\right) \le \gamma_{th}\right), \tag{5.33}$$

where $\gamma_{S_{m,\min}}^{\text{ub}} = \min_{j \in \{1,\cdots,M-1\}} \left(\gamma_{S_{m,\min}}^{(j),\text{lb}}\right)$ is defined in (D.13). Then, $P_{\text{out}}^{\text{ub}}$ is derived in closed-form by using (5.27) as

$$P_{\text{out}}^{\text{ub}} = 1 - \prod_{m=1}^{M} \prod_{j=1}^{M-1} \left(1 - F_{\gamma_{S_{m,\min}}^{(j),\text{lb}}}(\gamma_{th})\right), \tag{5.34}$$

where $F_{\gamma_{S_{m,\min}}^{(j),\text{lb}}}(x)$ is defined in (5.28).

### 5.3.3 High SNR asymptotic outage probability of MWRNs with pairwise ZF transmissions

In this subsection, the asymptotically exact high SNR approximations for the lower and upper bound of the overall outage probability are derived.

**High SNR approximation of the lower bound of $P_{\text{out}}$:**

The high SNR approximation for the lower bound of the outage probability of $m$th source can be derived as (see Appendix D.4 for the proof)

$$P_{\text{out,m}}^{\text{lb},\infty} = \left[ \sum_{j=1}^{M-1} \Omega_{\text{lb},m}^{(j)} \right] \left( \frac{\gamma_{th}}{\bar{\gamma}_{S,R}} \right)^{G_{d,m}^{\text{lb}}} + o\left( \bar{\gamma}_{S,R}^{-G_{d,m}^{\text{lb}}} \right), \tag{5.35}$$

where the lower bound of the diversity order is given by

$$G_{d,m}^{\text{lb}} = N_m - N_R + 1. \tag{5.36}$$

In (5.35), the system dependent constant, $\Omega_{\text{lb,m}}^{(j)}$, is given by

$$\Omega_{\text{lb,m}}^{(j)} = \frac{\left( \phi_m^{(j)} \right)^{N_m - N_R + 1}}{\Gamma(N_m - N_R + 2)\beta^{N_m - N_R + 1}}, \tag{5.37}$$

where $\bar{\gamma}_{m,R} = \bar{\gamma}_{S,R}$, $\bar{\gamma}_{R,m} = \bar{\gamma}_{R,S}$, $\bar{\gamma}_{R,S} = \beta\bar{\gamma}_{S,R}$, $\phi_m^{(j)} = \frac{\mathcal{T}_n(\mathcal{T}_j + \mathcal{T}_{j+1})}{\mathcal{T}_j}$, and $\phi_m^{(j)} = \frac{\mathcal{T}_n(\mathcal{T}_j + \mathcal{T}_{j+1})}{\mathcal{T}_{j+1}}$ for $m \in \{1, \cdots, M\}$, $j \in \{1, \cdots, M-1\}$ and $n \in \{1, \cdots, M-1\}$.

Now, the high SNR approximation for the lower bound of the overall outage probability is derived as

$$P_{\text{out}}^{\text{lb},\infty} = \left[ \sum_{m'} \sum_{j=1}^{M-1} \Omega_{\text{lb},m'}^{(j)} \right] \left( \frac{\gamma_{th}}{\bar{\gamma}_{S,R}} \right)^{G_d^{\text{lb}}} + o\left( \bar{\gamma}_{S,R}^{-G_d^{\text{lb}}} \right), \tag{5.38}$$

where $m' \in \{m' | G_{d,m'}^{\text{lb}} = \min(N_1, \cdots, N_{m'}, \cdots, N_M) - N_R + 1\}$. Moreover, the lower bound of the overall diversity order is given by

$$G_d^{\text{lb}} = \min_{m \in \{1, \cdots, M\}} (N_m) - N_R + 1. \tag{5.39}$$

**High SNR approximation of the upper bound of $P_{\text{out}}$:**

First, the high SNR approximation for the upper bound of the outage probability of $m$th source is derived by employing similar techniques to those in Appendix D.4 and by using

the high SNR approximation of the CDF of the minimum eigenvalue of the Wishart matrix in [136] as follows:

$$P_{\text{out,m}}^{\text{ub},\infty} = \left[ \sum_{j=1}^{M-1} \Omega_{\text{ub},m}^{(j)} \right] \left( \frac{\gamma_{th}}{\bar{\gamma}_{S,R}} \right)^{G_{d,m}^{\text{ub}}} + o\left( \bar{\gamma}_{S,R}^{-G_{d,m}^{\text{ub}}} \right), \tag{5.40}$$

where the upper bound of the diversity order is given by

$$G_{d,m}^{\text{ub}} = N_m - N_R + 1. \tag{5.41}$$

In (5.40), the system dependent constant, $\Omega_{\text{ub,m}}^{(j)}$, is given by

$$\Omega_{\text{ub,m}}^{(j)} = \frac{\nu_m \left( \phi_m^{(j)} \right)^{N_m - N_R + 1}}{(N_m - N_R + 1)\beta^{N_m - N_R + 1}}, \tag{5.42}$$

where $\phi_m^{(j)}$ and $\beta$ are defined in (5.37). Moreover, in (5.42), $\nu_m$ is given by

$$\nu_m = \begin{cases} \frac{\det(\boldsymbol{\Psi}_m)}{\prod_{l=1}^{N_R}[\Gamma(N_R-l+1)\Gamma(N_m-l+1)]}, & N_R \neq 1 \\ \frac{1}{\Gamma(N_m)}, & N_R = 1, \end{cases} \tag{5.43}$$

where $\boldsymbol{\Psi}_m$ for $m \in \{1, \cdots, M\}$ is an $(N_R - 1) \times (N_R - 1)$ matrix, where the $(u,v)$th element is given by $[\boldsymbol{\Psi}_m]_{u,v} = \Gamma(N_m - N_R + u + v + 1)$.

Next, the high SNR approximation for the upper bound of the overall outage probability can be derived as

$$P_{\text{out}}^{\text{ub},\infty} = \left[ \sum_{m'} \sum_{j=1}^{M-1} \Omega_{\text{ub},m'}^{(j)} \right] \left( \frac{\gamma_{th}}{\bar{\gamma}_{S,R}} \right)^{G_d^{\text{ub}}} + o\left( \bar{\gamma}_{S,R}^{-G_d^{\text{ub}}} \right), \tag{5.44}$$

where $m'$ is given by $m' \in \{m' | G_{d,m'}^{\text{lb}} = \min(N_1, \cdots, N_{m'}, \cdots, N_M) - N_R + 1\}$. Furthermore, in (5.44), $G_d^{\text{ub}}$ is the upper bound of the overall diversity order, and is given by

$$G_d^{\text{ub}} = \min_{m \in \{1, \cdots, M\}} (N_m) - N_R + 1. \tag{5.45}$$

**Remark III.1:** The lower and upper bounds of the diversity orders in (5.45) and (5.39), respectively, are the same, and consequently, the overall diversity order of the MIMO AF MWRN is given by $G_d = \min_{m \in \{1, \cdots, M\}} (N_m) - N_R + 1$.

### 5.3.4 DMT of MWRNs with pairwise ZF transmissions

In this subsection, the fundamental DMT [26] of MIMO AF MWRNs with pairwise Tx/Rx ZF transmissions is derived to obtain valuable insights into practical system designing. In

this system set-up, $M$ independent symbol vectors each having $N_R$ independent symbols are exchanged among $M$ users in $2(M-1)$ time-slots. In this context, the effective mutual information can be upper bounded as

$$\mathcal{I}_{\text{eff}} \lesssim \frac{MN_R}{2(M-1)} \log\left(1 + \min_{m \in \{1, \cdots, M\}} \left(\gamma_{S_m, \min}^{\text{ub}}\right)\right). \tag{5.46}$$

Consequently, the information rate outage probability can be lower bounded as

$$P_{\text{out}} \lesssim \Pr\left(\mathcal{I}_{\text{eff}} \leq \mathcal{R}_{th}\right) = \Pr\left(\min_{m \in \{1, \cdots, M\}} \left(\gamma_{S_m, \min}^{\text{ub}}\right) \leq 2^{\frac{2(M-1)\mathcal{R}_{th}}{MN_R}} - 1\right), \tag{5.47}$$

where $\mathcal{R}_{th}$ is the overall target information rate, and is defined a $\mathcal{R}_{th} = r \log\left(1 + \bar{\gamma}_{S,R}\right)$ [26]. By employing (5.38), $P_{\text{out}}$ can be lower bounded when $\bar{\gamma}_{S,R} \to \infty$ as

$$P_{\text{out}}^{\bar{\gamma}_{S,R} \to \infty} \gtrsim \bar{\gamma}_{S,R}^{-\left(\min_{m \in \{1, \cdots, M\}} (N_m) - N_R + 1\right)\left(1 - \frac{2r(M-1)}{MN_R}\right)}. \tag{5.48}$$

Next, the effective mutual information can be lower bounded as

$$\mathcal{I}_{\text{eff}} \gtrsim \frac{MN_R}{2(M-1)} \log\left(1 + \min_{m \in \{1, \cdots, M\}} \left(\gamma_{S_m, \min}^{\text{lb}}\right)\right). \tag{5.49}$$

Now, by using similar steps to those in (5.47), (5.48), and then employing (5.44), $P_{\text{out}}$ can be upper bounded $\bar{\gamma}_{S,R} \to \infty$ as

$$P_{\text{out}}^{\bar{\gamma}_{S,R} \to \infty} \lesssim \bar{\gamma}_{S,R}^{-\left(\min_{m \in \{1, \cdots, M\}} (N_m) - N_R + 1\right)\left(1 - \frac{2r(M-1)}{MN_R}\right)}. \tag{5.50}$$

In particular, the lower and upper bounds of $P_{\text{out}}$ in (5.48) and (5.50), respectively, coincide each other and hence the achievable DMT can be derived as [26]

$$G_d(r) = \left(\min_{m \in \{1, \cdots, M\}} (N_m) - N_R + 1\right)\left(1 - \frac{2r(M-1)}{MN_R}\right). \tag{5.51}$$

It is worth noticing that the achievable diversity order reduces as the number of antennas at the relay ($N_R$) increase; however, the achievable multiplexing gain increases. The maximum achievable diversity order and multiplexing gain are given by $G_d = \min_{m \in \{1, \cdots, M\}} (N_m) - N_R + 1$, and $r = \frac{MN_R}{2(M-1)}$, respectively. Interestingly, $r$ is maximized when $M = 2$, i.e., $r_{\max} = \lim_{M \to 2} \frac{MN_R}{2(M-1)} = N_R$. However, for large $M$, $r$ approaches $N_R/2$, i.e., $r_{\min} = \lim_{M \to \infty} \frac{MN_R}{2(M-1)} = \frac{N_R}{2}$. This result leads us to an important insight into practical system-design and implementation of MWRNs with pairwise transmissions; i.e., the multiplexing gain of MIMO AF MWRNs gradually reduces to $1/2$ as the number of sources increases, and consequently, the multiplexing gain asymptotically approaches that of AF OWRNs.

126

## 5.4 Performance Analysis of non-pairwise ZF transmission strategy

In this section, the performance metrics of MIMO AF MWRNs with non-pairwise Tx/Rx ZF transmissions are derived. To this end, the outage probability lower and upper bounds pertaining to an arbitrary source is derived, and thereby, the overall outage probability is deduced.

### 5.4.1 The outage probability of the $j$th BC phase of MWRNs with non-pairwise ZF transmissions

By following a similar argument to that of (5.24), the outage probability of the $i$th source for MWRNs with non-pairwise ZF transmissions is defined as

$$P_{\text{out,i}} = \Pr\left(\min_{\substack{k \in \{1, \cdots, N_{\min}\} \\ j \in \{1, \cdots, M-1\}}} \left(\left[\gamma_{S_i^{(j)}}\right]_k\right) \le \gamma_{th}\right), \quad \text{for } i \in \{1, \cdots, M\}, \tag{5.52}$$

where $\left[\gamma_{S_i^{(j)}}\right]_k$ is defined in (5.23). Again, the exact derivation of (5.52) is mathematically intractable due to the statistical correlation of $[\gamma_{S_i^{(j)}}]_k$ for $k \in \{1 \cdots N_{\min}\}$ for a given $j$. Thus, similar to case in Section 5.3.1 simple lower and upper bounds of the outage probability are derived in closed-form.

**Lower bound of $P_{\text{out,i}}$:**

The lower bound of the outage probability of the $i$th source can be derived as[13]

$$P_{\text{out,i}}^{\text{lb}} = \begin{cases} \dfrac{\gamma\left(N_R - MN_{\min} + 1, \frac{\mu_i x}{\eta_i - \zeta_i x}\right)}{\Gamma(N_R - MN_{\min} + 1)}, & 0 < x < \frac{\eta_i}{\zeta_i} \\ 1, & x \ge \frac{\eta_i}{\zeta_i}, \end{cases} \tag{5.53}$$

where $N_{\min} \triangleq \min_{m \in \{1, \cdots, M\}} (N_m)$, $\mu_i = N_i \bar{\gamma}_{R,i}$, $\eta_i = \bar{\gamma}_{R,i} \bar{\gamma}_{i,R}$, and $\zeta_i = N_i \mathcal{Q}' + N_i \mathcal{Q} \sum_{i=1}^{M} \dfrac{\bar{\gamma}_{i,R}}{N_i}$, for $i \in \{1, \cdots, M\}$. Moreover, $\mathcal{Q} = (MN_{\min})/(N_R - MN_{\min})$ and $\mathcal{Q}'$ is given by [137]

$$\mathcal{Q}' = \frac{\sum_{m=1}^{MN_{\min}} \det(\mathbf{M}_m)}{\prod_{l=1}^{MN_{\min}} \left[\Gamma(N_R - l + 1)\Gamma(MN_{\min} - l + 1)\Gamma(N_R - l + 1)\right]}, \tag{5.54}$$

where $\mathbf{M}_m^{(i,j)} = \Gamma(N_R - MN_{\min} + i - 1)\Gamma(N_R - MN_{\min} + i + j - 2)$ for $j = m$ and $\mathbf{M}_m^{(i,j)} = \Gamma(N_R - MN_{\min} + i)\Gamma(N_R - MN_{\min} + i + j - 1)$ for $j \ne m$.

---

[13]As per Remark II.3, the proof of (5.53) and (5.55) follows the similar techniques to those in Appendix D.2, and hence, is omitted for the sake of brevity.

**Upper bound of $P_{\text{out,i}}$:**

Similarly, the upper bound of the outage probability of the $i$th source can be derived as follows:

$$P_{\text{out,i}}^{\text{ub}} = \begin{cases} 1 - \dfrac{\det\left[\mathbf{Q}\left(\frac{\mu_i x}{\eta_i - \zeta_i x}\right)\right]}{\prod_{l=1}^{MN_{\min}}[\Gamma(MN_{\min}-l+1)\Gamma(N_R-l+1)]}, & 0 < x < \frac{\eta_i}{\zeta_i} \\ 1, & x \geq \frac{\eta_i}{\zeta_i}. \end{cases} \tag{5.55}$$

where the $(u,v)$th element of $MN_{\min} \times MN_{\min}$ matrix, $\mathbf{Q}_i(x)$, in (5.28) is given by [136, Eqn. (2.73)]

$$[\mathbf{Q}(x)]_{u,v} = \Gamma(MN_{\min} - N_R + u + v - 1, x). \tag{5.56}$$

In (5.55), $\mu_i$, $\eta_i$, $\zeta_i$ and $N_{\min}$ are defined under (5.53).

### 5.4.2 Overall outage probability of MWRNs with non-pairwise ZF transmissions

By employing a similar argument to that of Section 5.3.2, the overall outage probability of the non-pairwise ZF transmission strategy can be defined as the probability that the smallest subchannel of the weakest source falls bellow a preset threshold as follows:

$$P_{\text{out}} = \Pr\left( \min_{\substack{k \in \{1,\cdots,N_{\min}\}, j \in \{1,\cdots,M-1\} \\ i \in \{1,\cdots,M\}}} \left( \left[\gamma_{S_i^{(j)}}\right]_k \right) \leq \gamma_{th} \right). \tag{5.57}$$

As per Remark II.2, the derivation of (5.57) appears mathematically intractable as $\left[\gamma_{S_i^{(j)}}\right]_k$ and $\left[\gamma_{S_m^{(l)}}\right]_k$ are functions of the same random variables for $(i,m) \in \{1,\cdots,M\}$ and $i \neq m$.

### 5.4.3 High SNR asymptotic outage probability of MWRNs with non-pairwise ZF transmissions

In this subsection, the asymptotically exact high SNR approximations for the lower and upper bound of the outage probability at an arbitrary source are derived[14].

**High SNR approximation of the lower bound of $P_{\text{out,i}}$:**

The high SNR approximation for the lower bound of the outage probability of $m$th source can be derived by employing similar techniques to those in Appendix D.4 as follows:

$$P_{\text{out,i}}^{\text{lb},\infty} = \frac{N_i^{N_R - MN_{\min}+1}}{\Gamma(N_R - MN_{\min}+2)} \left( \frac{\gamma_{th}}{\bar{\gamma}_{S,R}} \right)^{G_{d,i}^{\text{lb}}} + o\left( \bar{\gamma}_{S,R}^{-G_{d,i}^{\text{lb}}} \right), \tag{5.58}$$

---

[14]The proofs of high SNR approximations of both lower and upper outage probability bounds follow similar techniques to those in Appendix D.4, and hence are omitted.

where the lower bound of the diversity order is given by

$$G_{d,i}^{\text{lb}} = N_R - M \left[ \min_{m \in \{1, \cdots, M\}} (N_m) \right] + 1. \tag{5.59}$$

where $\bar{\gamma}_{i,R} = \bar{\gamma}_{S,R}$, $\bar{\gamma}_{R,i} = \bar{\gamma}_{R,S}$, and $\bar{\gamma}_{R,S} = \beta \bar{\gamma}_{S,R}$ for $i \in \{1, \cdots, M\}$ and $j \in \{1, \cdots, M-1\}$.

**High SNR approximation of the upper bound of $P_{\text{out,i}}$:**

First, the high SNR approximation for the upper bound of the outage probability of $i$th source is derived as follows:

$$P_{\text{out,i}}^{\text{ub},\infty} = \Omega_{\text{ub},i} \left( \frac{\gamma_{th}}{\bar{\gamma}_{S,R}} \right)^{G_{d,i}^{\text{ub}}} + o\left( \bar{\gamma}_{S,R}^{-G_{d,i}^{\text{ub}}} \right), \tag{5.60}$$

where the upper bound of the diversity order is given by

$$G_{d,i}^{\text{ub}} = N_R - M \left[ \min_{m \in \{1, \cdots, M\}} (N_m) \right] + 1. \tag{5.61}$$

In (5.60), the system dependent constant, $\Omega_{\text{ub,i}}$, is given by

$$\Omega_{\text{ub,i}} = \frac{\det\left( \boldsymbol{\Psi}_i \right) N_i^{N_R - MN_{\min} + 1}}{(N_R - MN_{\min} + 1) \prod_{l=1}^{MN_{\min}} [\Gamma(MN_{\min} - l + 1)\Gamma(N_R - l + 1)]}, \tag{5.62}$$

where $\boldsymbol{\Psi}_i$ for $i \in \{1, \cdots, M\}$ is an $(MN_{\min}-1) \times (MN_{\min}-1)$ matrix with the $(u,v)$th element given by $[\boldsymbol{\Psi}_i]_{u,v} = \Gamma(N_R - MN_{\min} + u + v + 1)$, where $N_{\min} = \min_{m \in \{m, \cdots, M\}} (N_m)$.
**Remark IV.1:** An explicit high SNR approximation for lower and upper bounds of the overall outage probability appears mathematically intractable as the exact evaluation of (5.57) is not plausible. However, the overall diversity order of MIMO AF MWRNs with non-pairwise transmissions can readily be deduced by employing similar arguments to those in Appendix D.4 as the minimum operation over $i \in \{1, \cdots, M\}$ of (5.57) does not alter the achievable diversity order. Thus, the high SNR approximation of the overall outage probability of the MIMO AF MWRNs with non-pairwise transmissions is given by $P_{\text{out}}^\infty = \Omega \left( \frac{\gamma_{th}}{\bar{\gamma}_{S,R}} \right)^{G_d} + o\left( \bar{\gamma}_{S,R}^{-G_d} \right)$, where $\Omega$ is a system dependent parameter and the overall diversity order of is given by $G_d = N_R - MN_{\min} + 1$.

### 5.4.4 DMT of MWRNs with non-pairwise ZF transmissions

In this subsection, the achievable DMT of MIMO AF MWRNs with non-pairwise ZF transmissions is derived. In this subclass of MWRNs, $M$ independent symbol vectors each having $N_{\min} = \min_{i \in \{1, \cdots, M\}} (N_i)$ independent symbols are exchanged among $M$ sources in

$M$ time-slots. In this context, the effective mutual information of the overall system can be written as

$$\mathcal{I}_{\text{eff}} = N_{\min}\log\left(1 + \min_{\substack{k\in\{1,\cdots,N_{\min}\},j\in\{1,\cdots,M-1\}\\i\in\{1,\cdots,M\}}}\left(\left[\gamma_{S_i^{(j)}}\right]_k\right)\right). \tag{5.63}$$

The information rate outage probability is then given by

$$P_{\text{out}} = \Pr(\mathcal{I}_{\text{eff}} \leq \mathcal{R}_{th}) = \Pr\left(\min_{\substack{k\in\{1,\cdots,N_{\min}\},j\in\{1,\cdots,M-1\}\\i\in\{1,\cdots,M\}}}\left(\left[\gamma_{S_i^{(j)}}\right]_k\right) \leq 2^{\frac{\mathcal{R}_{th}}{N_{\min}}}-1\right), \tag{5.64}$$

where $\mathcal{R}_{th}$ is the overall target rate and is defined as follows: $\mathcal{R}_{th} = r\log\left(1 + \bar{\gamma}_{S,R}\right)$ [26]. Next, by employing Remark IV.1, $P_{\text{out}}$ can be approximated when $\bar{\gamma}_{S,R} \to \infty$ as

$$P_{\text{out}}^{\bar{\gamma}_{S,R}\to\infty} \approx \bar{\gamma}_{S,R}^{-(N_R-MN_{\min}+1)\left(1-\frac{r}{N_{\min}}\right)}. \tag{5.65}$$

From (5.65), the achievable DMT of MIMO MWRNs with non-pairwise transmissions can be derived as [26]

$$G_d(r) = \left(N_R - M\left[\min_{m\in\{1,\cdots,M\}}(N_m)\right] + 1\right)\left(1 - \frac{r}{N_{\min}}\right). \tag{5.66}$$

Interestingly, the achievable spatial multiplexing gain of MWRNs with non-pairwise ZF transmissions does not depend on the number of available sources, $M$, actively participating in the network. In fact, the maximum achievable multiplexing gain can be readily quantified by using (5.66) to be $r = N_{\min}$ and hence directly determines by the minimum antenna count at $S_i$ for $i \in \{1, \cdots, M\}$. Moreover, the achievable diversity order reduces as the total number of antennas at the sources increases for a fixed relay antenna array size.

## 5.5 Numerical Results

In this section, numerical results are presented to study the outage probability, the fundamental DMT and the achievable sum rate performance of MIMO AF MWRNs with both pairwise and non-pairwise ZF transmissions. To capture the effect of the network geometry, the average SNR of $S_i \to R$ channel is modeled by $\bar{\gamma}_{i,R} = \bar{\gamma}\left(\frac{d_0}{d_{i,R}}\right)^{\varpi}$ for $i \in \{1, \cdots, M\}$, where $\bar{\gamma}$ is the average transmit SNR, $d_0$ is the reference distance, and $\varpi$ is the path-loss exponent. The hop distance between $S_i$ and $R$ is denoted by $d_{i,R}$ for $i \in \{1, \cdots, M\}$.

In Fig. 5.5, the overall outage probability of the pairwise ZF transmission strategy is plotted for several antenna configurations. Specifically, the exact outage probability is plotted by using Monte Carlo simulation results, and the lower and upper bounds are plotted
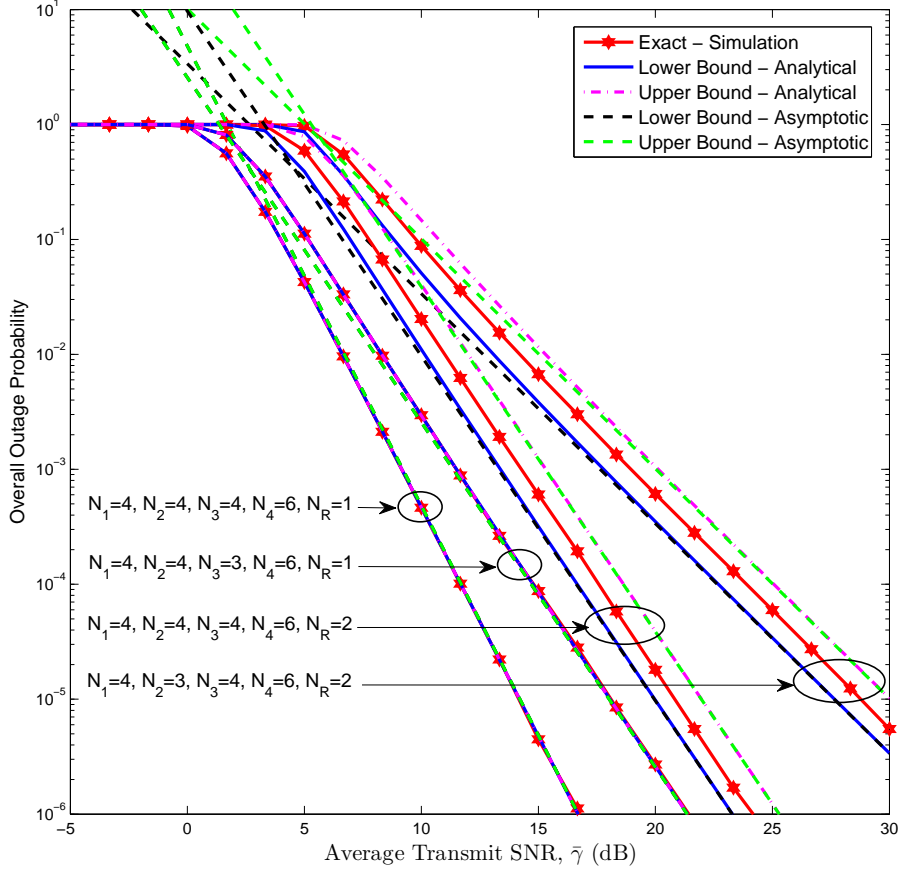
Figure 5.5: The overall outage probability of pairwise transmission strategy for MIMO four-way AF relay network with the SNR threshold $\gamma_{th} = 5.00$ dB. The hop distances are modeled as $d_{1,R} = 0.5d_0$, $d_{2,R} = 1.25d_0$, $d_{3,R} = 0.75d_0$ and $d_{4,R} = d_0$. Moreover, the path-loss exponent is assumed to be $\varpi = 3.5$.

by employing (5.32), and (5.34), respectively. Moreover, asymptotic outage bounds are also plotted by using (5.38) and (5.44) to compare the achievable diversity orders. Fig. 5.5 clearly reveals that the outage probability improves significantly as the number of antennas at the relay decreases. For instance, at $10^{-4}$ outage probability, single-antenna relay results in a 6 dB SNR gain over the dual-antenna relay. However, the single-antenna set-up achieves this outage gain over the latter at the expense of a significant spatial multiplexing loss as quantified in (5.51). In particular, for single-antenna relays, our outage bounds reduce to exact outage as $N_R = 1$ case results in a unit-rank Wishart matrix, $\mathbf{H}_{R,i}^H \mathbf{H}_{R,i}$.

Fig. 5.6 shows the outage probability bounds pertaining to the first source of MIMO AF MWRNs with non-pairwise ZF transmissions. Several antenna configurations are considered to study the effect of relay and source antenna counts on the outage probability
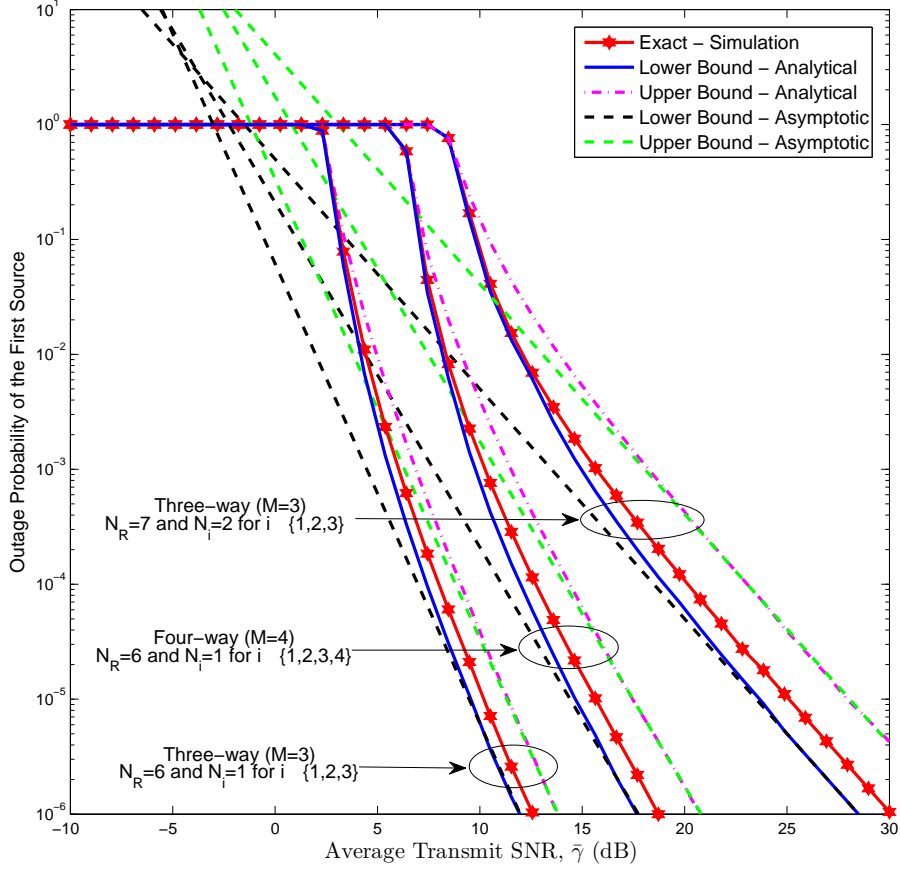
Figure 5.6: The outage probability of the first source of the non-pairwise ZF transmission strategy for the SNR threshold $\gamma_{th} = 6.00$ dB. The hop distances are modeled as $(d_{1,R} = 0.75d_0, d_{2,R} = d_0, d_{3,R} = 1.25d_0)$ for the three-way relay network and as $(d_{1,R} = 0.75d_0, d_{2,R} = d_0, d_{3,R} = 1.25d_0, d_{4,R} = 0.8d_0)$ for the four-way relay network. Moreover, the path-loss exponent is assumed to be $\varpi = 3.5$.

performance. The outage probability curves of three-way relay network pertaining to the single-antenna and dual-antenna sources clearly reveal that the achievable diversity gain reduces as the source antenna array size increases. For example, at an outage probability of $10^{-4}$, the three-way relay network with single-antenna sources achieves a SNR gain of 3 dB over the dual-antenna counterpart. However, as per Eqn. (5.66), the single-antenna sources in fact reduce the achievable maximum spatial multiplexing gain over the dual-antenna sources. This observation is a complete opposite to that we observed in outage performance study of pairwise MWRNs in Fig. 5.6, where the achievable diversity order increases with the number of antennas equipped at the sources for a fixed relay antenna array. Our outage bounds are thus useful to verify the important system-design parameters
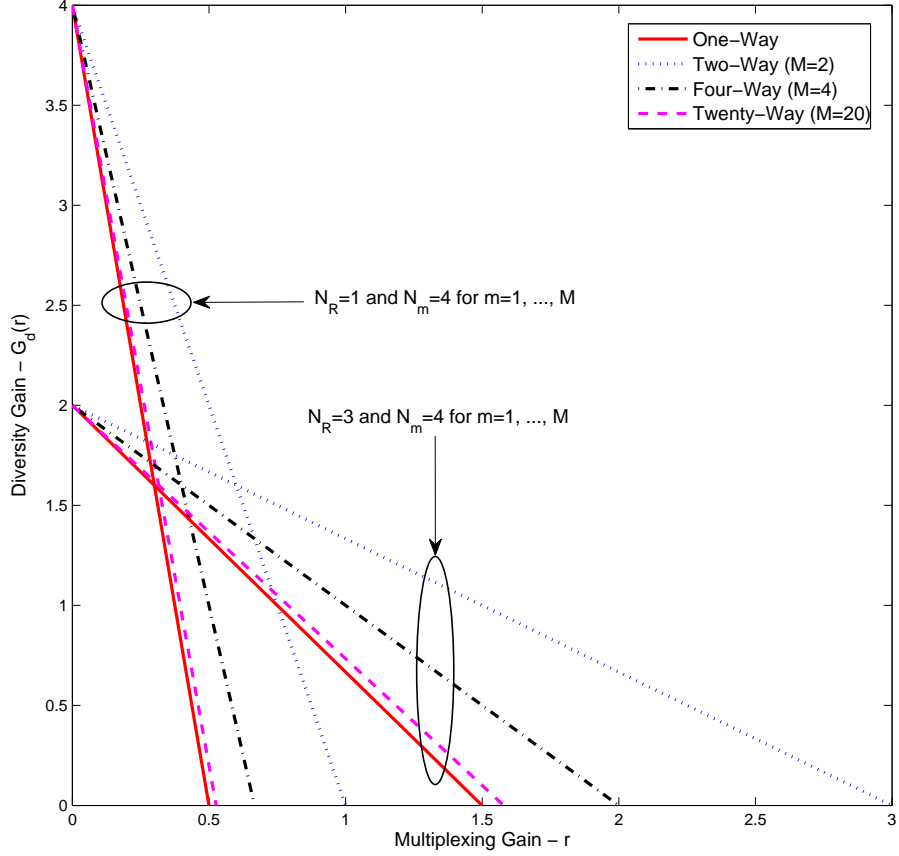
Figure 5.7: The achievable DMT of the pairwise ZF transmission strategy.

such as the diversity order and array gain.

In Fig. 5.7, the achievable DMT curves for the pairwise ZF transmission strategy are plotted for several system configurations. Specifically, the DMT of the MIMO AF OWRN serves as a benchmark to compare the performance of MWRNs. The achievable multiplexing gain gradually improves as the number of relay antennas increases. However, at the same time, higher number of relay antennas significantly reduces the achievable diversity gains. Interestingly, the TWRN provides the highest multiplexing gain for a given $N_R$. However, as the number of sources increases, the achievable spatial multiplexing gain gradually decreases to $N_R/2$, which is exactly the same multiplexing gain achieved by the MIMO AF OWRN. Thus, the MIMO AF MWRNs with pairwise ZF transmission exhibit diminishing multiplexing gains as the network size grows. Thus, our DMT analysis suggests the performance limits for practical MWRNs with optimal achievable diversity and multiplexing gains.
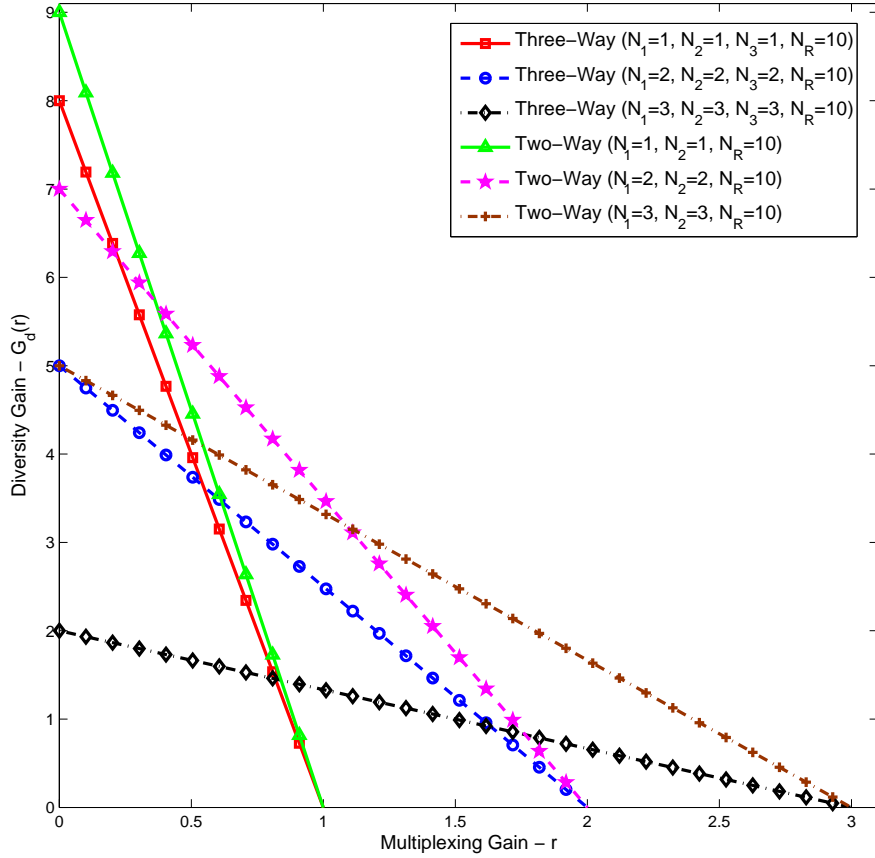
Figure 5.8: The achievable DMT of the non-pairwise ZF transmission strategy.

Fig. 5.8 shows the achievable DMT of the non-pairwise ZF transmission strategy for two specific system configurations. To this end, a three-way relay network and a two-way relay network with three specific antenna configurations as shown in the legend of Fig. 5.8 are treated. The DMT curves corresponding to three-way and two-way relay networks with the same antenna configuration at each terminal reveal that the achievable maximum spatial multiplexing gain does not depend on the number of sources available in the network. However, it is evident from Fig. 5.8 that the multiplexing gain in fact depends on the minimum antenna account at the sources. On the contrary, the achievable maximum diversity gain directly depends on the total number of antennas equipped at the sources for a fixed relay antenna array size. Our DMT analysis thus provides valuable insights into practical implementation of MIMO AF MWRNs.

## 5.6 Conclusion

The performance of (i) pairwise ZF transmission and (ii) non-pairwise ZF transmission for the MIMO AF MWRNs was studied over Rayleigh fading channels. Specifically, the lower and upper bounds of the overall outage probability were derived in closed-form. In particular, high SNR outage probability approximations were derived, and thereby, the achievable DMT, the maximum achievable diversity, and spatial multiplexing gains were quantified to obtain valuable insights into practical MIMO MWRN system-designing. Interestingly, our outage probability bounds reduce to exact outage probability for single-antenna relays, and hence, they serve as benchmarks for practical MIMO AF MWRNs with pairwise ZF transmissions. Furthermore, the pairwise ZF transmission strategy requires each source to know only its channel to the relay and consequently eliminates the requirement of the global CSI for each source. Our DMT analysis for this case reveals that increasing the number of relay antennas reduces the diversity gains, however improves the multiplexing gains. Counter intuitively, this multiplexing gain gradually diminishes as the number of participating sources linearly grows. Interestingly, the multiplexing gain of MWRNs with non-pairwise ZF transmissions does not depend on the number of sources in the network and hence are suitable for large network deployments despite the inherent higher relay processing complexity. Our transmission designs for MIMO MWRNs therefore provide flexibility in obtaining the desirable trade-offs among the system performance, implementation complexity, and wireless resource usage.

$\sim$

# Chapter 6

# Conclusion and Future Work

In this chapter, the conclusion and the summary of the contribution of this thesis are first outlined. Then, the future research directions are described.

## 6.1 Conclusion and summary of the contribution

This thesis focused on designing and analyzing new wireless transmission strategies for cooperative relay networks. The key design criterion of these physical-layer designs is to leverage the spatial diversity and/or spatial multiplexing gains available among distributed single-antenna and/or multiple-antenna wireless terminals through distributed transmission and efficient signal processing. The main objectives achieved in this thesis can be enumerated as follows:

1. Developed a comprehensive performance analysis framework for multi-hop amplify-and-forward (AF) relay networks yielding closed-form performance bounds.

2. Designed and analyzed the adaptive multiple relay selection (MRS) schemes for cooperative multi-relay AF networks and thereby optimizing the trade-offs among the implementation complexity, wireless resource usage, and overall performance.

3. Designed and analyzed the optimal joint antenna and relay selection strategies for multiple-input multiple-output (MIMO) AF one-way relay networks (OWRNs) and MIMO two-way relay networks (TWRNs) by aiming to achieve full diversity and array gain benefits.

4. Designed and analyzed the joint transmit/receive (Tx/Rx) zero forcing (ZF) beamforming strategies for MIMO AF multi-way relay networks (MWRNs) to optimize the trade-off between the achievable diversity-multiplexing trade-off (DMT) and implementation complexity.

5. Quantified the detrimental impact of practical transmission impairments such as feedback delays and spatially correlated fading on the performance of aforementioned transmission strategies.

6. Valuable insights and guidelines for practical usage were obtained, and thereby, the trade-offs among the overall system performance, resource usage, and implementation complexity were improved by refining the underlying physical layer transmission designs.

The contribution of Chapter 2 to Chapter 5 can be further elaborated as follows:

- The main focus of the Chapter 2 was to develop a comprehensive performance analysis framework for multi-hop AF relay networks. To this end, a new class of signal-to-noise ratio (SNR) upper bounds for the multi-hop relay networks were developed. A mathematically tractable statistical characterization of the SNR bounds was developed by deriving the cumulative distribution function (CDF), the probability density function (PDF), and the moment generating function (MGF) in closed-form. The resulting outage probability and the average symbol error rate bounds were proved to be asymptotically exact. Consequently, a generalized asymptotic performance analysis framework was developed. Usefulness of the proposed bounding techniques was illustrated through two practical examples.

- In Chapter 3, a new class of MRS scheme was designed and analyzed for cooperative relay networks. The key design criterion is to adaptively select a subset from the available relays to satisfy a preset output threshold SNR. The fundamental relationships among the basic performance metrics such as the outage probability, average symbol error rate (SER), and average number of selected relays were characterized to ascertain the practical viability of the proposed MRS schemes. The proposed adaptive MRS schemes indeed provide more flexibility in utilizing bandwidth and spatial diversity in cooperative relay networks over fading channels.

- Chapter 4 focused on developing joint antenna and relay selection strategies, which are optimal in the sense of the achievable diversity gains, for MIMO AF OWRNs and MIMO AF TWRNs. A comprehensive performance analysis framework was first developed for the optimal transmit antenna selection (TAS) strategy for single-relay MIMO OWRNs. The insights obtained through this analysis were then employed for designing the the optimal joint antenna and relay selection strategy for the multi-relay MIMO OWRNs.

Moreover, the optimal joint Tx/Rx antenna and relay selection strategy was designed and analyzed for the multi-relay MIMO TWRNs. The performance degradation due to practical transmission impairments such as the feedback delays and the spatially correlated fading was quantified to ascertain the practical viability of the proposed designs. Efficient channel prediction strategy to circumvent outdated channel-state information (CSI) incurred due to feedback delays for antenna selection was devised, and thereby, the proposed antenna and relay selection strategies were fined-tuned. Moreover, the SNR loss incurred due to correlated fading cases was quantified. Thereby, valuable insights/guidelines, which can be readily incorporated in the design of practical systems by introducing necessary fade margins in the link budget calculations, were obtained.

- In Chapter 5, two transmission strategies for MIMO AF MWRNs, namely (i) pairwise ZF transmission and (ii) non-pairwise ZF transmission, were designed and analyzed. The practical viability of the proposed strategies was ascertained by charactering the fundamental trade-offs among the outage probability, achievable diversity order, and spatial multiplexing gain. The proposed pairwise ZF transmission strategy enjoys lower relay processing complexity than that of the non-pairwise ZF transmission strategy. However, the former achieves this benefit at the expense of some loss in achievable spatial multiplexing gain. Our transmission designs provide flexibility in adapting various antenna configurations at the sources and the relay, and hence, they may be employed in MIMO MWRNs with various practical applications.

## 6.2 Future research directions

Our future research interests are primarily based on (i) system, channel and mobility modeling, (ii) physical layer transmission designing, (iii) interference modeling, and (iv) performance analyzing of next-generation multi-way relay networks (MWRNs). As elaborate in Chapter 5, the MWRNs are the next evolution of both OWRNs and TWRNs, and hence, the physical layer transmission designs and analysis have not yet been fully explored. To be more specific, the practically viable MIMO MWRN network topologies have not been explored by taking into account the important transmission impairments such as the miscellaneous interferences, feedback delays, channel estimation errors, and spatial correlated fading.

Moreover, the wireless data traffic demand is increasing exponentially mainly due to the recent proliferation of data-hungry portal wireless devices such as smart phones and net-

books. As the conventional techniques for increasing data rates, enhancing link-reliability, and reducing energy consumption are approaching their fundamental limits, new wireless network architectures are needed to satisfy the future wireless requirements. To this end, the future research specifically focuses on designing and analyzing novel energy efficient wireless transmission strategies for MIMO MWRNs.

**Objectives:** The goals of the future research plan are as follows:

1. To develop new energy-efficient system, channel, and signal models for MWRNs by considering realistic wireless propagation conditions and by using green radio signal processing techniques.

2. To design and analyze new physical layer transmission strategies by giving special emphasis to relay processing techniques, joint antenna and relay selection strategies, transmit/receive beamforming strategies, and multi-user scheduling schemes.

3. To develop and analyze distributed network coding strategies and source-grouping techniques to optimize the achievable diversity order, spatial multiplexing gain, and implementation complexity.

4. To design novel joint interference and radio resource management techniques for physical-layer transmissions to optimize the network resource usage and the overall quality-of-service.

5. To characterize the key relationships among the data rate, coverage, energy efficiency, and reliability.

**Methodology:** The aforementioned research objectives will be accomplished by employing tools from communications theory, probability and stochastic processes, stochastic geometry, graph theory, and green-radio signal processing techniques as follows:

- First, mathematical models will be developed to understand how MWRNs perform under realistic operating conditions. The joint effects of radio-wave propagation over wireless channels, such as time-frequency selectivity, signal fading, signal shadowing and pathloss will be considered.

- The fundamental design criterion of the transmission designs will be to optimize the trade-offs among the overall data rate, coverage, reliability and power consumption. Our preliminary results (see Chapter 5) show that the performance of MWRNs

139

greatly depends on the cooperative strategies, which include the selection of relay types and relaying partners, signaling protocols, and relay- processing algorithms (i.e., deciding when, how, and with whom to cooperate). Moreover, key design objective of the joint antenna and relay selection strategies will be to achieve a desirable trade-off among the system complexity and performance.

- New physical-layer distributed network coding strategies will be then designed for MIMO MWRNs to obtain desirable trade-off between the data rate and network resource usage. The key idea is that a particular wireless terminal can improve channel capacity significantly by aggregating additional spatial dimensions facilitated by other distributed wireless terminals. In this context, novel practical analog network coding (ANC) and physical layer network coding (PLNC) structures will be designed for high capacity multicasting from multiple-source groups to multiple-destination groups by exploiting MIMO multi-way relay channels. In general, these channels are referred to as the MIMO multiple-access multi-way relay interference channels (MA-MWR-IC), and would provide unprecedented challenges for the network designers. One efficient technique to circumvent MIMO MA-MWR-IC is to employ the concepts of ANC and PLNC to facilitate interference-free signaling between multi-source groups. To this end, three key design parameters of network codes (i) field size, (ii) generation size and (iii) block size are optimized to design practically implementable ANCs and PLNCs to achieve (i) lower delay, (ii) higher coding throughput, (iii) better network performance, and (iv) lower complexity subjected to system specific trade-offs.

- The inter-cell and intra-cell interferences are the major impediments to the performance gains promised by MIMO MWRNs. Physical-layer interference mitigation techniques will be therefore developed by using (i) coordinated beamforming, (ii) cooperative signal processing, (iii) adaptive transmit power control, and (iv) interference alignment techniques. Moreover, energy-efficient radio resource management strategies will be developed by using tools from cross-layer optimization and opportunistic resource-sharing in the time, frequency, and space dimensions. Our preliminary research reveals that the amount of inter-user interference of MWRNs indeed heavily depends on the source-grouping strategies. Thus, in order to circumvent the inter-user interferences and hence to improve the multiplexing gains, novel source-grouping strategies will be designed.

- The aforementioned transmission designs, networks coding strategies, and interference/resource management techniques will then be integrated into the new MWRN system models, and thereby, the overall performance will be investigated by deriving important performance metrics such as the outage probability, average probability of error, data rate, and diversity-multiplexing trade-off. The insights obtained through the analysis will be then employed to refine the physical layer transmission strategies and hence to achieve better trade-off between complexity and performance.

**Significance:** Our future research directions mainly focus on designing and analyzing new system models and transmission strategies for MIMO MWRNs, which are the next evolution of MIMO OWRNs and MIMO TWRNs. In particular, the MWRNs are of great practical interest as a potential candidate network topology for the next-generation wireless technologies because of their numerous practical applications as elaborated in Chapter 1 and Chapter 5. For example, some of the potential applications include voice-over-IP (VoIP) calls, video and audio streaming, videoconferencing, gaming, surveillance for public safety, connectivity to remote devices, and educational services at little or no incremental cost to network operators and subscribers. In summary, the research outcomes will potentially allow wireless networks to achieve higher data rates with improved trade-off between the link-reliability and extended-coverage. Our future research outcomes therefore could eventually contribute to the advancement of the fourth generation (4G) broadband wireless standards, especially in mobile-WiMAX (IEEE 802.16m) and 3GPP LTE-Advanced.

$\sim$

# Bibliography

[1] I. Gradshteyn and I. Ryzhik, *Table of integrals, Series, and Products*, 7th ed. Academic Press, 2007.

[2] M. Abramowitz and I. Stegun, *Handbook of Mathematical Functions*. Dover Publications, Inc., New York, 1970.

[3] R. A. Horn and C. R. Johnson, *Matrix Analysis*, 1st ed. New York, NY: Cambridge University Press, 1985.

[4] G. Strang, *Linear Algebra and Its Applications*, 2nd ed. Orlando, FL: Academic Press, Inc, 1980.

[5] M. Dohler, R. Heath, A. Lozano, C. Papadias, and R. Valenzuela, "Is the phy layer dead?" *IEEE Commun. Mag.*, vol. 49, no. 4, pp. 159–165, 2011.

[6] *Global Mobile Data Traffic Forecast Update, 2012-2017*, Cisco, Cisco Visual Networking Index, Feb. 2013.

[7] M. Ismail and W. Zhuang, "Network cooperation for energy saving in green radio communications," *Wireless Communications, IEEE*, vol. 18, no. 5, pp. 76–81, 2011.

[8] G. J. Foschini, "Layered space-time architecture for wireless communication in a fading environment when using multi-element antennas," *Bell Labs Technical Journal*, vol. 5, no. 2, pp. 41–59, Autumn 1996.

[9] A. Goldsmith, S. A. Jafar, N. Jindal, and S. Vishwanath, "Capacity limits of MIMO channels," *IEEE J. Sel. Areas Commun.*, vol. 21, no. 5, pp. 684–702, Jun. 2003.

[10] T. Cover and A. E. Gamal, "Capacity theorems for the relay channel," *IEEE Trans. Inf. Theory*, vol. 25, no. 5, pp. 572–584, Sep. 1979.

[11] A. Sendonaris, E. Erkip, and B. Aazhang, "User cooperation diversity–part I: system description," *IEEE Trans. Commun.*, vol. 51, no. 11, pp. 1927–1938, Nov. 2003.

[12] J. N. Laneman, D. N. C. Tse, and G. W. Wornell, "Cooperative diversity in wireless networks: Efficient protocols and outage behavior," *IEEE Trans. Inf. Theory*, vol. 50, no. 12, pp. 3062–3080, Dec. 2004.

[13] A. Nosratinia, T. E. Hunter, and A. Hedayat, "Cooperative communication in wireless networks," *IEEE Commun. Mag.*, vol. 42, no. 10, pp. 74–80, Oct. 2004.

[14] *Wireless LAN Medium Access Control (MAC) and Physical Layer (PHY) Specifications - Amendment 5: Enhancements for Higher Throughput*, IEEE Std 802.11n, Oct. 2009.

[15] *Air Interface for Fixed and Mobile Broadband Wireless Access Systems Amendment 2: Physical and Medium Access Control Layers for Combined Fixed and Mobile Operation in Licensed Bands and Corrigendum 1*, IEEE Std 802.16e-2005, Feb. 2006.

[16] *Technical Specification Group Radio Access Network; Evolved Universal Terrestrial Radio Access (E-UTRA); LTE physical layer; General description (Release 9)*, 3GPP 3GPP TS 36.201 V9.1, Mar. 2010.

[17] J. Lee, J.-K. Han, and J. Zhang, "MIMO technologies in 3GPP LTE and LTE-Advanced," *EURASIP Journal on Wireless Communications and Networking*, Jul. 2009.

[18] *Air Interface for Broadband Wireless Access Systems - Amendment 1: Multihop Relay Specification*, IEEE Std 802.16j-2009, Jun. 2009.

[19] R. U. Nabar, O. Oyman, H. Bölcskei, and A. J. Paulraj, "Capacity scaling laws in MIMO wireless networks," in *Proc. Allerton Conference on Communication, Control, and Computing*, Monticello, IL, Oct. 2003.

[20] Y. Fan and J. Thompson, "MIMO configurations for relay channels: Theory and practice," *IEEE Trans. Wireless Commun.*, vol. 6, no. 5, pp. 1774–1786, May 2007.

[21] M. Yuksel and E. Erkip, "Multiple-antenna cooperative wireless systems: A diversity-multiplexing tradeoff perspective," *IEEE Trans. Inf. Theory*, vol. 53, no. 10, pp. 3371–3393, Oct. 2007.

[22] Y. Yang, H. Hu, J. Xu, and G. Mao, "Relay technologies for WiMAX and LTE-advanced mobile systems," *IEEE Commun. Mag.*, vol. 47, no. 10, pp. 100–105, Oct. 2009.

[23] K. Loa, C.-C. Wu, S.-T. Sheu, Y. Yuan, M. Chion, D. Huo, and L. Xu, "IMT-advanced relay standards," *IEEE Commun. Mag.*, vol. 48, no. 8, pp. 40–48, Aug. 2010.

[24] A. Goldsmith, *Wireless Communications*, 1st ed.  New York, NY: Cambridge University Press, 2005.

[25] A. Paulraj, R. Nabar, and D. Gore, *Introduction to Space-Time Wireless Communications*, 1st ed.  Cambridge University Press, 2003.

[26] D. N. C. Tse, P. Viswanath, and L. Zheng, "Diversity-multiplexing tradeoff in multiple-access channels," *IEEE Trans. Inf. Theory*, vol. 50, no. 9, pp. 1859–1874, 2004.

[27] G. L. Stüber, *Principles of Mobile Communication*, 2nd ed.  New York, NY: Kluwer Academic Publishers, 2002.

[28] H. Bolcskei, M. Borgmann, and A. J. Paulraj, "Impact of the propagation environment on the performance of space-frequency coded MIMO-OFDM," *IEEE J. Sel. Areas Commun.*, vol. 21, no. 3, pp. 427–439, Apr. 2003.

[29] D. Tse and P. Viswanath, *Fundamentals of Wireless Communication*.  New York, NY: Cambridge University Press, Jun. 2005.

[30] A. Poon, R. Brodersen, and D. Tse, "Degrees of freedom in multiple-antenna channels: a signal space approach," *IEEE Trans. Inf. Theory*, vol. 51, no. 2, pp. 523–536, 2005.

[31] R. Somaraju and J. Trumpf, "Degrees of freedom of a communication channel: using DOF singular values," *IEEE Trans. Inf. Theory*, vol. 56, no. 4, pp. 1560–1573, Apr. 2010.

[32] J. G. Proakis, *Digital Communications*, 5th ed.  New York, NY: McGraw-Hill, Inc., 2007.

[33] L. Zheng and D. Tse, "Diversity and multiplexing: a fundamental tradeoff in multiple-antenna channels," *IEEE Trans. Inf. Theory*, vol. 49, no. 5, pp. 1073–1096, May 2003.

[34] I. E. Telatar, "Capacity of multi-antenna Gaussian channels," Bell Laboratories, Lucent Technologies, Murray Hill, NJ, Tech. Rep., Oct. 1995.

[35] B. Rankov and A. Wittneben, "Spectral efficient protocols for half-duplex fading relay channels," *IEEE J. Sel. Areas Commun.*, vol. 25, no. 2, pp. 379–389, 2007.

[36] Y. Han, S. H. Ting, C. K. Ho, and W. H. Chin, "Performance bounds for two-way amplify-and-forward relaying," *IEEE Trans. Wireless Commun.*, vol. 8, pp. 432–439, 2009.

[37] R. H. Y. Louie, Y. Li, and B. Vucetic, "Practical physical layer network coding for two-way relay channels: performance analysis and comparison," *IEEE Trans. Wireless Commun.*, vol. 9, pp. 764–777, 2010.

[38] P. Popovski and H. Yomo, "Physical network coding in two-way wireless relay channels," in *Proc. IEEE International Conference on Communications (ICC)*, Glasgow, Scotland, Jun. 2007, pp. 707–712.

[39] C. Li, L. Yang, and W.-P. Zhu, "Two-way MIMO relay precoder design with channel state information," *IEEE Trans. Commun.*, vol. 58, no. 12, pp. 3358–3363, 2010.

[40] J. Joung and A. Sayed, "Multiuser two-way amplify-and-forward relay processing and power control methods for beamforming systems," *IEEE Trans. Signal Process.*, vol. 58, no. 3, pp. 1833–1846, Mar. 2010.

[41] G. Amarasuriya, C. Tellambura, and M. Ardakani, "Two-way amplify-and-forward multiple-input multiple-output relay networks with antenna selection," *IEEE J. Sel. Areas Commun.*, vol. 30, no. 8, pp. 1513–1529, Sep. 2012.

[42] ——, "Performance analysis of zero-forcing for two-way MIMO AF relay networks," *IEEE Wireless Commun. Lett.*, vol. 1, no. 2, pp. 53–56, Apr. 2012.

[43] M. Peng, C. Yang, Z. Zhao, W. Wang, and H.-H. Chen, "Cooperative network coding in relay-based IMT-advanced systems," *IEEE Commun. Mag.*, vol. 50, no. 4, pp. 76–84, Apr. 2012.

[44] *Air Interface for Fixed and Mobile Broadband Wireless Access Systems Amendment 2: Physical and Medium Access Control Layers for Combined Fixed and Mobile Operation in Licensed Bands and Corrigendum 1*, IEEE Std 802.16e-2005, Feb. 2006.

[45] *Wireless Medium Access Control (MAC) and Physical Layer (PHY) Specifications for High Rate Wireless Personal Area Networks (WPANs) - Amendment 2: Millimeter-*

*wave-based Alternative Physical Layer Extension*, IEEE Std 802.15.3c-2009, Oct. 2009.

[46] R. Pabst, B. H. Walke, D. C. Schultz, P. Herhold, H. Yanikomeroglu, S. Mukherjee, H. Viswanathan, M. Lott, W. Zirwas, M. Dohler, H. Aghvami, D. D. Falconer, and G. P. Fettweis, "Relay-based deployment concepts for wireless and mobile broadband radio," *IEEE Commun. Mag.*, vol. 42, no. 9, pp. 80–89, Sep. 2004.

[47] G. K. Karagiannidis, T. A. Tsiftsis, and R. K. Mallik, "Bounds for multihop relayed communications in Nakagami-$m$ fading," *IEEE Trans. Commun.*, vol. 54, no. 1, pp. 18–22, Jan. 2006.

[48] G. K. Karagiannidis, "Performance bounds of multihop wireless communications with blind relays over generalized fading channels," *IEEE Trans. Wireless Commun.*, vol. 5, no. 3, pp. 498–503, Mar. 2006.

[49] T. Tsiftsis, "Performance of wireless multihop communications systems with cooperative diversity over fading channels," *International Journal of Communication Systems*, vol. 21, no. 5, pp. 559–565, May 2008.

[50] M. O. Hasna, "Average BER of multihop communication systems over fading channels," in *Proc. 10th IEEE International Conference on Electronics, Circuits and Systems (ICECS).*, vol. 2, Dec. 2003, pp. 723–726.

[51] M. Hasna and M.-S. Alouini, "A performance study of dual-hop transmissions with fixed gain relays," *IEEE Trans. Wireless Commun.*, vol. 3, no. 6, pp. 1963–1968, Nov. 2004.

[52] M. O. Hasna and M. S. Alouini, "Outage probability of multihop transmission over Nakagami fading channels," *IEEE Commun. Lett.*, vol. 7, no. 5, pp. 216–218, May 2003.

[53] M. Di Renzo, F. Graziosi, and F. Santucci, "A unified framework for performance analysis of CSI-assisted cooperative communications over fading channels," *IEEE Trans. Commun.*, vol. 57, no. 9, pp. 2551–2557, Sep. 2009.

[54] D. Michalopoulos and T. Tsiftsis, "Performance analysis of wireless multihop diversity systems," *International Journal of Communication Systems*, vol. 21, no. 9, pp. 955–969, Sep. 2008.

146

[55] M. Di Renzo, F. Graziosi, and F. Santucci, "A comprehensive framework for performance analysis of dual-hop cooperative wireless systems with fixed-gain relays over generalized fading channels," *IEEE Trans. Wireless Commun.*, vol. 8, no. 10, pp. 5060–5074, Oct. 2009.

[56] Z. Fang, L. Li, and Z. Wang, "Asymptotic performance analysis of multihop relayed transmissions over Nakagami-$m$ fading channels," *IEICE Trans. Comm.*, vol. E91B, no. 12, Dec. 2008.

[57] M. Di Renzo, F. Graziosi, and F. Santucci, "A comprehensive framework for performance analysis of cooperative multi-hop wireless systems over log-normal fading channels," *IEEE Trans. Commun.*, vol. 58, no. 2, pp. 531–544, Feb. 2010.

[58] A. Ribeiro, X. Cai, and G. B. Giannakis, "Symbol error probabilities for general cooperative links," *IEEE Trans. Wireless Commun.*, vol. 4, no. 3, pp. 1264–1273, May 2005.

[59] M. Labiod, H. Badra, *New Technologies, Mobility and Security*. Springer Netherlands, 2007.

[60] R. H. Y. Louie, Y. Li, and B. Vucetic, "Performance analysis of beamforming in two hop amplify and forward relay networks," in *Proc. IEEE International Conference on Communications (ICC)*, May 2008, pp. 4311–4315.

[61] Z. Wang and G. Giannakis, "A simple and general parameterization quantifying performance in fading channels," *IEEE Trans. Commun.*, vol. 51, no. 8, pp. 1389–1398, Aug. 2003.

[62] Y. Chen and C. Tellambura, "Distribution functions of selection combiner output in equally correlated Rayleigh, Rician, and Nakagami-m fading channels," *IEEE Trans. Commun.*, vol. 52, no. 11, pp. 1948–1956, Nov. 2004.

[63] A. Papoulis and S. U. Pillai, *Probability, Random Variables and Stochastic Processes*, 4th ed. New York, NY: McGraw-Hill Inc., Jan. 2002.

[64] A. Annamalai, C. Tellambura, and V. K. Bhargava, "Efficient computation of MRC diversity performance in Nakagami fading channel with arbitrary parameters," *Electron. Lett.*, vol. 34, no. 12, pp. 1189–1190, Jun. 1998.

[65] G. Amarasuriya, C. Tellambura, and M. Ardakani, "Multi-hop relay networks with multiple-antenna equipped source and destination," in *Proc. IEEE 72nd Vehicular Technology Conference-Fall (VTC-Fall)*, Sep. 2010, pp. 1–5.

[66] J. N. Laneman and G. W. Wornell, "Energy-efficient antenna sharing and relaying for wireless networks," in *Proc. IEEE Wireless Communications and Networking Conference (WCNC)*, vol. 1, Chicago, IL, Sep. 2000, pp. 7–12.

[67] ——, "Distributed space-time-coded protocols for exploiting cooperative diversity in wireless networks," *IEEE Trans. Inf. Theory*, vol. 49, no. 10, pp. 2415–2425, Oct. 2003.

[68] A. Sendonaris, E. Erkip, and B. Aazhang, "User cooperation diversity. part i. system description," *IEEE Trans. Commun.*, vol. 51, no. 11, pp. 1927–1938, Nov. 2003.

[69] ——, "User cooperation diversity. part II. implementation aspects and performance analysis," *IEEE Trans. Commun.*, vol. 51, no. 11, pp. 1939–1948, Nov. 2003.

[70] V. Sreng, H. Yanikomeroglu, and D. D. Falconer, "Relayer selection strategies in cellular networks with peer-to-peer relaying," in *Proc. IEEE 58th Vehicular Technology Conference (VTC 2003-Fall)*, vol. 3, Oct. 2003, pp. 1949–1953.

[71] A. K. Sadek, Z. Han, and K. J. R. Liu, "A distributed relay-assignment algorithm for cooperative communications in wireless networks," in *Proc. IEEE International Conference on Communication (ICC)*, vol. 4, Jun. 2006, pp. 1592–1597.

[72] A. Bletsas, A. Khisti, D. P. Reed, and A. Lippman, "A simple cooperative diversity method based on network path selection," *IEEE J. Sel. Areas Commun.*, vol. 24, no. 3, pp. 659–672, Mar. 2006.

[73] Y. Zhao, R. Adve, and T. J. Lim, "Improving amplify-and-forward relay networks: optimal power allocation versus selection," *IEEE Trans. Wireless Commun.*, vol. 6, no. 8, pp. 3114–3123, Aug. 2007.

[74] ——, "Symbol error rate of selection amplify-and-forward relay systems," *IEEE Commun. Lett.*, vol. 10, no. 11, pp. 757–759, Nov. 2006.

[75] D. S. Michalopoulos, G. K. Karagiannidis, T. A. Tsiftsis, and R. K. Mallik, "An optimized user selection method for cooperative diversity systems," in *Proc. IEEE Global Telecommunications Conference (GLOBCOM)*, Nov./Dec. 2006, pp. 1–6.

[76] R. Madan, N. Mehta, A. Molisch, and J. Zhang, "Energy-efficient cooperative relaying over fading channels with simple relay selection," *IEEE Trans. Wireless Commun.*, vol. 7, no. 8, pp. 3013–3025, Aug. 2008.

[77] Y. Jing and H. Jafarkhani, "Single and multiple relay selection schemes and their achievable diversity orders," *IEEE Trans. Wireless Commun.*, vol. 8, no. 3, pp. 1414–1423, Mar. 2009.

[78] S. S. Ikki and M. H. Ahmed, "Performance of multiple-relay cooperative diversity systems with best relay selection over Rayleigh fading channels," *EURASIP J. Adv. Signal Process*, Jan. 2008.

[79] S. W. Kim, D. S. Ha, and J. H. Reed, "Minimum selection GSC and adaptive low-power rake combining scheme," in *Proc. of International Symposium on Circuits and Systems, (ISCAS)*, vol. 4, May 2003, pp. 357–360.

[80] Y. Chen and C. Tellambura, "An adaptive maximal ratio combining scheme and its performance analysis," in *Wireless 2004, Calgary, Alberta, Canada*, Jul. 2004.

[81] H.-C. Yang and M. S. Alouini, "MRC and GSC diversity combining with an output threshold," *IEEE Trans. Veh. Technol.*, vol. 54, no. 3, pp. 1081–1090, May 2005.

[82] A. Lioumpas, G. Karagiannidis, and T. Tsiftsis, "Adaptive generalized selection combining (A-GSC) receivers," *IEEE Trans. Wireless Commun.*, vol. 7, pp. 5214–5219, Dec. 2008.

[83] Y. Ma, X. Dong, and H.-C. Yang, "Asymptotic performance of threshold-based generalized selection combining," *IEEE Trans. Veh. Technol.*, vol. 58, no. 5, pp. 2579–2585, Jun. 2009.

[84] S. S. Ikki and M. H. Ahmed, "Performance analysis of generalized selection combining for amplify-and-forward cooperative-diversity networks," in *Proc. IEEE International Conference on Communications ICC*, Dresden, Germany, Jun. 2009.

[85] K.-S. Hwang, Y.-C. Ko, and M. S. Alouini, "Performance analysis of incremental opportunistic relaying over identically and non-identically distributed cooperative paths," *IEEE Trans. Wireless Commun.*, vol. 8, no. 4, pp. 1953–1961, Apr. 2009.

[86] P. A. Anghel and M. Kaveh, "Exact symbol error probability of a cooperative network in a Rayleigh-fading environment," *IEEE Trans. Wireless Commun.*, vol. 3, no. 5, pp. 1416–1421, Sep. 2004.

[87] S. Ikki and M. H. Ahmed, "Performance analysis of cooperative diversity wireless networks over Nakagami-m fading channel," *IEEE Commun. Lett.*, vol. 11, no. 4, pp. 334–336, Apr. 2007.

[88] T. Nechiporenko, P. Kalansuriya, and C. Tellambura, "Performance of optimum switching adaptive $m$-QAM for amplify-and-forward relays," *IEEE Trans. Veh. Technol.*, vol. 58, no. 5, pp. 2258–2268, Jun. 2009.

[89] S. Berger, M. Kuhn, A. Wittneben, T. Unger, and A. Klein, "Recent advances in amplify-and-forward two-hop relaying," *IEEE Commun. Mag.*, vol. 47, no. 7, pp. 50–56, Jul. 2009.

[90] M. Ju and I.-M. Kim, "Relay selection with ANC and TDBC protocols in bidirectional relay networks," *IEEE Trans. Commun.*, vol. 58, no. 12, pp. 3500–3511, 2010.

[91] R. Zhang, Y.-C. Liang, C. C. Chai, and S. Cui, "Optimal beamforming for two-way multi-antenna relay channel with analogue network coding," *IEEE J. Sel. Areas Commun.*, vol. 27, no. 5, pp. 699–712, 2009.

[92] A. Y. Panah and R. W. Heath, "MIMO two-way amplify-and-forward relaying with imperfect receiver CSI," *IEEE Trans. Veh. Technol.*, vol. 59, no. 9, pp. 4377–4387, 2010.

[93] A. F. Molisch and M. Z. Win, "MIMO systems with antenna selection," *IEEE Microw. Mag.*, vol. 5, no. 1, pp. 46–56, 2004.

[94] N. Sollenberger, "Diversity and automatic link transfer for a TDMA wireless access link," in *Proc. IEEE Global Telecommunications Conference (GLOBCOM)*, Dec. 1993, pp. 532–536.

[95] Y. Jing and H. Jafarkhani, "Single and multiple relay selection schemes and their achievable diversity orders," *IEEE Trans. Wireless Commun.*, vol. 8, no. 3, pp. 1414–1423, Mar. 2009.

[96] S. Peters and R. W. Heath, "Nonregenerative MIMO relaying with optimal transmit antenna selection," *IEEE Signal Process. Lett.*, vol. 15, pp. 421–424, 2008.

[97] L. Cao, X. Zhang, Y. Wang, and D. Yang, "Transmit antenna selection strategy in amplify-and-forward MIMO relaying," in *Proc. IEEE Wireless Communications and Networking Conference (WCNC)*, Budapest, Apr. 2009.

[98] S. Chen, W. Wang, X. Zhang, and D. Zhao, "Performance of amplify-and-forward MIMO relay channels with transmit antenna selection and maximal-ratio combining," in *Proc. IEEE Wireless Communications and Networking Conference (WCNC)*, Apr 2009.

[99] C. Feng, L. Cao, X. Zhang, and D. Yang, "Diversity order analysis of a sub-optimal transmit antenna selection strategy for non-regenerative MIMO relay channel," in *Proc. IEEE 20th International Symposium on Personal, Indoor and Mobile Radio Communications (PIMRC)*, Sep. 2009, pp. 978 –982.

[100] I. H. Kim, D. J. Love, and S. Y. Park, "Recursive covariance design for multiple antenna physical layer multicasting," in *Proc. IEEE Radio and Wireless Symposium*, Orlando, FL, Jan. 2008, pp. 555–558.

[101] H. A. Suraweera, G. K. Karagiannidis, Y. Li, H. K. Garg, A. Nallanathan, and B. Vucetic, "Amplify-and-forward relay transmission with end-to-end antenna selection," in *Proc. IEEE Wireless Communications and Networking Conference (WCNC)*, Apr 2010.

[102] A. Muller and J. Speidel, "Outage-optimal transmit antenna selection for cooperative decode-and-forward systems," in *Proc. 69th IEEE Vehicular Technology Conference (VTC-Spring)*, Apr 2009, pp. 1–5.

[103] T. Duong, H.-J. Zepernick, T. Tsiftsis, and Q. B. V. Nguyen, "Performance analysis of amplify-and-forward MIMO relay networks with transmit antenna selection over Nakagami-$m$ channels," in *Proc. IEEE 21st International Symposium on Personal, Indoor and Mobile Radio Communications (PIMRC)*, Sep. 2010, pp. 368–372.

[104] L. Cao, L. Chen, X. Zhang, and D. Yang, "Performance analysis of two-hop amplify-and-forward MIMO relaying with transmit antenna selection," in *Proc. IEEE 21st International Symposium on Personal, Indoor and Mobile Radio Communications (PIMRC)*, Sep. 2010, pp. 373–378.

[105] ——, "Asymptotic performance of two-hop amplify-and-forward MIMO relaying with transmit antenna selection," in *Proc. IEEE Global Conference on Communications (GLOBCOM)*, Dec. 2010, pp. 1–6.

[106] A. Yilmaz and O. Kucur, "Error performance of joint transmit and receive antenna selection in two hop amplify-and-forward relay system over Nakagami-$m$ fading channels," in *Proc. IEEE 21st International Symposium on Personal, Indoor and Mobile Radio Communications (PIMRC)*, Sep. 2010, pp. 2198–2203.

[107] M. Eslamifar, W. H. Chin, C. Yuen, and G. Y. Liang, "Performance analysis of two-way multiple-antenna relaying with network coding," in *Proc. IEEE 70th Vehicular Technology Conference (VTC-Fall)*, 2009, pp. 1–5.

[108] M. Eslamifar, C. Yuen, W. H. Chin, and Y. L. Guan, "Max-min antenna selection for bi-directional multi-antenna relaying," in *Proc. IEEE 71st Vehicular Technology Conference (VTC-Spring)*, 2010, pp. 1–5.

[109] H. Park, J. Chun, and R. Adve, "Computationally efficient relay antenna selection for AF MIMO two-way relay channels," *IEEE Trans. Signal Process.*, vol. 60, no. 11, pp. 6091–6097, 2012.

[110] Y. Li, R. H. Y. Louie, and B. Vucetic, "Relay selection with network coding in two-way relay channels," *IEEE Trans. Veh. Technol.*, vol. 59, no. 9, pp. 4489–4499, 2010.

[111] Y. Fan and J. Thompson, "On the outage capacity of MIMO multihop networks," in *Proc. IEEE Global Telecommunications Conference (GLOBCOM)*, Dec. 2005.

[112] J. Huang, T. Wu, X. Yu, and Y. Wang, "Statistical joint antenna and node selection for multi-antenna relay networks," in *Proc. IEEE Wireless Communications and Networking Conference (WCNC)*, Mar. 2008, pp. 2021–2026.

[113] D. Gore, R. Heath Jr., and A. Paulraj, "On performance of the zero forcing receiver in presence of transmit correlation," in *Proc. IEEE International Symposium on Information Theory (ISIT)*, Lausanne, Switzerland, Jun. 2002.

[114] R. H. Y. Louie, Y. Li, and B. Vucetic, "Zero forcing processing in two hop networks with multiple source, relay and destination nodes," in *Proc. IEEE International Conference on Communications (ICC)*, Dresden, Germany, Jun. 2009.

[115] A. Annamalai and C. Tellambura, "Error rates for Nakagami-$m$ fading multichannel reception of binary and M-ary signals," *IEEE Trans. Commun.*, vol. 49, no. 1, pp. 58–68, Jan. 2001.

[116] M. Abramowitz and I. Stegun, *Handbook of Mathematical Functions*. Dover Publications, Inc., New York, 1970.

[117] Golub, G. H., Welsch, and J. H., "Calculation of Gauss quadrature rules," Stanford, CA, USA, Tech. Rep., 1967.

[118] S. Zhou and G. Giannakis, "Adaptive modulation for multiantenna transmissions with channel mean feedback," *IEEE Trans. Wireless Commun.*, vol. 3, no. 5, pp. 1626–1636, Sep. 2004.

[119] G. Amarasuriya, C. Tellambura, and M. Ardakani, "Feedback delay effect on dual-hop MIMO AF relaying with antenna selection," in *Proc. IEEE Global Communications Conference (GLOBCOM)*, Miami, FL, USA, Dec. 2010, pp. 1–5.

[120] J. Makhoul, "Linear prediction: A tutorial review," *IEEE Proceedings*, vol. 63, no. 4, pp. 561–580, Apr. 1975.

[121] T. Ekman, "Prediction of mobile radio channels, modeling and design," Ph.D. dissertation, Uppsala Univ., Uppsala, Sweden, Sept. 2002.

[122] Y. Tong, *The multivariate Normal Distribution*, 3rd ed. New York: Spring-Verlag, 1990.

[123] E. van der Meulen, "A survey of multi-way channels in information theory: 1961-1976," *IEEE Trans. Inf. Theory*, vol. 23, no. 1, pp. 1–37, Jan. 1977.

[124] D. Gunduz, A. Yener, A. Goldsmith, and H. Poor, "The multi-way relay channel," in *Proc. IEEE Int. Sympo. on Info. Theory., (ISIT)*, Jul. 2009, pp. 339–343.

[125] L. Ong, S. Johnson, and C. Kellett, "An optimal coding strategy for the binary multi-way relay channel," *IEEE Commun. Lett.*, vol. 14, no. 4, pp. 330–332, Apr. 2010.

[126] ——, "The capacity region of multiway relay channels over finite fields with full data exchange," *IEEE Trans. Inf. Theory*, vol. 57, no. 5, pp. 3016–3031, May 2011.

[127] L. Ong, C. Kellett, and S. Johnson, "Capacity theorems for the awgn multi-way relay channel," in *Proc. IEEE Int. Symp. Info. Theory (ISIT)*, Jun. 2010, pp. 664–668.

[128] V. R. Cadambe, "Multi-way relay based deterministic broadcast with side information: Pair-wise network coding is sum-capacity optimal," in *46th Annual Conf. on Info. Sci. and Sys., Princeton NJ*, Mar. 2012.

[129] G. Amarasuriya, C. Tellambura, and M. Ardakani, "Performance analysis of pairwise amplify-and-forward multi-way relay networks," *accepted for publication in IEEE Wireless Commun. Lett.*, Jul. 2012.

[130] A. Amah and A. Klein, "A transceive strategy for regenerative multi-antenna multi-way relaying," in *Proc. 3rd IEEE Int. Workshop on Computational Advances in Multi-Sensor Adaptive Processing (CAMSAP)*, Dec. 2009, pp. 352–355.

[131] ——, "Non-regenerative multi-way relaying with linear beamforming," in *Proc. IEEE Personal, Indoor and Mobile Radio Commun., (PIMRC)*, Sep. 2009, pp. 1843–1847.

[132] Z. Zhao, Z. Ding, M. Peng, W. Wang, and K. Leung, "A special case of multi-way relay channel: When beamforming is not applicable," *IEEE Trans. Wireless Commun.*, vol. 10, no. 7, pp. 2046–2051, Jul. 2011.

[133] A. Amah and A. Klein, "Non-regenerative multi-antenna multi-group multi-way relaying," *EURASIP J. Wireless Commun. and Netw.*, vol. 2011, pp. 1–19, Jul. 2011.

[134] J. Heath, R.W., S. Sandhu, and A. Paulraj, "Antenna selection for spatial multiplexing systems with linear receivers," *IEEE Commun. Lett.*, vol. 5, no. 4, pp. 142–144, Apr. 2001.

[135] J. A. Tague and C. I. Caldwell, "Expectations of useful complex wishart forms," *Multidimens. Syst. Signal Process.*, vol. 5, no. 3, pp. 263–279, Jul. 1994.

[136] L. G. Ordóñez, "Performance limits of spatial multiplexing MIMO systems," Ph.D. dissertation, Technical University of Catalonia (UPC), Barcelona, Spain, Mar. 2009.

[137] R. Louie, Y. Li, and B. Vucetic, "Zero forcing in general two-hop relay networks," *IEEE Trans. Veh. Technol.*, vol. 59, no. 1, Jan. 2010.

[138] H. A. David, *Order Statistics*, 2nd ed.   Wiley, New York, 1981.

[139] I. Wolfram Research. The Wolfram functions site. [Accessed: April 2012]. [Online]. Available: http://functions.wolfram.com/07.34.21.0002.01

[140] J. Ritcey and M. Azizoglu, "Impact of switching constraints on selection diversity performance," in *Conference Record of the Thirty-Second Asilomar Conference on Signals, Systems Computers*, Nov. 1998, pp. 795 –799.

[141] A. Erdelyi, W. Magnus, F. Oberhettinger, and F. G. Tricomi, *Tables of Integral Transforms*, ser. Bateman Manuscript Project, California Institute of Technology. McGraw-Hill Book Company, Inc, 1954, vol. 1.

[142] D. Gore, J. Heath, R.W., and A. Paulraj, "On performance of the zero forcing receiver in presence of transmit correlation," in *Proc. IEEE Int. Sympo. on Inf. Theory (ISIT)*, Lausanne, Switzerland, Jul. 2002, pp. 1–2.

$\sim$

# Appendix A

# Proofs for Chapter 2

## A.1   The proof of Theorem 2.1

**Proof**: Let the random variable $\Gamma$ be

$$\Gamma = \frac{\Gamma_1 \Gamma_2}{\Gamma_1 + \Gamma_2}, \tag{A.1}$$

where $\Gamma = \gamma_{\text{e2e}}^{\text{ub}}$, $\Gamma_1 = \min\limits_{n \in \{1, \cdots, P\}} (\gamma_n)$ and $\Gamma_2 = \min\limits_{n \in \{P+1, \cdots, N\}} (\gamma_n)$. The CDF of $\Gamma$ can then be expressed as

$$F_\Gamma(x) = \Pr\left(\frac{\Gamma_1 \Gamma_2}{\Gamma_1 + \Gamma_2} \leq x\right). \tag{A.2}$$

Alternatively, the CDF of $\Gamma$ can be rewritten in a single-integral form as

$$F_\Gamma(x) = \int_0^\infty \Pr\left(\frac{\Gamma_1 z}{\Gamma_1 + z} \leq x\right) f_{\Gamma_2}(z)\, \mathrm{d}z, \tag{A.3}$$

which follows from the fact that $\Gamma_1$ and $\Gamma_2$ are statistically independent. After some mathematical manipulations, $F_\Gamma(x)$ can be expanded as [86]

$$F_\Gamma(x) = \int_0^x \underbrace{\Pr\left(\Gamma_1 \geq \frac{xz}{z-x}\right)}_{\doteq 1} f_{\Gamma_2}(z)\, \mathrm{d}z + \int_x^\infty \Pr\left(\Gamma_1 \leq \frac{xz}{z-x}\right) f_{\Gamma_2}(z)\, \mathrm{d}z. \tag{A.4}$$

After some further manipulations, (A.4) can be written in an more tractable form as follows:

$$F_\Gamma(x) = 1 - \int_0^x \left[1 - F_{\Gamma_1}\left(\frac{xz}{z-x}\right)\right] f_{\Gamma_2}(z)\, \mathrm{d}z. \tag{A.5}$$

By using (A.5), the complimentary cumulative distribution function (CCDF) of $\Gamma$ can be expressed in a single-integral form as

$$\bar{F}_\Gamma(x) = \int_0^\infty \bar{F}_{\Gamma_1}\left(\frac{(z+x)x}{z}\right) f_{\Gamma_2}(z+x)\mathrm{d}z. \tag{A.6}$$

The CCDF of $\Gamma_1$ for independent and identically distributed (i.i.d.) Nakagami-$m$ fading with integer $m$ can be derived by using [1, Eqn. (8.352.2)] and [115, Eqn. (44)] as follows:

$$\bar{F}_{\Gamma_1}(x) = \prod_{n=1}^{P} \bar{F}_{\gamma_n}(x) = \left[ \Gamma\left(m, \frac{mx}{\bar{\gamma}}\right) / \Gamma(m) \right]^P \tag{A.7}$$

$$= \exp\left(-\frac{mPx}{\bar{\gamma}}\right) \sum_{k=0}^{P(m-1)} \beta_{k,P} \left(\frac{mx}{\bar{\gamma}}\right)^k, \tag{A.8}$$

where $\beta_{k,P}$ is defined in (2.6b). The PDF of $\Gamma_2$ for i.i.d. Nakagami-$m$ fading is given by

$$f_{\Gamma_2}(x) = \frac{d}{dx}\left[1 - \left(\bar{F}_{\gamma_n}(x)\right)^{N-P}\right] = P\left[\bar{F}_{\gamma_n}(x)\right]^{N-P-1} f_{\gamma_n}(x) \tag{A.9}$$

$$= \frac{(N-P)}{\Gamma(m)} \sum_{k=0}^{(m-1)(N-P-1)} \beta_{k,N-P-1} \left(\frac{m}{\bar{\gamma}}\right)^{m+k} x^{m+k-1} \exp\left(-\frac{m(N-P)x}{\bar{\gamma}}\right).$$

By substituting (A.7) and (A.9) into (A.6), and by evaluating the resulting integral by using [1, Eqn. (3.471.9)], the desired result given in (2.6a) can be derived.

The PDF of $\Gamma$ defined in (A.1) can be derived by differentiating (A.4) as follows:

$$f_{\Gamma}(x) = \frac{d}{dx}\left[\int_0^x f_{\Gamma_2}(z)\, dz\right] + \frac{d}{dx}\left[\int_x^\infty \Pr\left(\Gamma_1 \leq \frac{xz}{z-x}\right) f_{\Gamma_2}(z)\, dz\right]. \tag{A.10}$$

By using the Leibniz integral rule, (A.10) can readily be evaluated as follows:

$$f_{\Gamma}(x) = f_{\Gamma_2}(x) - f_{\Gamma_2}(x) \lim_{z \to x}\left[F_{\Gamma_1}\left(\frac{xz}{z-x}\right)\right]$$
$$+ \int_x^\infty \left(\frac{z}{z-x}\right)^2 f_{\Gamma_1}\left(\frac{xz}{z-x}\right) f_{\Gamma_2}(z)\, dz. \tag{A.11}$$

By first noticing the fact that $\lim_{x\to\infty} F_X(x) = 1$ and then by substituting the dummy variable $t = z - x$, the PDF of $\Gamma$ can be written in a compact integral form as

$$f_{\Gamma}(x) = \int_0^\infty \left(\frac{t+x}{t}\right)^2 f_{\Gamma_1}\left(\frac{x(t+x)}{t}\right) f_{\Gamma_2}(t+x)\, dt \tag{A.12a}$$

$$= \sum_{i=1}^{3} \alpha_i(x) \int_0^\infty t^{1-i} f_{\Gamma_1}\left(\frac{x(t+x)}{t}\right) f_{\Gamma_2}(t+x)\, dt, \tag{A.12b}$$

where $\alpha_1(x) = 1$, $\alpha_2(x) = 2x$, and $\alpha_3(x) = x^2$.

The PDF of $\Gamma_1$ can readily be derived as

$$f_{\Gamma_1}(x) = \frac{d}{dx}\left[1 - \left(\bar{F}_{\gamma_n}(x)\right)^P\right] = P\left[\bar{F}_{\gamma_n}(x)\right]^{P-1} f_{\gamma_n}(x) \tag{A.13}$$

$$= \frac{P}{\Gamma(m)} \sum_{k=0}^{(m-1)(P-1)} \beta_{k,P-1} \left(\frac{m}{\bar{\gamma}}\right)^{m+k} x^{m+k-1} \exp\left(-\frac{mPx}{\bar{\gamma}}\right).$$

The PDF of $\Gamma_2$ has already been derived in (A.9). By first substituting (A.13) and (A.9) into (A.12b), and then by evaluating the residue integral by employing [1, Eqn. (3.471.9)], the desired result given in (2.7) can be derived.

The MGF of $\Gamma$ can be derived by substituting (2.6a) into

$$\mathcal{M}_\Gamma(s) = \mathcal{E}_\Gamma\{\exp(-sx)\} = 1 - \int_0^\infty s\bar{F}_\Gamma(x)\exp(-sx)\mathrm{d}x, \tag{A.14}$$

and by evaluating the resulting integral by using [1, Eqn. (6.621.3)]. ∎

## A.2 The proof of Theorem 2.2

**Proof**: If the MacLaurin series expansion of the PDF of $\gamma_n$ for $n \in \{1, \cdots, N\}$ is given by $f_{\gamma_n}(x) = \frac{\beta_n}{(C_n\bar{\gamma})^{d_n}}x^{d_n-1} + o(x^{d_n-1})$, then the corresponding MacLaurin series expansion of the CDF is given by

$$F_{\gamma_n}(x) = \frac{\beta_n}{(C_n)^{d_n}\,d_n}\left(\frac{x}{\bar{\gamma}}\right)^{d_n} + o(x^{d_n}). \tag{A.15}$$

The MacLaurin series expansion of the CDF of $\Gamma_1 = \min_{n\in\{1,\cdots,P\}}(\gamma_n)$ is derived by first substituting (A.15) into

$$F_{\Gamma_1}(x) = 1 - \prod_{n=1}^{P}(1 - F_{\gamma_n}(x)) \tag{A.16}$$

and by then employing the identity

$$\prod_{n=1}^{P}(1 - x_n) = 1 + \sum_{n=1}^{P}(-1)^n \sum_{\lambda_1=1}^{P-l+1}\sum_{\lambda_2=\lambda_1+1}^{P-l+2}\cdots\cdots\sum_{\lambda_n=\lambda_{n-1}}^{P}\prod_{q=1}^{n}x_{\lambda_q} \tag{A.17}$$

as follows:

$$F_{\Gamma_1}(x) = \sum_{l\in\{n|d_n=\min_{n\in\{1,\cdots,P\}}(d_n)\}}\frac{\beta_n}{d_n(C_n)^{d_n}}\left(\frac{x}{\bar{\gamma}}\right)^{d_1^{\min}} + o\left(x^{d_1^{\min}}\right), \tag{A.18}$$

where $d_1^{\min} = \min_{n\in\{1,\cdots,P\}}(d_n)$. Similarly, the MacLaurin series expansion of $\Gamma_2 = \min_{n\in\{P+1,\cdots,N\}}(\gamma_n)$ can be derived as

$$F_{\Gamma_2}(x) = \sum_{n\in\{n|d_n=\min_{n\in\{P+1,\cdots,N\}}(d_n)\}}\frac{\beta_n}{d_n(C_n)^{d_n}}\left(\frac{x}{\bar{\gamma}}\right)^{d_2^{\min}} + o\left(x^{d_2^{\min}}\right), \tag{A.19}$$

where $d_2^{\min} = \min_{n\in\{P+1,\cdots,N\}}(d_n)$.

The MacLaurin series expansion of CDF of $\Gamma = \Gamma_1 \Gamma_2 / (\Gamma_1 + \Gamma_2)$ can then be derived by using (A.4) as follows:

$$\lim_{x \to 0^+} F_\Gamma(x) = \lim_{x \to 0^+} \int_0^x f_{\Gamma_2}(z) \, \mathrm{d}z + \lim_{x \to 0^+} \int_x^\infty \mathrm{Pr}\left( \Gamma_1 \leq \frac{xz}{z-x} \right) f_{\Gamma_2}(z) \, \mathrm{d}z. \quad \text{(A.20)}$$

Next, one observes that if $\lim_{x \to 0^+}$, then $z/(z-x) \to 1$ and $xz/(z-x) \to x$. Thus, the MacLaurin series expansion of CDF of $\Gamma$ can further be simplified as

$$\begin{aligned} \lim_{x \to 0^+} F_\Gamma(x) &= \lim_{x \to 0^+} F_{\Gamma_2}(x) + \lim_{x \to 0^+} \mathrm{Pr}(\Gamma_1 \leq x) \int_x^\infty f_{\Gamma_2}(z) \, \mathrm{d}z \\ &= \lim_{x \to 0^+} F_{\Gamma_1}(x) + \lim_{x \to 0^+} F_{\Gamma_2}(x) - \lim_{x \to 0^+} F_{\Gamma_1}(x) \, F_{\Gamma_2}(x). \quad \text{(A.21)} \end{aligned}$$

By substituting (A.18) and (A.19) into (A.21), the desired result given in (2.15) can be readily derived. Moreover, the MacLaurin series expansions of the PDF and MGF of $\Gamma$ can then be derived by first differentiating (A.21) and then taking the Laplace transformation of the resulting PDF, respectively.

∎

$\sim$

# Appendix B

# Proofs for Chapter 3

## B.1 Proof of average SER of OT-MRS scheme

The lower bound on the average SER of the output-threshold multiple relay selection (OT-MRS) scheme can be derived by averaging the conditional error probability (CEP) over the PDF of the upper-bounded output SNR as follows:

$$
\begin{aligned}
\bar{P}_e &= \int_0^\infty \zeta \mathcal{Q}(\sqrt{\eta x}) f_{\gamma_c}(x) \mathrm{d}x \\
&= \int_0^{\gamma_{th}} \zeta \mathcal{Q}(\sqrt{\eta x}) \left( \beta_{sd,L} \exp\left( -\frac{x}{\bar{\gamma}_{S,D}} \right) + \sum_{l=1}^{L} \frac{\beta_{l,L}}{(l-1)!} x^{l-1} \exp\left( \frac{x}{\bar{\gamma}} \right) \right) \mathrm{d}x \\
&\quad + \int_{\gamma_{th}}^\infty \zeta \mathcal{Q}(\sqrt{\eta x}) \left( \beta_{sd,1} \exp\left( -\frac{x}{\bar{\gamma}_{S,D}} \right) + \frac{\lambda}{\bar{\gamma}} \exp\left( -\frac{x}{\bar{\gamma}} \right) \right) \mathrm{d}x \\
&= \zeta \beta_{sd,L} \mathcal{I}_1 + \zeta \sum_{l=1}^{L} \beta_{l,L} \mathcal{I}_l + \zeta \beta_{sd,1} \mathcal{I}_2 + \frac{\zeta \lambda}{\bar{\gamma}} \mathcal{I}_3,
\end{aligned}
\tag{B.1}
$$

where $\lambda$ is defined in (3.12a). Moreover, in (B.1), the integrals $\mathcal{I}_1, \mathcal{I}_2, \mathcal{I}_3$, and $\mathcal{I}_l$ are defined as

$$
\begin{aligned}
\mathcal{I}_1 &= \int_0^{\gamma_{th}} \mathcal{Q}(\sqrt{\eta x}) \exp\left( -\frac{x}{\bar{\gamma}_{S,D}} \right) \mathrm{d}x, \quad \mathcal{I}_2 = \int_{\gamma_{th}}^\infty \mathcal{Q}(\sqrt{\eta x}) \exp\left( -\frac{x}{\bar{\gamma}_{S,D}} \right) \mathrm{d}x, \\
\mathcal{I}_3 &= \int_{\gamma_{th}}^\infty \mathcal{Q}(\sqrt{\eta x}) \exp\left( -\frac{x}{\bar{\gamma}} \right) \mathrm{d}x, \quad \text{and} \quad \mathcal{I}_l = \int_0^{\gamma_{th}} \frac{\mathcal{Q}(\sqrt{\eta x})}{(l-1)!} x^{l-1} \exp\left( -\frac{x}{\bar{\gamma}} \right) \mathrm{d}x.
\end{aligned}
$$

The integrals $\mathcal{I}_1$, $\mathcal{I}_2$, and $\mathcal{I}_3$ can be evaluated in closed-form by employing techniques similar to those in [88]. The integral $\mathcal{I}_l$ can be evaluated by first using the identity [116]

$$
\int_0^x t^{l-1} \exp\left( -\frac{t}{\bar{\gamma}} \right) \mathrm{d}t = (\bar{\gamma})^l \gamma\left( l, \frac{x}{\bar{\gamma}} \right)
\tag{B.2}
$$

and then integration by parts as follows:

$$
\begin{aligned}
\mathcal{I}_l &= \frac{(\bar{\gamma})^l}{(l-1)!}\mathcal{Q}(\sqrt{\eta\gamma_{th}})\gamma\left(l,\frac{\gamma_{th}}{\bar{\gamma}}\right) + 0.5\bar{\gamma}^l\left(1 - 2\mathcal{Q}(\sqrt{\eta\gamma_{th}})\right) \\
&\quad + \sum_{j=0}^{l-1}\frac{2^{j-1}(\bar{\gamma})^{l-j}}{\sqrt{\pi}\eta^j\, j!}\left(\frac{\eta\bar{\gamma}}{2+\eta\bar{\gamma}}\right)^{j+0.5}\gamma\left(j+0.5,\frac{\gamma_{th}}{2\bar{\gamma}}(2+\eta\bar{\gamma})\right).
\end{aligned}
\tag{B.3}
$$

The desired result (3.19) can be derived by using the identities $\gamma\left(\frac{1}{2},x\right)=\sqrt{\pi}\left(1-2\mathcal{Q}(\sqrt{2x})\right)$ and $\Gamma(a,x)+\gamma(a,x)=\Gamma(x)$ [116].

## B.2 Proof of average number of selected relays

The average number of selected relays ($L_c$) by the proposed OT-MRS scheme can be derived as follows:

$$
\bar{L}_c = \sum_{l=1}^{L} l\ \Pr(L_c = l),
\tag{B.4}
$$

where $\Pr(L_c = l)$ denotes the probability that the selected number of relays equals to $l$. In order to derive $\bar{L}_c$ in closed-form, $\Pr(L_c = l)$ is first derived by using the definition of $\gamma_{\text{out}}$ given in (3.6) as follows:

$$
\Pr(L_c{=}l) = \begin{cases}
\Pr\left(\gamma_{S,D} + \gamma_{R_1} \geq \gamma_{th}\right), & l = 1 \\
\Pr\left(\left[\gamma_{S,D}+\sum_{i=1}^{l}\gamma_{R_i} \geq \gamma_{th}\right]\cap\left[\gamma_{S,D}+\sum_{i=1}^{l-1}\gamma_{R_i} < \gamma_{th}\right]\right), & l\in\{2,\cdots,L-1\} \\
\Pr\left(\gamma_{S,D} + \sum_{i=1}^{L-1}\gamma_{R_i} < \gamma_{th}\right), & l=L.
\end{cases}
\tag{B.5}
$$

After some mathematical manipulations, (B.5) can be expressed in a more tractable form as

$$
\Pr(L_c = l) = \begin{cases}
1 - F_{\Gamma_1}(\gamma_{th}), & l = 1 \\
\int_0^{\gamma_{th}}\int_{\gamma_{th}-\Gamma_{l-1}}^{\infty} f_{\Gamma_{l-1},\gamma_{R_l}}(\Gamma_{l-1},\gamma_{R_l})\,\mathrm{d}\gamma_{R_l}\mathrm{d}\Gamma_{l-1}, & l\in\{2,\cdots,L-1\} \\
F_{\Gamma_{L-1}}(\gamma_{th}), & l = L.
\end{cases}
\tag{B.6}
$$

By substituting (3.10), (3.11) into (B.5) and after applying some mathematical manipulations, a lower bound for $\Pr(L_c = l)$ can be derived as

$$
\Pr(L_c = l) \geq \begin{cases}
\beta_{sd,1}\bar{\gamma}_{S,D}\exp\left(-\frac{\gamma_{th}}{\bar{\gamma}_{S,D}}\right) + \beta_{1,1}\bar{\gamma}\exp\left(-\frac{\gamma_{th}}{\bar{\gamma}}\right), & l = 1 \\
\beta_{sd,l-1}\left(\frac{\bar{\gamma}\bar{\gamma}_{S,D}}{\bar{\gamma}-\bar{\gamma}_{S,D}}\right)\exp\left(-\frac{\gamma_{th}}{\bar{\gamma}}\right)\left(1 - \exp\left(-\frac{\gamma_{th}(\bar{\gamma}-\bar{\gamma}_{S,D})}{\bar{\gamma}\bar{\gamma}_{S,D}}\right)\right) \\
\quad + \sum_{i=1}^{l-1}\frac{\beta_{i,l-1}(\gamma_{th})^i}{i!}\exp\left(-\frac{\gamma th}{\bar{\gamma}}\right), & l\in\{2,\cdots,L-1\} \\
\beta_{sd,L-1}\bar{\gamma}_{S,D}\left(1 - \exp\left(-\frac{\gamma_{th}}{\bar{\gamma}_{S,D}}\right)\right) + \sum_{i=1}^{L-1}\frac{\beta_{i,L-1}(\bar{\gamma})^i}{(i-1)!}\gamma\left(i,\frac{\gamma_{th}}{\bar{\gamma}}\right), & l = L.
\end{cases}
\tag{B.7}
$$

161

Next, by substituting (B.7) into (B.4), a lower bound on the average number of selected relays $\bar{L}_c$ can be then derived as given in (3.21).

$$\sim$$

# Appendix C

# Proofs for Chapter 4

## C.1 Proof of the CDF of SNR lower bound of optimal TAS for OWRNs

In the optimal TAS, the antenna indexes $I$ and $K$ at $S$ and $R$, respectively, are selected based the criterion given in (4.6). An upper bound for the CDF of the end-to-end SNR can be derived as follows:

$$
\begin{aligned}
F_{\gamma_{e2e}}(x) &= \Pr\left(\max_{i\in\{1,\cdots,N_S\}}\left(\gamma_{e2e}^{(i,K)}\right) \leq x\right) = P\left(\max_{i\in\{1,\cdots,N_S\}}\left(\gamma_{S,D}^{(i)} + \gamma_{SRD}^{(i,K)}\right) \leq x\right) \\
&\leq \Pr\left(\max_{i\in\{1,\cdots,N_S\}}\left(\gamma_{S,D}^{(i)}, \gamma_{SRD}^{(i,K)}\right) \leq x\right),
\end{aligned}
\tag{C.1}
$$

where $\gamma_{SRD}^{(i,K)} = \frac{\gamma_{S,R}^{(i)}\gamma_{R,D}^{(K)}}{\gamma_{S,R}^{(i)}+\gamma_{R,D}^{(K)}}$.

The probability measure denoted by $\Pr\left(\max_{i\in\{1,\cdots,N_S\}}\left(\gamma_{S,D}^{(i)}, \gamma_{SRD}^{(i,K)}\right) \leq x\right)$ can be lower bounded by $F_{\gamma_{SD}^{(I)}}(x)\, F_{\gamma_{SRD}^{(I,K)}}(x)$, where the corresponding CDFs are defined as $F_{\gamma_{S,D}^{(I)}}(x) = \Pr\left(\max_{i\in\{1,\cdots,N_S\}}\left(\gamma_{S,D}^{(i)}\right) \leq x\right)$ and $F_{\gamma_{SRD}^{(I,K)}}(x) = \Pr\left(\max_{i\in\{1,\cdots,N_S\}}\left(\gamma_{SRD}^{(i,K)}\right) \leq x\right)$. The CDF of $\gamma_{S,D}^{(I)}$ is given by

$$
\begin{aligned}
F_{\gamma_{SD}^{(I)}}(x) &= \left[1 - \exp\left(-\frac{x}{\beta_0}\right) \sum_{t=0}^{M_0-1} \frac{1}{t!}\left(\frac{x}{\beta_0}\right)^t\right]^{N_S} \\
&= \sum_{u=0}^{N_S} \sum_{v=0}^{u(M_0-1)} \binom{N_S}{u} \frac{(-1)^u \phi_{v,u,M_0}}{(\beta_0)^v} x^v \exp\left(-\frac{ux}{\beta_0}\right),
\end{aligned}
\tag{C.2}
$$

where $M_0 = m_o N_d$ and $\phi_{n,m,M_0}$ is given by (4.14). The $F_{\gamma_{SRD}^{(I,K)}}(x)$ is written as

$$
\begin{aligned}
F_{\gamma_{SRD}^{(I,K)}}(x) &= \int_0^\infty \Pr\left(\max_{1\leq i\leq N_s}\left(\frac{\gamma_{S,R}^{(i)}\lambda}{\gamma_{S,R}^{(i)}+\lambda}\right) \leq x\right) f_{\gamma_{R,D}^{(K)}}(\lambda)\, \mathrm{d}\lambda \\
&= F_{\gamma_{R,D}^{(K)}}(x) + \int_0^\infty F_{\gamma_{S,R}^{(I)}}\left(\frac{x(x+\lambda)}{\lambda}\right) f_{\gamma_{R,D}^{(K)}}(\lambda)\, \mathrm{d}\lambda,
\end{aligned}
\tag{C.3}
$$

where the CDF of $\gamma_{R,D}^{(K)}$ is the derived as

$$
\begin{aligned}
F_{\gamma_{R,D}^{(K)}}(x) &= \left[1 - \exp\left(-\frac{x}{\beta_2}\right)\sum_{t=0}^{M_2-1}\frac{1}{t!}\left(\frac{x}{\beta_2}\right)^t\right]^{N_R} \\
&= \sum_{p=0}^{N_R}\sum_{q=0}^{p(M_2-1)}\binom{N_R}{p}\frac{(-1)^p\phi_{q,p,M_2}}{(\beta_2)^q}x^q\exp\left(-\frac{px}{\beta_2}\right),
\end{aligned}
\tag{C.4}
$$

and the PDF of $\gamma_{R,D}^{(K)}$ can be obtained by differentiation (C.4) as

$$
\begin{aligned}
f_{\gamma_{R,D}^{(K)}}(x) &= \frac{\mathrm{d}}{\mathrm{d}x}\left\{F_{\gamma_{R,D}^{(K)}}(x)\right\} = \sum_{p=0}^{N_R-1}\sum_{q=0}^{p(M_2-1)}\frac{(-1)^pN_R\binom{N_R-1}{p}\phi_{q,p,M_2}}{\Gamma(M_2)(\beta_2)^{M_2+q}} \\
&\quad\times\ x^{M_2+q-1}\exp\left(-\frac{(p+1)x}{\beta_2}\right).
\end{aligned}
\tag{C.5}
$$

In (C.4) and (C.5), $M_2 = m_2 N_D$. The CDF of $\gamma_{S,R}^{(I)}$ is next derived as

$$
\begin{aligned}
F_{\gamma_{S,R}^{(I)}}(x) &= \left[1 - \exp\left(-\frac{x}{\beta_1}\right)\sum_{t=0}^{M_1-1}\frac{1}{t!}\left(\frac{x}{\beta_1}\right)^t\right]^{N_S} \\
&= \sum_{a=0}^{N_S}\sum_{b=0}^{a(M_1-1)}\binom{N_S}{a}\frac{(-1)^a\phi_{b,a,M_1}}{(\beta_1)^b}x^b\exp\left(-\frac{ax}{\beta_1}\right),
\end{aligned}
\tag{C.6}
$$

where $M_1 = m_2 N_d$. Next, by substituting (C.4), (C.5), and (C.6) into (C.3), a single integral expression, involving $\int_0^\infty \lambda^{M_2+q-b-1}(x+\lambda)^b\exp\left(-\frac{(p+1)\lambda}{\beta_2} - \frac{ax^2}{\beta_1\lambda}\right)\mathrm{d}\lambda$, for $\gamma_{SRD}^{(I,K)}$ can be obtained. This integral can be evaluated closed-form by first using the binomial expansion of $(x+\lambda)^b$ and then using [1, Eqn. (3.471.9)]. Finally, the desired result (4.13a) can be obtained in closed-form by substituting $\gamma_{SRD}^{(I,K)}$, and (C.2) into (C.1).

## C.2 Proof of the CDF of the SNR of optimal TAS for OWRNs without direct channel

The end-to-end SNR of the optimal TAS for MIMO OWRNs without the direct channel is given by

$$
\gamma_{e2e}^{(I,K)} = \gamma_{SRD}^{(I,K)} = \frac{\gamma_{S,R}^{(I)}\gamma_{R,D}^{(K)}}{\gamma_{S,R}^{(I)} + \gamma_{R,D}^{(K)}},
\tag{C.7}
$$

where $I$ and $K$ are the optimal transmit antenna indices at $S$ and $R$, respectively. The CDF of $\gamma_{SRD}^{(I,K)}$ can be then derived as follows:

$$
\begin{aligned}
F_{\gamma_{SRD}^{(I,K)}}(x) &= \Pr\left(\gamma_{S,R}^{(I)}\gamma_{R,D}^{(K)}/(\gamma_{S,R}^{(I)} + \gamma_{R,D}^{(K)}) \le x\right) \\
&= F_{\gamma_{S,R}^{(I)}}(x) + \int_x^\infty \Pr\left(\gamma_{R,D}^{(K)} \le (xy/(y-x))\right)f_{\gamma_{S,R}^{(I)}}(y)\,\mathrm{d}y.
\end{aligned}
\tag{C.8}
$$

By using the variable change $z = y - x$, $F_{\gamma_{\text{e2e}}}(x)$ is written in a compact form as

$$F_{\gamma_{SRD}^{(I,K)}}(x) = 1 - \int_0^\infty \bar{F}_{\gamma_{R,D}^{(K)}}((x+y)x/y) \, f_{\gamma_{S,R}^{(I)}}(x+y) \, \mathrm{d}y, \tag{C.9}$$

where $f_{\gamma_{S,R}^{(I)}}(x)$ is the PDF of $\gamma_{S,R}^{(I)}$ and $\bar{F}_{\gamma_{R,D}^{(K)}}(x)$ is the CCDF of $\gamma_{R,D}^{(K)}$. By employing (C.4), $\bar{F}_{\gamma_{R,D}^{(K)}}(x)$ can be obtained as follows:

$$\bar{F}_{\gamma_{R,D}^{(K)}}(x) = 1 - \sum_{p=0}^{N_R} \sum_{q=0}^{p(M_2-1)} \binom{N_R}{p} \frac{(-1)^p \phi_{q,p,M_2}}{(\beta_2)^q} x^q \exp\left(-\frac{px}{\beta_2}\right), \tag{C.10}$$

The $f_{\gamma_{S,R}^{(I)}}(x)$ is next derived by differentiating (C.6)

$$f_{\gamma_{S,R}^{(I)}}(x) = \sum_{a=0}^{N_S-1} \sum_{b=0}^{a(M_1-1)} \frac{(-1)^a N_S \binom{N_S-1}{a} \phi_{b,a,M_1}}{\Gamma(M_1)(\beta_1)^{M_1+b}} x^{M_1+b-1} \exp\left(-\frac{(a+1)x}{\beta_1}\right). \tag{C.11}$$

B first substituting (C.10) and (C.11), into (C.9), and then evaluating the residue integral by employing [1, Eqn. (3.471.9)], the desired result can be derived in closed-form as given in (4.15a).

## C.3   Proof of the asymptotic performance metrics for OWRNs

In this section, the proofs of the asymptotic outage probability and the average SER at high SNRs are sketched.

The end-to-end SNR of the optimal TAS for MIMO OWRNs is given by

$$\gamma_{\text{e2e}}^{(I,K)} = \gamma_{S,D}^{(I)} + \frac{\gamma_{S,R}^{(I)} \gamma_{R,D}^{(K)}}{\gamma_{S,R}^{(I)} + \gamma_{R,D}^{(K)}}, \tag{C.12}$$

where $I$ and $K$ are the optimal transmit antenna indices at $S$ and $R$, respectively. The first part and the second part of (C.12) represent the SNRs of the direct channel and relayed-channel, respectively. For the sake of simplicity, the relayed-channel SNR is denoted as

$$\gamma_{SRD}^{(I,K)} = \frac{\gamma_{S,R}^{(I)} \gamma_{R,D}^{(K)}}{\gamma_{S,R}^{(I)} + \gamma_{R,D}^{(K)}}. \tag{C.13}$$

Interestingly, $\gamma_{SRD}^{(I,K)}$ also accounts for the exact end-to-end SNR of the optimal TAS for OWRNs without having the direct channel.

Our first goal is to derive the first order expansion of the CDF of $\gamma_{SRD}^{(I,K)}$, and thereby, to derive the same for the CDF of $\gamma_{\text{e2e}}^{(I,K)}$. To this end, the first order expansion of $F_{\gamma_{S,R}^{(I)}}(x)$ is derived as

$$\lim_{x \to 0^+} F_{\gamma_{S,D}^{(I)}}(x) = \Pi_{SD}\left(\frac{x}{\bar{\gamma}}\right)^{m_0 N_D N_S} + o\left(x^{m_0 N_D N_S}\right), \tag{C.14}$$

where $k_0 = \bar{\gamma}_{S,D}/\bar{\gamma}$ and $\Pi_{SD} = \frac{(m_0/k_0)^{m_0 N_D N_S}}{(\,(m_0 N_D)!\,)^{N_S}}$. The achievable diversity order of the direct channel is therefore given by $G_{d,SD} = m_0 N_D N_S$.

By employing (C.8), the first order expansion of $\gamma_{SRD}^{(I,K)}$ can be derived as

$$\lim_{x\to 0^+} F_{\gamma_{SRD}^{(I,K)}}(x) = \lim_{x\to 0^+} F_{\gamma_{S,R}^{(I)}}(x) + \lim_{x\to 0^+} \int_x^\infty F_{\gamma_{R,D}^{(K)}}\left(\frac{xy}{y-x}\right) f_{\gamma_{S,R}^{(I)}}(y)\, \mathrm{d}y. \quad \text{(C.15)}$$

One immediately observes that if $\lim_{x\to 0^+}$, then $x/(y-x) \to 0^+$. By employing this fact, (C.15) is then simplified as

$$\lim_{x\to 0^+} F_{\gamma_{SRD}^{(I,K)}}(x) = \lim_{x\to 0^+} F_{\gamma_{S,R}^{(I)}}(x) + \lim_{x\to 0^+} \left[ F_{\gamma_{R,D}^{(K)}}(x)\left(1 - F_{\gamma_{S,R}^{(I)}}(x)\right) \right]. \quad \text{(C.16)}$$

The first order expansion of $F_{\gamma_{S,R}^{(I)}}(x)$ is next derived by using (C.4) as follows:

$$\lim_{x\to 0^+} F_{\gamma_{S,R}^{(I)}}(x) = \Pi_1 \left(\frac{x}{\bar{\gamma}}\right)^{m_1 N_S N_R} + o\left(x^{m_1 N_S N_R}\right), \quad \text{(C.17)}$$

where $\Pi_1 = \frac{(m_1/k_1)^{m_1 N_S N_R}}{(\,(m_1 N_R)!\,)^{N_S}}$. Similarly, the first order expansion of $F_{\gamma_{R,D}^{(K)}}(x)$ is then derived as

$$\lim_{x\to 0^+} F_{\gamma_{R,D}^{(K)}}(x) = \Pi_2 \left(\frac{x}{\bar{\gamma}}\right)^{m_2 N_R N_D} + o\left(x^{m_1 N_R N_D}\right), \quad \text{(C.18)}$$

where $\Pi_2 = \frac{(m_2/k_2)^{m_2 N_R N_D}}{(\,(m_2 N_D)!\,)^{N_R}}$. Besides, in (C.17) and (C.18), $k_1 = \bar{\gamma}_{S,R}/\bar{\gamma}$ and $k_2 = \bar{\gamma}_{R,D}/\bar{\gamma}$. By first substituting (C.17) and (C.18) into (C.16), and then taking the single-term polynomial with the lowest power of $x$, the first order expansion of $F_{\gamma_{SRD}^{(I,K)}}(x)$ can be derived as follows:

$$\lim_{x\to 0^+} F_{\gamma_{SRD}^{(I,K)}}(x) = \Pi_{SRD} \left(\frac{x}{\bar{\gamma}}\right)^{G_{d,SRD}} + o\left(x^{G_{d,SRD}}\right), \quad \text{(C.19)}$$

where $\Pi$ is defined as

$$\Pi_{SRD} = \begin{cases} \Pi_1, & m_1 N_S < m_2 N_D \\ \Pi_2, & m_1 N_S > m_2 N_D \\ (\Pi_1 + \Pi_2), & m_1 N_S = m_2 N_D = mN. \end{cases} \quad \text{(C.20)}$$

where $\Pi_1$ and $\Pi_2$ are defined in (C.17) and (C.18). Moreover, the diversity order $G_{d,SRD}$ is given by $G_{d,SRD} = N_R \min(m_1 N_S, m_2 N_D)$. The asymptotic outage probability of the optimal TAS for OWRNs without having the direct channel can be then obtained by evaluating (C.19) at the threshold SNR as given in (4.26).

The first order expansion of the end-to-end SNR of the optimal TAS for OWRNs with the direct channel is next derived as follows: To this end, the first order expansions of the MGFs of $\gamma_{S,D}^{(I)}$ is derived by substituting (C.14) into (4.16) as follows:

$$\mathcal{M}_{\gamma_{SD}^{(I)}}(s) = \frac{\Pi_{SD}\Gamma(G_{d,SD}+1)}{(\bar{\gamma}s)^{G_{d,SD}}} + o\left(s^{-G_{d,SD}}\right). \quad \text{(C.21)}$$

Similarly, the first order expansion of the MGF of $\gamma_{SRD}^{(I,K)}$ is derived as

$$\mathcal{M}_{\gamma_{SRD}^{(I,K)}}(s) = \frac{\Pi_{SRD}\Gamma(G_{d,SRD}+1)}{(\bar{\gamma}s)^{G_{d,SRD}}} + o\left(s^{-G_{d,SRD}}\right). \tag{C.22}$$

The first order expansion of the CDF of $\gamma_{e2e}^{(I,K)}$ given in (C.12) can be then derived by using $\mathcal{L}^{-1}\left(\frac{1}{s}\mathcal{M}_{\gamma_{SD}^{(I)}}(s)\mathcal{M}_{\gamma_{SRD}^{(I,K)}}(s)\right)$, where $\mathcal{L}^{-1}(\cdot)$ denotes the inverse Laplace transform, as follows:

$$\begin{aligned}
\lim_{x\to 0^+} F_{\gamma_{e2e}^{(I,K)}}(x) &= \frac{\Pi_{SD}\Pi_{SRD}\Gamma(G_{d,SD}+1)\Gamma(G_{d,SRD})}{\Gamma(G_{d,SD}+G_{d,SRD}+1)}\left(\frac{x}{\bar{\gamma}}\right)^{G_{d,SD}+G_{d,SRD}} \\
&\quad + o\left(x^{G_{d,SD}+G_{d,SRD}}\right).
\end{aligned} \tag{C.23}$$

By first substituting the corresponding values of $\Pi_{SD}$, $\Pi_{SRD}$, $G_{d,SD}$, and $G_{d,SRD}$ defined in (C.14) and (C.15) into (C.23), and then evaluating it at the threshold SNR, the desired asymptotic outage probability at high SNRs can be obtained as in (4.25a).

The asymptotic average SER at high SNRs can the be derived by substituting the first order expansion of the CDF of the end-to-end SNR into the integral representation of the average SER $\bar{P}_e^\infty = \frac{\alpha}{2}\sqrt{\frac{\varphi}{2\pi}}\int_0^\infty x^{-\frac{1}{2}}e^{-\frac{\varphi x}{2}}F_{\gamma_{e2e}^\infty}(x)\,\mathrm{d}x$.

## C.4 Proof of the CDF of effective SNR of optimal Tx/Rx antenna selection for TWRNs

The proof of the CDF of the effective end-to-end SNR, which is defined as the end-to-end SNR of the worst source, is sketched as follows:

$$\begin{aligned}
F_Z(z) &= \Pr\left[Z = \max_{\substack{j\in\{1,\cdots,N_1\},l\in\{1,\cdots,N_2\}\\m\in\{1,\cdots,N_R\}}}\left(\min\left(\gamma_{S_1}^{(j,l,m)},\gamma_{S_2}^{(j,l,m)}\right)\right) \le z\right] \\
&= \Pr\left[\max_{m\in\{1,\cdots,N_R\}}\left(\min\left(\gamma_{S_1}^{(J,L,m)},\gamma_{S_2}^{(J,L,m)}\right)\right) \le z\right], \tag{C.24}
\end{aligned}$$

where $\gamma_{S_1}^{(j,l,m)}$ and $\gamma_{S_2}^{(j,l,m)}$ are defined in (4.5). Besides, $\gamma_{S_1}^{(J,L,m)}$ and $\gamma_{S_2}^{(J,L,m)}$ are the end-to-end SNR at $S_1$ and $S_2$, respectively, and are given by

$$\gamma_{S_1}^{(J,L,m)} = \max_{j\in\{1,\cdots,N_1\},l\in\{1,\cdots,N_2\}}\left(\gamma_{S_1}^{(j,l,m)}\right) = \frac{X_m Y_m}{\alpha X_m + \beta Y_m + \eta} \tag{C.25a}$$

$$\gamma_{S_2}^{(J,L,m)} = \max_{j\in\{1,\cdots,N_1\},l\in\{1,\cdots,N_2\}}\left(\gamma_{S_2}^{(j,l,m)}\right) = \frac{X_m Y_m}{\beta X_m + \alpha Y_m + \eta}, \tag{C.25b}$$

where the random variables $X_m$ and $Y_m$ are defined as

$$X_m = \left|h_{S_1,R}^{(m,J)}\right|^2 = \max_{j\in\{1,\cdots,N_1\}}\left(\left|h_{S_1,R}^{(m,j)}\right|^2\right) \tag{C.25c}$$

$$Y_m = \left|h_{S_2,R}^{(m,L)}\right|^2 = \max_{l\in\{1,\cdots,N_2\}}\left(\left|h_{S_2,R}^{(m,l)}\right|^2\right) \tag{C.25d}$$

In (C.25c) and (C.25d), $\alpha = (\bar{\gamma}_S + \bar{\gamma}_R)/\bar{\gamma}_S\bar{\gamma}_R$, $\beta = 1/\bar{\gamma}_R$ and $\eta = 1/\bar{\gamma}_S\bar{\gamma}_R$, where $\bar{\gamma}_S = \mathcal{P}_S/\sigma_S^2$ and $\bar{\gamma}_R = \mathcal{P}_R/\sigma_R^2$ are the average transmit SNRs at the source nodes and the relay[1].

We then define $Z_m = \min\left(\gamma_{S_1}^{(J,L,m)}, \gamma_{S_2}^{(J,L,m)}\right)$ and simplify it as follows[2]:

$$Z_m = \begin{cases} \gamma_{S_1}^{(J,L,m)}, & Y_m \leq X_m \\ \gamma_{S_2}^{(J,L,m)}, & Y_m > X_m. \end{cases} \tag{C.26}$$

The CDF of $Z_m$ can be next derived as

$$F_{Z_m}(z) = \Pr[Z_m \leq z] = P_1(z) + P_2(z), \tag{C.27a}$$

where $P_1(z)$ and $P_2(z)$ are given by

$$P_1(z) = \Pr\left[\left\{\gamma_{S_1}^{(J,L,m)} \leq z\right\} \cap \{Y_m \leq X_m\}\right] \tag{C.27b}$$

$$P_2(z) = \Pr\left[\left\{\gamma_{S_2}^{(J,L,m)} \leq z\right\} \cap \{X_m < Y_m\}\right]. \tag{C.27c}$$

After some manipulations, the probability $P_1(z)$ can be expressed in a more mathematically tractable form as follows:

$$\begin{aligned} P_1(z) &= \Pr[\{X_m \leq \beta z\} \cap \{Y_m \leq X_m\}] \\ &+ \Pr\left[\left\{Y_m \leq \frac{z(\alpha X_m + \eta)}{X_m - \beta z}\right\} \cap \{Y_m \leq X_m\}\right], \end{aligned} \tag{C.28a}$$

where the first probability measure of (C.28a) is given by

$$\mathbb{I}_1(z) = \Pr[\{X_m \leq \beta z\} \cap \{Y_m \leq X_m\}] = \int_{x=0}^{\beta z} \int_{y=0}^{x} f_{X_m}(x) \, f_{Y_m}(y) \, \mathrm{d}y\mathrm{d}x. \tag{C.28b}$$

Similarly, the second probability measure of (C.28a) is expanded as

$$\begin{aligned} \mathbb{I}_1'(z) &= \Pr\left[\left\{Y_m \leq \frac{z(\alpha X_m + \eta)}{X_m - \beta z}\right\} \cap \{Y_m \leq X_m\}\right] \\ &= \int_{t=0}^{\infty} \Pr\left[Y_m \leq \min\left(\frac{z(\alpha(t+\beta z) + \eta)}{t}, t+\beta z\right)\right] f_{X_m}(t+\beta z) \, \mathrm{d}t, \end{aligned} \tag{C.28c}$$

where the term $\min(\cdot, \cdot)$ in $\mathcal{I}_1'(z)$ can be simplified as

$$\min\left(\frac{z(\alpha(t+\beta z) + \eta)}{t}, t+\beta z\right) = \begin{cases} t + \beta z, & 0 \leq t \leq \phi(z) \\ \frac{z}{t}\left[\alpha(t+\beta z) + \eta\right], & t \geq \phi(z), \end{cases} \tag{C.28d}$$

---

[1]Without loss of generality, the transmit powers and the additive white Gaussian noise (AWGN) noise variances at the both $S_1$ and $S_2$ are assumed to be identical; i.e., $\mathcal{P}_{S_1} = \mathcal{P}_{S_2} = \mathcal{P}_S$ and $\sigma_{S_1}^2 = \sigma_{S_2}^2 = \sigma_S^2$.

[2]It is important to note that the random variables $\gamma_{S_1}^{(J,L,m)}$ and $\gamma_{S_2}^{(J,L,m)}$ are not statistically independent.

where $\phi(z)$ is derived by first solving the quadratic equation

$$t^2 + (\beta - \alpha)zt - z(\alpha\beta z + \eta) = 0 \tag{C.28e}$$

and then taking the viable root as

$$\phi(z) = 0.5(\alpha - \beta)z + 0.5\sqrt{(\alpha - \beta)^2 z^2 + 4z(\alpha\beta z + \eta)}. \tag{C.28f}$$

Consequently, $\mathcal{I}'_1(z)$ can be simplified as follows:

$$\mathcal{I}'_1(z) = \mathbb{I}_2(z) + \mathbb{I}_3(z), \tag{C.29a}$$

where the integrals $\mathbb{I}_2(z)$ and $\mathbb{I}_3(z)$ are given by

$$\mathbb{I}_2(z) = \int_{t=0}^{\phi(z)} F_{Y_m}(t + \beta z) f_{X_m}(t + \beta z)\,\mathrm{d}t \tag{C.29b}$$

$$\mathbb{I}_3(z) = \int_{t=\phi(z)}^{\infty} F_{Y_m}\left(\frac{z(\alpha(t + \beta z) + \eta)}{t}\right) f_{X_m}(t + \beta z)\,\mathrm{d}t. \tag{C.29c}$$

Next, $P_1(z)$ in (C.27b) is derived as follows:

$$P_1(z) = \mathcal{I}_1(z) + \mathcal{I}_2(z) + \mathcal{I}_3(z). \tag{C.30a}$$

In (C.28a), $F_{X_m}(x)$ and $F_{Y_m}(y)$ are the CDFs of $X_m$ and $Y_m$ (C.25a), respectively, and are given by [138]

$$F_{X_m}(x) = \left[F_{|h^{(m,j)}|^2}(x)\right]^{N_1} = \sum_{p=0}^{N_1} \binom{N_1}{p}(-1)^p \exp\left(\frac{px}{\zeta_1}\right) \tag{C.30b}$$

$$F_{Y_m}(y) = \left[F_{|h^{(m,l)}|^2}(y)\right]^{N_2} = \sum_{q=0}^{N_2} \binom{N_2}{q}(-1)^q \exp\left(\frac{-qy}{\zeta_2}\right). \tag{C.30c}$$

Moreover, $f_{X_m}(x)$ and $f_{Y_m}(y)$ are the PDFs of $X_m$ and $Y_m$, respectively, and are given by

$$f_{X_m}(x) = \sum_{p=0}^{N_1-1} \frac{N_1\binom{N_1-1}{p}(-1)^p}{\zeta_1} \exp\left(\frac{-(p+1)x}{\zeta_1}\right) \tag{C.30d}$$

$$f_{Y_m}(y) = \sum_{q=0}^{N_2-1} \frac{N_2\binom{N_2-1}{q}(-1)^q}{\zeta_2} \exp\left(\frac{-(q+1)y}{\zeta_2}\right). \tag{C.30e}$$

By substituting (C.30b) and (C.30d) into (C.28a), $\mathcal{I}_1(z)$ and $\mathcal{I}_2(z)$ can be evaluated exactly in closed-form as given in the first and second terms of (4.21). Specifically, $\mathcal{I}_3(z)$ is too mathematically intractable to be exactly solved, and thus, two efficient evaluation techniques are provided as follows:

### C.4.1 Derivation of $\mathcal{I}_3(z)$ by using GLQ [116, Eq. (25. 4. 45)]:

The integral $\mathcal{I}_3$ is given by

$$
\begin{aligned}
\mathcal{I}_3(z) &= \sum_{p=0}^{N_1-1} \sum_{q=0}^{N_2} \frac{N_1 \binom{N_1-1}{p} \binom{N_2}{q} (-1)^{p+q}}{\zeta_1} \exp\left(-z\left(\frac{(p+1)\beta}{\zeta_1} + \frac{q\alpha}{\zeta_2}\right)\right) \\
&\times \int_{\phi(z)}^{\infty} \exp\left(-\left(\frac{(p+1)t}{\zeta_1} + \frac{pz(\alpha\beta z + \eta)}{\zeta_2 t}\right)\right) \mathrm{d}t,
\end{aligned} \tag{C.31a}
$$

where $\alpha$, $\beta$, $\eta$, and $\phi(z)$ are defined in (4.21). Now, (C.31a) is re-arranged to obtain the Gauss-Laguerre quadrature (GLQ) integral form as

$$
\begin{aligned}
\mathbb{I}_3(z) &= \sum_{p=0}^{N_1-1} \sum_{q=0}^{N_2} \frac{N_1 \binom{N_1-1}{p} \binom{N_2}{q} (-1)^{p+q}}{p+1} \\
&\times \exp\left(-\left[z\left(\frac{(p+1)\beta}{\zeta_1} + \frac{q\alpha}{\zeta_2}\right) + \frac{(p+1)\phi(z)}{\zeta_1}\right]\right) \int_0^{\infty} \Psi(x) \mathrm{e}^{-x} \mathrm{d}x, \tag{C.31b}
\end{aligned}
$$

where $\Psi(x) = \exp\left(-\frac{qz(p+1)(\alpha\beta z+\eta)}{\zeta_2[\zeta_1 x + (p+1)\phi(z)]}\right)$. The integral in (C.31b) can be readily evaluated by using the GLQ rule as follows:

$$
\int_0^{\infty} \Psi(x) \mathrm{e}^{-x} \mathrm{d}x = \sum_{t=1}^{T_g} w_t \Psi(x_t) + \mathcal{R}_{T_g}, \tag{C.32}
$$

where $x_t$ and $w_t$ for $t \in \{1, \cdots, T_g\}$ are the abscissas and weights of the GLQ, respectively [116, Eqn. (25.4.45)]. Specifically, $x_t$ is the $t$th root of the Laguerre polynomial $\mathcal{L}_n(x)$ [116, Chap. 22], and the corresponding $t$th weight is given by $w_t = \frac{(t!)^2 x_t}{(t+1)^2 [\mathcal{L}_{t+1}(x_t)]^2}$. Both $x_t$ and $w_t$ can be efficiently computed by using the classical algorithm proposed in [117]. Furthermore, $T_g$ is the number of terms used in the GLQ summation, and $\mathcal{R}_{T_g}$ is the remainder term, which readily diminishes as $T_g$ approaches as small as 10 [117].

### C.4.2 Derivation of $\mathbb{I}_3(z)$y using the Taylor series expansion

The integral in (C.31a) can be written by applying the Taylor series to $\mathrm{e}^{-\frac{pz(\alpha\beta z+\eta)}{\zeta_2 t}}$ as follows:

$$
\mathcal{J}(z) = \sum_{i=0}^{\infty} \frac{(-1)^i}{i!} [acz(\alpha\beta z + \eta)]^i \exp\left(a\phi(z)\right) \int_{a\phi(z)}^{\infty} \frac{\exp\left(-t\right)}{t^i} \mathrm{d}t, \tag{C.33a}
$$

where $\alpha$, $\beta$ and $\phi(z)$ are defined in (4.21), and $a = \frac{p+1}{\zeta_1}$, $c = \frac{q}{\zeta_2}$, respectively. The integral in (C.33a) can be evaluated by using [1, Eqn. (3.381.6)] as

$$
\mathcal{J}(z) = \sum_{i=0}^{\infty} \frac{(-1)^i [acz(\alpha\beta z\eta)]^i \exp\left(\frac{a\phi(z)}{2}\right) \mathcal{W}_{\frac{-i}{2}, \frac{1-i}{2}}(a\phi(z))}{(i)! [a\phi(z)]^{\frac{i}{2}}}, \tag{C.33b}
$$

where $\mathcal{W}_{\nu,\mu}(z)$ is the Whittaker function [1, Eqn. (9.220.4)]. Eqn. (C.33b) can be further simplified by using [139] as

$$\mathcal{J}(z) = \sum_{i=0}^{\infty} \frac{(-1)^i}{i!} [acz(\alpha\beta z + \eta)]^i \exp\left(a\phi(z)\right) \Gamma\left(1 - i, a\phi(z)\right), \tag{C.33c}$$

where $\Gamma(\mu, z)$ is the complementary incomplete gamma function [116, Eqn. (8.350.2)].

Next, we test the convergence of the infinite series expansion in (C.33c) as follows: To this end, we denote the summand of (C.33c) by $\mathcal{A}_i(z)$.

$$\lim_{i\to\infty} \frac{\mathcal{A}_{i+1}}{\mathcal{A}_i} = \lim_{i\to\infty} \frac{-[acz(\alpha\beta z + \eta)]}{i+1} \frac{\Gamma(-i, a\phi(z))}{\Gamma(-i+1, a\phi(z))} \to 0. \tag{C.34}$$

Eqn. (C.34) follows from the fact that $\Gamma(-i, z)$ is monotonically decreasing with $i \geq 0$ and for a given $z$, and thus the ratio $\frac{\Gamma(-i,a\phi(z))}{\Gamma(-i+1,a\phi(z))}$ is bounded as $i \to \infty$. Since $\lim_{i\to\infty} \frac{\mathcal{A}_{i+1}}{\mathcal{A}_i} < 1$, by using the Ratio test, it can be shown that the infinite series in (C.33c) is convergent.

Now, by following similar steps to those of $P_1$, the second part of (C.27b) i.e., $P_2$ can be evaluated readily. Then the CDF of $Z_m$ can be derived as $F_{Z_m}(z) = P_1 + P_2$.

By identifying that the $Z_m$ for $m \in \{1, \cdots, N_R\}$ are statistically independent and identically distributed random variables, the CDF of $Z$ in (C.24) can be derived readily as $F_Z(z) = (F_{Z_m}(z))^{N_R}$ (4.20).

## C.5 Proof of the asymptotic performance metrics for TWRNs

In this section, the proofs of the asymptotic outage probability of the optimal antenna selection for TWRNs is sketched. In this context, the first order expansion of the CDFs of $X_m$ and $Y_m$ in (C.30b) can be derived as[3] [61]

$$F_{X_m}^{\infty}(x) = \frac{x^{N_1}}{\zeta_1^{N_1}} + o\left(x^{N_1}\right) \quad \text{and} \quad F_{Y_m}^{\infty}(y) = \frac{y^{N_2}}{\zeta_2^{N_2}} + o\left(y^{N_2}\right). \tag{C.35}$$

Similarly, the first order expansions of the PDFs of $X_m$ and $Y_m$ are given by [61]

$$f_{X_m}^{\infty}(x) = \frac{N_1 x^{N_1-1}}{\zeta_1^{N_1}} + o\left(x^{N_1-1}\right) \quad \text{and} \quad f_{Y_m}^{\infty}(y) = \frac{N_2 y^{N_2-1}}{\zeta_2^{N_2}} + o\left(y^{N_2-1}\right). \tag{C.36}$$

We first consider $P_1(z)$ in (C.28a). By substituting (C.36) and (C.35) into (C.28b) and (C.29b), the first order expansion of $\mathbb{I}_1(z)$ and $\mathbb{I}_2(z)$ can be derived as follows:

$$\mathbb{I}_1^{\infty}(z) = \frac{N_1(\beta z)^{N_1+N_2}}{(N_1+N_2)\zeta_1^{N_1}\zeta_2^{N_2}} + o\left(z^{N_1+N_2+1}\right), \tag{C.37a}$$

$$\mathbb{I}_2^{\infty}(z) = \frac{N_1(\alpha z)^{N_1+N_2}}{(N_1+N_2)\zeta_1^{N_1}\zeta_2^{N_2}} + o\left(z^{N_1+N_2+1}\right). \tag{C.37b}$$

---

[3]The first order expansion of $F_X(x)$, i.e., $\lim_{x\to 0^+} F_X(x)$, is also denoted by $F_X^{\infty}(x)$

The first order expansion of $\mathbb{I}_3(z)$ can be next derived follows: To this end, the Integral $\mathbb{I}_3(z)$ in (C.29c) can be re-written by applying a change of variable; $t + \beta z \to t$ as

$$\mathbb{I}_3(z) = \int_{t=\phi(z)+\beta z}^{\infty} \Pr\left[Y_m \le \frac{z(\alpha t + \eta)}{t - \beta z}\right] f_{X_m}(t)\, \mathrm{d}t. \tag{C.38}$$

We next consider the first order expansion of $\mathbb{I}_3(z)$ in (C.38). One observes that if $\lim_{z\to 0^+}$, then $\frac{z(\alpha t + \eta)}{t-\beta z} \to 0^+$. Thus, $\mathbb{I}_3(z)$ in (C.38) can be approximated whenever $z \to 0^+$ as follows:

$$\mathbb{I}_3^\infty(z) = F_{Y_m}^\infty(\alpha z)\left(\lim_{z\to 0^+}\int_{t=\phi(z)+\beta z}^{\infty} f_{X_m}(t)\, \mathrm{d}t\right) = F_{Y_m}^\infty(\alpha z)\left[1 - F_{X_m}^\infty(\phi(z)+\beta z)\right]. \tag{C.39}$$

By first substituting (C.35) into (C.39) and then by selecting the lowest powers of $z$, the first order expansion of $\mathbb{I}_3(z)$ can be derived as

$$\mathbb{I}_3^\infty(z) = \frac{(\alpha z)^{N_2}}{\zeta_2^{N_2}} + o\left(z^{N_2}\right). \tag{C.40}$$

The first order expansion of $P_1(z)$ is then given by $P_1^\infty(z) = \mathbb{I}_1^\infty(z) + \mathbb{I}_2^\infty(z) + \mathbb{I}_3^\infty(z)$. In particular, the behavior of $P_1(z)$ at the origin is completely governed by $\mathbb{I}_3^\infty(z)$ as it has the lowest powers of $z$, and thus $P_1^\infty(z)$ can be simplified as

$$P_1^\infty(z) = \frac{(\alpha z)^{N_2}}{\zeta_2^{N_2}} + o\left(z^{N_2}\right). \tag{C.41}$$

By following similar techniques to those of $P_1^\infty(z)$, the first order expansion pf $P_2(z)$ in (C.27a) can be next derived as

$$P_2^\infty(z) = \frac{(\alpha z)^{N_1}}{\zeta_1^{N_1}} + o\left(z^{N_1}\right). \tag{C.42}$$

The first order expansion of the CDF of $Z_m$ can be now derived by using (C.41) and (C.42) as follows:

$$F_{Z_m}^\infty(z) = P_1^\infty(z) + P_2^\infty(z) = \begin{cases} \frac{1}{(\zeta_1)^{N_1}}\left(\frac{\bar\gamma_S + \bar\gamma_R}{\bar\gamma_S\bar\gamma_R}\right)^{N_1} z^{N_1} + o\left(z^{N_1}\right), & N_1 < N_2 \\ \frac{1}{(\zeta_2)^{N_2}}\left(\frac{\bar\gamma_S + \bar\gamma_R}{\bar\gamma_S\bar\gamma_R}\right)^{N_2} z^{N_2} + o\left(z^{N_2}\right), & N_1 > N_2 \\ \left(\frac{1}{(\zeta_1)^N} + \frac{1}{(\zeta_2)^N}\right)\left(\frac{\bar\gamma_S + \bar\gamma_R}{\bar\gamma_S\bar\gamma_R}\right)^N z^N + o\left(z^N\right), & N_1 = N_2 = N. \end{cases} \tag{C.43}$$

The asymptotic outage probability at high SNRs can be then derived as in (4.30a) by first obtaining the first order expansion of $Z$ by substituting (C.43) into $F_Z^\infty(z) = (F_{Z_m}^\infty(z))^{N_R}$ and then evaluating it at $\gamma_{th}$.

## C.6 Proof of the CDF of the SNR of optimal TAS for OWRNs with feedback delays

We first suppose that $\tilde{\gamma}_{S,R}^{(i)}$ denotes the delayed version of $\gamma_{S,R}^{(i)}$ by time $\tau_1$. The average fading power is assumed to remain constant over the time delay $\tau_1$. By following the analysis techniques pertinent to the outdated CSI of [140], the joint PDF of $\tilde{\gamma}_{SR}^{(i)}$ and $\gamma_{SR}^{(i)}$ can be written as follows:

$$
\begin{aligned}
f_{\tilde{\gamma}_{S,R}^{(i)}, \gamma_{S,R}^{(i)}}(x,y) &= \frac{m_1^{m_1 N_R+1}(xy)^{\frac{m_1 N_R-1}{2}}}{(m_1 N_R-1)! \rho_1^{m_1 N_R-1}\left(1-\rho_1^2\right)(\bar{\gamma}_{S,R})^{m_1 N_R+1}} \\
&\times \exp\left(-\frac{m_1(x+y)}{\left(1-\rho_1^2\right)\bar{\gamma}_{S,R}}\right) \mathcal{I}_{m_1 N_R-1}\left(\frac{2m_1\rho_1\sqrt{xy}}{\left(1-\rho_1^2\right)\bar{\gamma}_{S,R}}\right),
\end{aligned}
\tag{C.44}
$$

where $\rho_1^2$ is the normalized correlation coefficient between $\tilde{\gamma}_{S,R}^{(i)}$ and $\gamma_{S,R}^{(i)}$. The feedback delay $\tau_1$ can be related to $\rho_1$ by following Clarke's scattering model, as $\rho_1 = \mathcal{J}_0(2\pi f_1 \tau_1)$, where $f_1$ is the Doppler fading frequency. In fact, (C.44) is the joint PDF of two correlated Gamma distributed random variables.

The CDF of the end-to-end SNR ($\tilde{\gamma}_{\text{e2e}}$) of the optimal TAS for OWRNs without having the direct channel can be derived as

$$
F_{\gamma_{\text{e2e}}}(x) = 1 - \int_0^\infty \left[1 - F_{\tilde{\gamma}_{S,R}^{(I)}}\left(\frac{(z+x)x}{z}\right)\right] f_{\tilde{\gamma}_{R,D}^{(K)}}(z+x)\,\mathrm{d}z.
\tag{C.45}
$$

One now needs to obtain the CDF of $\tilde{\gamma}_{S,R}^{(I)}$ and the PDF of $\tilde{\gamma}_{R,D}^{(K)}$. To this end, we start deriving the CDF of $\tilde{\gamma}_{S,R}^{(I)}$. In fact, $\tilde{\gamma}_{S,R}^{(I)}$ is the induced order statistic of the original order statistic $\gamma_{S,R}^{(I)}$ [138]. The PDF of $\tilde{\gamma}_{S,R}^{(I)}$ can be therefore derived as [138,140]

$$
f_{\tilde{\gamma}_{S,R}^{(I)}}(x) = \int_0^\infty f_{\tilde{\gamma}_{S,R}^{(I)}|\gamma_{S,R}^{(I)}}(x\,|\,y) f_{\gamma_{S,R}^{(I)}}(y)\,\mathrm{d}y,
\tag{C.46}
$$

where $f_{\tilde{\gamma}_{S,R}^{(I)}|\gamma_{S,R}^{(I)}}(x\,|\,y) = \dfrac{f_{\tilde{\gamma}_{S,R}^{(i)}, \gamma_{S,R}^{(i)}}(x,y)}{f_{\gamma_{S,R}^{(i)}}(y)}$ is the PDF of $\tilde{\gamma}_{S,R}^{(I)}$ conditioned on $\gamma_{S,R}^{(I)}$. The PDF of $\gamma_{S,R}^{(I)}$ is given by $f_{\gamma_{S,R}^{(I)}}(y) = N_R\left[F_{\gamma_{S,R}^{(i)}}(y)\right]^{N_R-1} f_{\gamma_{S,R}^{(i)}}(y)$. By first substituting (C.44) into (C.46) and then solving the resulting integral by using [141, Eqn. (4.16.20)], the PDF of $\tilde{\gamma}_{S,R}^{(I)}$ can be derived as follows:

$$
\begin{aligned}
f_{\tilde{\gamma}_{S,R}^{(I)}}(x) &= \sum_{a=0}^{N_S-1}\sum_{b=0}^{a(M_1-1)} \frac{N_S(-1)^a\binom{N_S-1}{a}\phi_{b,a,M_1}\Gamma(M_1+b)}{\Gamma^2(M_1)\rho_1^{M_1}\beta_1^{\frac{M_1}{2}}} \\
&\times \frac{(1-\rho_1^2)^\xi}{\left(1+a(1-\rho_1^2)\right)^\xi} x^{\frac{M_1-2}{2}}\exp\left(-\Xi x\right)\mathbf{M}_{-\xi,\vartheta}(\theta x),
\end{aligned}
\tag{C.47}
$$

where $\xi = \frac{M_1+2b}{2}$, $\vartheta = \frac{M_1-1}{2}$, $\Xi = \frac{2+2a(1-\rho_1^2)-\rho_1^2}{2\beta_1(1-\rho_1^2)(1+a(1-\rho_1^2))}$ and $\theta = \frac{\rho_1^2}{\beta_1(1-\rho_1^2)(1+a(1-\rho_1^2))}$. By first using the Confluent Hypergeometric function $_1\mathcal{F}_1(\cdot;\cdot;\cdot)$ representation of Whittaker-M function [1, Eqn. (9.220.2)] and then by expressing $_1\mathcal{F}_1(\cdot;\cdot;\cdot)$ as a finite series expansion [139], a mathematically tractable form for (C.47) can be next derived as follows:

$$
\begin{aligned}
f_{\tilde{\gamma}_{S,R}^{(I)}}(x) \;=\; & \sum_{a=0}^{N_S-1}\sum_{b=0}^{a(M_1-1)}\sum_{k=0}^{b} \frac{N_S(-1)^a\binom{N_S-1}{a}\binom{b}{k}\phi_{b,a,M_1}}{\Gamma(M_1)\Gamma(M_1+k)\beta_1^{M_1+k}} \\
& \times \frac{\Gamma(M_1+b)\rho_1^k(1-\rho_1^2)^{b-k}}{\left(1+a(1-\rho_1^2)\right)^{M_1+b+k}} x^{M_1+k-1}\exp\left(-\Phi x\right),
\end{aligned}
\tag{C.48}
$$

where $\Phi = \frac{(a+1)}{\beta_1(1+a(1-\rho_1^2))}$. The CDF of $\tilde{\gamma}_{S,R}^{(I)}$ can be then derived as

$$
\begin{aligned}
F_{\tilde{\gamma}_{S,R}^{(I)}}(x) \;=\; & 1-\sum_{a=0}^{N_S-1}\sum_{b=0}^{a(M_1-1)}\sum_{k=0}^{b}\sum_{l=0}^{M_1+k-1} \frac{N_S(-1)^a\binom{N_S-1}{a}\binom{b}{k}}{\Gamma(M_1)\beta_1^l(\,l!)} \\
& \times \frac{\phi_{b,a,M_1}\Gamma(M_1+b)\rho_1^{2k}(1-\rho_1^2)^{b-k}}{(a+1)^{M_1+k-l}\left(1+a(1-\rho_1^2)\right)^{b+l}} x^l\exp\left(-\Phi x\right).
\end{aligned}
\tag{C.49}
$$

By using similar techniques to those of used for the derivation of $f_{\tilde{\gamma}_{S,R}^{(I)}}(x)$, the PDF of $\tilde{\gamma}_{R,D}^{(K)}$, $f_{\tilde{\gamma}_{R,D}^{(K)}}(x)$, can be derived as well. The desired result can be then derived by employing (C.45) as given in (4.51a).

The proof of the first order expansion of $F_{\gamma_{e2e}}(x)$ is next sketched. To this end, the first order expansion of $F_{\tilde{\gamma}_{S,R}^{(I)}}(x)$ is derived as follows:

$$
\lim_{x\to 0^+} F_{\tilde{\gamma}_{S,R}^{(I)}}(x) = \Phi_1\left(\frac{x}{\bar{\gamma}}\right)^{m_1 N_R} + o\left(x^{m_1 N_R}\right),
\tag{C.50}
$$

where $\Phi_1$ is defined in (4.52b). Similarly, the first order expansion of $F_{\tilde{\gamma}_{R,D}^{(K)}}(x)$ is derived as

$$
\lim_{x\to 0^+} F_{\tilde{\gamma}_{R,D}^{(K)}}(x) = \Phi_2\left(\frac{x}{\bar{\gamma}}\right)^{m_2 N_D} + o\left(x^{m_2 N_D}\right),
\tag{C.51}
$$

where $\Phi_2$ is defined in (4.52c). By first substituting (C.50) and (C.51) into (C.16) and then selecting the single-term with the lowest power of $x$, the first order expansion of $F_{\gamma_{e2e}}(x)$ is derived as follows:

$$
\lim_{x\to 0^+} F_{\gamma_{e2e}}(x) = \Phi\left(\frac{x}{\bar{\gamma}}\right)^{G_d} + o\left(x^{G_d}\right),
\tag{C.52}
$$

where $\Phi$ and $G_d$ are defined in (4.55b) and (4.53), respectively. The asymptotic outage probability can then be derived by evaluating (C.52) at the threshold SNR as given in (4.52a).

## C.7 Proof of the CDF of the SNR of optimal antenna selection for TWRNs with feedback delays

Whenever the antennas are selected by using outdated CSI due to feedback delays, $\gamma_{S_1}^{(J,L)}$ and $\gamma_{S_2}^{(J,L)}$ in (C.25a) can be expressed as[4]

$$
\gamma_{S_1}^{(\hat{J},\hat{L})} = \max_{j \in \{1,\cdots,N_1\}, l \in \{1,\cdots,N_2\}} \left( \gamma_{S_1}^{(j,l)} \right) = \frac{\hat{X}\hat{Y}}{\alpha\hat{X} + \beta\hat{Y} + \eta} \quad \text{and}
$$

$$
\gamma_{S_2}^{(\hat{J},\hat{L})} = \max_{j \in \{1,\cdots,N_1\}, l \in \{1,\cdots,N_2\}} \left( \gamma_{S_2}^{(j,l)} \right) = \frac{\hat{X}\hat{Y}}{\beta\hat{X} + \alpha\hat{Y} + \eta}, \tag{C.53}
$$

where $\hat{X} = \max_{j \in \{1,\cdots,N_1\}} \left( \left| \hat{h}_{S_1,R}^{(j)} \right|^2 \right)$ and $\hat{Y} = \max_{l \in \{1,\cdots,N_2\}} \left( \left| \hat{h}_{S_2,R}^{(l)} \right|^2 \right)$. Here, $\hat{h}_{S_1,R}^{(j)}$ and $\hat{h}_{S_2,R}^{(l)}$ are the $j$th and $l$th elements of the outdated channel vectors defined in (4.57). In fact, $\hat{X}$ and $\hat{Y}$ are the induced order statistics of original random variables $X$ and $Y$ [138]. Thus, the CDF and the PDF of $\hat{X}$ can be derived by using techniques similar those used in [119] as follows:

$$
F_{\hat{X}}(x) = 1 - \sum_{p=0}^{N_1-1} (-1)^p \binom{N_1}{p+1} \exp\left( -\frac{(p+1)x}{\zeta_1 \left( 1 + p \left( 1 - \rho_1^2 \right) \right)} \right) \quad \text{and}
$$

$$
f_{\hat{X}}(x) = \sum_{p=0}^{N_1-1} \frac{(-1)^p N_1 \binom{N_1-1}{p}}{\zeta_1 \left( 1 + p \left( 1 - \rho_1^2 \right) \right)} \exp\left( -\frac{(p+1)x}{\zeta_1 \left( 1 + p \left( 1 - \rho_1^2 \right) \right)} \right). \tag{C.54}
$$

Similarly, the CDF and PDF of $\hat{Y}$ can be derived as

$$
F_{\hat{Y}}(y) = 1 - \sum_{q=0}^{N_2-1} (-1)^q \binom{N_2}{q+1} \exp\left( -\frac{(q+1)y}{\zeta_2 \left( 1 + q \left( 1 - \rho_2^2 \right) \right)} \right) \quad \text{and}
$$

$$
f_{\hat{Y}}(y) = \sum_{q=0}^{N_2-1} \frac{(-1)^q N_2 \binom{N_2-1}{q}}{\zeta_2 \left( 1 + p \left( 1 - \rho_1^2 \right) \right)} \exp\left( -\frac{(q+1)y}{\zeta_2 \left( 1 + q \left( 1 - \rho_2^2 \right) \right)} \right). \tag{C.55}
$$

By substituting (C.54) and (C.55) into (C.28a) and following techniques similar to those in Appendix C.4, the CDF of $\hat{Z}$, and thereby, outage probability can be derived as given in (4.58a).

The first order expansion of $F_{\hat{X}}(x)$ and $f_{\hat{X}}(x)$ can be derived as

$$
F_{\hat{X}}^{\infty}(x) = \sum_{p=0}^{N_1-1} \frac{(-1)^p N_1 \binom{N_1-1}{p}}{\zeta_1 (1 + p(1 - \rho_1^2))} x + o(x) \quad \text{and}
$$

$$
f_{\hat{X}}^{\infty}(x) = \sum_{p=0}^{N_1-1} \frac{(-1)^p N_1 \binom{N_1-1}{p}}{\zeta_1 (1 + p(1 - \rho_1^2))} + o(1). \tag{C.56}
$$

---

[4]Since the system model is relaxed by considering a single-antenna relay, the dependency of end-to-end SNR on relay antenna index ($m$) is ignored.

Similarly, the first order expansion of $F_{\hat{Y}}(y)$ and $f_{\hat{Y}}(y)$ is given by

$$
\begin{aligned}
F_{\hat{Y}}^{\infty}(y) &= \sum_{q=0}^{N_2-1} \frac{(-1)^q N_2 \binom{N_2-1}{q}}{\zeta_2(1+q(1-\rho_2^2))} y + o(y) \quad \text{and} \\
f_{\hat{Y}}^{\infty}(y) &= \sum_{q=0}^{N_2-1} \frac{(-1)^q N_2 \binom{N_2-1}{q}}{\zeta_2(1+q(1-\rho_2^2))} + o(1).
\end{aligned}
\tag{C.57}
$$

By first substituting (C.56) and (C.57) into (C.37a), (C.37b) and (C.39), and then by following techniques similar to those in Appendix C.5, the asymptotic outage probability of the optimal antenna selection for TWRNs under feedback delays can be derived as given in (4.59a).

$$\sim$$

# Appendix D

# Proofs for Chapter 5

## D.1 Proof of the end-to-end SNR

To begin with, the signal vector belonging to the $n$th source, received at the $m$th source in the $j$th time-slot of the broadcast (BC) phase is re-written as

$$\mathbf{y}_{S_m}^{(j,n)} = G_j g_n \mathbf{x}_n + G_j \mathbf{n}_R^{(j)} + \mathbf{V}_m^{(j)} \mathbf{n}_m^{(j)}, \tag{D.1}$$

where $G_j = \sqrt{\mathcal{P}_R/(g_j^2 + g_{j+1}^2 + \sigma_R^2)}$, $g_n = \sqrt{\mathcal{P}_n/\mathcal{T}_n}$, $\mathcal{T}_n = N_R/(N_n - N_R)$, $j \in \{1, \cdots, M-1\}$, $m \in \{1, \cdots, M\}$, $n \in \{1, \cdots, M\}$, and $m \neq n$. The post-processing end-to-end SNR of the $k$th data subchannel of $\mathbf{y}_{S_m}^{(j,n)}$ can then be derived as follows:

$$\left[\gamma_{S_m^{(j,n)}}\right]_k = \frac{G_j^2 g_n^2}{G_j^2 \sigma_R^2 + \sigma_m^2 \left[\mathbf{V}_m^{(j)} \left(\mathbf{V}_m^{(j)}\right)^H\right]_{k,k}}. \tag{D.2}$$

By substituting $G_j$ and $\mathbf{V}_m^{(j)}$ in (5.7) into (D.2), the end-to-end SNR of the desired data subchannel can be re-written as

$$\left[\gamma_{S_m^{(j,n)}}\right]_k = \frac{\mathcal{P}_R g_n^2}{\mathcal{P}_R \sigma_R^2 + \sigma_m^2 (g_j^2 + g_{j+1}^2 + \sigma_R^2) \left[\left(\left(\mathbf{H}_{R,m}^{(j)}\right)^H \mathbf{H}_{R,m}^{(j)}\right)^{-1}\right]_{k,k}}. \tag{D.3}$$

Next, by substituting $g_n^2 = \mathcal{P}_n/\mathcal{T}_n$, $g_j^2 = \mathcal{P}_j/\mathcal{T}_j$ and $g_{j+1}^2 = \mathcal{P}_{j+1}/\mathcal{T}_{j+1}$ into (D.3) and performing some mathematical manipulations, the desired result can be derived as shown in (5.11).

## D.2 Proof of the outage probability lower bound of pairwise ZF transmission strategy

In this Appendix, the lower bound of the outage probability of the $m$th source is sketched. To this end, the maximum diagonal element of the inverse of a Wishart matrix can be lower

bounded by its arbitrary $a$th diagonal element as

$$\max_{k\in\{1\cdots N_R\}}\left(\left[\left(\left(\mathbf{H}_{R,m}^{(j)}\right)^H\mathbf{H}_{R,m}^{(j)}\right)^{-1}\right]_{k,k}\right)\geq\left[\left(\left(\mathbf{H}_{R,m}^{(j)}\right)^H\mathbf{H}_{R,m}^{(j)}\right)^{-1}\right]_{a,a}, \quad (\mathrm{D.4})$$

where $a\in\{1,\cdots,N_R\}$. Next, the smallest post-processing subchannel SNR of $S_m$ received in the $j$th time-slot of the BC phase can be upper bounded as

$$\min_{k\in\{1\cdots N_R\}}\left(\left[\gamma_{S_m^{(j)}}\right]_k\right)\leq\gamma_{S_m,\min}^{(j),\mathrm{ub}}=\frac{\eta_m^{(j)}}{\zeta_m^{(j)}+\mu_m^{(j)}\left[\left(\left(\mathbf{H}_{R,m}^{(j)}\right)^H\mathbf{H}_{R,m}^{(j)}\right)^{-1}\right]_{a,a}}, \quad (\mathrm{D.5})$$

where $\mu_m^{(j)}$, $\eta_m^{(j)}$, and $\zeta_m^{(j)}$ are defined in (5.26). By substituting (D.5) into (5.24), $P_{\mathrm{out,m}}$ can be lower bounded as

$$P_{\mathrm{out,m}}\geq P_{\mathrm{out,m}}^{\mathrm{lb}}=\mathrm{Pr}\left(\min_{j\in\{1,\cdots,M-1\}}\left(\gamma_{S_m,\min}^{(j),\mathrm{ub}}\right)\leq\gamma_{th}\right). \quad (\mathrm{D.6})$$

In order to derive $P_{\mathrm{out,m}}^{\mathrm{lb}}$ in closed-form, the CDF of $\gamma_{S_m,\min}^{(j),\mathrm{ub}}$ is obtained as follows:

$$F_{\gamma_{S_m,\min}^{(j),\mathrm{ub}}}(x)=1-\mathrm{Pr}\left(X_m^{(j)}\leq\frac{\eta_m^{(j)}-\zeta_m^{(j)}x}{\mu_m^{(j)}x}\right), \quad (\mathrm{D.7})$$

where $X_m^{(j)}=\left[\left(\left(\mathbf{H}_{R,m}^{(j)}\right)^H\mathbf{H}_{R,m}^{(j)}\right)^{-1}\right]_{a,a}$. For $x\geq\eta_m^{(j)}/\zeta_m^{(j)}$, $F_{\gamma_{S_m,\min}^{(j),\mathrm{ub}}}(x)=1$, and for $x<\eta_m^{(j)}/\zeta_m^{(j)}$, $F_{\gamma_{S_m,\min}^{(j),\mathrm{ub}}}(x)$ becomes

$$F_{\gamma_{S_m,\min}^{(j),\mathrm{ub}}}(x)=1-\int_0^{\frac{\eta_m^{(j)}-\zeta_m^{(j)}x}{\mu_m^{(j)}x}}f_{X_m^{(j)}}(y)\,\mathrm{d}y, \quad (\mathrm{D.8})$$

where $f_{X_m^{(j)}}(x)$ can be obtained by substituting the PDF of $1/X_m^{(j)}$, which is given by $f_{1/X_m^{(j)}}(x)=\frac{x^{N_m-N_R}e^{-x}}{\Gamma(N_m-N_R+1)}$ [142] into the transformation $f_{X_m^{(j)}}(x)=\frac{1}{x^2}f_{1/X_m^{(j)}}(1/x)$ as follows:

$$f_{X_m^{(j)}}(x)=\frac{e^{-1/x}}{\Gamma(N_m-N_R+1)x^{N_m-N_R+2}}. \quad (\mathrm{D.9})$$

Next, by substituting (D.9) into (D.8), and by applying a change of variable, $y=1/t$, (D.8) can be rearranged as

$$F_{\gamma_{S_m,\min}^{(j),\mathrm{ub}}}(x)=1-\int_{\frac{\mu_m^{(j)}x}{\eta_m^{(j)}-\zeta_m^{(j)}x}}^{\infty}\frac{t^{N_m-N_R}e^{-t}}{\Gamma(N_m-N_R+1)}\mathrm{d}t. \quad (\mathrm{D.10})$$

By using [1, Eqn. (8.350.2)], (D.10) can now be evaluated in closed-form as in (5.26). By substituting (D.10) into the CDF of minimum of $M-1$ independent random variables, the desired results can be derived as in (5.25).

## D.3 Proof of the outage probability upper bound for pairwise ZF transmission strategy

In this Appendix, the outage upper bound of the $m$th source is derived. To this context, the maximum diagonal element of the inverse of a Wishart matrix is upper bounded as [134]

$$\max_{k\in\{1\cdots N_R\}}\left(\left[\left(\left(\mathbf{H}_{R,m}^{(j)}\right)^H \mathbf{H}_{R,m}^{(j)}\right)^{-1}\right]_{k,k}\right) \leq \lambda_{\min}^{-1}\left(\left(\mathbf{H}_{R,m}^{(j)}\right)^H \mathbf{H}_{R,m}^{(j)}\right). \quad \text{(D.11)}$$

The smallest subchannel SNR of $S_m$ received in the $j$th time-slot of the BC phase can then be lower bounded by substituting (D.11) into (5.11) as follows:

$$\min_{k\in\{1\cdots N_R\}}\left(\left[\gamma_{S_m^{(j)}}\right]_k\right) \geq \gamma_{S_m,\min}^{(j),\text{lb}} = \frac{\eta_m^{(j)}}{\zeta_m^{(j)} + \mu_m^{(j)}\lambda_{\min}^{-1}\left(\left(\mathbf{H}_{R,m}^{(j)}\right)^H \mathbf{H}_{R,m}^{(j)}\right)}, \quad \text{(D.12)}$$

where $\mu_m^{(j)}$, $\eta_m^{(j)}$, and $\zeta_m^{(j)}$ are defined in (5.26). By substituting (D.12) into (5.24), $P_{\text{out,m}}$ can now be upper bounded for $0 < \gamma_{th} < \eta_m^{(j)}/\zeta_j^{(m)}$ as

$$\begin{aligned}
P_{\text{out,m}} \leq P_{\text{out,m}}^{\text{ub}} &= \Pr\left(\min_{j\in\{1,\cdots,M-1\}}\left(\gamma_{S_m,\min}^{(j),\text{lb}}\right) \leq \gamma_{th}\right) \\
&= 1 - \prod_{j=1}^{M-1}\left(1 - F_{\lambda_{\min}^{(j,m)}}\left(\frac{\mu_m^{(j)}\gamma_{th}}{\eta_m^{(j)} - \zeta_m^{(j)}\gamma_{th}}\right)\right), \quad \text{(D.13)}
\end{aligned}$$

where $\lambda_{\min}^{(j,m)} = \lambda_{\min}\left(\left(\mathbf{H}_{R,m}^{(j)}\right)^H \mathbf{H}_{R,m}^{(j)}\right)$ and the CDF of $\lambda_{\min}^{(j,m)}$ is given by [136, Eqn. (2.73)]. By using similar steps to those in Appendix D.2, we can show that $P_{\text{out,m}} = 1$ for $\gamma_{th} \geq \eta_m^{(j)}/\zeta_j^{(m)}$.

## D.4 Proof of the high SNR outage probability approximation for pairwise ZF transmission

In this Appendix, the proof of the lower bound for the diversity order is sketched. To begin with, the PDF of $\gamma_{S_m,\min}^{(j),\text{ub}}$ for $j \in \{1,\cdots,M-1\}$ is derived by differentiating (5.25) with respect to variable $x$ by using the Leibniz integral rule as follows:

$$\begin{aligned}
f_{\gamma_{S_m,\min}^{(j),\text{ub}}}(x) &= \frac{e^{-\frac{\mu_m^{(j)}x}{\eta_m^{(j)} - \zeta_m^{(j)}x}}}{\Gamma(N_m - N_R + 1)}\left(\frac{\mu_m^{(j)}x}{\eta_m^{(j)} - \zeta_m^{(j)}x}\right)^{N_m - N_R}\frac{d}{dx}\left[\frac{\mu_m^{(j)}x}{\eta_m^{(j)} - \zeta_m^{(j)}x}\right], \\
&= \frac{\eta_m^{(j)}\left(\mu_m^{(j)}\right)^{N_m - N_R + 1}x^{N_m - N_R}e^{\frac{-\mu_m^{(j)}x}{\eta_m^{(j)} - \zeta_m^{(j)}x}}}{\Gamma(N_m - N_R + 1)\left(\eta_m^{(j)} - \zeta_m^{(j)}x\right)^{N_m - N_R + 2}}, \quad \text{(D.14)}
\end{aligned}$$

179

where $0 \leq x < \frac{\eta_m^{(j)}}{\zeta_m^{(j)}}$. By substituting $\mu_m^{(j)}$, $\eta_m^{(j)}$, and $\zeta_m^{(j)}$, defined in (5.26) into (D.14), and then by taking the Taylor series expansion around $x = 0$, the first order expansion of $f_{\gamma_{S_m,\min}^{(j),\text{ub}}}(x)$ when $\lim_{x \to 0}$ is derived as

$$f_{\gamma_{S_m,\min}^{(j),\text{ub}}}^{x \to 0}(x) = \frac{\left(\phi_m^{(j)}\right)^{N_m - N_R + 1} x^{N_m - N_R}}{(N_m - N_R)! \left(\beta \bar{\gamma}_{SR}\right)^{N_m - N_R + 1}} + o\left(x^{N_m - N_R}\right). \tag{D.15}$$

The first order expansion of the PDF of $\gamma_{S_m,\min}^{(j),\text{ub}}$ in (D.15) is indeed the single-term polynomial approximation of the exact PDF of $\gamma_{S_m,\min}^{(j),\text{ub}}$ consisting with the lowest power of $x$ [61]. The first order expansion of the CDF of $\gamma_{S_m,\min}^{(j),\text{ub}}$ when $\lim_{x \to 0}$ is derived by using (D.15) as follows [61]:

$$F_{\gamma_{S_m,\min}^{(j),\text{ub}}}^{x \to 0}(x) = \Omega_{\text{lb},m}^{(j)} \left(\frac{\gamma_{th}}{\bar{\gamma}_{S,R}}\right)^{G_{d,m}^{\text{lb}}} + o\left(\bar{\gamma}_{S,R}^{-G_{d,m}^{\text{lb}}}\right), \tag{D.16}$$

where $G_{d,m}^{\text{lb}}$ and $\Omega_{\text{lb},m}^{(j)}$ are defined in (5.36) and (5.37). Next, the first order expansion of the CDF of $Y_m = \min_{j \in \{1,\cdots,M-1\}} \left(\gamma_{S_m,\min}^{(j),\text{lb}}\right)$ can be derived by first substituting (D.16) into $F_{Y_m}(x) = 1 - \prod_{j=1}^{M-1}\left(1 - F_{\gamma_{S_m,\min}^{(j),\text{ub}}}(x)\right)$ and then by using the well-known identity [1] $\prod_{l=1}^{L}(1-y_l) = 1 + \sum_{l=1}^{L}(-1)^l \sum_{\lambda_1=1}^{L-l+1} \sum_{\lambda_2=\lambda_1+1}^{L-l+2} \cdots \cdots \sum_{\lambda_l=\lambda_{l-1}}^{L} \prod_{n=1}^{l} y_{\lambda_n}$ as follows:

$$F_{Y_m^\infty}(x) = \left[\sum_{j=1}^{M-1} \Omega_{\text{lb},m}^{(j)}\right] \left(\frac{x}{\bar{\gamma}_{S,R}}\right)^{G_{d,m}^{(j),\text{lb}}} + o\left(x^{G_{d,m}^{(j),\text{lb}}}\right). \tag{D.17}$$

By using a similar technique, the first order expansion of the CDF of $Z = \min_{j \in \{1,\cdots,M-1\}} (Y_m)$ can be derived by substituting (D.17) into the expansion of $F_Z(x) = 1 - \prod_{m=1}^{M}\left(1 - F_{Y_m^\infty}(x)\right)$ to obtain the desired result in (5.38).

$$\sim$$